Institut de Ciència i Tecnologia Ambientals
Universitat Autònoma de Barcelona

Application of tetraether membrane lipids as proxies for continental climate reconstruction in Iberian and Siberian lakes

Marina Escala Pascual

Tesi doctoral

Institut de Ciència i Tecnologia Ambientals

Universitat Autònoma de Barcelona

Application of tetraether membrane lipids as proxies for continental climate reconstruction in Iberian and Siberian lakes

Memòria presentada per Marina Escala Pascual per optar al títol de Doctor per la Universitat Autònoma de Barcelona, sota la direcció del doctor Antoni Rosell Melé.

Marina Escala Pascual

Abril 2009

icta Institut de Ciència i Tecnologia Ambientals • UAB

Universitat Autònoma de Barcelona

Cover photograph: Lake Baikal (Jens Klump, Continent Project)

Als meus pares i al meu germà.

INDEX

Appendices

Agraïments - Acknowledgements

Vull donar les gràcies a l'Antoni Rosell, per donar-me l'oportunitat d'investigar en el camp del paleoclima i per tot el que n'he anat aprenent al llarg d'aquests anys a la universitat.

També vull agrair al Pere Masqué el suport en la fase inicial d'aquesta tesi.

Vull agrair a l'Alba Eustaquio i al Josep M. Paulís tot el suport i la motivació durant els anàlisis al Servei d'Anàlisi Química de la UAB. També vull agrair a la Montse Carrascal i al Joaquín Abián el seu recolzament durant els anàlisis al laboratori de Proteòmica CSIC-UAB.

I would like to thank Hedi Oberhänsli for the opportunity to sample sediment cores from Lake Baikal and the constructive discussions about the paleoclimate of this lake. Martin Schmid and Carsten Schubert are thanked for providing temperature information from the Lake Baikal sediment trap moorings.

Agraeixo al Carles Borrego i l'Emili Casamayor l'experiència del mostreig del llac del Vilar i el coneixement que han compartit sobre els arquees.

Quiero dar las gracias a Blas Valero y Ana Moreno por las muestras de lagos de la Península Ibérica que nos ofrecieron y por compartir su conocimiento y experiencia.

Emma Pearson is thanked for provision of samples and productive discussions about the Iberian Peninsula lakes.

Hiroyuki Morii is thanked for provision of a caldarchaeol sample and Thierry Benvegnu for preparation of compound GR.

I would like to thank Stefan Schouten, Ellen Hopmans and Jaap S.S. Damsté for their hospitality and the fruitful analyses and discussions during my short stays at the NIOZ, on Texel. I thank as well the colleagues at NIOZ, with whom I learned a lot and who made my stays very enjoyable: Angela, Isla, Thorsten, Arjan, Francien, Cornelia and Johann.

Agraeixo a la Generalitat de Catalunya el seu suport en forma d'una beca d'investigació predoctoral FI i una beca d'estada BE.

Moltes gràcies als coleguis de l'ICTA, especialment a la Nata, l'Alfredo, el Migue, la Gemma, la Gema, la Susanne, el Bastian, la Núria, la Saioa, el César, el Sergi i des de fa poquet, a l'Anna, per tantíssimes converses i experiències compartides, des dels cafès a les discussions *freakis*, els aniversaris, les llargues tardes al laboratori i totes les rialles. I perquè em feu venir ganes de no marxar.

Moltes gràcies a la Dril, la Mafi, la Montse, l'Anna i la Sílvia perquè les trobades han estat una porta oberta que hem travessat parlant i escoltant, rient i mirant pel·lis, sopant i filosofant sobre la vida. Gràcies també al David, al Luís, la Mireia, l'Andrés, l'Arnau i la Sara, perquè també formen part del camí que m'ha dut fins aquí.

També vull donar les gràcies al Lluís, el Jordi i la Gemma, perquè trobar-me amb ells m'ha ajudat a obrir els ulls.

Moltes gràcies a la meva família, en especial als meus pares i al meu germà. Gràcies, mare, per tot el suport en incomptables vegades, per escoltar-me i cuidar-me i sobretot, per l'acceptació i la valentia de viure. Gràcies, pare, per mostrar-me el camí de la millora contínua, per l'alegria retrobada i també especialment, per la valentia de viure. Gràcies, *Brother*, per la quantitat de coses que ens uneixen i ens diferencien i per mostrar-me què pot ser expressar-se i no rendir-se.

Vielen Dank, Jörg, unsere Weg ist eine Herausforderung und ich bin glüclklich mit dir zu wandern.

Marina

Abstract

Since 2002, several climate proxies based on biomarkers of Archaea and Bacteria have been developed and applied in sedimentary archives worldwide. These biomarkers are the glycerol dialkyl glycerol tetraethers or GDGTs. Among the proposed proxies, the TEX_{86} index is applied in sediments to reconstruct sea surface temperatures (SST) and lake surface temperatures (LST); The MBT and CBT indices are together applied as a proxy for past surface air temperature and the BIT index is measured in sediments to assess qualitatively relative inputs of pelagic-originated material versus soil material. Given the novelty of these proxies, there is plenty of scope to improve upon a range of issues regarding their measurement and application. Consequently, the aim of this thesis has been to tackle analytical methodological issues to gain in analytical reliability and sample throughput, and expand the range of environments where GDGT proxies have been appraised, particularly in lake environments.

In the analytical section of the thesis, two sample clean-up methods, i.e. alumina fractionation and alkaline hydrolysis are compared. Additional tests compare alumina and silica in their activated and deactivated states as adsorbents onto which GDGTs are fractionated. Results show that TEX_{86} values are robust using these methodologies, while BIT values are dependant on adsorbent activation state. Regarding the chromatographic analysis, an increase in the analysis velocity and a reduction of flow are effectively implemented without loss of chromatographic peak resolution. Additionally, two mass spectrometer designs, i.e. an ion-trap system and a quadrupole system, are used for the measurement of a wide range of values of TEX_{86} and BIT indices, and results confirm the comparability of both systems. However, BIT values are found to be extremely sensitive to the MS tuning conditions.

In order to find out the main factors influencing the GDGTs distribution in lacustrine environments, a suite of surface sediments from 38 Iberian lakes are surveyed. Principal component analysis of the relative concentrations of GDGTs indicates that terrestrial versus lacustrine origin, combined with degree of cyclization and degree of methylation of the lipids are the principal factors accounting for the GDGT distribution in the sediments. The measurement of the MBT/CBT proxy represents a pioneer application of these indices in lake sediments. TEX_{86} and MBT/CBT are shown to have a limited applicability in predicting the lake temperature, likely due to a complex combination of factors influencing the GDGT abundances. Using cluster analysis a subset of lakes is selected with a rather linear relationship of TEX_{86} and CBT/MBT with instrumental air temperatures.

In the study conducted in lake Baikal in Siberia, sediment traps, surface sediments and two cores spanning the last glacial-interglacial cycle are analysed in the north and south basins of the lake. BIT values both for the particulate material collected and the surface sediments suggest low influence of soil-derived material. TEX_{86} derived LST from the water column particulate material and sediments are in the range of measured annual LST. The down-core variations of the TEX_{86} and MBT/CBT proxies reveal a climatic signal, inferred both from the reconstructed transition from glacial to interglacial conditions and the partial agreement with reconstructed changes in Lake Baikal region derived from other proxies applied in the sediments.

Finally, an exploratory study in the Bosumtwi impact structure in Africa reveals the presence of GDGTs in the deeply buried impacted rocks and three hypotheses are discussed for their origin and relative age.

The work presented extends the range of analytical techniques that can be reliably used for the measurement of the GDGT indices and provides deeper knowledge on the application and validation of GDGTs as climate proxies in lacustrine sediments, in particular from the Iberian and Siberian regions.

Resum

Des del 2002, s'han desenvolupat una sèrie de *proxies* climàtiques basades en biomarcadors derivats d'arquees i bacteris. Aquests biomarcadors són els glicerol dialquil glicerol tetraèters o GDGTs. D'entre aquestes *proxies*, l'índex TEX_{86} s'aplica en sediments per tal de reconstruir les temperatures superficials del mar i dels llacs; els índexs MBT i CBT són utilitzats conjuntament per a reconstruir la temperatura superficial de l'aire i l'índex BIT permet avaluar la contribució relativa de material provinent del sòl i material pelàgic en els sediments. A causa del recent desenvolupament d'aquestes *proxies*, hi ha encara un gran nombre d'aspectes metodològics i d'aplicació que han estat poc estudiats. Per això, l'objectiu d'aquesta tesi ha estat la comparació i optimització de diversos procediments analítics implicats en la determinació dels GDGTs, així com l'estudi d'aquests biomarcadors en nous ambients, amb especial atenció en els llacs.

En la part analítica d'aquesta tesi, s'ha comparat el mètode estàndard de *clean-up* de les mostres basat en el fraccionament de lípids en alúmina amb la hidròlisi alcalina; a més, s'han comparat diversos adsorbents i graus d'activació per al fraccionament dels lípids. Els resultats demostren que el TEX_{86} és robust respecte a aquestes tècniques, mentres que l'índex BIT depèn del grau d'activació de l'adsorbent. En la cromatografia, s'han dut a terme una reducció del flux i un augment de la velocitat dels anàlisis sense pèrdua de resolució cromatogràfica. Finalment, s'han utilitzat dos espectròmetres de masses de disseny diferent per a mesurar els índexs TEX_{86} i BIT i se n'ha confirmat la comparabilitat. Per altra banda, s'ha observat una sensibilitat extrema del BIT respecte a les condicions d'optimització dels espectròmetres.

S'ha estudiat les concentracions dels GDGTs en els sediments superficials d'un conjunt de 38 llacs de la Península Ibèrica per tal d'identificar els factors que en determinen la distribució relativa. L'anàlisi de components principals indica que la major part de la variança pot explicar-se amb l'origen dels GDGTs (del sòl o lacustre), el grau de ciclització interna i el grau de metilació dels GDGTs. Els resultats demostren que les *proxies* MBT/CBT i el TEX_{86} tenen una utilitat limitada en la predicció de les temperatures d'aquests llacs, possiblement perquè la distribució de GDGTs és determinada per una mescla complexa de factors. Utilitzant l'anàlisi de *clusters* s'ha identificat un subconjunt de llacs on els índexs TEX_{86} i MBT/CBT mantenen una relació linial forta amb les temperatures instrumentals de l'aire.

L'estudi dut a terme al llac Baikal (Sibèria) combina els resultats de trampes de sediment, sediments superficials i dos testimonis sedimentaris que corresponen a l'últim cicle glacial-interglacial. Els valors per a l'índex BIT al sediment suggereixen una contribució minsa de material provinent del sòl i les temperatures superficials del llac derivades de l'índex TEX_{86} es troben dins el rang anual de les mesures de temperatures superficials. En els testimonis sedimentaris, les variacions en profunditat del TEX_{86} i l'MBT/CBT revelen un senyal climàtic que es concreta en el registre de la transició de condicions glacials a interglacials i l'acord parcial amb les reconstruccions climàtiques existents per a la regió del llac Baikal derivades d'altres *proxies*.

En darrer lloc, l'estudi exploratori dut a terme al cràter del Bosumtwi (Àfrica) revela la presència de GDGTs en les roques impactades i es discuteixen tres hipòtesis en referència a l'origen dels GDGTs trobats.

El treball presentat amplia el rang de tècniques analítiques que poden utilitzar-se de forma fiable per a la mesura dels índexs basats en GDGTs i profunditza en l'aplicació i validació dels GDGTs com a *proxies* climàtiques en sediments lacustres, particularment de la Península Ibèrica i Sibèria.

Chapter 1

Introduction

1.1. Paleoclimate and biomarker proxies

The prospect of future climate is of great concern in the international agenda. This partly stems from the realization that the recent increase in global average surface air and ocean temperatures is to some degree caused by anthropogenic activities (IPCC, 2007). Consequently, there is a large deal of interest worldwide to find out to what extent humankind can influence the state of climate and how can this affect human welfare and ecosystems. In the quest for understanding the climate system, **paleoclimate** has emerged as a field of research that looks into the past to unveil the cycles and patterns of natural climate variability, looking for the causes and consequences of changes in the several components of the climatic system.

Climate on Earth has an intrinsic variability, i.e. it has always been changing since our planet was formed, about 4600 million years (Myr) ago. The planet has experienced drastic changes, starting by a considerable cooling from its original extremely high temperatures, the growth and retreat of ice-caps, as well as experiencing periods of higher than present atmospheric greenhouse gas (GHG) concentrations, tens of millions of years ago (e.g. IPCC, 2007). More recently, during the Quaternary, the period spanning the last 1.8 Myr, long-term climatic changes are dominated by glacial-interglacial cycles linked to changes in orbital parameters and to non-linear responses, such as changes in global ice volume and thermohaline circulation (e.g. Hays et al., 1976; Paillard, 2001). Intense research is focused on the amplitude of temperature and GHG concentration changes, the global biogeochemical cycle's patterns, especially those of nitrogen and carbon, the changes in productivity in the oceans following the glacial-interglacial cycles and the coupling of changes between land and ocean in different regions of the globe.

Most instrumental records of temperature and other climatic variables such as precipitation or wind strength span less than the last two centuries (e.g. Le Treut et al., 2007). Reconstruction of pre-industrial past environmental and climatic change, therefore requires the use of indirect, or **proxy** methods. A proxy is a measurable descriptor that stands in for a target but unobservable parameter, such as temperature, salinity and productivity (Wefer et al., 1999). One of the key parameters to define the

state of climate in a specific period is the sea surface temperature (SST). Several proxies have been developed to reconstruct SST, such as microfossil assemblages of foraminifera and diatoms (Erez et al., 1983; Pichon et al., 1987), oxygen isotopic composition of biogenic carbonate (Emiliani, 1955), Mg/Ca ratios in carbonate shells (Chave, 1954a,b; Lea, 2003) and biomarker proxies based on algal and archaeal lipids (Brassell et al., 1986; Schouten et al., 2002). On land, these or similar proxies are applied to reconstruct lake surface temperature (LST) (e.g. Walker et al., 1991; Mackay et al., 2007; Zink et al., 2001; Powers et al., 2004). LST can be a good indicator of continental climate in a specific region, and provides key information to study the coupling between ocean and land climates; this is a consequence of lakes integrating a signal of the whole basin through the storage of organic and inorganic compounds transported by streams and runoff into their sediments. Furthermore, lake sedimentary archives record fluctuations in water level, water chemistry and productivity, which can be strongly influenced by climate. Among the temperature proxies that have been applied in lakes to reconstruct LST, biomarkers are probably the least studied.

Biomarkers are organic compounds (primarily lipids) that have particular biosynthetic origins and are resistant to degradation, so that they can be preserved in sediments and sedimentary rocks (e.g. Rosell-Melé, 2003). The most valuable biomarkers are taxonomically specific, i.e., they can be attributed to a defined group of organisms, and by means of their chemical and/or sterical configuration they carry a signal from the past environments in which they were synthesized. Both alkenones derived from Haptophyceae algae (Brassell et al., 1986; Prahl and Wakeham, 1987; Li et al., 1996) and **glycerol dialkyl glycerol tetraethers** (**GDGTs**) from Archaea (Schouten et al., 2002; Powers et al., 2004) are biomarkers used in proxies for reconstructing past SST and LST. Published studies on the application of archaeal GDGT-based proxies in lacustrine systems are still scarce and results suggest that their climatic interpretation is not consistent in all lakes (e.g. Powers, 2005). Much more investigation is needed to understand in which conditions these biomarker proxies can be reliably applied. The following sections summarize what is known about the presence of Archaea in freshwater environments and the use of Archaeal-derived lipids as proxies for lake surface temperature reconstruction.

1.2. Distribution of Archaea in freshwater environments

Three decades ago, the use of ribosomal RNA (ribonucleic acid) analyses allowed Woese and collaborators to reclassify organisms by their phylogenetic relationships, prompting the replacement of the traditional tree with the prokaryotes and eukaryotes as the two life domains. The revision distinguished three domains called Eukarya, Bacteria and Archaeabacteria (Woese et al., 1977) and the latter was subsequently renamed **Archaea** (Woese et al., 1990). While the first two groups had long been studied, little was known about Archaea. Not long ago it was assumed that the occurrence of this group of organisms was restricted to extreme environments, either with low pH, extreme high temperatures and salinity, and/or anaerobic conditions. But this picture was strongly influenced by the bias in the range of physiologies observed in cultured Archaea (e.g. Casamayor and Borrego, 2009). Several studies in the last decade, using new cultivation-independent molecular ecological techniques such as fluorescence *in situ* hybridization (FISH) and microautoradiography able to monitor active populations, RNA isolation and gene sequencing, have radically changed this view. They have uncovered vast numbers of Archaea that occur ubiquitously in relatively cold environments (see Figure 1.1), including the ocean water column and sediments, as well as ice, soils and freshwater environments on land (Hershberger et al., 1996; Cavicchioli, 2006). Moreover, there is increasing evidence of their importance in the global biogeochemical cycles, especially those of carbon and nitrogen (e.g. Könneke et al., 2005; Herndl et al., 2005; Ingalls et al., 2006; Leininger et al., 2006).

The domain Archaea includes at present two main most widespread and abundant phyla: **Crenarchaeota** and **Euryarchaeota**. Three other phyla within the Archaea have been suggested, namely Korarchaeota, Nanoarchaeota and Thaumarchaeota, but they are still minor groupings with few described representatives (Barns et al., 1996; Huber et al., 2002; Brochier-Armanet et al., 2008). Among Crenarchaeota and Euryarchaeota several **methanogenic**[*] species have been cultured (e.g. Tornabene et al., 1979) but only a few cold non-methanogenic representatives have hitherto proved amenable for cultivation techniques. A recent landmark study was the isolation of the first free-living marine archaeon belonging to Crenarchaeota from a tank in an aquarium in the city of

[*] Words in grey are described in the glossary.

Seattle, United States (*Nitrosopumilus maritimus*, Könneke et al., 2005). Additionally, a marine crenarchaeon that lives associated with sponges from the family Axinellidae (*Cenarchaeum symbiosum*, Preston et al., 1996; Schleper et al., 1997b, 1998) has been sufficiently enriched to allow sequencing its complete genome (Hallam et al., 2006).

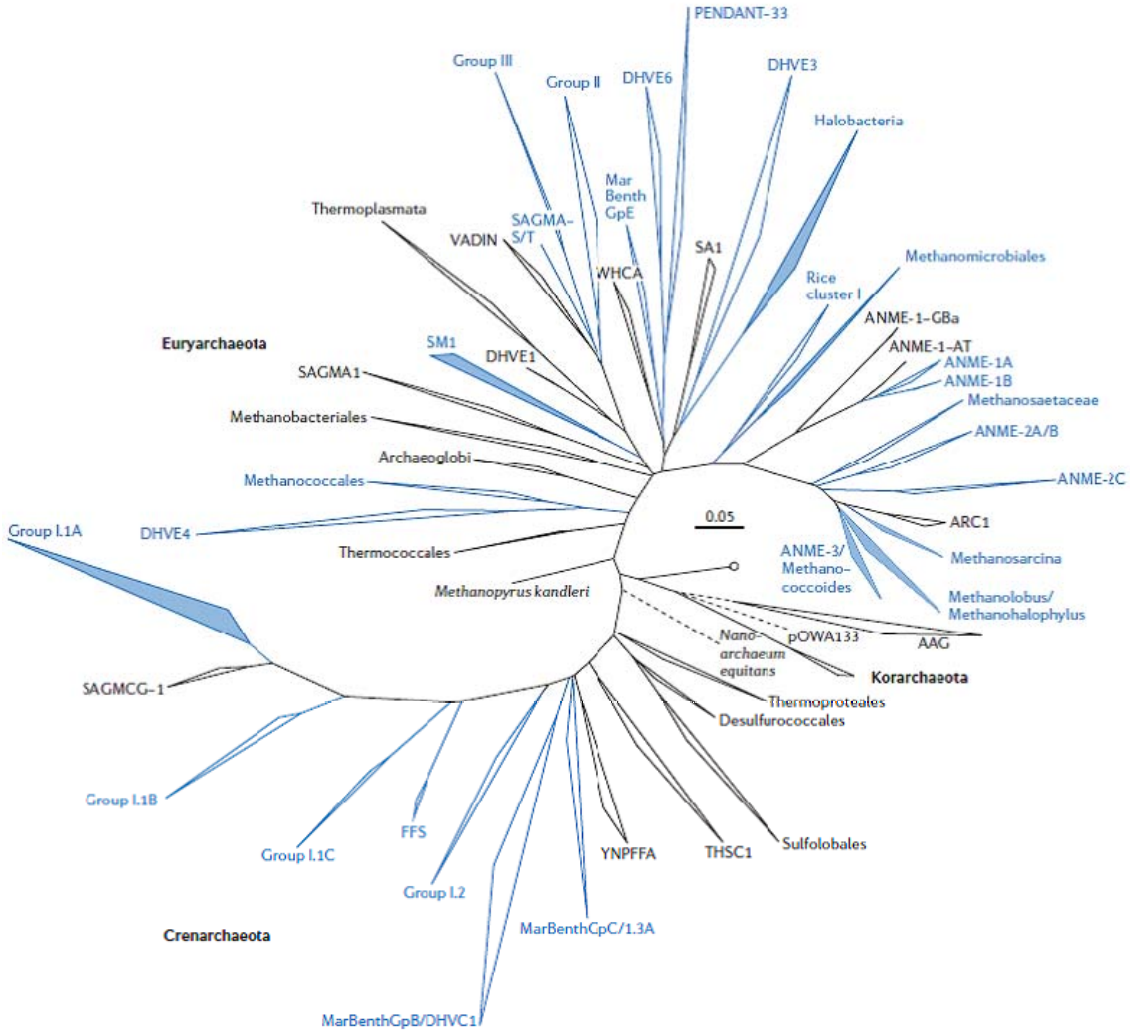

Figure 1.1 16S-RNA tree showing the recognized diversity of Archaea from naturally cold environments (in blue) and other archaeal groups for comparison (in black). Isolated phylotypes are indicated by filled blue. Source: Cavicchioli (2006).

In cold inland waters, Crenarchaeota and Euryarchaeota have been found in lakes, rivers, marshes and salty lakes and salterns (e.g. Casamayor and Borrego, 2009). Euryarchaeotal representatives in these environments embrace a wide variety of **mesophilic** phylotypes, including methanogens (widely spread in anoxic environments

and fairly easy to culture) and the halophiles, found in large numbers in salty environments and of which a few representatives have been isolated (e.g. Franzmann et al., 1988). On the other hand, the vast majority of mesophilic Crenarchaeota phenotypes discovered have not yet been cultured and therefore the ecology and metabolism of most of these organisms remain elusive.

Published studies on the presence of Archaea in **lacustrine systems** are concentrated in the last decade. A first observation is that archaeal cells in the water column are metabolically active *in situ* (e.g. Jurgens et al, 2000). The reported numbers suggest that Archaea contribute a lower percentage of the picoplankton than in the marine realm, where Archaea constitute around 20% of the picoplankton, reaching in some cases 84% (Karner et al., 2001; Herndl et al., 2005). A survey of 8 large lakes in North America (Lakes Erie, Huron, Michigan, Ontario, and Superior), Russia (Lakes Ladoga and Onega) and Africa (Lake Victoria) revealed that Archaea contributed 1% to 10% of the total picoplankton RNA pool (Keough et al., 2003). Other studies in lakes Michigan, Wintergreen and Lawrence (North America) found that crenarchaeotal RNA represented 10% of the total planktonic RNA (Schleper et al., 1997a; MacGregor et al., 1997). These findings suggest that a small number of crenarchaeons inhabit the freshwater environments.

A particular case seem to be the polar and high altitude lakes, of which some representatives have been studied in Antarctica, Arctic as well as the Alps and Pyrenean mountain regions. In these ultraoligotrophic and mostly well-oxygenated water bodies, the reported abundances of Archaea are higher (1-37% of total prokaryotic plankton), and highest cell concentrations are detected during autumn thermal mixing and formation of ice-cover in early winter (e.g. Pernthaler et al., 1998; Urbach et al., 2001; Auguet and Casamayor, 2008). There are also evidences of higher archaeal diversity among lakes in these cold environments.

Moreover, stratified lakes, environments characterized by strong gradients of oxygen concentration, light availability and water chemical composition, are niche of depth-distributed distinct archaeal populations. In the upper well-oxygenated water layers both mesophilic Crenarchaeota and Euryarchaeota are found, although they are usually less

abundant than Bacteria. Anoxic bottom waters and sediments are instead rich in the relatively well-known methanogens (Euryarchaeota) and a few phylotypes of planktonic Crenarchaeota distantly related to the marine benthic relatives (Casamayor and Borrego, 2009). Observations also coincide on the increase of archaeal abundance with depth, especially below the chemocline, as observed in lake Sælenvannet in Norway (Øvreås et al., 1997) and lake Vilar in Spain (Casamayor et al., 2001). Another significant study in a stratified Finnish boreal forest lake found that Crenarchaeota, only detected in the anoxic layer, were not related to surrounding soil Crenarchaeota, supporting the idea of *in situ* metabolically active cells (Jurgens et al., 2000).

Salt lakes are also extreme environments worth looking at, given their worldwide occurrence in inland water systems. Mesohaline uncultured Euryarchaeota constitute the archaeal community in lakes with salinities ranging from 50-70 g/L, while in hypersaline environments (>200 g/L) Haloarchaea dominate the whole microbial community, accounting for up to 75% of cells (Casamayor and Borrego, 2009). Euryarchaeota seem to have specific adaptations to thrive in such extreme environments; for instance, the group Haloarchaea has developed especial proteins resistant to denaturing effects of salt and DNA-repairing systems, which explains the wide occurrence of this group in salt lakes, where Crenarchaeota are virtually absent (Casamayor and Borrego, 2009). The stratified hypersaline lake Solar in Egypt (Cytryn et al., 2000) and the alkaline lake Qinghai in China (Dong et al., 2006) are two representatives of these studies.

Besides RNA, other characteristic archaeal molecules have been studied both in ocean and freshwater environments: the membrane lipids. Among these we find the so-called glycerol dialkyl glycerol tetraethers (GDGTs), biomarkers that have been the focus of geochemical surveys carried out in freshwater environments (e.g. Schouten et al., 1998; Powers et al., 2004). These geochemical analyses greatly benefit from the results provided by molecular studies, since the origin of the membrane lipids can not be inferred solely from their presence in the sediments. Thus, information on the occurrence of active Archaea in lakes, taxonomic diversity and distribution in the water column are of great interest for the interpretation of the GDGT pool contained in sediments.

1.3. Origin and significance of GDGTs

Polar lipids are the basic constituents of the cell membrane and are usually composed of a polar head group bonded to an apolar structure of hydrocarbon chains. In the prokaryotic domain, four differences allow distinguishing archaeal from bacterial lipids: (i) the glycerophosphate backbone is composed of *sn*-glycerol-1-phosphate in Archaea while its enantiomer *sn*-glycerol-3-phosphate is found in bacterial phospholipids; (ii) hydrocarbon chains are bonded to the glycerol moiety exclusively by ether linkages in Archaea, while in Bacteria ester bonds predominate in the fatty acid – glycerol connection; (iii) the **isoprenoidal** hydrocarbon chains are common in the archaeal domain, while Bacteria exhibit mostly **branched** chains; (iv) archaeal membranes show a significant number of bipolar tetraether lipids, with hydrocarbon chains spanning through the membrane, but such bipolar structure is rare in Bacteria (Koga et al., 1993).

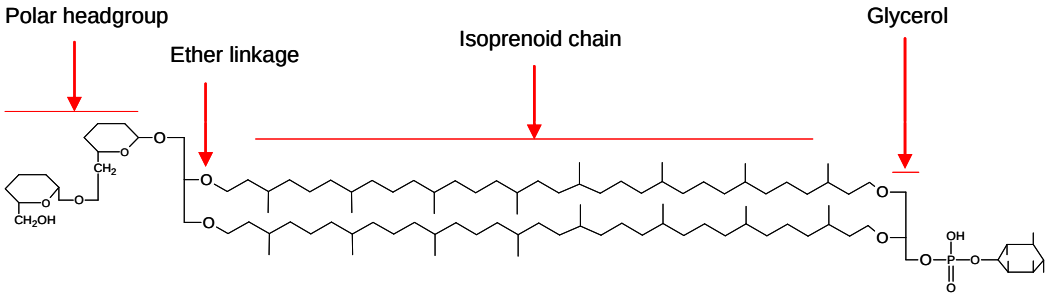

Figure 1.2 Archaeal tetraether lipid (gentiobiosyl caldarchatidyl-inositol from *Methanobacterium thermoautotophicum*. Source: Koga et al., 1993). Two polar head groups are bonded to glycerol moieties that are in turn ether-linked to the core double C_{40} isoprenoidal chains.

A typical archaeal tetraether lipid structure has two isoprenoidal chains bonded to two terminal glycerols by ether linkages, which in turn hold two polar head groups, thus providing the bipolar nature (see Fig. 1.2). The polar head groups are rapidly detached (within weeks) after the cell's decay, presumably by enzimatic hydrolization (White et al., 1979; Harvey et al., 1986) and easily degraded. In aquatic systems, this process may already happen in the water column, while the dead cell material sinks to the floor

sediment. In contrast, the core structure remains intact for longer periods and can therefore be accumulated in sediments. This core structure is called **glycerol dialkyl glycerol tetraether** or **GDGT**.

The key attribute that makes GDGTs valuable as temperature proxies is their structural dependence on temperature. At increasing temperatures, cyclopentane moieties are formed within the isoprenoidal chains, an effect first observed in cultured extremophilic archaeons (e.g. Gliozzi et al., 1983; DeRosa and Gambacorta, 1988; Uda et al., 2001). This is presumably related to the fluidity of the membrane, i.e. the rigid cyclopentane rings keep the membrane in a liquid crystalline state and reduce the proton permeation rate when temperatures increase, thus helping membrane stability, similarly to what double bonds and chain length do in membrane lipids from Bacteria and Eukarya (Albers et al., 2000; van de Vossenberg, 1995).

This temperature-dependant cyclopentane formation has not yet been directly observed for mesophilic archaeons, due to the virtual lack of isolated species. At the time this thesis is written, only marine water incubation studies have provided some hints pointing at a similar response of mesophilic Crenarchaeota to temperature compared to their cultured **thermophilic** relatives (Wuchter et al., 2004; Schouten et al., 2007a). These two studies tested incubation temperatures ranging from 5 to 25 ºC and 25 to 40 ºC, respectively, and a clear change in the cyclization of the GDGT pool after a few months of incubation could be observed. However, as the DNA composition suggested some changes in the number of archaeal phylotypes present in the tanks, there is no complete evidence of the cell membrane response, as species distribution changes could partly explain the evolution observed in the lipid distribution. Anyway, the results from these studies are in agreement with the hypothesis that cold environment-inhabiting Archaea respond to temperature using a similar strategy than their thermophilic relatives.

A typical C_{40} isoprenoidal chain from a GDGT can contain none or a maximum of four cyclopentane rings (Itoh et al., 2001 and references therein). Because every GDGT has two hydrocarbon chains, 9 combinations exist, ranging from 0 to 8 cyclopentanes present in the molecule (e.g. Schouten et al., 2008a). Additionally, a GDGT containing

a total of 4 cyclopentane rings and one cyclohexyl has been reported (Sinninghe Damsté et al., 2002b). This GDGT was named Crenarchaeol and it has one regioisomer that occurs in smaller amounts in the environment. While these **isoprenoidal GDGTs** are known to originate from Archaea, similar but smaller **branched GDGTs** first detected in peat bogs and later in soils and sediments have been ascribed to presumably anaerobic as yet unidentified soil bacteria (Schouten et al., 2000; Weijers et al., 2006a). Figure 1.3 shows the isoprenoidal and branched GDGT structures that have been used as biomarker proxies for paleoclimate studies.

Table 1.1 summarizes what has been published on the source organisms of these GDGTs. It is noteworthy that the acyclic GDGT I (caldarchaeol) is a widespread occurring GDGT in the domain Archaea and very abundant in methanogens (e.g. Koga et al., 1993). GDGTs II-IV are usually not as abundant as GDGT I, and although initially thought to be produced by thermophilic and non-methanogenic mesophiles, some studies have indicated that a few mesophilic methanogens can also synthesize them (Gattinger et al., 2002). Structure V (crenarchaeol) and its regioisomer V' were initially thought to be biomarkers of mesophilic aquatic Crenarchaeota (Sinninghe Damsté et al., 2002b), but were recently shown to be also synthesized by a thermophilic crenarchaeon (de la Torre et al., 2008); their occurrence in Euryarchaeota, and thus in methanogens, has not been reported. It is also important to indicate that all these structures, GDGTs I – V', have been reported to occur not only in aquatic environments but also in soils, and thus in the lacustrine sediments there is probably an admixture of autochthonous GDGTs I- V' derived from Archaea living in the lake water column plus identical allochthonous GDGTs transported from soils by runoff (e.g. Weijers et al., 2006b). Finally, the branched structures VI – XIV are ascribed to soil bacteria (Weijers et al., 2006a), but no representative of these organisms has been hitherto isolated for membrane lipid analysis.

As aforementioned, several paleoclimate proxies based on the environmental GDGT distribution have been developed. The next section gives an overview of the calibration of the GDGT-derived proxies.

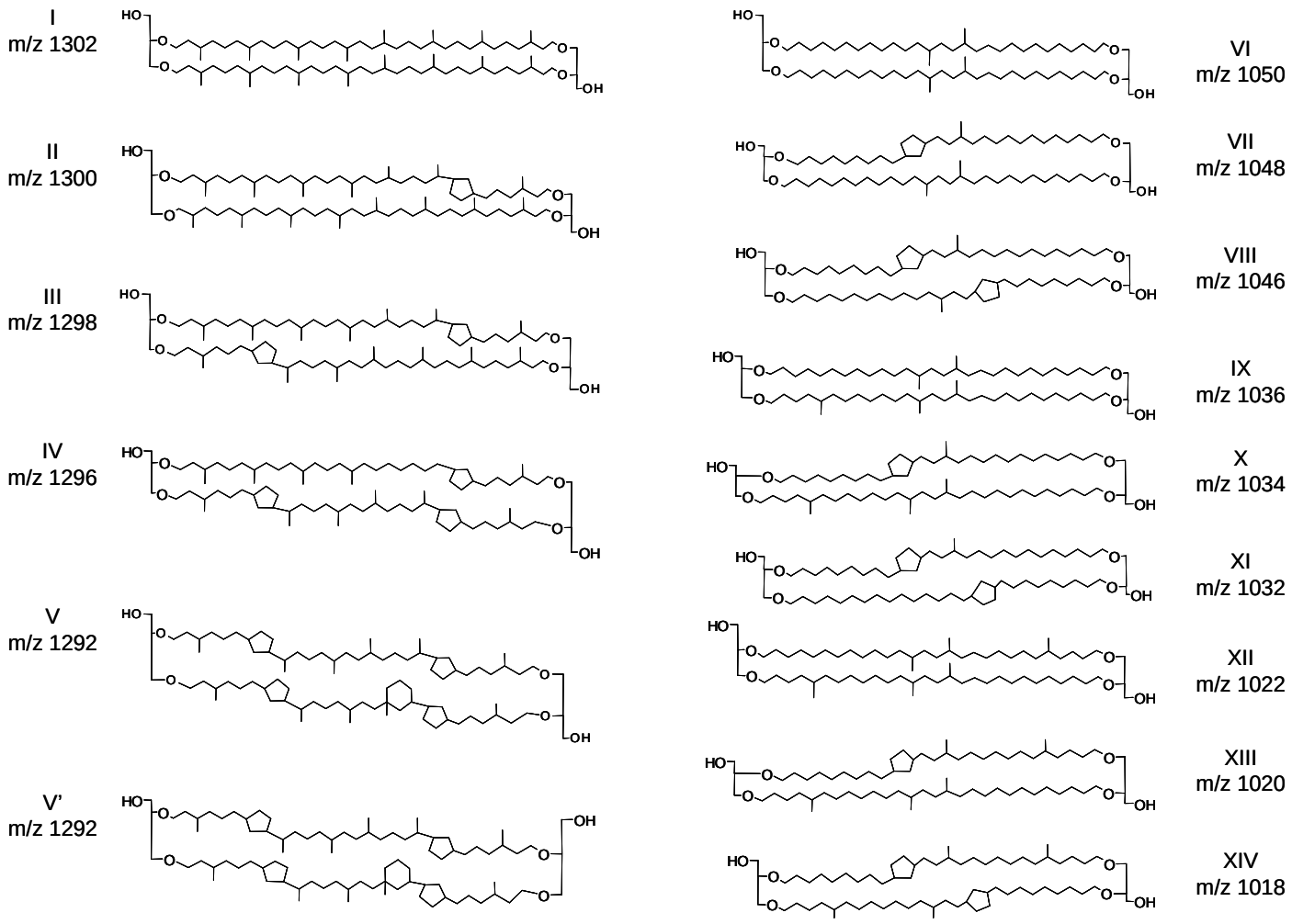

Figure 1.3 Structures of the glycerol dialkyl glycerol tetraethers (GDGTs) commonly used as biomarkers. Note that structure V' is a regioisomer of structure V. Structures I to V' are isoprenoidal GDGTs synthesized by several archaeal species. Conversely, structures VI to XIV are branched GDGTs synthesized by as yet unidentified soil bacteria. *m/z* refers to the mass/charge ratio of the protonated molecules (see Chapther 2 for analytical methodology).

Isoprenoidal GDGTs		
Structure	**Source organisms**	**References**
I (caldarchaeol) absence of rings	Euryarchaeota - mesophilic AOM - *mesophilic methanogens* - *thermophilic* Crenarchaeota - *mesophilic* - *thermophilic*	Tornabene and Langworthy (1979) Koga et al. (1993) De Long et al. (1998) Pancost et al. (2001) Aloisi et al. (2002) Bouloubassi et al. (2006) de la Torre et al. (2008) Schouten et al. (2008a)
II – IV 1-3 rings	Euryarchaeota - mesophilic AOM - *mesophilic methanogens* - *thermophilic* Crenarchaeota - *mesophilic* - *thermophilic*	De Long et al. (1998) Koga et al. (1998) Pancost et al. (2001) Uda et al., (2001) Aloisi et al. (2002) Gattinger et al. (2002) Bouloubassi et al. (2006) de la Torre et al. (2008) Schouten et al. (2008a)
V and V' (crenarchaeol and its regioisomer) 5 rings	Euryarchaeota - not found Crenarchaeota - *mesophilic* - *thermophilic*	Sinninghe Damsté et al. (2002b) Schouten et al. (2008a) de la Torre et al. (2008)

Branched GDGTs		
Structure	**Source organisms**	**References**
VI-XIV 0-2 rings	unidentified (presumably anaerobic) soil bacteria	Sinninghe Damsté et al. (2000) Weijers et al. (2006a)

Table 1.1 Identified source organisms of the GDGTs used as biomarkers in paleoclimate. Roman numbers of structures refer to Figure 1.3. AOM refers to organisms capable of anaerobic oxidation of methane. In italics, source organisms identified by extracting the lipids directly from cultured or isolated cells. The other source organisms are assumed based on the occurrence and distribution of GDGTs in specific environments, their ^{13}C values and/or RNA analyses at collection site.

1.4. Calibration of GDGT-based proxies

At present there are four proxies based on the relative abundances of GDGTs that are applied in paleoclimate studies to derive reconstructions of past sea and lake surface temperature (TEX_{86}), past air temperature (MBT/CBT), soil pH (CBT) and soil vs aquatic-derived concentrations of organic matter (BIT) (see Table 1.2).

The TetraEther indeX of 86 carbon atoms or **TEX_{86}** was first proposed as a paleotemperature proxy for reconstructing SST using a core-top calibration of 44 sediments from 15 oceanographic sites, mostly located near coastal areas (Schouten et al., 2002). This initial sample set was extended over 280 sediments in a follow-up study, which also tested depth-weighted temperatures to clarify the depth at which the temperature signal stored in sediments originated from. The best correlation was obtained using mean annual temperatures from the mixed layer (Kim et al., 2008) (see table 1.2). The paleothermometer TEX_{86} has been used to reconstruct temperatures from virtually all oceanic provinces and at very different time scales, from quasi-annual (Huguet et al., 2007b), decadal (e.g. Rueda et al., 2009) to centennial (e.g. Huguet et al., 2006) and multimillennial (e.g. Forster et al., 2007), going back as far as Cretaceous, approximately 120 Myr ago (e.g. Kuypers et al., 2002).

In 2004, Powers and collaborators published the first results of TEX_{86} on lake sediments. The four large lakes surveyed at that time (Michigan, Superior, Malawi and Issyk Kul) showed TEX_{86}-temperature values that fitted with the marine calibration, and the addition one year later of 5 more lakes to this set prompted the first lacustrine calibration, which was still not very different from the marine one (Powers et al., 2005). A subsequent study increased considerably the number of explored lakes to 48, but only 22 sites gave sufficient GDGT signal in their sediments to measure TEX_{86} (Powers, 2005). Of these 22 lakes, only 15 sites were included in the final calibration, arguing that the rest gave unreliable reconstructed temperatures (see Table 1.2). The authors also concluded that only large lakes are suitable for TEX_{86} application, since high amounts of terrestrially-derived GDGTs in lake sediments can bias the TEX_{86} (e.g. Weijers et al., 2006b), and this is more likely to happen in small-sized lakes (see discussion below for BIT index). Recently, Blaga and collaborators published an extensive study of 47

European lakes along a north-south transect and found that only 9 lakes were suitable for TEX_{86} application (Blaga et al., 2009). Lake surface temperature records have been reconstructed for the last glacial-interglacial cycle for lakes Malawi (Powers et al., 2005) and Tanganyika (Tierney et al., 2008) in subtropical Africa, and there is an ongoing study in African lake Challa (Sinninghe Damsté et al., 2006).

TEX_{86} was calibrated to reconstruct mean annual surface temperatures. However, some research has been undertaken to explore which season is reflected by the proxy, which should be connected to the maximum GDGT exported productivity. The first marine survey suggested good correlation of TEX_{86} with winter temperatures (Schouten et al., 2002) an this was supported by a later study in the North Sea where higher abundances of marine Crenarchaeota were observed in that season (Herfort et al., 2006a). On the other hand, the extended calibration of TEX_{86} indicated that mean annual temperatures were more likely represented in the sediment signal (Kim et al., 2008). This last hypothesis was further supported by a sediment trap study in the Arabian Sea (Wuchter et al., 2006) and a comparison of TEX_{86} and instrumental temperatures in a two centuries-spanning sediment record in the Skagerrak strait (Rueda et al., 2009).

In the lacustrine systems, initial work by Powers and collaborators suggested that the TEX_{86} reflected mean annual temperature rather than a seasonal signal (Powers et al., 2004). However, expanding the lake calibration set gave slightly better correlation of TEX_{86} with winter than with annual surface temperatures (Powers, 2005). Archaeal productivity patterns, which would be the first direct cause of abundance of GDGTs, has been repeatedly suggested to increase in autumn and early winter, at least in high altitude lakes, which would support this last observation. However, the timing of the growing season might be site-dependant, both in the marine and the continental regions, due to the high diversity of environments that exist. In any case, the working hypothesis at present is that mean annual temperatures are reconstructed when TEX_{86} is applied in lakes (e.g. Tierney et al., 2008).

Concerning the water depth at which the temperature signal is originated, i.e. from which depth do the scavenged GDGTs come, particulate organic matter surveys in the ocean (Wuchter et al., 2005) as well as the recent core-top calibration of TEX_{86} (Kim et

al., 2008) suggest that generally temperatures of the upper mixed layer (100-200 m) are integrated in the GDGT signal at the ocean floor. This has been connected to the efficient scavenging of GDGTs by particles produced in the dynamic food web of the surface (e.g. Wuchter et al., 2005). Yet it has been found that not all regions follow the same pattern and for instance in Santa Barbara basin colder than measured surface temperatures were reconstructed using the TEX_{86} in sediments (Huguet et al., 2007a). In lakes, it is assumed that the paleothermometer TEX_{86} is reconstructing surface temperatures, in agreement with some successful present-day LST reconstructions in several of the lake sediments explored (Powers, 2005). On the other hand, molecular studies suggest that active Archaea thrive throughout the water column and very strong temperature gradients can occur in lakes, which raises the question of whether all lakes integrate a LST signal in their sedimentary record. Furthermore, when GDGTs are analysed for reconstructing SST and LST in the lakes and the ocean, thermophilic input of GDGTs can be assumed negligible but care has to be taken with possible methanogenic-derived GDGTs I-IV, since the depth distribution of methanogens might be different from other Archaea and their temperature response is not known.

Aside from temperature, other variables such as salinity or nutrient abundance have been discussed as possible influences on TEX_{86} values. Incubation studies of North Sea water (Wuchter et al., 2004) suggest no influence of salinity (27-35‰), but in hypersaline environments a distinct lipid distribution with virtually no crenarchaeol (structure V) and high abundances of caldarchaeol (structure I) has been reported by Turich et al. (2007). The same study presented data from GDGT distribution on ocean suspended particulate matter and suggested nutrient-induced increase of TEX_{86} values in mesopelagic waters, although this is still under debate (Schouten et al., 2008b; Turich et al., 2008). Another noteworthy indication of Turich et al. is that Euryarchaeota in the water column could be contributing to the GDGT sedimentary pool, a hypothesis that has not been considered in most papers published so far, where Crenarchaeota are regarded as the sole source organisms of TEX_{86} related GDGTs in the water column. DNA analyses have shown however that Euryarchaeota can represent 1 to 73% of the total marine Archaea (Turich et al., 2008). Because the temperature response of these Euryarchaeota remains hitherto unknown (they were not detected in incubation studies), their impact on the GDGT distribution in the ocean and lakes is still concealed.

Proxy	Equation	Reconstructed parameter	Calibration	Parameter range	Observations / Environments applied in
TEX_{86}	$\frac{1298+1296+1292'}{1300+1298+1296+1292'}$	Sea surface temperature (SST)	$SST = (TEX_{86} - 0.28) / 0.015$ $N = 43 \quad R^2 = 0.92$	0 – 30 ºC Schouten et al. (2002)	Calibrated with World Ocean Atlas and World Ocean Database SST. Applied in ocean water column and sediments. Only core-top calibrations are included in this table.
			$SST = -10.78 + 56.2 \cdot TEX_{86}$ $N = 223 \quad R^2 = 0.94$	5 – 30 ºC Kim et al. (2008)	
		Lake surface temperature (LST)	$LST = (TEX_{86} - 0.25) / 0.017$ $N = 9 \quad R^2 = 0.96$	5 – 27 ºC Powers et al. (2005)	Applied in lake water column and sediments. 7 outliers are discarded in Powers (2005) calibration.
			$LST = (TEX_{86} - 0.21) / 0.019$ $N = 15 \quad R^2 = 0.94$	4 – 28 ºC Powers (2005)	
BIT	$\frac{1050+1036+1022}{1292+1050+1036+1022}$	Relative proportion of soil vs. aquatic-derived organic matter	*Qualitative proxy* End members: 0 → no soil organic matter input 1 → dominant soil organic matter	Hopmans et al. (2004)	Applied in open ocean, estuaries and lake water column and sediments, river particulate matter and soils.
MBT	$\frac{1022+1020+1018}{all\ branched}$	Air temperature (MAT)	$MAT = (MBT - 0.122 - 0.187 \cdot CBT) / 0.020$ $N = 135 \quad R^2 = 0.77$	-2.9 – 27 ºC Weijers et al. (2007b)	Calibrated with soil samples. Applied in soils and estuaries.
CBT	$-\log\left(\frac{1020+1034}{1022+1036}\right)$	Soil pH	$pH = (3.33 - CBT) / 0.38$ $N = 135 \quad R^2 = 0.70$	3.3 – 8.2 Weijers et al. (2007b)	

Table 1.2 Climate proxies based on relative abundances of glycerol dialkyl glycerol tetraethers (GDGTs). Numbers in the proxy equations refer to the m/z value of the protonated GDGTs (see Figure 1.3).

The second GDGT proxy is the Branched vs Isoprenoid Tetraether or **BIT** index (Hopmans et al., 2004), which quantifies the relative abundance of the soil-originated branched GDGTs versus the isoprenoidal predominantly aquatic-derived crenarchaeol (see table 1.2). BIT is used to assess the relative changes in fluvial or run off input of soil organic matter, which can be used to gain information on the past hydrological cycle. This index is also used to assess the reliability of TEX_{86} as this is compromised as a SST/LST proxy if the sediment sample contains significant amounts of soil-derived isoprenoidal GDGTs (Weijers et al., 2006b). However, there is no definitive BIT threshold beyond which TEX_{86} is not applicable, since the BIT value will depend not only on soil organic matter input, but also on soil GDGT abundance and distribution and crenarchaeol productivity in the water column. For instance, the BIT values of the lake sediments included in the final calibration in Powers (2005) range from 0.09, indicating virtually negligible soil organic matter input, to 0.72, which indicates predominant soil organic matter input, although all lakes seem to have a reliable TEX_{86}. The value of the BIT index as a climate proxy has also been demonstrated in several recent multiproxy studies focusing on the abundance and distribution of terrestrial organic matter in continental margins (Huguet et al., 2007b; Kim et al., 2006, 2007; Herfort et al., 2006b; van Dongen et al., 2008), and in tracing the reactivation of the European hydrological system at the onset of the last deglaciation (Ménot et al., 2006).

In 2007, two more GDGT proxies were presented: the Methylation index of Branched Tetraethers (**MBT**) and the Cyclisation index of Branched Tetraethers (**CBT**) (Weijers et al., 2007b). These two indices were built based on relative abundances of branched GDGTs found in worldwide surface soils (n = 134), and were found to correlate with soil pH (CBT) and mean annual surface air temperature or MAT (MBT/CBT) (see table 2.1). They were later appraised in a series of heated soils (12 - 41 ºC) close to hot springs in Yellowstone National Park (USA) and found to be also correlated to soil temperatures and pH (Peterse et al. 2009), further supporting the proxies performance in soils. While calibrated on soil samples, the MBT and CBT proxies have been applied in the pool of branched GDGTs accumulated in the sediments of coastal areas (e.g. Weijers et al., 2007a; Rueda et al., 2009; Bendle et al., in prep.) but their application has not yet been reported in lake sediments.

1.5. Objective and outline of this thesis

The recent discovery of the potential of archaeal and bacterial membrane lipids for climate and environmental reconstructions has prompted several lines of research focused on the development of climate proxies, the analytical methodology, the survey of new archives of application and the reconstruction of past temperatures and environmental processes. Given the novelty of the GDGT proxies there is plenty of scope to improve upon a range of issues regarding their measurement and application. The general objective of this thesis is therefore to further develop the analytical methodology to gain in analytical reliability and sample throughput, and expand the range of locations where GDGT proxies have been appraised, particularly in lake environments.

The specific goals concerning the analytical methodology (Chapter 2) are:

- To test the comparability of the standard method of GDGT cleanup in sediment samples (alumina fractionation) with a widely used cleanup technique in the biomarker field (alkaline hydrolysis) in terms of TEX_{86} and BIT values.
- In relation to this, to compare the effect on TEX_{86} and BIT of using several adsorbents and degree of activation for the fractionation of GDGTs during the sample cleanup.
- To evaluate the possibility of increasing sample throughput for the analysis of GDGTs employing High Performance Liquid Chromatography - Mass Spectrometry (HPLC-MS).
- To appraise a reduction of the solvent volume required in the analysis using HPLC-MS by changing the HPLC column and solvent flow.
- To assess the comparability of two mass spectrometers with an ion-trap design and a quadrupole design for the measurement of TEX_{86} and BIT indices.

Besides, the specific goals regarding the application of the GDGT proxies in natural archives are:

- To explore the main factors influencing the GDGT distribution in the surface sediments of a range of lakes from the Iberian Peninsula (Chapter 3).
- To investigate the performance of TEX_{86}, BIT and MBT/CBT proxies in the surface sediments of these Iberian lakes.
- To identify the most suitable candidates among the Iberian lakes surveyed for undertaking paleoclimate reconstructions using the GDGT proxies.
- To assess the validity of the TEX_{86}, BIT and MBT/CBT proxies in the Lake Baikal (Siberia) by studying GDGT fluxes in annual sediment traps and GDGT distributions in sediment traps and surface sediments from the North and the South basins (Chapter 4).
- To inspect further the climatic control on the GDGT proxies in Lake Baikal region by reconstructing a record of TEX_{86}, BIT and MBT/CBT for the last glacial-interglacial cycle in two cores from the North and South basins of the lake.
- To survey the impacted rocks of the Bosumtwi crater (Ghana, Africa), currently buried under 150-300 m of post-impact lake sediments, for the presence of GDGTs as biomarkers of extant or past archaeal communities (Chapter 5).

Chapter 2

Methodology

2.1. A review of GDGT analysis

2.1.1. Development of GDGT analysis

The membrane lipids from Archaea were isolated and characterized for the first time in the early 1960s (e.g. Kates et al., 1963). The methods concerned have evolved since then, but the basic procedure remains the same (e.g. Koga and Morii, 2006).

The first **extractions** of archaeal lipids were performed using the Bligh and Dyer method (Bligh and Dyer, 1959) directly on the isolated archaeal cells. In essence, this method includes a series of liquid-liquid extractions using different ratios of methanol, chloroform and water to isolate the archaeal membrane lipids (diethers and tetraethers) in the organic phase. A modified version of this method (e.g. Nishihara and Koga, 1987) is still used nowadays to extract cell material. For the extraction of environmental samples such as sediments and filtered water, the sample is first freeze-dried and the archaeal lipids are usually removed from the matrix using Soxhlet and ultrasonic bath-assisted extraction with organic solvents, typically dichloromethane and methanol (e.g. King et al., 1998; Schouten et al., 2000). More recently, new methods in which both temperature and pressure can be controlled have become standard for the GDGT extraction, namely using Accelerated Solvent Extraction (ASE) and Microwave Assisted Extraction (MAE) (e.g. Schouten et al., 2007b; Escala et al., 2007). In a recent paper comparing several methods for the extraction of the organic matter from sediment samples, Schouten and collaborators showed that ASE, Soxhlet and ultrasonic extraction were comparable there was no significant difference between Soxhlet, ultrasonic and Accelerated Solvent Extraction methods in terms of distribution of GDGTs (Schouten et al., 2007b).

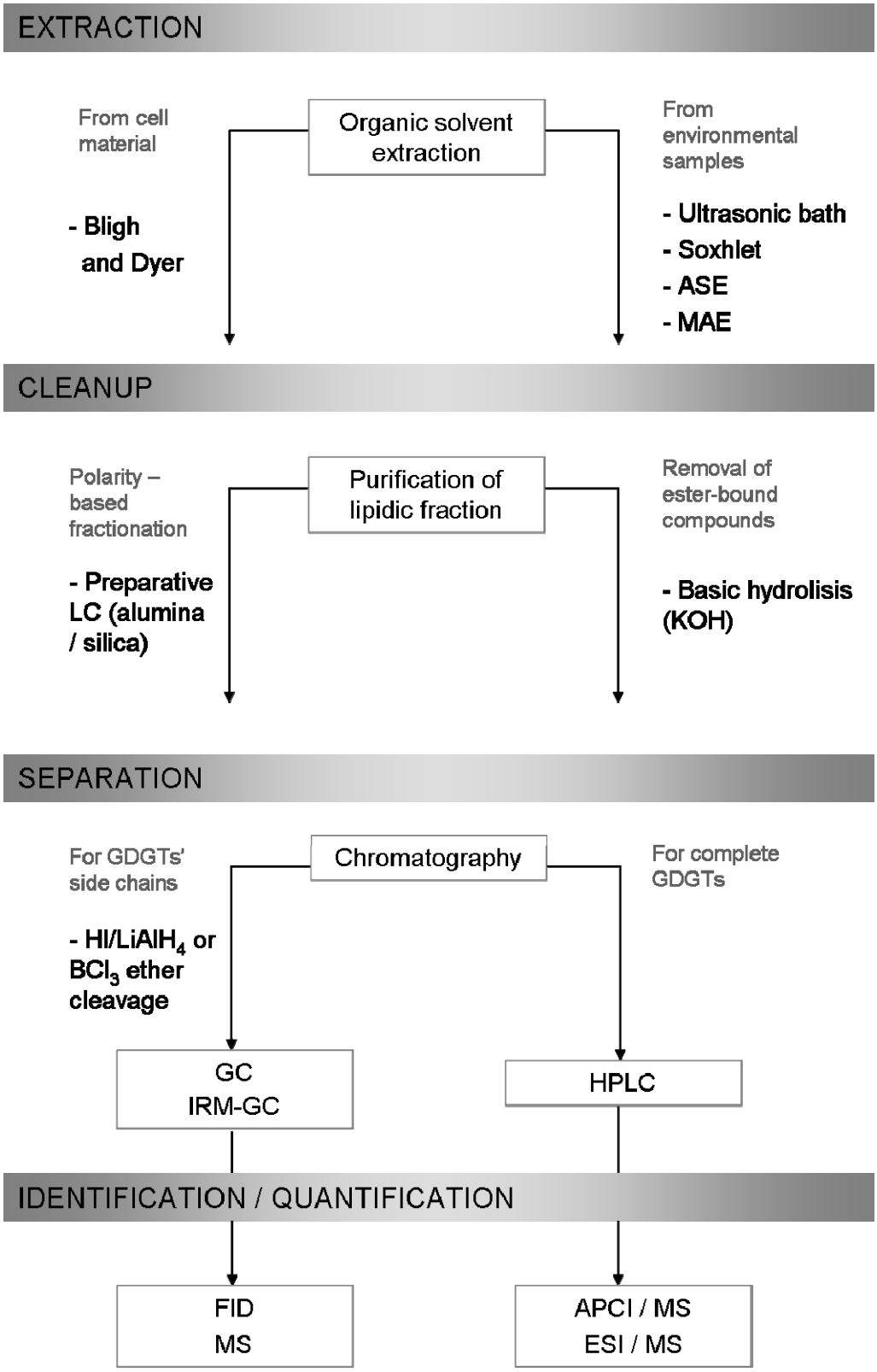

Figure 2.1 Schematic laboratory protocol for GDGT extraction and analysis. LC: liquid chromatography; GC: gas chromatography; IRM: isotope ratio monitoring; FID: flame ionisation detector; HPLC: high performance liquid chromatography APCI: atmospheric pressure chemical ionisation; ESI: electrospray; MS: mass spectrometry.

The **clean-up** of the samples, intended to purify the GDGT fraction, is traditionally achieved by means of liquid chromatography (LC) that separates the lipids according to their polarity. Thin-layer chromatography (e.g. Mancuso et al., 1986) has been replaced by preparative column chromatography using alumina (or silica), nowadays the most extensively used clean-up method for the GDGT analysis (e.g. Schouten et al., 2007b). In these polarity-based separations the GDGTs are collected in the polar fraction. Alternatively, hydrolysis (or saponification) with potassium hydroxide (KOH) has been reported in a few studies (e.g. Escala et al., 2007; Schouten et al., 2008a). This method hydrolyses the ester bonds and thus allows the removal of most of the labile fraction of the organic matter, while the ether-bonded GDGTs remain intact.

The final steps are the **separation**, **identification** and **quantification** of the GDGTs. Here two trends exist. The first one targets the biphytanes (the isoprenoidal side chains contained in the tetraether lipids), and therefore the ether linkage between the glycerol and the hydrocarbon chains is cleaved, either by hydroiodic acid (HI) degradation followed by lithium aluminium hydride ($LiAlH_4$) reduction or by trichloroborane (BCl_3) treatment (e.g. Koga and Morii, 2006). The released biphytanes are usually separated by gas chromatography and identified/quantified using a flame ionisation detector (GC-FID) or a mass spectrometer (GC-MS). The disadvantage of this technique is that the information of the whole GDGT structure is lost, so it does not allow the elucidation of the number of cyclopentane rings in each molecule, and thus it is not suitable for TEX_{86} measurements. However, it has been used to assess the diversity of biphytanes in water or sedimentary environments, and as a preparation step for stable isotopes measurements in these biphytanes (e.g. Hoefs et al., 1997; DeLong et al., 1998; Sinninghe Damsté et al., 2002a).

The second trend is the analysis of the complete GDGT structure, which is mandatory for the assessment of the GDGT-based proxies aforementioned. Given the high mass of GDGTs (1000-1300 Da) they are not amenable for gas chromatographic separation. Back in 1986, Mancuso et al. proposed using high performance lipid chromatography (HPLC) coupled to a refractive index detector, and applied the method to extracts from several archaeal species. The separation of different diether and tetraether lipids was indeed achieved, confirming that HPLC was a simple and fast technique for separation

of these compounds. But the detection was more problematic, since the refractive index did not provide unambiguous identification of the analytes. In 2000, Hopmans et al. reported the analysis of tetraether lipids by **normal phase** HPLC coupled to atmospheric pressure chemical ionisation/mass spectrometry (APCI-MS). As can be seen in Figure 2.2, this method allows chromatographic separation of GDGTs plus determination of their exact composition according to their *m/z* values (mass-to-charge ratio of the ionised molecules). These results enabled the identification of the complete core tetraether lipids, and paved the way for the development of the proxy TEX_{86}. At present, **HPLC/APCI-MS** is widely used in the studies that measure TEX_{86} and the other GDGT-based proxies.

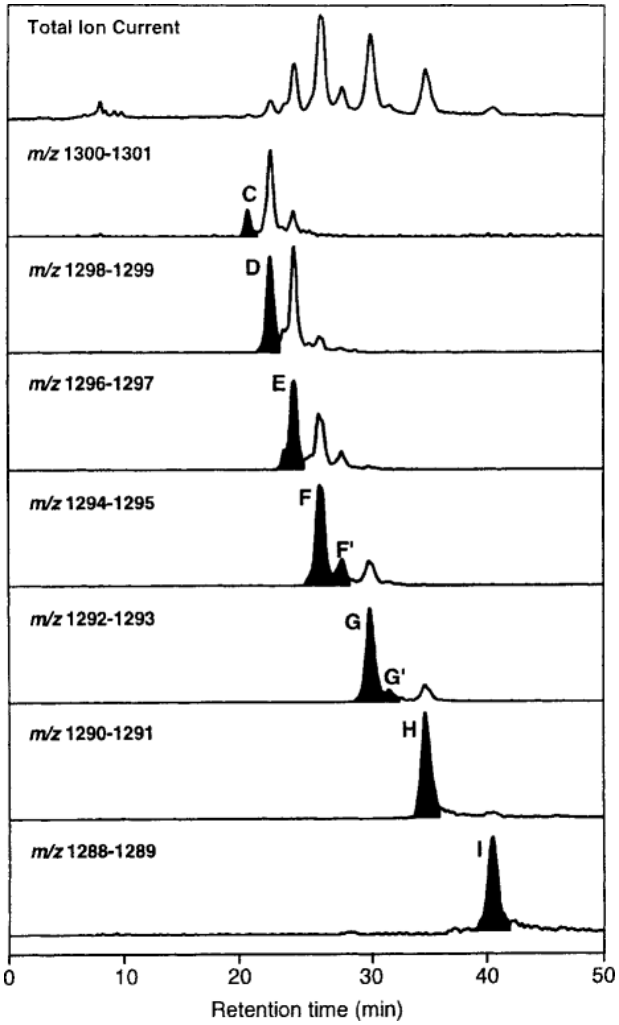

Figure 2.2 Total ion current (upper panel) and individual mass chromatograms of the GDGTs isolated from *Sulfolobus solfataricus* (Hopmans et al., 2000).

Figure 2.3 shows a schematic of the components of an HPLC/APCI-MS system. **HPLC** functions by partitioning of the analytes of interest into two phases: a stationary phase, located inside the HPLC column, and a mobile phase (a mixture of organic and/or inorganic solvents) that elutes through the stationary phase. Different affinity of the analytes for these phases will determine their retention time in the stationary phase, the final objective being a sequential elution of the analytes. The mobile phase traditionally used to separate GDGTs is a mixture of hexane (apolar) and a small proportion of the polar solvent propanol, while the stationary phase is usually cyanopropilsilane (CN) or aminopropylsilane (NH_2) (e.g. Hopmans et al., 2000; Schouten et al., 2007b).

Mass spectrometry (**MS**) is a powerful technique to elucidate the structure and molecular weight of compounds, and quantify the abundance of an analyte. There are several mass spectrometer designs, among which the quadrupole and the ion-trap are widely used systems. The quadrupole analyzer is the most commonly employed for GDGT analyses (e.g. Hopmans et al., 2000). This system is made of four parallel, stainless steel rods in which opposite pairs are electrically connected. The analyte ions are introduced into this quadrupole and the electric potentials applied alternately to the two pairs of rods create a fluctuating electric field that affect the path of the ions. All ions (if operating in full scan mode) or alternatively single pre-selected masses (if operating in single ion monitoring mode) will have stable trajectories inside the diameter of the quadrupole and thus will reach the detector, while all other ions will be deflected out of the quadrupole. Initial GDGT measurements in quadrupole MS were conducted by full scan technique; however, a recent paper considered the advantages of single ion monitoring (SIM) mode, where individual masses corresponding to the ionised GDGTs are monitored ($[M+H]^+$), therefore increasing the sensitivity (Schouten et al., 2007b).

Conversely, in the ion trap, the analyte ions transferred into the MS are stored in a space between a circular ring electrode in the *x* axis and two end-cap electrodes in the *y* axis (the ion trap) and their trajectories are stable as long as a certain radio frequency potential is applied to the circular electrode. Changing the radio frequency signal will make the ions trajectories unstable according to their *m/z* ratio, and they will be ejected from the trap and will strike the detector. This system enables the detection of ions in a

selected *m/z* range, since ions are progressively ejected from the trap according to their *m/z* (Poole, 2003). The *m/z* of the ionised branched GDGTs extend from 1018 to 1050, while the isoprenoidal GDGTs range from 1292 - 1302 (see structures in Figure 1.3).

A critical component in the HPLC/MS system is the interface connecting both instruments. At present the **APCI** interface is the most widely used for this purpose. Its task is to vaporize and ionise the liquid sample eluting from the HPLC and introduce the sample in the MS, which is at vacuum. The eluent from the HPLC (i.e. solvent plus analytes) enters the APCI interface where it is converted into a spray of fine droplets by a heated pneumatic nebuliser. The droplets are transported by a gas flow through a desolvation chamber and to the ion formation region where a corona discharge ionises the solvent molecules at atmospheric pressure. A series of collisions and charge exchanges between solvent and gas molecules results in the formation of a reagent gas plasma, which initiates the chemical ion-molecule reactions with the analyte. The result is the ionisation of the analyte (M) that in the case of GDGTs occurs by protonation of the molecules in the form of $[M+H^+]$. Following ionisation, a voltage applied to a capillary leads the ions into the mass spectrometer while other non-ionised molecules are removed by a flux of dry heated nitrogen (N_2) gas (Poole, 2003).

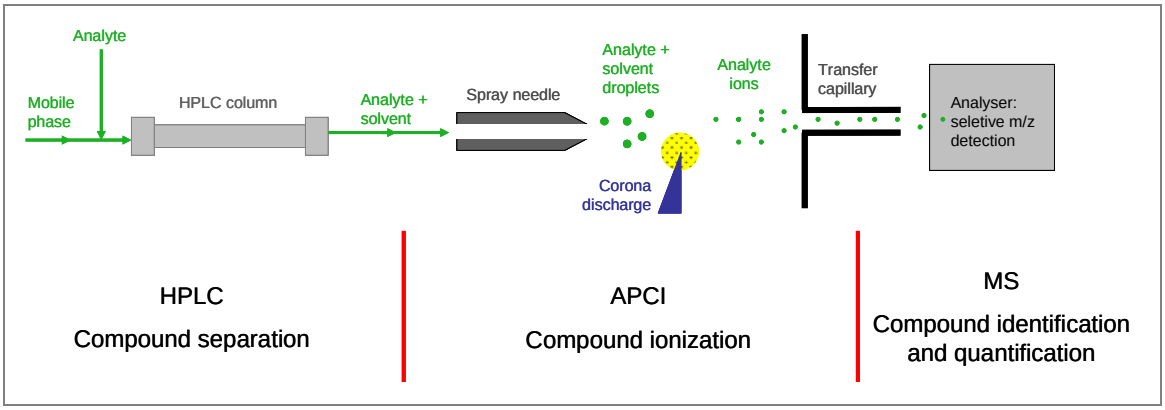

Figure 2.3 Scheme of the components of the HPLC/APCI-MS system.

The analytical reproducibility (one standard deviation of replicate analyses) of the published TEX_{86} index has increased from the first reported value of 0.022, equivalent to 2.0 ºC (Schouten et al., 2002), to recent values of 0.004 which translates in a temperature of 0.3 ºC (Schouten et al., 2007b).

2.1.2. The future: intact polar lipids analysis

The subsurface of several sedimentary marine environments has been proven to contain a relatively large number of active prokaryotic cells, especially from Archaea, at least down to 800 m below the sea floor, in sediments tens of millions of years old (e.g. Parkes et al., 1994). These Archaea are producing membrane lipids, among which GDGT-based structures, although presumably at very low rates, since these low-energy environments can not support fast metabolisms (D'Hondt et al., 2002). Nevertheless, this is a critical issue, since proxy-based reconstructions using GDGTs found in sediments might be derived from an admixture of lipids originally synthesized in the water column, and lipids from subsurface-dwelling Archaea. Thus, the surface water temperature reconstruction might be compromised if the later fraction is important. It is therefore becoming apparent the need to distinguish these two sources of GDGTs in paleoclimate studies (e.g. Pitcher et al., 2009).

There is some evidence that the polar head groups of intact bacterial lipids rapidly detach (sometimes within days or weeks) after the bacterial cell decay (e.g. White et al., 1979; Harvey et al., 1986), and the pattern is assumed to be the same for Archaea (e.g. Sturt et al., 2004). Therefore, analytically distinguishing archaeal lipids that keep their polar head group, i.e. **intact polar lipids** (**IPL**), from those that do not (core lipids) appears as a logical solution to discriminate between contributions of extant and dead Archaea. The sediments usually contain a complex mixture of IPLs but recent advances in separation and identification including HPLC/MS techniques are paving the way for such studies.

Guckert et al. (1985) already proposed silica-based fractionations to separate bacterial IPLs but detection was still dependant on headgroup cleavage and subsequent GC analysis. By the end of the 1990s, intact polar lipids could be analysed by HPLC/MS (e.g. Fang and Barcelona, 1998). Sturt et al. (2004) showed that the separation and identification of intact polar ether lipids was feasible by means of normal phase HPLC/MS using electrospray ionisation (HPLC/ESI-MS). Eventually, Pitcher et al. (2009) achieved the effective separation of intact polar GDGTs and core GDGTs via fractionation on silica gel and subsequent analysis by HPLC/ESI-MS. Although the

precision of the silica gel fractionation is hindered by the matrix from which the lipids are extracted, the efforts to separate IPL from core lipids guarantee more precise paleoclimate studies in the future.

Beyond their value to distinguish extant and dead Archaeal production, intact polar lipids are attractive analytical targets because they are taxonomically more specific than their apolar derivatives (e.g. Sturt et al., 2004; Rossel et al., 2008). Besides, IPL concentrations can be used to detect and quantify total viable biomass in subsurface sediments both marine (e.g. Biddle et al., 2006; Lipp et al., 2008) and lacustrine (e.g. Zink et al., 2008), although the different polar headgroups confer differential ionisation efficiencies to the molecules and thus still hamper the quantification by mass spectrometry (e.g. Zink et al., 2008).

2.2. GDGT analysis in the present thesis

2.2.1. Material and chemicals

The following paragraphs give an overall description of the material cleaning, solvents and standards used.

2.2.1.1. Laboratory material cleaning

Prior to use, reusable glassware was successively soaked in HNO_3 1% for 24 hours and in a *BioSel* (phosphate-free alkaline detergent) solution 2% for 24 hours. After rinsing with distilled water, the volumetric glassware was rinsed with acetone and wrapped in aluminum fold. The non-volumetric glassware was dried in an oven, wrapped in aluminum foil and fired at 450 ºC for 12 hours.

Disposable glassware was fired at 450ºC for 6-12 hours before use.

2.2.1.2. Solvents

The solvents used for rinsing material were of analytical grade (Carlo Erba), and included acetone, methylene chloride and methanol. All solvents used for the analysis of the samples (dichloromethane, methanol, hexane, acetone) were of GC grade (Suprasolv®, Merck). HPLC mobile phase solvents were of HPLC grade (Lichrosolv®, Merck) and included hexane and *n*-propanol.

2.2.1.3. Standards

A standard solution of GDGT-I (provided by Dr Hiroyuki Morii, University of Occupational and Environmental Health, Kitakyushu, Japan) and a standard solution of GR (provided by Dr Thierry Benvegnu, Ecole Nationale Supérieure de Chimie de Rennes, France) were used for HPLC/MS tuning. GDGT-I (caldarchaeol) is an acyclic tetraether widespread in archaeal membranes, with a *m/z* ratio of 1302 (see Figure 1.3 and Table 1.1). Compound GR is a synthetic tetraether with one cyclopentane ring (e.g. Réthoré et al., 2007), presumably not occurring in the environment and with a *m/z* ratio of 1208.

Several grams of sediment from lake Banyoles (Catalunya, Spain) were freeze-dried and homogenised. This sample was used as standard sediment and extracted in each batch of samples to check the analytical stability of the TEX_{86} index.

Extracts from lake Banyoles sediment and North Sea sediments were used for assessing the instrumental (HPLC/MS) precision of TEX_{86} measurements in each period of analysis and long-term reproducibility, i.e. between periods of analysis.

2.2.2. Analytical instrumentation

2.2.2.1. HPLC/APCI-MS systems

The GDGTs were separated and quantified by means of HPLC/APCI-MS. Samples reported in this thesis were analysed using two systems, an ion trap and a quadrupole, and a study of their comparability can be found in Section 2.4. The systems were the following:

a. Agilent 1100 HPLC coupled to a Bruker ion trap Esquire 3000 MS (Chemical Analytical Service, Science Faculty, Autonomous University of Barcelona). Sample extracts were eluted using a cyanopropilsilane (CN) column at 30ºC in a gradient flow using a mixture of hexane/*n*-propanol.

b. Dionex P680 HPLC system coupled to a Thermo Finnigan TSQ Quantum Discovery Max quadrupole mass spectrometer (Proteomics Laboratory CSIC-Autonomous University of Barcelona). Sample extracts were eluted using a CN column in a gradient flow with a mixture of hexane/*n*-propanol.

2.2.2.2. GDGT identification

Positive ion spectra were generated for GDGT detection. The relevant GDGTs for quantification of TEX_{86}, BIT and MBT/CBT were monitored at the *m/z* of their $[M+H]^+$ at masses 1302, 1300, 1298, 1296, 1292, 1050, 1048, 1046, 1036, 1034, 1032, 1022, 1020 and 1018.

The GDGTs were identified by the mass spectra of the eluting compounds combined with their HPLC retention times. Further confirmation of the identity of the first eluting compound, GDGT-I, was accomplished by fragmentation (MS^2) of the ionised molecule in the ion trap. The major fragments yielded by the fragmentation process (intensity over 20% of that of the intact GDGT-I signal) are listed in table 2.1. Similar fragmentation patterns are reported in Hopmans et al. (2000).

Fragment (*m/z*)	Intensity (% of the I_{max})	Structure information
1284	89	loss of a water molecule
743	49	loss of a side chain
651	38	loss of a side chain and a glycerol
725	30	loss of a side chain and one oxygen atom
1228	28	loss of a glycerol
707	23	loss of a side chain and two oxygen atoms

Table 2.1. Major fragments yielded in the fragmentation process (MS^2) of ionised GDGT-I.

Due to the presence of stable isotopes, chiefly of carbon, in the molecules of the GDGTs, each lipid gives a signal in more than one *m/z*. Principally four isotopic ions could be distinguished in the mass spectra that characterized each GDGT peak (see Figure 2.4). The observed isotopic distribution closely followed the theoretical distribution calculated by means of the software I*sotope Calculator*. The protonated molecule $[M+H]^+$ was always the most abundant ion formed, followed by the ions at $[M+H]^+$+1 and $[M+H]^+$+2. Given that the masses of some of the GDGTs are only 2 mass units apart (e.g. 1296 and 1298), the ion at $[M+H]^+$+2 will be isobaric, with the resolution of our instrument (~3000), with that of the $[M+H]^+$ from a GDGT that is two mass units heavier. This hampered the accurate integration of the $[M+H]^+$ of some GDGTs if they were not sufficiently chromatographically resolved from the $[M+H]^+$+2 ion of another GDGT. Therefore, the chromatographic conditions were developed seeking sufficient chromatographic resolution of isobaric ions to ensure reliable peak area integrations (see Figure 2.5).

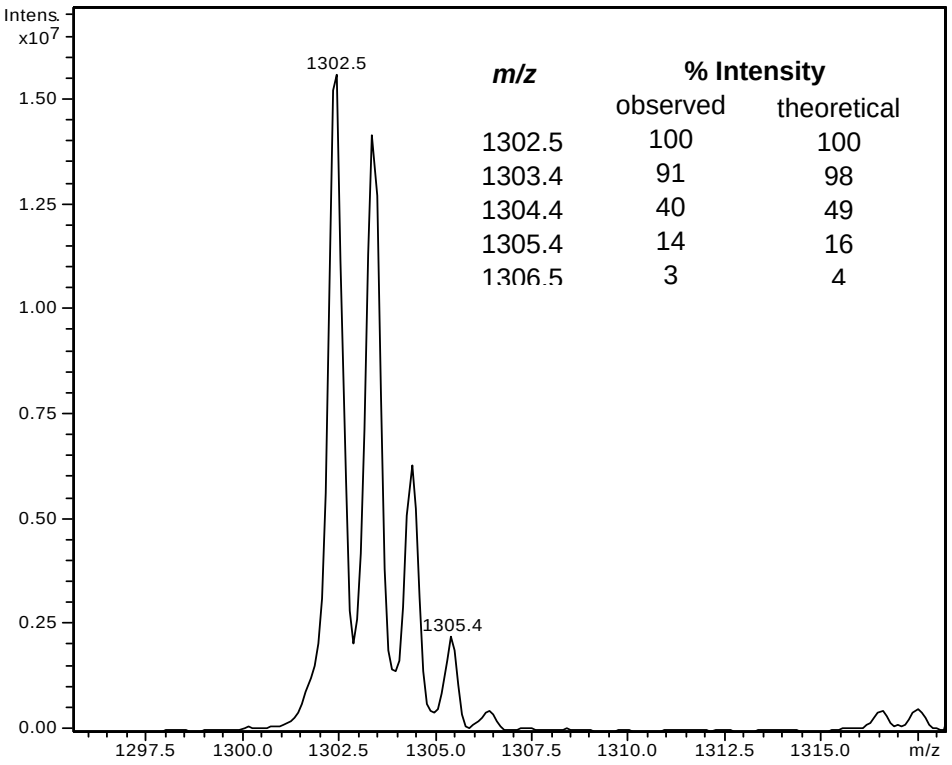

Fig. 2.4. Mass spectrum of GDGT-I with theoretical (*Isotope Calculator* software) and observed isotopic distribution. Note that the decimal part of the m/z ratio can slightly vary, due to mass spectrometer precision.

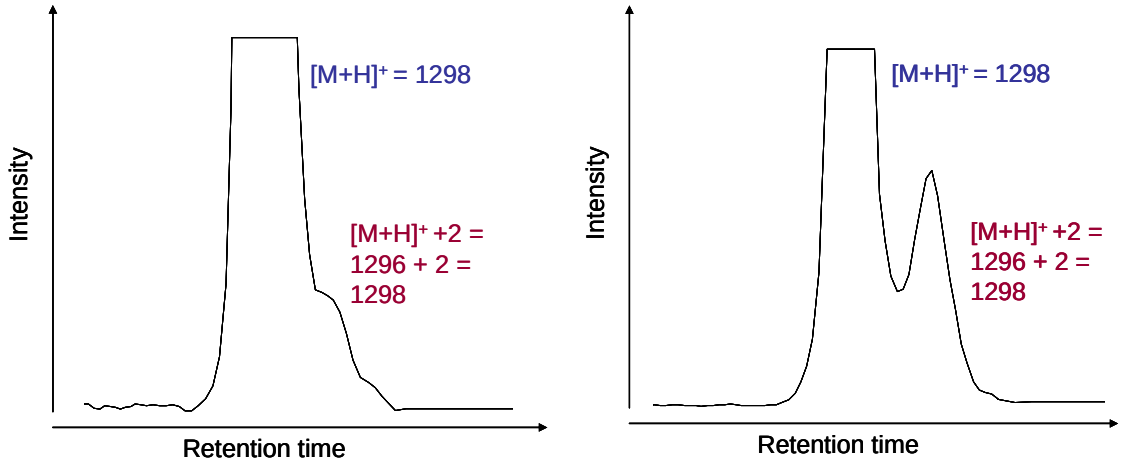

Figure 2.5 Example of isobaric ions overlapping in a developing chromatography (left) and final chromatographic method (right).

2.2.2.3. Linear range

The sensitivity of the mass spectrometers was optimized by monitoring the area in the chromatogram of the protonated GDGT-I (*m/z* 1302) and GR (*m/z* 1208) from the standard solution. Quantification of the abundances of GDGTs requires the determination of the range of the instrument over which the relationship between concentration of the analyte and detector response is linear. The linear range was calculated by injecting successive dilutions of the standard solution and monitoring the area of the peak in the chromatograms. Results show that for the Agilent HPLC – Bruker ion-trap MS, the response factor for GDGT-I is linear in the range 0.01 to 31.2 ng of injected analyte, i.e. 3 orders of magnitude (Figure 2.6a). For the Dionex HPLC – Thermo Finnigan quadrupole MS, the linear range could only be tested between 0.01 and 20 ng injected, which also represents 3 orders of magnitude (see Figure 2.6b). Because the rest of isoprenoidal GDGTs have a structure very similar to GDGT-I, they are in principally assumed to behave in the same pattern, i.e. to have the same response factor and linear range. However, for branched GDGTs, the response could differ from the one for GDGT-I, due to larger mass and structural differences. This is further explored in Section 2.4.

Another tetraether was available by June 2008, i.e. the synthetic compound GR. A series of dilutions of GR were tested in the Dionex HPLC – Thermo Finnigan quadrupole MS. A basic conclusion can be drawn from comparison of its response and that of GDGT-I (see Figure 2.6c), namely that GDGT-I triggers a more intense response in the quadrupole MS compared to GR. The linear range of GR in the quadrupole MS spans from 0.1 to at least 135.8 ng, i.e. 4 orders of magnitude, which is longer linear range than that established for GDGT-I in the ion-trap MS. These results, combined with the fact that GR is not occurring in the environment, show that GR can be a good internal standard for future quantification studies of GDGTs.

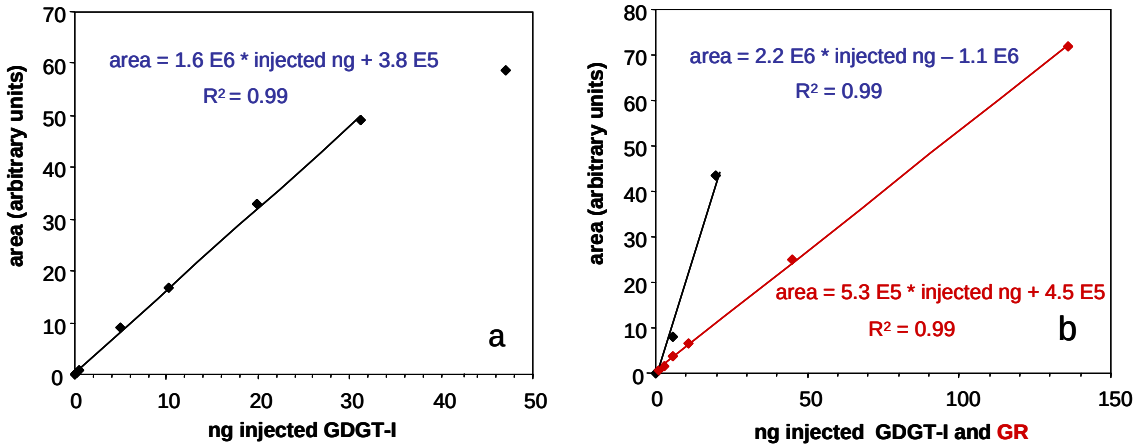

Figure 2.6 Response factor for the APCI/MS systems used in this study: a) Agilent HPLC – Bruker ion-trap MS response to GDGT-I. Note that the linear range is restricted to 0.01- 31.2 injected ng; b) Dionex HPLC – Thermo Finnigan quadrupole MS response to GDGT-I (black dots, the linear range extends from 0.01 to at least 20 injected ng) and to compound GR (red dots; the linear range spans 0.1 to 135.8 injected ng).

2.2.2.4. Limit of detection

The limit of detection (LOD), as the IUPAC* defined it in 1975, is "a number, expressed in units of concentration that describes the lowest concentration level of the element that an analyst can determine to be statistically different from an analytical blank". Although several methods are currently applied, the following equation is frequently used for the appraisal of LOD:

$$Y_B + k * S_B$$

where Y_B is the signal of a blank sample, S_B is the standard deviation of the blank signal and k is a numerical factor chosen in accordance with the confidence level desired, usually $k = 3$.

Blank samples containing only hexane:*n*-propanol (99:1) were injected over several days, intercalated between routine measurements, to obtain Y_B and S_B. As the level of noise may be different depending on the mass range recorded by de MS, these values were calculated for each *m/z* monitored, and represent the area of a baseline (noise) at the exact retention time of the GDGT of interest.

* IUPAC: International Union of Pure and Applied Chemistry.

The values obtained with the two HPLC/MS systems used are shown in Table 2.2. Results are reported as the injected amount of GDGT that would result in the area measured on the blank sample chromatogram, calculated by means of the calibration curve of area *vs* amount injected for GDGT-I. Note that there is a difference of one order of magnitude between both systems, i.e. LOD is ca. 70 pg for the Agilent HPLC – Bruker ion-trap MS, but ca. 7 pg for the Dionex HPLC – Thermo Finnigan system.

These results imply that, for the Agilent HPLC – Bruker ion-trap MS, the new linear range for each GDGT will have a higher threshold than suggested by the calibration curve, i.e. higher than 0.01 injected ng. Consequently, the linear range is finally set between 0.07 and 31.2 injected ngs for this system. Regarding the Dionex HPLC – Thermo Finnigan quadrupole MS, the linear range is kept between 0.1 to 135.8 injected ngs. Quantitative results from samples yielding concentrations outside the linear range were discarded.

LOD (injected ng)	**m/z of GDGT**								
	1302	**1300**	**1298**	**1296**	**1292**	**1292 Reg**	**1050**	**1036**	**1022**
Agilent HPLC -Bruker ion-trap MS	0.077	0.075	0.075	0.077	0.075	0.075	0.070	0.070	0.070
Dionex HPLC – Thermo Finnigan MS	0.010	0.007	0.007	0.007	0.009	0.007	0.007	0.007	0.007

Table 2.2. Limits of detection (LOD) for the GDGTs related to TEX_{86} and BIT monitored in the Agilent HPLC -Bruker ion-trap MS and Dionex HPLC – Thermo Finnigan MS systems. Values were calculated by means of the analysis of 9 and 15 blank samples, respectively.

2.2.2.5. Precision and reproducibility

The precision of the analytical instruments was assessed with TEX_{86} values from triplicate injections of the standard sediment in each period of analysis, and comparison of the averages of these triplicates over up to two years were used to calculate the reproducibility of the analysis.

GDGT measurements in sediment samples were undertaken with the Agilent HPLC – Bruker ion-trap MS system between April 2006 and May 2008, and precision was assessed with triplicate injections of Banyoles standard sediment. Precision ranged between 0.004 and 0.023 TEX_{86} units (1σ), which is equivalent to 0.2 and 1.2 ºC (using a marine calibration, see Table 1.2). The confidence intervals at 95% confidence were ± 0.009 (± 0.6 ºC) and ± 0.056 (± 3.7ºC). As can be seen in Figure 2.7a, the largest deviations in a single triplicate injection were obtained in April 2006 and in December 2007. In April 2006 the first analyses were undertaken and the low precision can be attributed to the limited experience and instrumental instability due to on-going method development. In the later period, December 2007, a technical problem was detected after performing the analyses, namely that the cone of the nebuliser in the APCI interface was not correctly aligned with the ion source at the entrance of the spectrometer, and thus a variable proportion of the ionised molecules was not efficiently transferred into the detector, resulting in high instability of the recorded intensity and low precision. Long-term reproducibility spanning two years of instrumental use shows fairly stable TEX_{86} values from April 2006 to December 2007, but the last triplicate, in May 2008 shows the largest deviation from the average value. This could be related to the fact that a new extract of Lake Banyoles sediment was prepared in May 2008 and that, according to changes in the preparation protocol for samples, this extract was clean-up by alumina fractionation instead of basic hydrolysis, although these two clean-up methods are in general comparable (see Section 2.4).

GDGTs were measured with the Dionex HPLC – Thermo Finnigan quadrupole MS system between January 2008 and November 2008, and precision was assessed with triplicate injections of North Sea standard sediment. Standard deviation (1σ) ranged between 0.001 and 0.015 TEX_{86} units, which are equivalent to 0.1 and 0.8 ºC using marine calibration. The confidence intervals at 95% confidence were therefore ± 0.002 (± 0.2 ºC) and ± 0.038 (± 2.5ºC). The precision is thus slightly better than the one obtained with the ion-trap system. The long-term reproducibility shows fairly stable values from January to March 2008 and a higher value in November 2008 (see Figure 2.7b). This shift is likely related to a change in the tuning parameters of the mass spectrometer, including internal temperatures and voltage and a new automatic mass

calibration. These results highlight the sensitivity of GDGT detection to tuning parameters, an issue further discussed in section 2.4.

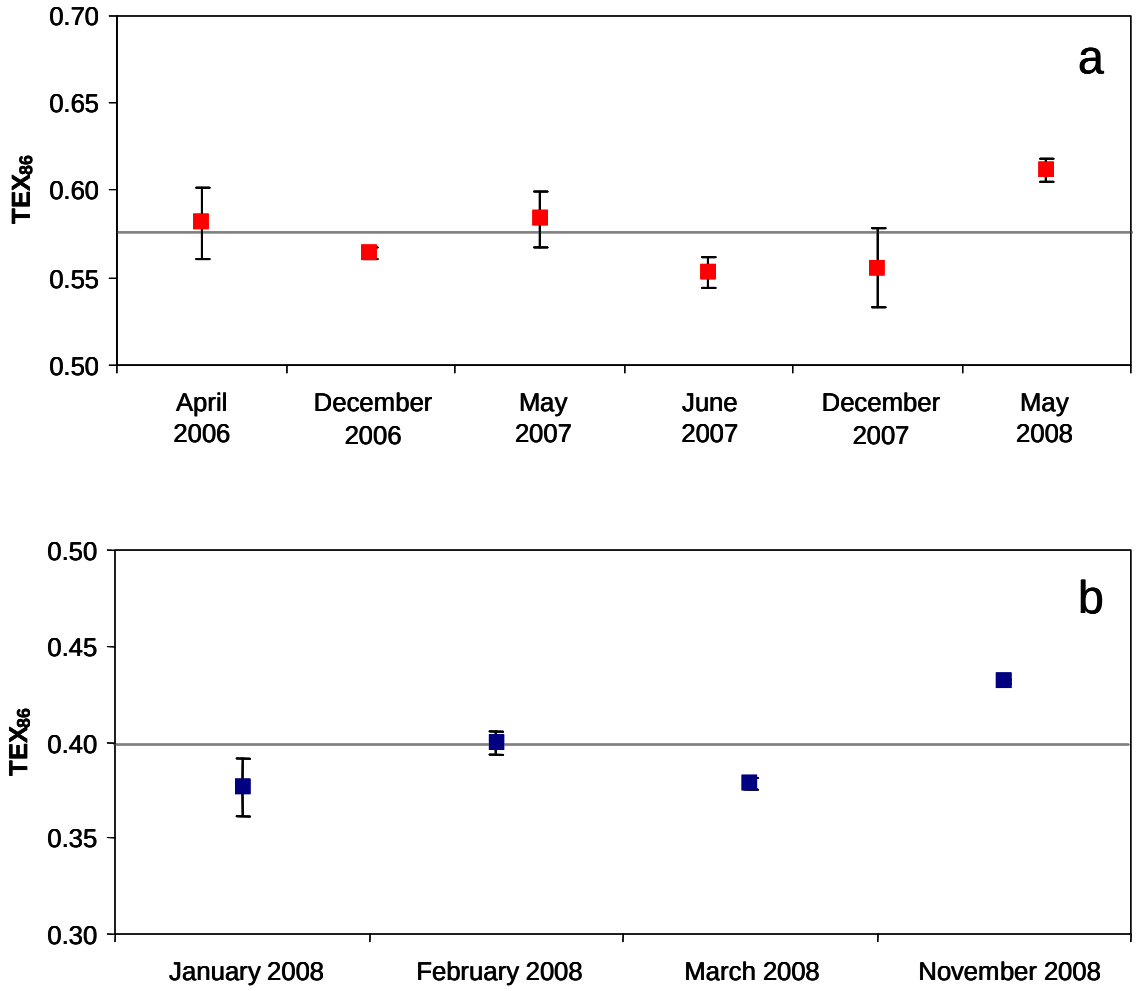

Figure 2.7 Long-term reproducibility of TEX_{86} analyses for the two HPLC/APCI-MS systems, **a)** Agilent HPLC coupled to Bruker ion-trap MS, used for analysis between April 2006 to May 2008, using standard sediment from lake Banyoles; **b)** Dionex HPLC coupled to Thermo Finnigan quadrupole MS, used for analyses between January and November 2008, with standard sediment from North Sea. Error bars indicate ± 1σ from a triplicate injection. The horizontal grey line indicates the average TEX_{86} value: 0.58 in panel a) and 0.40 in panel b).

2.2.3. Laboratory intercomparison

An anonymous interlaboratory comparison was undertaken in 2007-2008 with fifteen participating laboratories, which provided TEX_{86} and BIT measurements of two sample extracts prepared at the Royal Netherlands Institute for Sea Research (NIOZ, Netherlands). The resultant publication (Schouten et al., 2009) can be found complete in Appendix 3 and the basic conclusions are briefly described in this section.

The exercise was strictly concerned with the comparison of the HPLC/APCI-MS procedures used in different laboratories, which included MS using ion-traps, quadrupoles and one time-of-flight (TOF) system. Intralaboratory variation of TEX_{86} index measured for two sediments, S1 and S2, averaged 0.028 and 0.017 (± 1.1-1.9 ºC) respectively, after removal of statistically-identified outliers. Inter-laboratory reproducibility was higher, i.e. 0.050 for S1 and 0.067 for S2 (± 3.3-4.5 ºC). This analytical instrumental precision was compared to values obtained in interlaboratory comparison exercises undertaken for other more established temperature proxies, namely U^{K}_{37}', and Mg/Ca, and found to be higher (in terms of reconstructed temperature) than the precision associated to the complete sample process and analysis for these other proxies.

Regarding the BIT index, intralaboratory variation averaged 0.029 and 0.004 for S1 and S2, while interlaboratory reproducibility was 0.028 for S2 and reached 0.410 for S1, a number that indicates a large dispersion of results between laboratories. Systematic differences were suggested for TEX_{86} analyses and especially for BIT index (see Figure 2.8). The differences in BIT index were especulatively attributed to mass calibration and tuning differences between laboratories, although it could not be related to a specific instrumental setting considered in the study. In relation to the potential of TEX_{86} for temperature reconstructions, the relatively good intralaboratory precision values underscored the likely good assessment of relative changes in temperature by single laboratories. However, consistent with larger interlaboratory variation, caution was summoned when interpreting absolute temperature values.

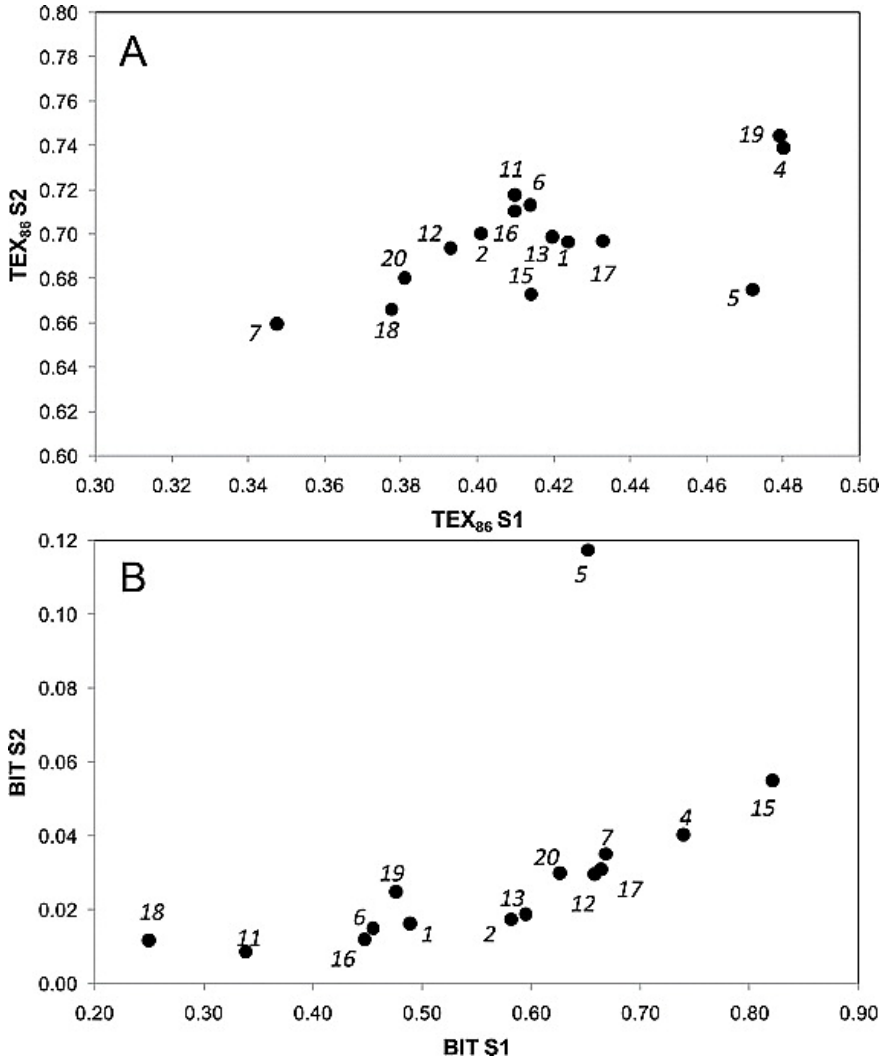

Figure 2.8 Cross-plots of a) TEX_{86} and b) BIT indices, for the two extract samples S1 and S2 compared in the interlaboratory study. Numbers represent the fifteen laboratories that reported results. Source: Schouten et al. (2009).

2.3. Rapid screening of glycerol dialkyl glycerol tetraethers in continental Eurasia samples using HPLC/APCI-ion trap mass spectrometry

This section contains a reduced version of a published manuscript (Escala et al., 2007) which can be found complete in the Appendix 3. Methodological protocols are described in detail in Appendix 1.

Here an optimized method which allows a rapid screening of GDGTs in different samples extracts is described. The method performance is appraised through the analysis of lacustrine sediments and water particulate matter from lakes located at different latitudes.

2.3.1. Experimental section

Late Holocene sediment samples from Iberian Peninsula lakes were provided by Dr B.Valero-Garcés (IPE-CSIC, Zaragoza, Spain). Core top sediments, water column particulate material obtained from sediment traps (one year integrated signal) and discrete near-surface water samples (2 liters filtered through 0.7 μm glass microfiber filters) from the north and south basins of Lake Baikal were sampled in summer 2001 (Russell and Rosell-Melé, 2005). GDGT relative abundances and TEX_{86} values were assessed in the samples. The analytical protocol included microwave assisted extraction, alkaline hydrolysis (with water extraction) and instrumental analysis using the Agilent 1100 HPLC coupled to the Bruker ion-trap MS (see Appendix 1). The HPLC column used was an Econosphere NH_2 column (4.6 x 150 mm; 5 μm, Alltech) equipped with a pre-column filter.

2.3.2. Results and discussion

Using our HPLC conditions, GDGT-I (caldarchaeol) eluted at 4.5 minutes, prior to the other tetraether molecules. GDGTs were identified by their mass spectra and the elution order coincided with that reported elsewhere (e.g. Schouten et al., 2002). Elution of the relevant compounds was complete in 7 minutes (Figure 2.9). After every four samples the column was flushed with a gradient elution program increasing the percentage of *n*-propanol in hexane from 2 to 8% to avoid peak retention time shifts due to possible system contamination. This enabled four samples to be analysed every hour. Previous TEX_{86} measurements are reported to take an hour (Hopmans et al., 2000), so that the method presented here increases four fold the sample throughput.

The optimized method enabled the detection of the target GDGTs in most of the samples from the Iberian lakes and the Lake Baikal (see Figure 2.9b). A comparison of the estimated temperatures based on the TEX_{86} measurements and reference temperatures is shown in Table 2.3. In Lake Baikal sediment trap material and sediment samples, GDGT-I and crenarchaeol (structure I and V in Figure 1.3) were the predominant GDGTs, which is in agreement with the typical GDGT distribution found in cold sites and low temperature incubations (Schouten et al., 2002; Wuchter et al., 2004). The estimated temperatures for Lake Baikal are similar to those reported for surface water (e.g. Bolgrien et al., 1995). None of the GDGTs were detected in filtered particulate matter from Lake Baikal, which may be due to the small amount of water filtered (2 liters). As for the Iberian lakes, estimated late Holocene temperatures are in the range of present day temperatures, as could be expected because of the fairly stable temperatures in south-western Europe throughout the Holocene (e.g. Davis et al., 2003).

The results show that the optimized method allows a reproducible and rapid screening of GDGTs in different samples significantly reducing the time required per analysis, therefore enhancing the potential for TEX_{86} use in paleoclimate studies.

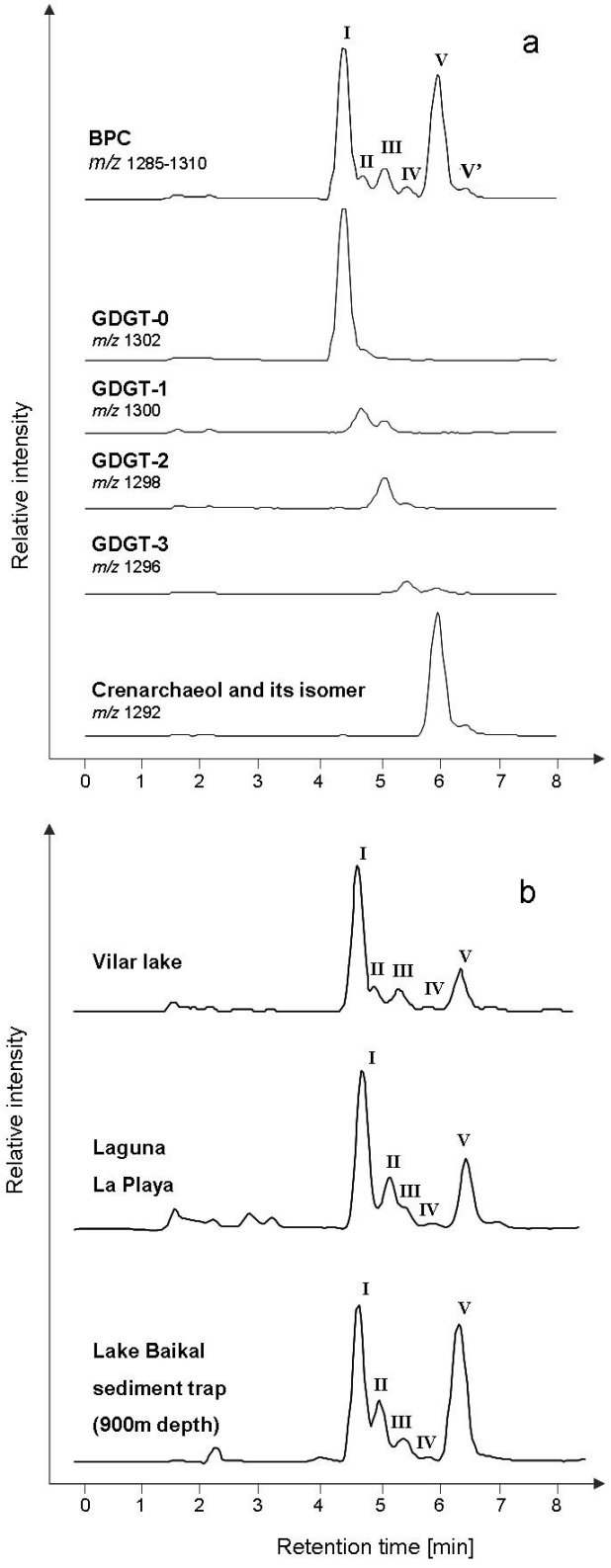

Figure 2.9 a) Base peak chromatogram and extracted ion chromatograms of GDGTs in sediments from lake Villarquemado (Teruel, Spain); **b)** Base peak chromatograms of sediments analysed with the rapid screening method: sediment from lake El Vilar; sediment from Laguna La Playa; material from a sediment trap deployed at 900 m depth in the north basin of Lake Baikal.

Sample		TEX_{86}	Estimated temperature (ºC)	Reference temperatures (ºC)
Lake Baikal (North Basin)				
Sediment trap (300 m depth)		0.312	1.4	Ice-covered from December until May; <4ºC in at the end of June, 6ºC in early July and 12-14ºC in early August.
Sediment trap (900 m depth)		0.342	3.5	
Filter (10 m depth)		n.d.		
Surface sediment (390 m depth)		0.371	5.4	
Lake Baikal (South Basin)				
Sediment trap (40 m depth)		0.411	8.1	Ice-covered from January until April; <4ºC in the end of June, 8-12ºC in early July.
Sediment trap (1396 m depth)		0.393	6.8	
Filter (10 m depth)		n.d.		
Surface sediment (632 m depth)		0.322	2.1	
Iberian Peninsula Lakes				
Villarquemado	1º 02' W, 40º 03' N	0.683	26.2	Min. -1.7 Max. 30.6 Av. 11.7
Caicedo (litoral sample)	2° 06´W, 42° 47´N	0.520	15.3	Min. 0.4 Max. 26.0 Av. 11.0
La Playa (1)	0º 11' W, 41º 25' N	0.652	24.1	Min. 1.4 Max. 31.9 Av. 14.6
La Playa (2)		0.762	31.4	
La Playa (3)		0.705	27.7	
El Tobar	3º 57' W, 40º 33' N	0.360	4.7	Min. 1.8 Max. 31.8 Av. 13.6
Sanabria	06º 42' W, 42º 07' N	0.549	17.2	Min. -1.7 Max. 26.1 Av. 9.8
Caicedo	2° 06´W, 42° 47´N	0.471	12.0	Min. 0.4 Max. 26.0 Av. 11.0
Montcortés	1º 00' E, 42º 20'N	0.542	16.8	Min. -3.3 Max. 26.9 Av. 9.6
Enol	4º 09' W, 43º 11' N	0.470	12.0	Min. 0.8 Max. 23.7 Av. 10.7
Taravilla	1º 59' W, 40º 39' N	0.486	13.1	Min. -1.7 Max. 30.3 Av. 11.0
Zoñar	4º 41' W, 37º 29' N	0.557	17.8	Min. 4.0 Max. 18.0 Av. 16.1
Estaña Grande	0º 32' E, 42º 02' N	0.205	-5.6	Min. -1.6 Max. 29.7 Av. 12.0
El Vilar (1)	2º 45', 42º 07' N	0.540	16.7	Min. 2.0 Max. 27.8 Av. 14.1
El Vilar (2)		0.562	18.1	
El Vilar (3)		0.547	17.1	

Table 2.3 TEX_{86} values and estimated temperatures (extended core-top calibration from Wuchter et al., 2005) for the samples analysed with the rapid screening method. Present day temperatures are reported for the sampling sites for comparison with estimated temperatures. Lake Baikal reference temperatures from Bolgrien et al. (1995). Iberian Peninsula lakes minimum (Min), maximum (Max) and average (Av) annual present day temperatures correspond to air temperatures from Digital Climatic Atlas of the Iberian Peninsula (Ninyerola et al., 2005). n.d.: GDGTs not detected.

2.4. Analytical considerations for the use of the paleothermometer Tetraether Index$_{86}$ and the Branched vs Isoprenoid Tetraether index regarding the choice of clean-up and instrumental conditions

This section contains a reduced version of a published manuscript (Escala et al., in press) which can be found complete in the Appendix 3. Methodological protocols are described in detail in Appendix 1.

The aim here is to discuss the comparability of alternative analytical methods to measure the TEX_{86} and BIT, using procedures and equipment which are not employed commonly to measure the GDGT proxies but are nonetheless frequently used by organic geochemists. For instance, it might be desirable in some cases to remove certain compounds in samples with a rich organic content in order to facilitate the detection of compounds such as the GDGTs. For this purpose alkaline hydrolysis (saponification) is tested as an alternative option to column fractionation for the clean-up of organic extracts, since hydrolysis breaks ester-bound compounds (typically present in several Eukarya and Bacteria-derived lipids) but does not affect the ether bounds (typical of Archaea-derived GDGT core lipids). Different adsorbents and their degree of activation are also tested for the fractionation of the extracts. In addition, different analytical instrumental configurations are explored, in particular, to measure TEX_{86} and BIT with an ion trap mass spectrometer as an alternative to using a quadrupole mass spectrometer.

2.4.1. Experimental section

A detailed account of the analytical protocol can be found in Appendix 1. The following paragraphs are a summary of the sample preparation and GDGT determination. Results were treated with SPSS 15.0 software.

2.4.1.1. Comparison of clean-up procedures

A set of 23 marine and lacustrine sediments, including both organic-rich ocean sediment surface and below-surface sediment samples were freeze-dried, homogenised and between 1-2 g of each sediment were extracted by microwave assisted extraction (MAE). Half of each extract was subject to **alkaline hydrolysis** whereas the other half was fractionated with **preparative column chromatography**. Alkaline hydrolysis typically includes one step where water is used to remove remaining salts from a hexane fraction. To assess the recovery of GDGTs when water was used, 8 aliquots of a GDGT-I standard solution were saponified and only in 4 of them water was used. A non-saponified aliquot was used as a control for GDGT recovery.

2.4.1.2. Comparison of adsorbents in preparative column chromatography

An extract of ~15g of sediment from Lake Banyoles (Catalunya, Spain) was split in several aliquots to test different **adsorbents** in preparative column chromatography. These were activated alumina, activated silica, and their deactivated homologues. Triplicates of the experiments and a blank control were performed.

2.4.1.3. GDGT determination by HPLC/APCI-MS

The equipment used included the Dionex P680 HPLC coupled to a Thermo Finnigan TSQ Quantum Discovery Max quadrupole mass spectrometer, hereafter referred as the **quadrupole system**. A second system composed by the Agilent HPLC 1100 Series coupled to a Bruker 3000 ion-trap MS, hereafter referred as the **ion-trap system**, was also used for comparison. The samples were eluted in a Prevail CN column (150 x 2.1 mm; 3 μm, Alltech). Flow rate was 0.3 mL/min and injection volume was 10 μL.

The TEX_{86} and BIT indices were calculated and TEX_{86} was converted to temperature values using the marine calibration by Kim et al. (2008) (see Chapter 1). We are aware that the conversion of lacustrine-derived TEX_{86} values to absolute lake surface temperature would require using the lacustrine calibration derived for this purpose. However, because we used both marine and lacustrine sediments in the experiments, and our interest in giving temperature values here is solely to give a physical interpretation of the observed TEX_{86} differences, the marine calibration is used for all the conversions.

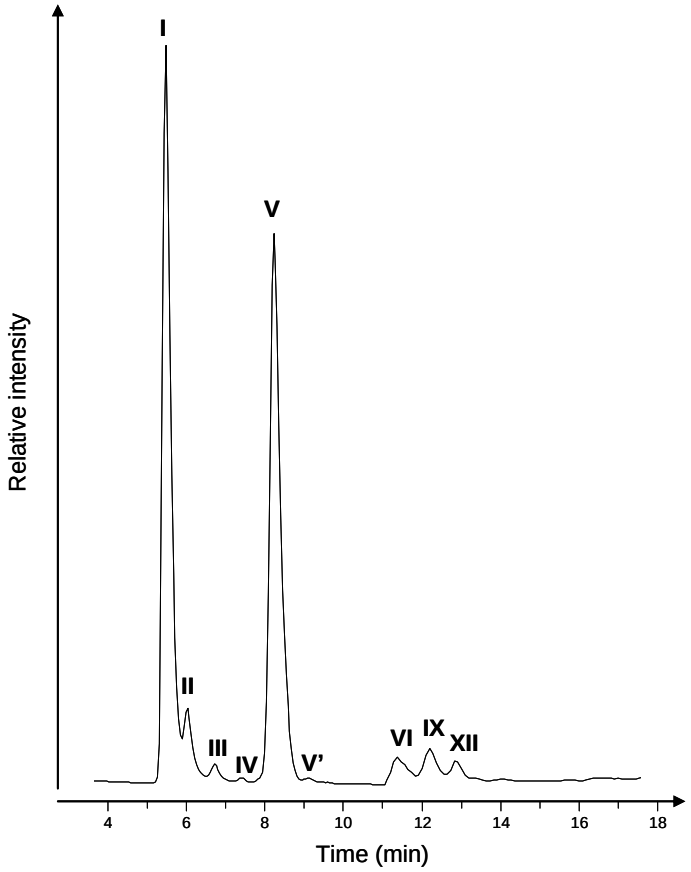

I. *m/z* 1302
II. *m/z* 1300
III. *m/z* 1298
IV. *m/z* 1296
V. *m/z* 1292
VI. *m/z* 1050
IX. *m/z* 1036
XII. *m/z* 1022

Figure 2.10. Base peak chromatogram, and the corresponding masses of the protonated molecules. Roman numbers refer to structures in Figure 1.3.

2.4.1.4. Comparison of HPLC columns and conditions

The analysis of a large amount of samples in paleoclimatology studies requires detail consideration on cost and waste management issues during the analysis, and in particular for the GDGTs analysis the volume of organic solvents used in the HPLC is a relevant concern. We tested an HPLC flow reduction with the aim to observe the change impinged on the stability of the GDGTs indices, given the resulting change in GDGTs peak shape and resolution. Alongside flow reduction we used a smaller-particle size column to keep a comparable head pressure in the HPLC system. Thus, the **Tracer Nucleosil CN** column (4 x 150 mm, 5 μm; Teknokroma), which had been used in our laboratory for previous analysis at a flow rate of 1 mL/min, was compared to a **Prevail CN** column (150 x 2.1 mm, 3 μm; Alltech) at a flow rate of 0.3 mL/min. This flow reduction and column comparison was tested on the ion-trap system.

2.4.1.5. Comparison of mass spectrometers

To investigate the reproducibility of the analysis using different designs of mass spectrometer, we compared the TEX_{86} and BIT values for 22 samples obtained with the ion-trap and the quadrupole spectrometers, using the Prevail CN column and respective APCI interfaces. An example of a chromatogram is shown in Figure 2.10.

2.4.2. Results and discussion

2.4.2.1. Clean-up methods: saponification vs alumina fractionation

A set of sediment extracts were subjected to two different clean-up methods, alkaline hydrolysis and fractionation through activated alumina columns, and their GDGT distribution was analysed by means of an HPLC/APCI- quadrupole MS. The resulting TEX_{86} and BIT values obtained with the two procedures are plotted in Figure 2.11, which shows no sign of systematic difference between the two methods. We identified and discarded outliers (1 found) for TEX_{86}, if any point fell beyond 3 standard deviations of the linear regression between saponified vs fractionated index. A paired t-test of the remaining 22 TEX_{86} values indicated that the alkaline hydrolysis and alumina fractionation clean-up methods did not result in significantly different TEX_{86} values (t critical value = 2.83, t empirical value = 2.41, P = 0.01). The standard deviation of the regression including the 22 values is 0.013 or ca. 0.7 ºC. This was half the precision we routinely obtain with the HPLC/quadrupole-MS, 1σ being 0.006 or ca. 0.3 ºC. Regarding the BIT, a paired t-test based on the 23 values also points at a non-significant difference between alkaline hydrolysis and alumina fractionation (t critical value = 2.82, t empirical value = 2.50, P = 0.01). Therefore, both methods are in principle comparable in terms of TEX_{86} and BIT measurement in lake and ocean sediment samples with different contents of organic matter. However, the saponification step may have a critical drawback if in the extraction process after saponification water is used to remove excess salt in the hexane extracts. We used a standard solution of GDGT-I to calculate recoveries of the procedure. When the water extraction step was removed, the recovery of GDGT-I of four replicate analyses was on average 104.6% (σ = 4.5%, n = 4), which dropped to 6.1% (σ = 4.1%, n = 4) when water extraction after hydrolysis was

undertaken. This could lead to a massive underestimation of the amounts of GDGTs in the samples and clearly should be avoided.

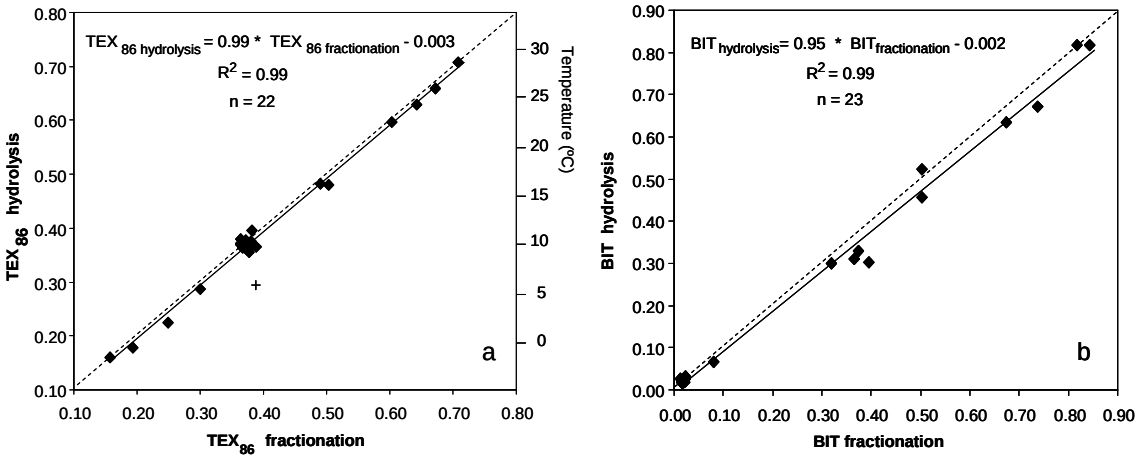

Figure 2.11 Cross-plots of TEX_{86} (a) and BIT values (b) obtained with the two clean-up methods tested: activated alumina column fractionation and alkaline hydrolysis (saponification). The cross symbol indicates an outlier data point. The standard deviation of the injections is not represented as it is smaller than the dots size. The dashed line indicates the 1:1 correspondence and is drawn only for illustration purpose.

2.4.2.2. Clean-up methods: comparison of adsorbents

Four different adsorbents were tested in preparative chromatography. The resulting TEX_{86} and BIT values obtained from triplicate analyses are compared in Figure 2.12. We confirmed the normal distribution of the data sets with a Kolmogorov-Smirnov test ($P = 0.925$ for TEX_{86} and $P = 0.765$ for BIT) and the homogeneity of variance ($P = 0.600$ for TEX_{86} and $P = 0.626$ for BIT) previous to the analysis of variance (one-way ANOVA test). According to the ANOVA, the five methods tested (four adsorbents and a control) yielded significantly different results in terms of BIT ($P < 0.001$) but not for TEX_{86} ($P = 0.105$). There was a maximum TEX_{86} difference between methods of 0.020 or 1.1 ºC (activated silica vs deactivated silica) and a minimum difference of 0.002 or 0.1 ºC (deactivated silica vs deactivated alumina). Thus, it seems that the fractionation with the compared adsorbents is not discriminating between the isoprenoidal GDGTs related to TEX_{86}. On the other hand, the maximum difference between the average BIT values of the tested methods is 0.050 (control vs activated alumina and silica). It can be argued that for the qualitative nature of the proxy and its

range of possible values (0-1) this difference raises no restriction for the selection of the clean-up method. However, results shown in Figure 2.12 suggest that the values of BIT in the hitherto published studies (e.g. Hopmans et al., 2004; Weijers et al., 2006b; Huguet et al., 2007b) might contain a certain degree of bias if activated alumina was used for the clean-up of samples, and this hampers the comparability of the published results.

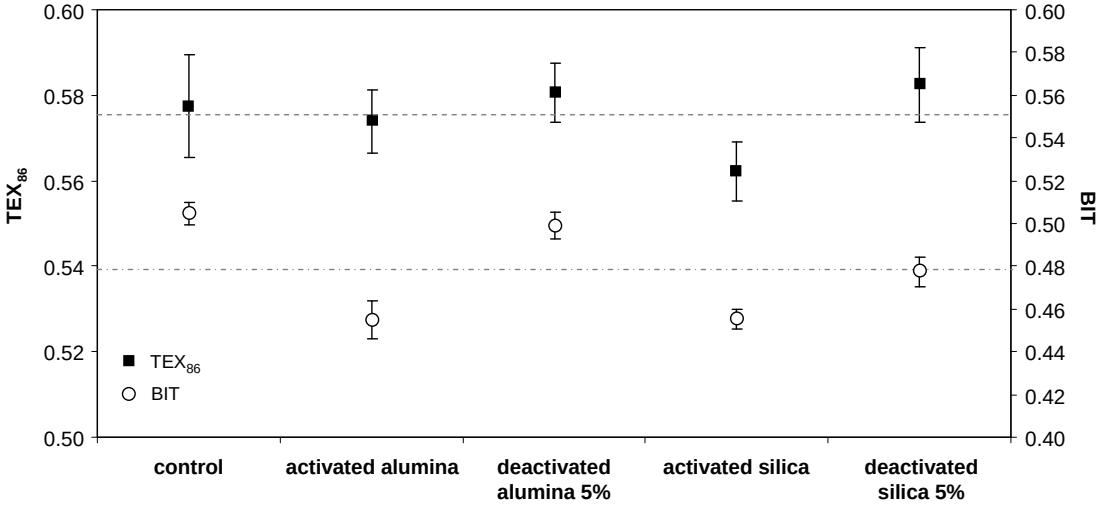

Figure 2.12 Comparison of the effect of the adsorbent type in column fractionation on TEX_{86} and BIT values for a sediment from lake Banyoles. Error bars indicate ± 1σ (n = 3) and the dashed lines show the average index value.

2.4.2.3. HPLC column effects

The indices TEX_{86} and BIT were calculated for a set of 19 samples injected in two different HPLC columns operated at 0.3 and 1 mL/min. The columns had the same stationary phase but were different in terms of particle size, column diameter and manufacturer. Given that the efficiency of a column is inversely proportional to the squared diameter and to the particle size, theoretically this gives a maximum increase of efficiency of ~5.7 times in changing columns from the Tracer Nucleosil CN to the Prevail CN. As the root square of column efficiency is proportional to the resolution it can provide, theoretically the resolution could be increased ~2.4 times with the Prevail CN in comparison to the Tracer CN tested. However this is compensated by the flow reduction, which was the final objective of the experiment. Column head pressure was comparable for both columns: in the Tracer Nucleosil CN column at 1 mL/min it was 59

bars, while a similar pressure (56 bars) was reached with the Prevail CN at 0.3 mL/min. The tested chromatographies did not produce significantly different TEX_{86} results (paired t-test; n = 19, t critical value = 2.88, t empirical value = 1.43, P = 0.01). However, there is a certain degree of dispersion of the TEX_{86} results, indicated by a standard deviation of Tracer Nucleosil CN over Prevail CN results of 0.041 equivalent to 2.1 ºC. Some samples show important differences in TEX_{86} values calculated with the two HPLC columns (6 samples show a difference larger than 1.7 ºC, which is the current error of the TEX_{86} calibration with SST (Kim et al., 2008)). At present, we have no explanation for the cause of the divergent TEX_{86} values with the two columns, but generally, the high correlation between both sets of results allows the intercomparability of the TEX_{86} values. The tested columns did also not produce significantly different BIT values (paired t-test; n = 18, t critical value = 2.90, t empirical value = 1.92, P = 0.01) and only one sample shows a difference larger than 0.10. An important advantage of the Prevail CN column is that the narrower and smaller particle size column requires about three times less solvent volume compared to the Trace CN, a significant cost and environmental advantage even if the run is lengthened by 7 minutes.

2.4.2.4. Comparison of mass spectrometers

With the aim of verifying whether BIT and TEX_{86} values obtained with the ion-trap MS are comparable to and as precise as the ones obtained with the quadrupole MS, a set of 22 sample extracts were injected in both systems using the same chromatographic conditions. The ion-trap system yielded a standard deviation of TEX_{86} from a triplicate injection of 0.007 or ca. 0.4 ºC, while for the quadrupole system the standard deviation was 0.006 or ca. 0.3 ºC. The BIT values from the same injections yielded a standard deviation of 0.002 for the ion-trap and 0.009 for the quadrupole system. Thus, no apparent difference in precision was obtained using both systems.

The cross-plot for TEX_{86} values (Figure 2.13a) suggests little systematic bias between the two HPLC/MS systems tested. The differences in TEX_{86} values for 18 out of the 22 samples range between 0.1 ºC and 1.7 ºC. However, four samples show differences of >3 ºC. They have in common that the GDGT III was slightly overestimated and the GDGT II slightly underestimated in the ion-trap MS compared to the quadrupole MS. Furthermore, three of these samples belong to the lower range of the TEX_{86} index,

below 0.3. However, at present the cause of this difference is not clear to us. A systematic difference between both systems is clearly observed for BIT, as the quadrupole yielded lower values than the ion-trap MS (Figure 2.13b). This could be related to the different analytical conditions employed in the MS system and a different response or ionisation efficiency of isoprenoidal vs branched GDGTs, given that conditions in both systems were optimized with the isoprenoidal GDGT-I but not with a branched GDGT.

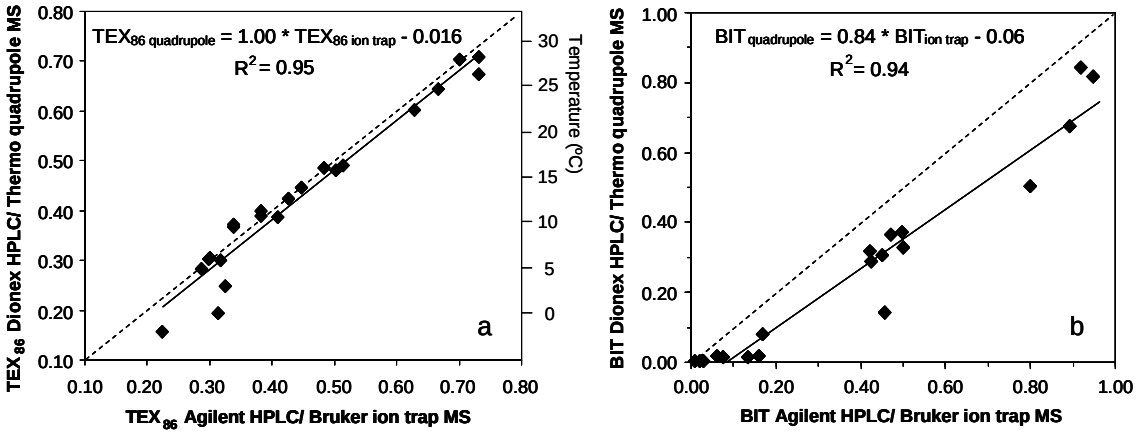

Figure 2.13 Cross-plots of TEX_{86} and BIT values obtained using the Dionex HPLC/Thermo quadrupole MS and the Agilent HPLC/Bruker ion-trap MS. The standard deviation of the injections is not represented as it is smaller than the dots size. The dashed line indicates the 1:1 correspondence and is drawn only for illustration purpose.

To appraise further the effects of the MS conditions on the TEX_{86} and BIT, we investigated the effect on GDGT yields of changes in the corona current and the temperatures involved in the vaporization of the sample (vaporizer temperature) and the ion transfer to the vacuum region in the detector (capillary temperature). While the tested corona intensities (3 to 15 μA) did not change significantly the relative GDGT yields, a larger effect was observed for the temperatures (Figure 2.14). The ionisation and transfer efficiency as derived from the peak areas differed between isoprenoidal GDGTs and branched GDGTs at different vaporizer temperatures (300 ºC to 500 ºC; Figure 2.14.b), and even more at different capillary temperatures (100 to 250 ºC; Figure 2.14.a).

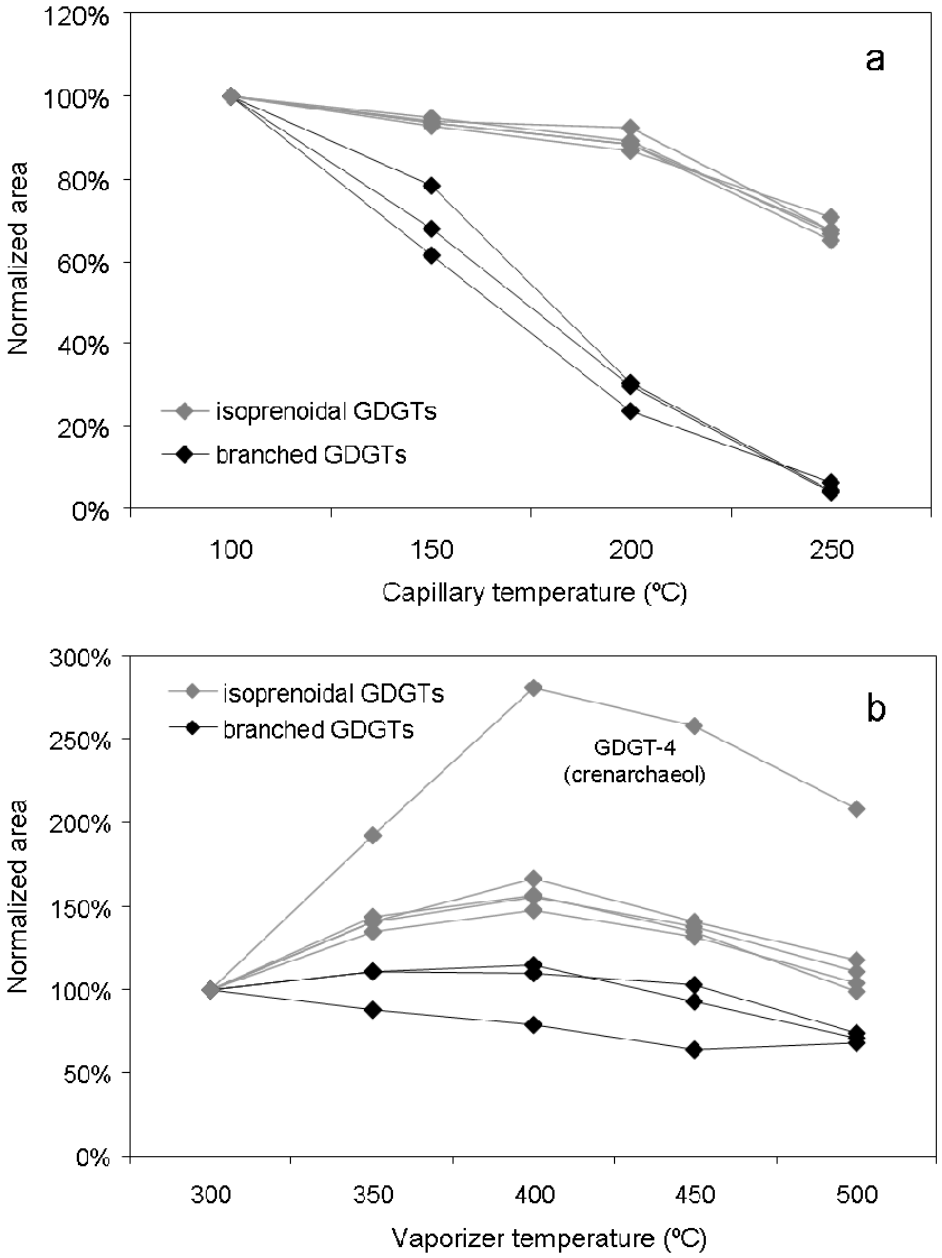

Figure 2.14 Effect of vaporizer temperature and capillary temperature on the branched (structures VI, IX and XII) and isoprenoidal (structures I to V') GDGTs yields. Data points reflect only one injection and were obtained with a Dionex HPLC coupled to a Thermo Finnigan TSQ Quantum Disovery Max mass spectrometer via an APCI interface.

This raises the question of how the indices TEX_{86} and BIT are affected by the optimization or tuning of the APCI. We observed a maximum difference in TEX_{86} of 0.05 or ca. 2.5 ºC (result from a single analysis). However, the BIT value of a marine sample rose from 0.15 to 0.45 when capillary temperature was lowered from 200 ºC to

100 ºC. The BIT values are more sensitive to the APCI conditions than $TEX_{86,}$ as the BIT index is based on measuring two types of GDGTs, i.e. the branched and isoprenoidal, while TEX_{86} is based only on the isoprenoidal ones (see Chapter 1). Given that the APCI conditions are usually not optimized using simultaneously both isoprenoidal and branched GDGTs, it is likely that values of BIT between various instruments are not comparable. Clearly much more investigation is needed to fully understand the ionisation and transfer process of GDGTs in the APCI and the repercussions on the derived TEX_{86} and BIT indices, but we urge special caution when comparing BIT values between laboratories.

2.4.3. Conclusions

In this study we show the applicability and investigate the reliability of alternatives to the common analytical protocols and equipment used to analyse archaeal and bacterial GDGTs in sediments for the measurement of the TEX_{86} and BIT indices. The clean-up experiments show that alkaline hydrolysis (saponification) is a valid alternative to the fractionation on activated alumina as long as the water extraction of the hexane fraction is avoided to minimize low recoveries of the GDGTs. Although alumina fractionation and alkaline hydrolysis are both widely used clean-up methods in paleoceanographic studies, alkaline hydrolysis might be especially useful to purify samples that are very rich in certain organic compounds, such as wax esters. Thus, GDGT analyses can be readily performed in multiproxy biomarkers studies in samples which require saponification of the organic extracts. Regarding the low recovery of GDGT-I when water is used to remove salts from hexane, we hypothesize that the GDGT might be preferentially solubilised by water due to the relative polarity of the compound. Silica and alumina used for column fractionation either activated or deactivated at 5% provide comparable results for TEX_{86}, but not for BIT. The degree of adsorbent activation seems to bias the BIT index and hence the use of non-activated adsorbents is preferable. A reduction of flow in the HPLC after a change of HPLC columns with the same phase but different particle size, diameter and manufacturer did not yield statistically significant differences of TEX_{86} and BIT values. Finally, TEX_{86} and BIT measurements on an ion-trap MS are compared for the first time to measurements obtained with a

quadrupole MS. The ion-trap system is shown to be as precise as the quadrupole analyser for both indices, and they also provide comparable TEX_{86} but significantly different BIT values. It appears that the ionisation and transfer efficiency between branched and isoprenoidal GDGTs is different enough so that BIT values are very sensitive to MS operational conditions. This is especially important as at present much of the calibration work and provision of reference values to interpret the GDGT indices in a paleoclimatic context is derived from a single laboratory (Schouten et al., 2002; Hopmans et al., 2004). Our results suggest that to use such reference values, the MS conditions should first be optimized so that the relative responses of the branched vs isoprenoidal GDGTs are comparable to the published reference values. This would be facilitated if a reference sample was available with which laboratories could tune their HPLC/MS systems to obtain comparable values among the increasing community analysing the GDGT indices.

Chapter 3

Exploration of GDGT distribution in Iberian lakes and their potential for climate reconstruction

3.1. Introduction

Archaea are known to occur widely in lacustrine environments (see Chapter 1). The use of their characteristic lipids, the isoprenoidal GDGTs, as well as branched GDGTs from bacteria living in soils has been applied in a few recent paleostudies in order to reconstruct lake surface temperature (LST) and annual mean air temperature (MAT) using the proxies TEX_{86} and MBT/CBT, respectively. The calibration of TEX_{86} includes large lakes located in the continental areas of America, Africa, Asia and one lake in Iceland. However, the number of large lakes, where TEX_{86} predominantly seems to work as a paleotemperature proxy, is limited. In fact, 90% of the estimated 304 million lakes worldwide have an area of less than 0.01 km^2 (Downing et al., 2006). Therefore investigating the applicability of this proxy in smaller, more frequent lakes is of primary interest in order to extend the area where quantitative continental temperature reconstructions can be achieved. Furthermore, the increase of practical sites where TEX_{86} and MBT/CBT proxies can be applied would also contribute significantly to the climate reconstruction at regional scale.

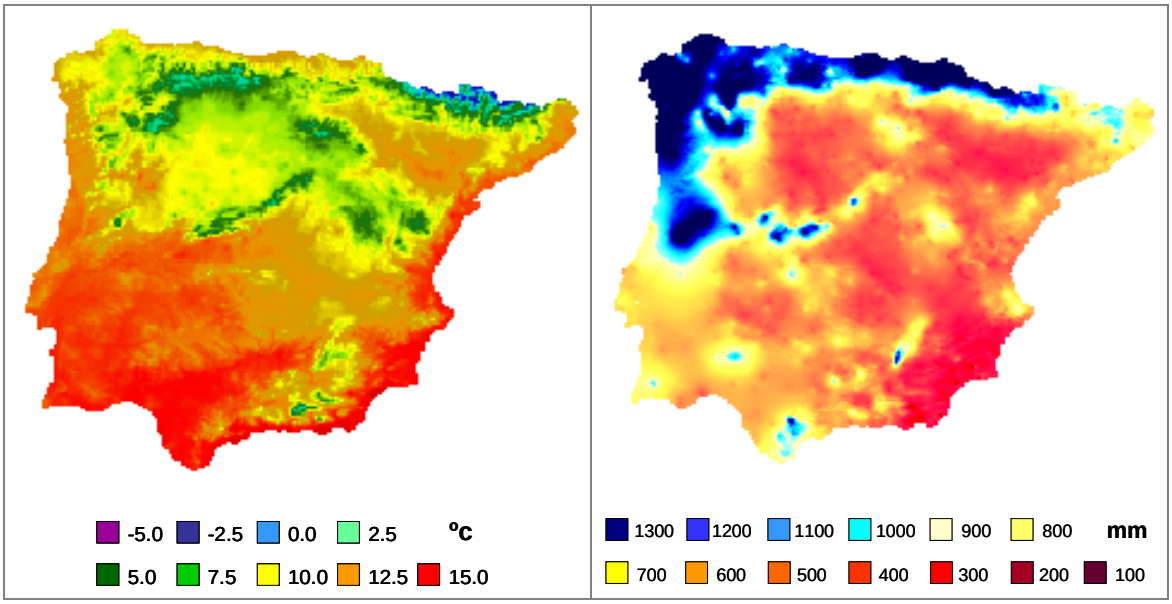

Figure 3.1 Distribution of mean annual air temperatures and annual precipitation in the Iberian Peninsula. Source: Digital Climatic Atlas of the Iberian Peninsula (Ninyerola et al., 2005).

Our study is focused on the Iberian Peninsula, south-west Europe, where there is a large number of small inland water bodies. This region is a key site to study land-ocean climatic interactions, with both the Atlantic Ocean and Mediterranean Sea playing an

important role in climatic changes occurring on land (e.g. Naughton et al., 2007). The present climatic distribution in the Iberian Peninsula is highly heterogeneous, since influences of the Atlantic, continental and subtropical regimes are present (Figure 3.1a). Furthermore, the varied relief and consequent rain shadow effect further contribute to this heterogeneity and determine a remarkably irregular spatial distribution of rainfall (Figure 3.1b). This explains the large inter-annual variations experienced by the Iberian inland aquatic system, composed of ephemeral *lagunas* and some semi-permanent and permanent lakes (e.g. Pearson et al., 2007).

Paleoclimate studies in Iberian Peninsula have been traditionally based on pollen studies (e.g. Peñalba et al., 1997; Naughton et al., 2007), which can be good indicators of the vegetation present in basins and relative changes in humidity. In contrast, they lack the temporal and spatial resolution needed to record short-term fluctuations and, furthermore, they are not able to reconstruct temperatures in a quantitative manner (e.g. Riera et al., 2004; Mighall et al., 2006). Dendroclimatology has also been used to derive relative changes in humidity (e.g. Nicault et al., 2008) and sedimentological and mineralogical studies have contributed to unveil the history of lake-level and water chemistry changes in Iberian lakes related to climate and human activity (e.g. Valero-Garcés et al., 2008; Moreno et al., 2008). In the last years, an increasing number of publications have focused on the reconstruction of late Quaternary climate in the Iberian Peninsula, in order to unravel the timing and mechanisms of rapid climatic change in south-western Europe. Furthermore, recent high-resolution studies for the Holocene underscore the rapid climatic variability experienced by the Iberian Peninsula during this period, opposite to what was previously thought (e.g. Riera et al., 2004). Thus, finding appropriate proxies that can track the (often rapid) changes occurring in the basins as in response to climate and human pressure is an important issue for paleostudies as well as for prediction of future evolution of aquatic system.

The objective of this chapter is to explore the potential of lakes in the Iberian Peninsula for applying quantitative temperature reconstructions using the GDGT distribution found in their sediments. For this purpose, a suite of lake surface sediment samples were collected and their GDGT distribution was analysed and interpreted in combination with the lake characteristics and climate parameters.

3.2. Study area and sample collection

Surface sediment samples used in this study come from a suit of 38 lakes in the Iberian Peninsula (see Figure 3.2 and Table 3.1) provided by collaborations with B. Valero-Garcés, A. Moreno and E. Pearson. The lakes considered are located mainly along four river basins, i.e. the Ebro, Duero, Guadiana and Guadalquivir basins, and the mountainous areas in the Cantabria region (north-west), the Iberian range and the Pyrenees (north-east). The studied lakes are mostly endorheic, i.e. closed drainage basins without water inflows or outflows, and where precipitation and evaporation patterns dominate the water regime. The Iberian lakes are usually shallow and small, except from some lakes in elevated areas in the north, and our data set reflects this pattern (50% of our lakes are 1 m deep or less, and have a surface of less than 0.3 km^2). Short sediment cores were collected either with a short Renberg corer, a Kullenberg probe or a Mac probe, while for some lakes directly surface sediment samples were collected using either an Eckman grab or a metallic spade. Sediments were collected as far from the coast as possible. For some lakes, subsurface rather than surface material was analysed (see table 3.1). The sedimentation rates are probably highly variable among the lakes and little information is published on this issue; hence different temporal ranges (decades to centuries) are integrated in the collected sediments. Given that for most of the lakes a minimum of 2 cm of surface sediment are analysed, the rapid changes that perturbed the lakes (e.g. interannual temperature variability) are likely not to be resolved and the signal of the sediments is rather an integration of climate during the time span of deposition, which is more suitable for a validation/calibration study.

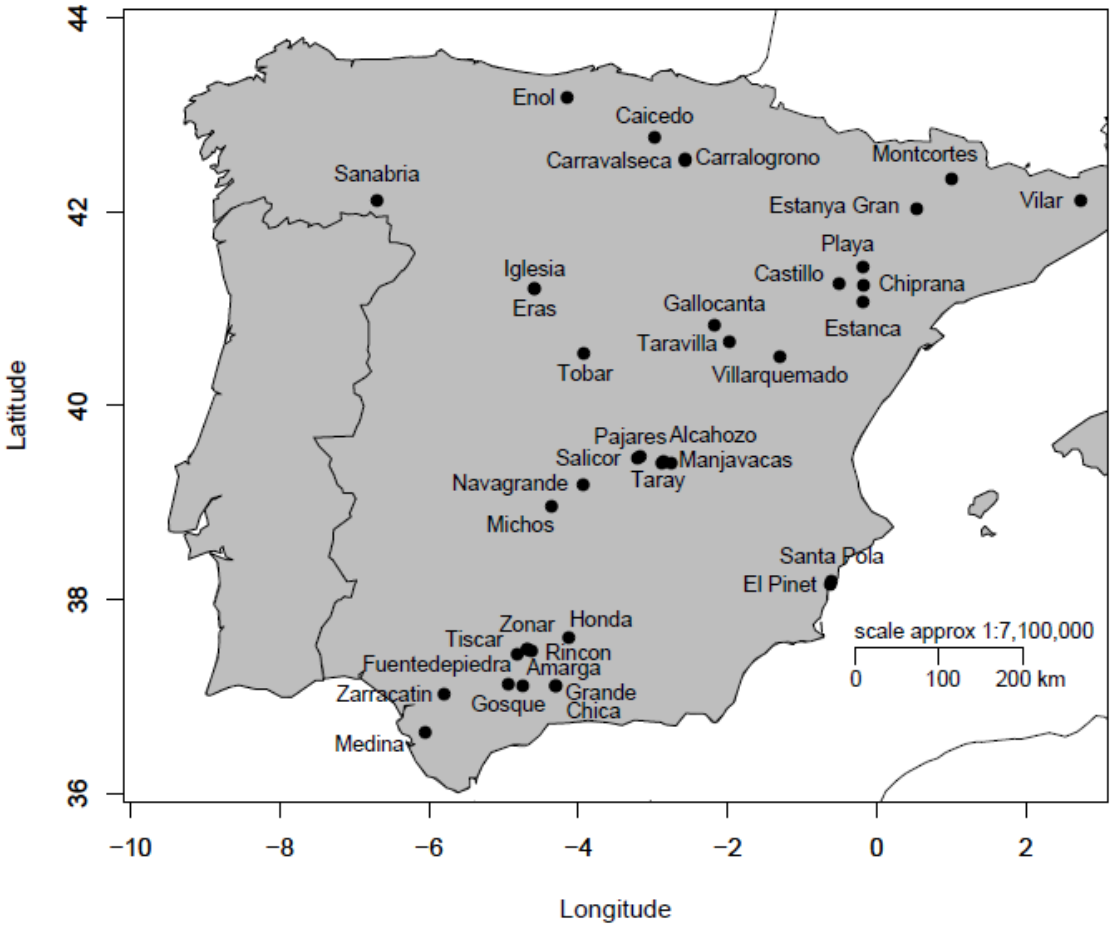

Figure 3.2 Location of surveyed lakes in the Iberian Peninsula.

Lake	River basin / mountain area /region	Latitude Nº	Longitude Eº	Altitude (m.a.s.l)**	Maximum depth (m)	Conductivity (mS / cm)	Origin of lake	Surface (km^2)	Sample depth (cm)	pH	TDS* (g/L)
Alcahozo	Guadiana	39.39	-2.88	670	0.02	105.9		0.50	0-2	8.2	68
Amarga	Guadalquivir	37.48	-4.69	370	4.5	4.84		0.20	0-2	8.2	3.91
Caicedo	Ebro	42.77	-2.98	655	25	1.4	karstic	0.07	5-8 / 7-10	8.0	0.95
Carralogroño	Ebro	42.54	-2.57	170	1.25	12.76		0.20	0-2	8.3	9.44
Carravalseca	Ebro	42.53	-2.57	560	0.3	22.5		0.20	0-2	8.5	13.6
Castillo	Ebro	41.26	-0.51	430	2.3	13.8		0.80	0-2	8.3	10.6
Chica	Guadalquivir	37.10	-4.31	790	4.7	4.74		0.20	0-2	6.6	4.45
Chiprana	Ebro	41.24	-0.18	150	4.8	42		0.23	0-2	8.1	25.3
El Pinet	Med. coast	38.16	-0.63	0	0.1				*surface*		
Enol	Cantabric Range	43.18	-4.15	1070	23		glacial	0.12	4-7 / 5-8		
Eras	Duero	41.20	-4.59	790	0.8	3.64		0.30	0-2	9.0	2.19
Estanca	Ebro	41.06	-0.19	337	5.6	0.8		1.20	0-2	7.6	0.46
Estanya Gran	Pre-Pyrenees	42.03	0.53	670	22	3.3	karstic	0.19	*surface*	8.1	
Fuentedepiedra	Guadalquivir	37.11	-4.75	680	0.03	52.5		0.90	0-2	8.4	36.4
Gallocanta	Ebro	40.83	-2.18	995	0.05	62.5	tectonic	5.60	0-2	8.1	37.5
Gosque	Guadalquivir	37.13	-4.94	410	0.02	103.8		0.80	0-2	8.0	9.88
Grande	Guadalquivir	37.11	-4.30	790	9.2	3.36		0.30	0-2	8.7	2.97
Honda	Guadalquivir	37.60	-4.13	450	3.2	31.2		0.10	0-2	9.5	22.2
Iglesia	Duero	41.20	-4.59	770	0.5	2.17		0.15	0-2	8.9	1.3
Manjavacas	Guadiana	39.42	-2.86	670	0.4	48.5		1.50	0-2	8.5	34.7
Medina	Guadalquivir	36.62	-6.05	20	0.6	7.91		1.20	0-2	8.1	6.39

Lake	River basin / mountain area /region	Latitude Nº	Longitude Eº	Altitude (m.a.s.l)**	Maximum depth (m)	Conductivity (mS / cm)	Origin of lake	Surface (km^2)	Sample depth (cm)	pH	TDS* (g/L)
Michos	Guadiana	38.96	-4.36	680	0.04	0.51	crater	0.50	0-2	7.1	0.25
Montcortès	Pyrenees	42.33	1.00	1065	30		karstic	0.19	10-13		
Navagrande	Guadiana	39.18	-3.94	620	0.2	22.6		0.90	0-2	7.6	16.5
Pajares		39.46	-3.21	670				0.24	*surface*		
Playa	Ebro	41.42	-0.19	340	0.45	71.5	karstic	2.50	1-2	8.2	43
Rincón	Guadalquivir	37.46	-4.63	310	4.5	1.74		0.20	0-2	7.3	1.34
Salicor	Guadiana	39.47	-3.17	670	0.02	105.9		0.50		8.2	68
Sanabria	Tera river	42.12	-6.70	1000	51	14.5	glacial	3.46	14-17	6.3	10.25
Santa Pola	Mediterranean coast	38.18	-0.61	0	0.2		*artificial saltworks*		*surface*		
Taravilla	Iberian Range Tajo basin	40.65	-1.98	1100	11	0.55	karstic	0.02	4-7	7.8	
Taray	Guadiana	39.41	-2.76	560	0.3	11.82		0.20	0-2	8.7	7.2
Tiscar	Guadalquivir	37.43	-4.82	250	0.03	57.6		0.10	0-2	8.7	34.5
Tobar	Iberian Range	40.53	-3.93	1250	28		karstic	0.41	0-2		
Vilar	Pre-Pyrenees	42.12	2.73	173	12	1.00	karstic	0.01	0-1	7.5	
Villarquemado	Alto Jiloca river	40.50	-1.30	990	2.8***		tectonic	11.30	2-4		
Zarracatín	Guadalquivir	37.03	-5.80	690	1.2	2.68		0.20	0-2	7.8	2.44
Zóñar	Guadalquivir	37.48	-4.69	290	15.4	2.46	karstic	0.49	0-2	7.4	2.28

Table 3.1 Iberian lakes included in the present study and their considered characteristics in terms of morphology, location and chemistry. *TDS = total dissolved solids. **m.a.s.l.= meters above sea level. *** Villarquemado is dry since 18th century due to human water exraction; this depth is the last depth known. Exact cm for surface sediments collected with a metallic spade are not available and hence *surface* is shown in the sample depth column. For a list of references, see Appendix 2.

3.3. Methodology

3.3.1. GDGT analysis

Samples were extracted by MAE, saponified and analysed by HPLC/APCI-MS either with the ion-trap or quadrupole MS. The detailed analytical protocols are described in Appendix 1. The concentrations of the 15 targeted GDGTs (see Chapter 1) were measured in sediment samples from the 38 Iberian lakes available to calculate the proxies TEX_{86}, MBT, CBT and BIT (see equations in Chapter 1). For two lakes, Enol and Caicedo, two samples taken from the littoral and central parts of the lakes were also analysed. The distribution of the GDGTs was also analysed statistically (see below), and all these indices were compared to the chemical, morphological and geographical location variables collected for each site.

3.3.2. Statistics

Because the main objective of the study was to assess the climatic and environmental influences on the GDGT distribution, all Iberian lakes were included in the statistical exercise, without discriminating possible outlier values a priori.

The results were treated with software SPSS 15.0. Two main statistical analyses were performed, the Principal Component Analysis (PCA) and Hierarchical Cluster Analysis (HCA). We applied PCA in order to study the distribution of the 15 GDGT concentrations in the lakes. PCA is a routine procedure used to reduce the dimensions in which the variation of the original data is distributed. This method identifies the orthogonal dimensions of maximum variation of the data and redefines these in terms of vectors which are linear combinations of the original variables. Usually a small number of these new vectors will explain most of the initial variance and they are called factors or Principal Components (PC).

Common procedures applied to the original data before performing the PCA are the normalisation and standardization (autoscaling) of the data. In the present study, the individual concentrations of GDGTs were normalised, so that the sum of all concentrations equals 1, in order to eliminate the effect of the "sample size", since our interest is more in the distribution of the GDGTs rather than the absolute abundances of each lipid. On the other hand, autoscaling the data implies changing the distribution of the values to have a mean of 0 and a variance equal to 1, in order to avoid the variables with larger range of values to dominate over the others. This standardization was also applied to the concentrations of the GDGTs, due to large differences in the typical environmental concentrations between these lipids. This procedure also can have a minor side effect, which is the amplification of the noise associated to the variables with lower values. In our case, we can expect as a consequence higher noise in the autoscaled concentration of the crenarchaeol regioisomer (*m/z* 1292), which is typically the less abundant GDGT in sediment samples. It is also common to rotate the resulting coordinates of the PCA, which yields a new arrange of vectors (Principal Components) that, still accounting for the same amount of variance than the non-rotated output, distributes more evenly the variance between the several PCs extracted, thus slightly simplifying the interpretation step. We used the *Varimax* rotation method (Kaiser, 1958).

Hierarchical cluster analysis (HCA) is another common analysis, employed to make groups of similar objects. HCA calculates similarities between objects and aggregates them forming successively larger clusters until all objects are comprised in one single cluster. In this study we performed an HCA for the cases (lakes) and we used three criteria for clustering: chemical variables (total dissolved solids, pH, and conductivity), morphological variables (area and maximum depth) and location variables (latitude, longitude and altitude). A fourth HCA was performed taking into account all variables at the same time. There are also several possible cluster methods to apply in the HCA. We used here the method of the complete linkage and the single linkage. In complete linkage, the distance between two clusters is the maximum distance between an observation in one cluster and an observation in the other cluster. As this method can be severely distorted with the presence of outliers (Milligan, 1980), single linkage was also used in a parallel HCA for each of the four analyses in order to compare the results. The squared Euclidean distance was used for computing the distances between clusters.

3.3.3. Lake surface temperature versus air surface temperature

Air surface temperatures are a widespread measured climatological parameter, whereas lake surface temperatures (LST) are seldomly recorded periodically, given that meteorological stations use less complicated technology for measuring air temperature than biological stations need for water monitoring. That is especially true for regions where small aquatic systems are the norm, as usually only relatively large lakes are monitored. For our set of Iberian lakes there is published information on water temperature only for a few of them. For this reason, we used air temperatures to compare to our GDGT-based reconstructions. In the following paragraphs, this approximation is discussed. Reference air temperatures were obtained from the Digital Climatic Atlas of the Iberian Peninsula (Ninyerola et al., 2005) and compared to the reconstructed mean annual air temperature (MAT) and lake surface temperature (LST). The Digital Climatic Atlas has a spatial resolution of 200 m, and monthly as well as annual temperature and rainfall values are available. Only meteorological stations with data spanning more than 15 years for temperature and 20 years for precipitation (period 1950-1999) were used to produce the Atlas, and the spatial interpolation between stations was performed with a multiple regression where independent variables were elevation, latitude, continentality, solar radiation and geomorphology (Ninyerola et al., 2005). Data for each lake studied has been extracted from the coordinates of the lake.

Water temperature in a lake is a result of the heat budget in the water body. The dominant source of heat income is direct absorption of solar radiation; additionally, transfer of heat from the air and from sediments, condensation of water vapour at the water surface and heat transfer from water inputs such as precipitation, runoff and groundwater flows all influence the heat budget (Wetzel, 2001). On the other hand, heat losses occur mainly by specific conduction of heat to the air, evaporation and outflow of surface waters (ibid.). Most of these processes occur at the water surface and wind patterns are the main driving force that distributes the heat in the lake water column. Lake surface and air surface temperatures should in principle be well coupled because they are connected by several elements of the heat budget, such as solar radiation, evaporation and precipitation. For instance, Powers et al. (2005) observed the following linear relationship between both temperatures for 9 lakes included in the initial

calibration of TEX_{86} in lakes: LST = 1.09 * SAT + 0.70, R^2= 0.95. According to this finding, large lakes would have a well coupled LST-air temperature. However, there are a number of complicating factors that might affect this coupling between water and air temperature (e.g. Webb and Nobilis, 1997; Tague et al., 2007):

- Water depth: the deeper a water body is, the higher the thermal capacity of the whole system will be. This can produce a two-way influence, i.e. the water temperature also affecting the air temperature. Furthermore, it could also give rise to a lagged response of the water temperature over the air temperature. Indeed, the higher specific heat of water compared to air gives rise to smaller variations of water temperature than those observed for air temperatures. In that sense, smaller lakes should in principle have better coupled water and air temperatures.

- Lake circulation: a parameter connected to the depth. Large lakes can develop a certain degree of internal circulation which can affect the temperature distribution in the water column.

- Lake surface inflows and outflows: the renovation of water in the lake system is also a parameter affecting the coupling of air and water temperature, as the heat budget is more complex. A particular case are the lakes affected by cold snow-melt discharges. Thus endorheic basins, where no surface inputs or outputs need to be accounted for, will have in principle a simpler relationship between air and water temperatures.

- Groundwater input: it is well known that groundwater-fed systems can deviate from the expected relationship between air and water temperature, due to the additional input in the heat budget that represent groundwater flows, which are usually colder and less sensitive to air temperature variability. This is typically occurring in lakes developed in karstic systems.

- Riparian vegetation: shading effect will restrict the solar radiation, an effect that might be relevant only in small lakes.

- Human impacts: water discharge from human sources can change the lake water temperature, usually to higher values.

As most of the lakes discussed in this study are shallow and small, circulation or water thermal inertia are not expected to be important factors. However there are a number of deeper lakes (5 lakes deeper than 20 m) and large lakes (7 lakes larger than 1 km^2). There are also some lakes located in karstic systems (see table 3.1); and some lakes are fed by snow-melt water and/or experience air temperatures (monthly means from the Iberian Climatic Atlas) slightly below 0 ºC (Estanya Gran, Gallocanta, Montcortès, Sanabria, Taravilla and Villarquemado). Thus some noise is expected in the air-water temperature relationship in our lake data set due to the high diversity of environments studied.

3.4. Results from Iberian lakes

3.4.1. Distribution of GDGTs and proxy indices

All lake sediments surveyed contained both isoprenoidal and branched GDGTs, but abundances widely differed. The percentage of branched GDGTs to the total abundance of GDGTs (branched and isoprenoidal) was highly variable in our lakes and ranged between 13% (Villarquemado) to 84% (Taray), with an average value of 51% and a median of 56% (see Figure 3.3). The BIT index in the studied lakes (see Appendix 2) averaged 0.77, with minimum and maximum values of 0.21 (Villarquemado and Manjavacas) and 0.99 (Sanabria), and a median of 0.85. The relatively high percentages of the branched GDGTs are not surprising, since most of the lakes are small and shallow and thus terrestrial material advected by runoff and streams will be relatively abundant compared to the in situ-produced isoprenoidal GDGTs. No trends were observed when relative or absolute abundances of branched GDGTs were compared with lake depth, lake surface and lake altitude. Unfortunately, catchment basin size is not available for the majority of the studied lakes and thus no comparison could be undertaken between the amount of soil-derived branched GDGTs in the sediments and size of the drainage basin.

TEX_{86} values in the Iberian lakes ranged from 0.10 (Alcahozo) to 0.83 (Zarracatín), with an average of 0.52 and a median of 0.53 (see Appendix 2). A high contribution of terrestrial organic matter is known to bias sometimes the TEX_{86} index via the introduction of isoprenoidal GDGTs advected from the soil. However, this effect will depend on the amount and distribution of isoprenoidal GDGTs that are washed from the soils, which can widely vary from site to site (Weijers et al., 2006b). The degree of correlation of TEX_{86} vs BIT might anyway be used as a first approximation to decipher whether TEX_{86} is being affected by the input of terrestrial organic matter in a site (ibid.). Figure 3.4 plots TEX_{86} values of Iberian Peninsula lakes against the proportion of branched GDGTs over total GDGTs found in sediments.

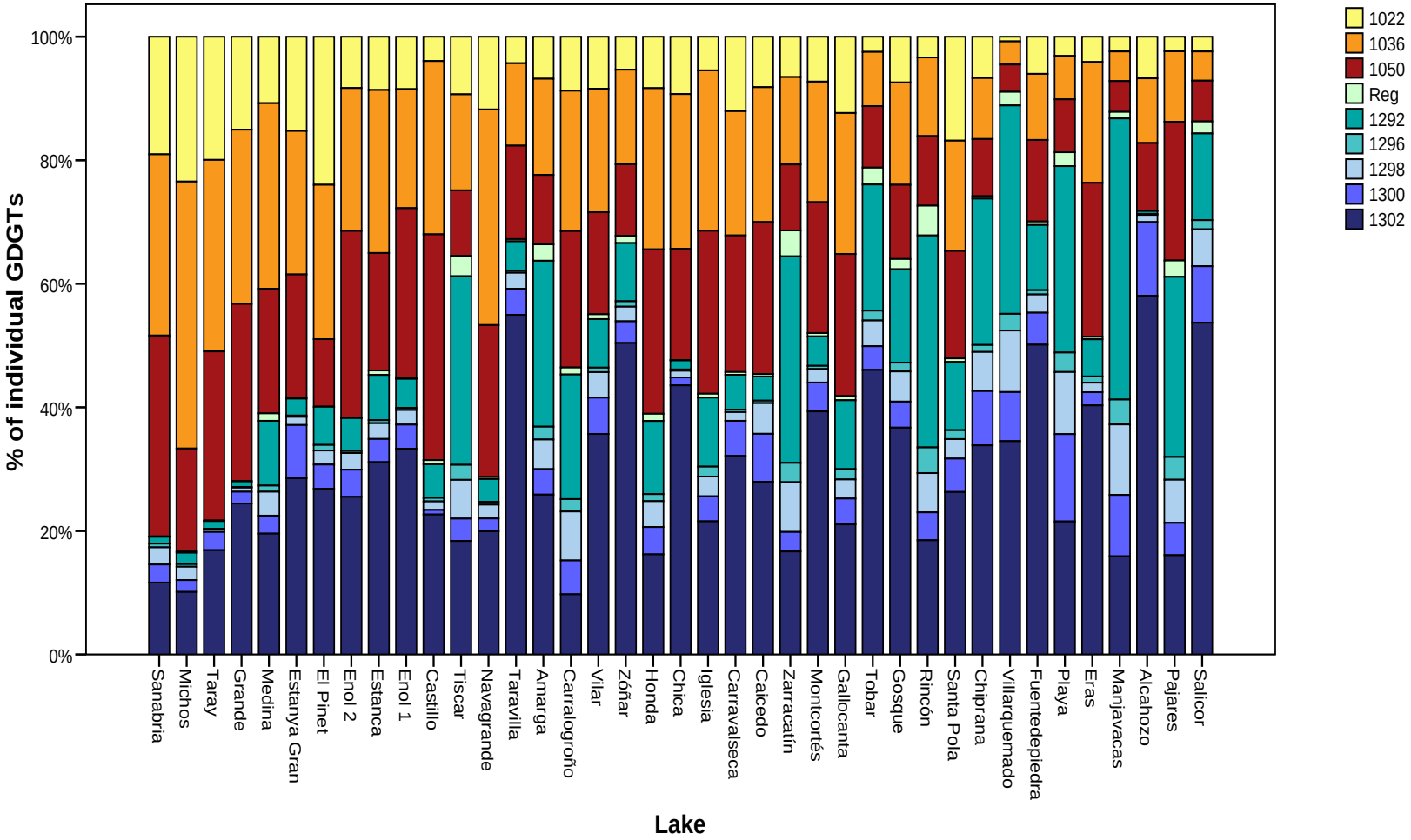

Figure 3.3 Relative abundances of GDGTs for the 38 Iberian lakes studied. GDGTs are identified with their *m/z*: 1022, 1036 and 1050 are branched lipids, while the rest are isoprenoidal GDGTs. Minor abundances of the terrestrial GDGTs with *m/z* 1048, 1046, 1034, 1032, 1020 and 1018 are not represented.

A visual inspection of Figure 3.4 reveals a cloud of points with TEX_{86} values between 0.4 and 0.8 and proportions of branched GDGTs between 0.15 and 0.85, and 5 points which show the lowest TEX_{86} values and have a variable proportion of GDGTs. A linear correlation between both variables is not significant (Sig. = 0.112) and therefore there is overall no evident effect of the relative terrestrial input on the TEX_{86} values. These five lakes characterized by the lower TEX_{86} values (< 0.30) are Carravalseca, Grande, Estanya Gran, Alcahozo and Taray. In fact, below a TEX_{86} of 0.25 (Estanya Gran, Taray and Alcahozo) the reconstructed lake surface temperatures (LST) would be negative. However, it is unlikely that in our Iberian lakes there is a signal of temperature below 0 ºC, since these are only reached in certain periods during winter.

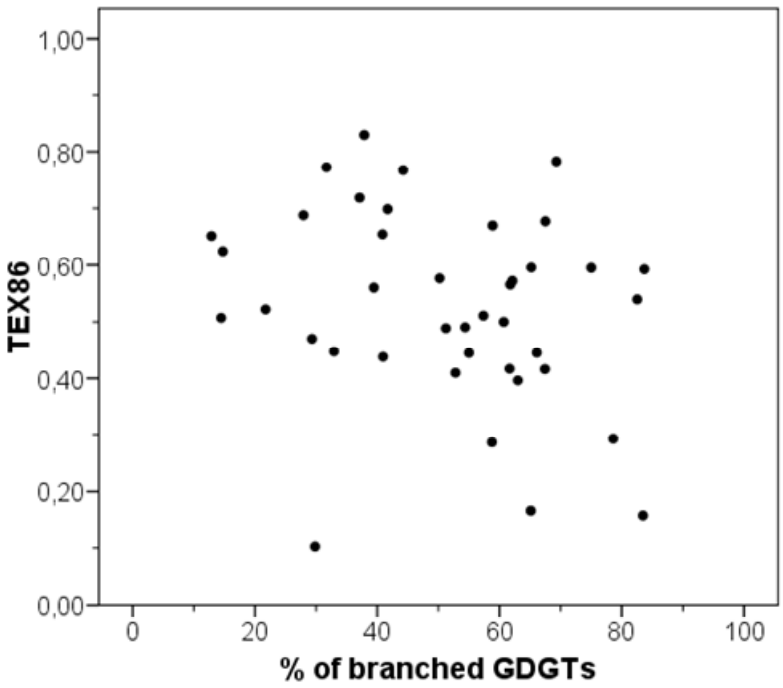

Figure 3.4 TEX_{86} values of Iberian lake surface sediments plotted versus proportion of branched GDGTs in the sediments.

A regression of TEX_{86} over the mean annual temperature (Atlas MAT, air temperature from the Digital Climatic Atlas) gave the equation $TEX_{86} = 0.182 + 0.024 * \text{Atlas MAT}$. Despite being significant in a statistical sense (P = 0.017), the relationship between both variables evidences considerable scatter ($R^2 = 0.14$). It also has a relatively high slope compared to the published lacustrine calibration, which is 0.017 (Powers et al., 2005).

This regression and a distribution of the residuals are shown in Figure 3.5. The 5 dots with the largest negative residuals (beyond -10 ºC) are ascribed again to lakes Carravalseca, Grande, Estanya Gran, Alcahozo and Taray. On the other hand, Carralogroño, Castillo, Pajares, Rincón, Tobar, Villarquemado and Zarracatín are the lakes with residuals larger than +10ºC. The regression with annual mean air temperatures gave a better correlation compared to seasonal mean temperatures, although the differences were small: the determination coefficients (R^2) were 0.12 (for spring and summer temperature) and 0.11 (for autumn and winter temperatures).

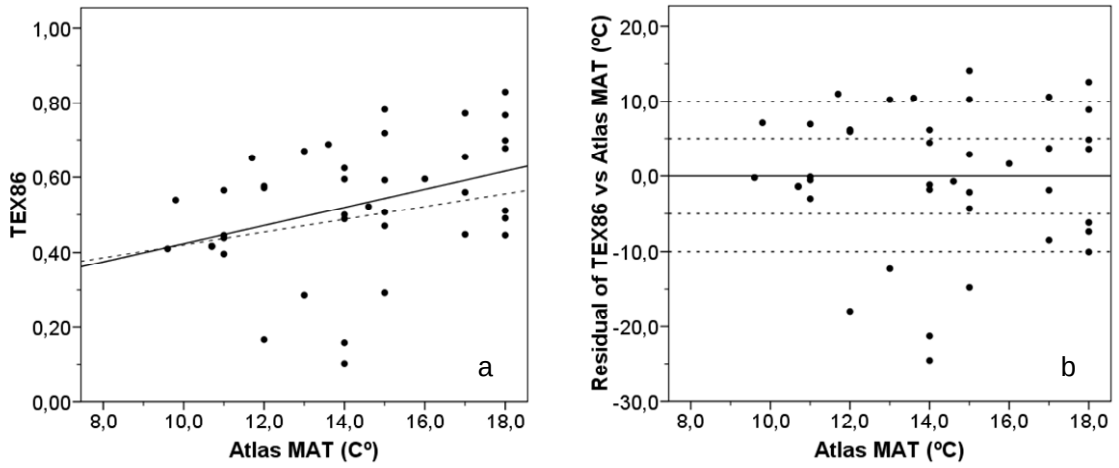

Figure 3.5 a) Linear regression of TEX_{86} over Atlas MAT. Determination coefficient is R^2= 0.14 (P = 0.017). Dashed line corresponds to the lacustrine calibration for TEX_{86} (Powers et al., 2005) and is plotted for comparison; b) distribution of residuals of TEX_{86} vs Atlas MAT. Residuals are represented in temperature units using calibration in Powers et al. (2005).

In our Iberian lake data set, MBT has a mean value of 0.21, a median of 0.20 and minimum and maximum values of 0.06 (Castillo) and 0.47 (El Pinet), respectively. CBT has a mean value of 0.58, a median of 0.53 and minimum and maximum values of 0.09 (Villarquemado) and 1.52 (Michos), respectively (see Appendix 2). These two indices are combined to derive an estimation of mean annual temperature (MAT_{est}). Figure 3.6 shows the relationship between the MAT_{est} and Atlas MAT, as well as the distribution of the residuals. The regression shows that only 9% of the MAT_{est} data can be explained by the Atlas instrumental mean annual temperature and the significance is very low (P = 0.060). The scatter is considerable and it is interesting to note that the MAT_{est} is always colder than the the digital Atlas MAT. The differences range from 6 to 29 ºC with an average of 15 ºC. It is also worth pointing out the high variability of MAT_{est} for groups

of lakes that would have in principle the same mean annual air temperature, especially the groups at 12, 15 and 18 ºC. There are clearly other factors than temperature affecting the estimated MAT, since only 12 of the 38 surveyed lakes have positive estimated mean annual temperatures.

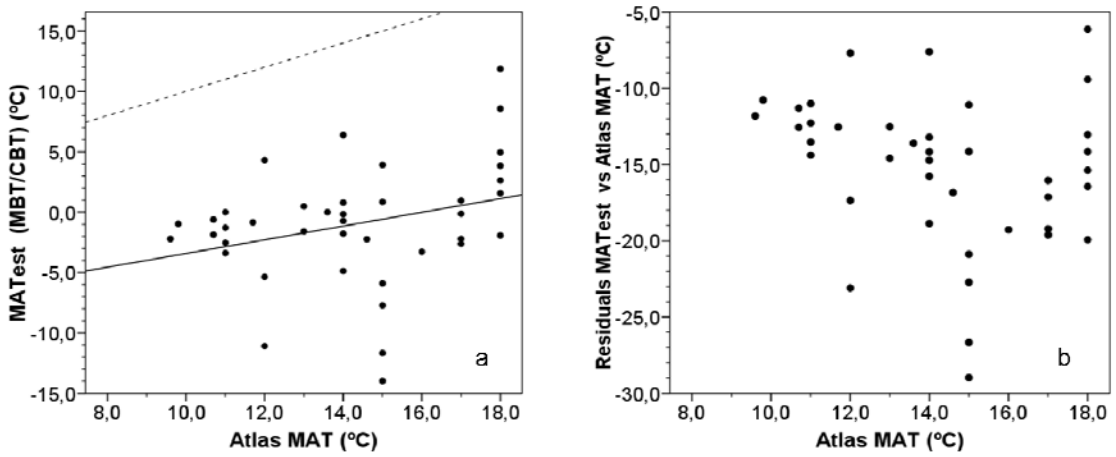

Figure 3.6 a) Linear regression of estimated MAT (MBT/CBT) over digital Atlas instrumental MAT; dashed line corresponds to the 1:1 relationship and is shown for comparison. b) Distribution of residuals vs. Atlas MAT.

According to literature, the best estimation of mean annual temperature using the GDGT distribution is derived from the indices MBT and CBT, which together are able to explain about 77% of the variability in the soil calibration data set (Weijers et al., 2007b). However, there is no calibration of these indices in sediments from lacustrine environments. In order to test whether the unreliable MAT_{est} was produced by a different relationship of MBT/CBT and MAT in Iberian lakes, we performed a multiple regression using both indices as predictor variables. In our data set of 38 lakes from the Iberian Peninsula, MBT and CBT together are able to explain 18.6% of the mean annual temperature variability (multiple linear regression, $P = 0.024$), but CBT is not significant as a predictor variable ($P = 0.600$).

Finally, in this initial description of GDGT distributions in the Iberian lake sediments, estimated LST and MAT_{est} were compared. Figure 3.7 shows the relationship of both reconstructed parameters, where two trends can be observed. One of decreasing estimated LST concomitant with increasing MAT_{est}, opposite as what could be expected,

with lakes Castillo, Pajares, Carravalseca, Grande, Estanya Gran and Taray clearly following this trend (blue slashed line in Figure 3.7). Interestingly, from these lakes, Castillo and Pajares are also the lakes with largest differences of MAT_{est} vs Atlas instrumental MAT, while the other four lakes are the ones with higher residuals of TEX_{86} vs Atlas MAT. A second trend in the data could be that of coupled increase of both reconstructed temperatures, easier to explain, although the scatter is considerable (red slashed line in Figure 3.7).

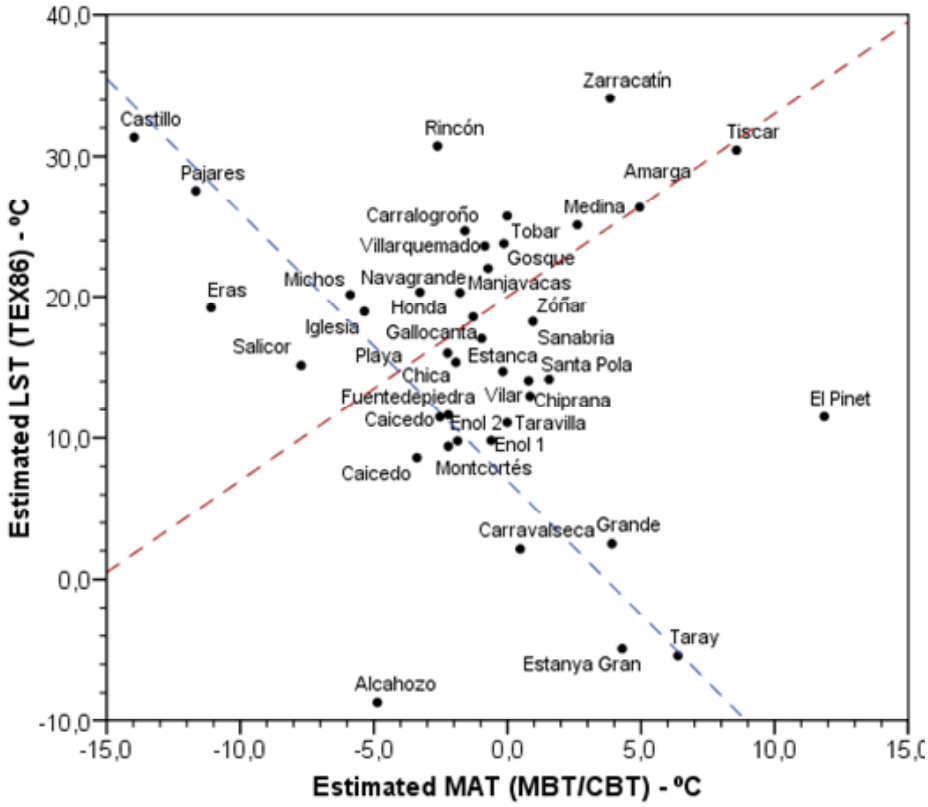

Figure 3.7 Estimated lake surface temperature (LST) from TEX_{86} vs estimated mean annual temperature (MAT_{est}) from MBT and CBT indices.

It is clear from these results that other factors aside from temperature are influencing the distribution of the GDGTs in the lake sediments. The proxies proposed so far based on these GDGTs have a limited applicability in the set of lakes studied unless the dispersion of the data can be explained. Thus, the following paragraphs are aimed to go deeply into the relationships between the GDGT distribution and the limnological data gathered.

3.4.2. Results from Principal Component Analysis

The principal component analysis (PCA) was applied to the normalised and autoscaled abundances of 15 GDGTs (15 initial variables) in the lake data set in order to reduce the amount of variables explaining the distribution of the data. The Kaiser criterion (Kaiser, 1960) and *scree* test (Cattell, 1966) were used to select the number of principal components (PC) to extract. The first method proposes to extract only the PCs with eigenvalues greater than 1, which are those that explain more variance than any initial variable. According to this, 4 components should be extracted (see Figure 3.8). Instead, the *scree* test is a graphical method that proposes to extract components with successively lower eigenvalues until the steep slope of decreasing eigenvalues levels off. According to this test, 6 PCs should be extracted (see Figure 3.8). As a compromise between Kaiser criterion and *scree* test, 5 PCs were extracted, which after the Varimax rotation were able to explain 90.9% of the total variance associated to the initial data, i.e. the distribution of the 15 GDGTs studied in the lake sediments (see Table 3.2). Although the amount of extracted PCs suggests that there is a complex group of factors determining the distribution of the GDGTs, half of the initial variance could be explained using only the first 2 principal components.

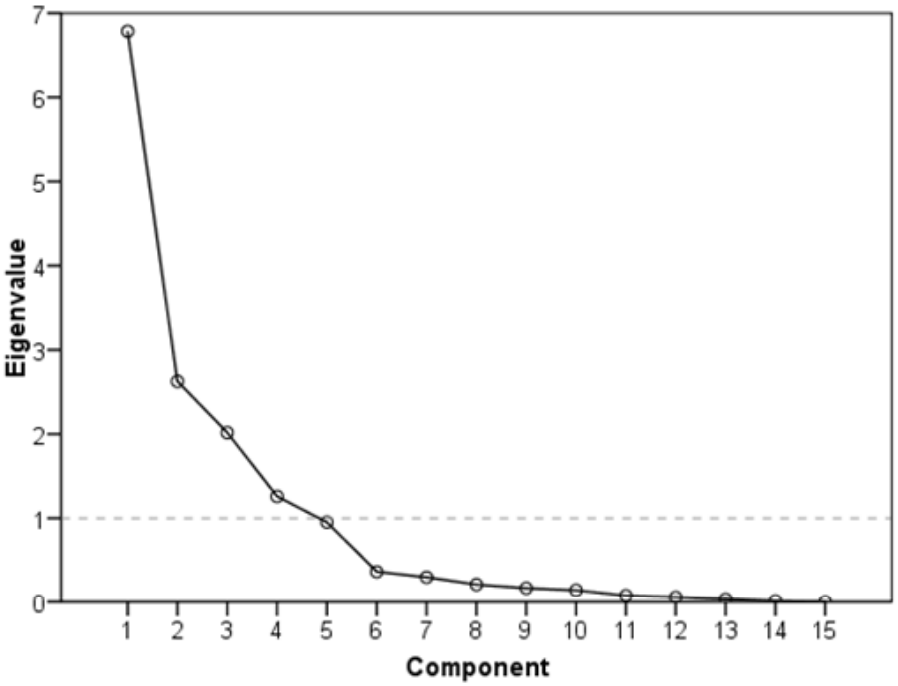

Figure 3.8 Plot of eigenvalues for the components of the Principal Component Analysis. As a compromise between Kaiser criterion and *scree* test, the first 5 components were extracted.

Total variance explained		Rotation sums of squared loadings	
Principal Component	**Total variance (eigenvalue)**	**Total % of variance**	**Cumulative %**
1	4.3	28.4	28.4
2	3.5	22.8	51.2
3	2.4	16.2	67.4
4	1.9	12.8	80.2
5	1.6	10.8	90.9

Table 3.2. Total variance explained by the 5 extracted principal components in the PCA. Initial data set included the normalised and autoscaled concentrations of the 15 GDGTs studied. The solution was rotated using the *Varimax* method.

Some information about the physical interpretation of each extracted component can be drawn from the loadings of the initial variables onto these extracted PC. These loadings are the multipliers of the original variables in the new vectors, with an absolute magnitude proportional to the importance of the original variables in defining the PC. The initial variables with absolute loadings larger than 0.5 are typically considered relevant. Figure 3.9 shows the distribution of the loadings; each panel corresponds to one of the 5 PCs extracted after the *Varimax* rotation process.

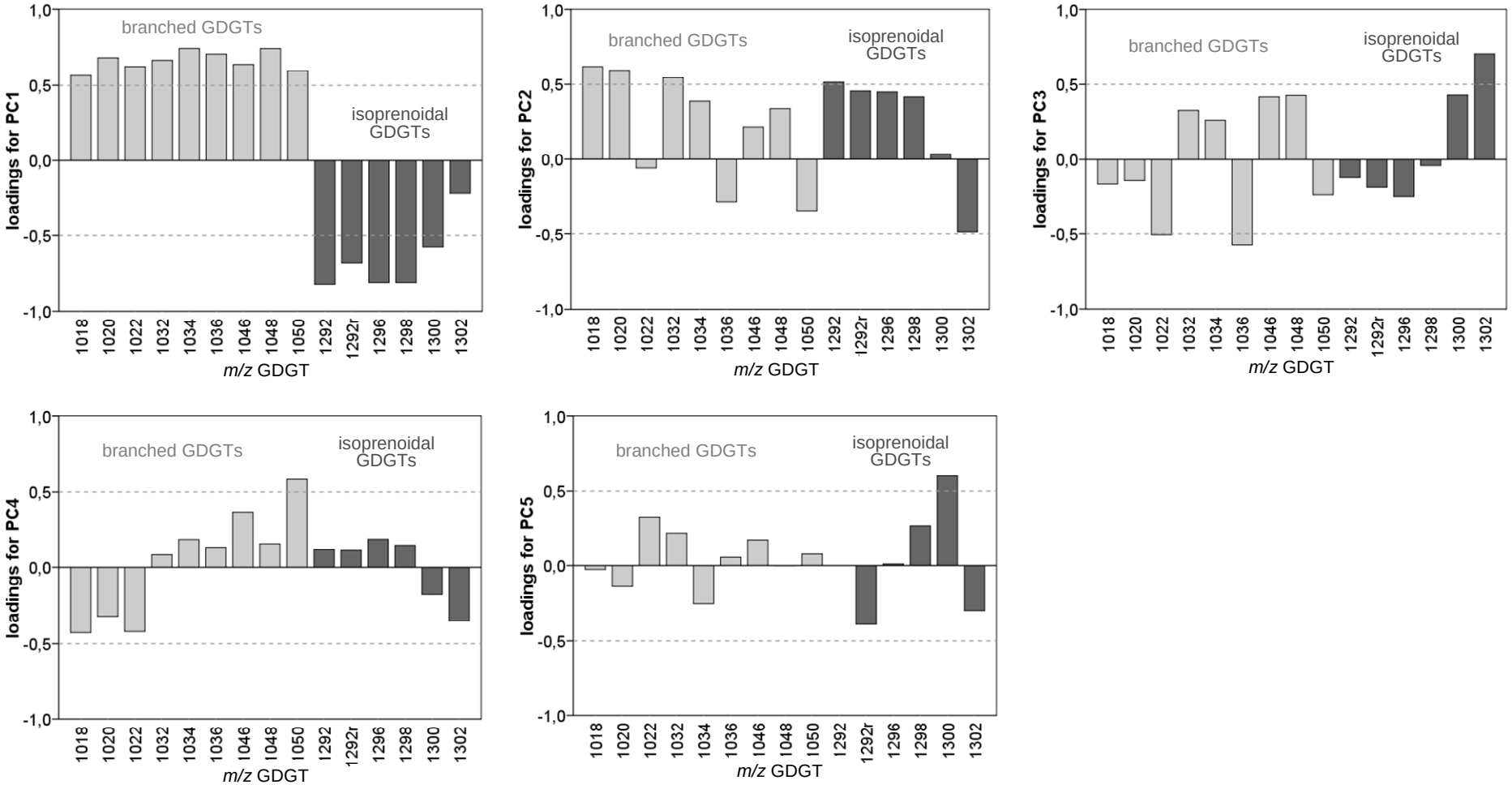

Figure 3.9 Loadings of the initial variables (normalised and autoscaled concentrations of the 15 analysed GDGTs) for the 5 extracted principal components. Slashed lines show reference values for loadings at 0.5 and -0.5. The *m/z* 1292r refers to regioisomer of crenarchaeol.

Principal Component 1 (Figure 3.9) shows a distribution of loadings which makes a clear distinction between soil GDGTs (those with m/z between 1018 and 1050) and GDGTs presumably synthesized within the lake but with possible contribution from the soil environment (m/z between 1292r-1302). This distinction can be readily observed from the sign of the loadings (positive vs negative) and interestingly, all loadings are above 0.5. An exception is 1302, with a very low loading, which can be explained because this GDGT is known to occur in high abundances in soils (e.g. Weijers et al., 2006b). Thus, PC1 seems to be related to the origin of the GDGTs, terrestrial vs lacustrine. It is not surprising, then, that it has a high linear correlation with the index BIT as they are both providing the same information (see Fig. 3.10a). The PC1 also shows a significant correlation with TEX_{86} (see Figure 3.10b), although large residuals are associated to the dots belonging to lakes Alcahozo, Taray, Estanya Gran, Grande, Michos and Castillo. The first four have also large residuals for the regression of TEX_{86} vs Atlas MAT (see Figure 3.5) and Castillo has a large residual for the regression MAT_{est} vs Atlas MAT (see Figure 3.6).

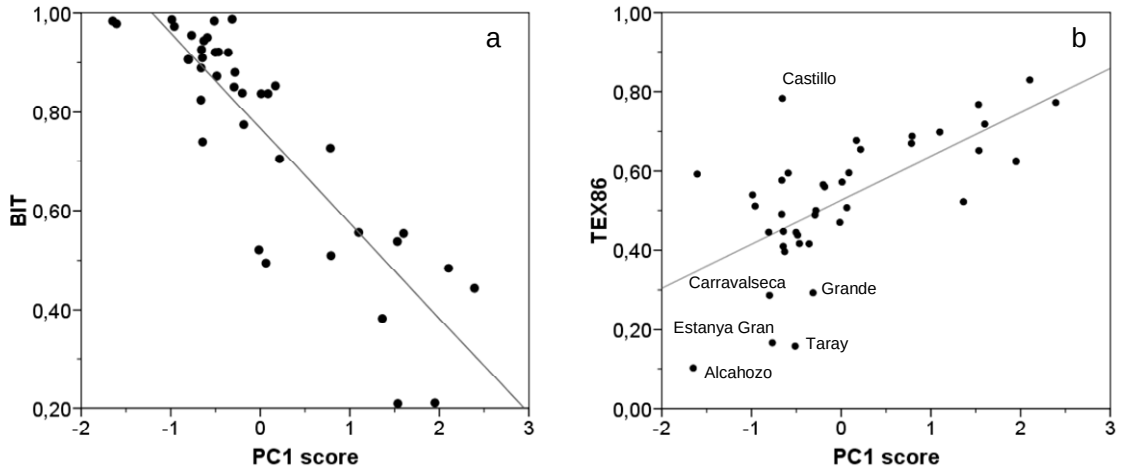

Figure 3.10 Correlation of a) index BIT vs principal component 1 scores and b) index TEX_{86} vs principal component 1 scores. PC1 explains 28.4% of the total variance in the initial data set (relative distributions of the GDGTs) and probably reflects soil *vs* lacustrine origin of GDGTs. The linear regressions with BIT and TEX_{86} have determination coefficients of R^2= 0.76 (Sig. < 0.001) and 0.43 (Sig. < 0.001), respectively.

The main characteristic of Principal Component 2 (Figure 3.9) is the connection between the sign of the loadings and the cyclization of the GDGTs. Positive loading values correspond to GDGTs with internal cycles, while non-cyclized GDGTs (those

with *m/z* 1302, 1050, 1036 and 1022) have negative values. That explains that CBT, which was designed as an index of Cyclization of Branched Tetraethers, is correlated to the PC2 (linear regression coefficient R^2 = 0.40, Sig. < 0.001). Thus, this PC is suggested to be related to the cyclization of the GDGTs, with probably an influence of the lipid mass for non-cyclized GDGT, since their loading values are more negative at increasing mass.

Regarding Principal Component 3, the loadings suggest important contribution from GDGTs with *m/z* 1302, 1050 and 1036, again lipids without cyclization (Figure 3.9). This PC has a high correlation with the index MBT and consequently as well with the estimated MAT (Figure 3.11), with determination coefficients of 0.82 (P < 0.001) and 0.76 (P < 0.001), respectively.

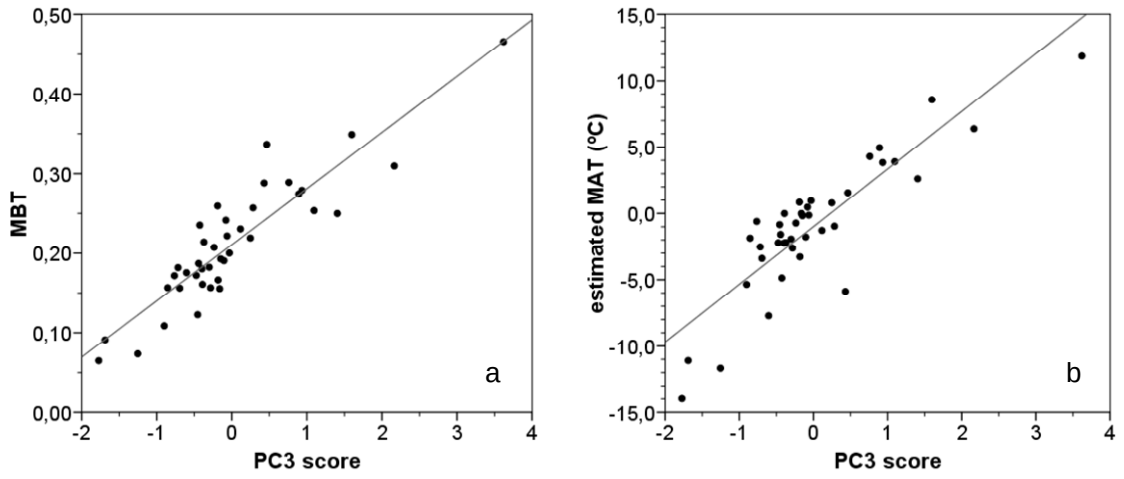

Figure 3.11 Correlation of a) index MBT with principal component 3 scores and b) estimated MAT (derived from MBT and CBT) with PC3 scores. PC3 accounts for 13.6% of the total initial variance (distribution of normalised GDGTs).

The distribution of loadings for the Principal Component 4 (Figure 3.9) suggests that only the branched GDGT with *m/z* 1050 is important in defining this PC. However, it can also be noted the negative sign of loadings for the peripheral masses, opposite to the positive loading values for intermediate masses. This suggests the existence of a factor related to the lengths of the carbon chains, although the cause remains still elusive, since no significant correlations were found with the limnological parameters tested.

The last principal component extracted, PC5, shows a very high loading for GDGT with *m/z* 1300, followed by the *m/z* 1292r, 1022 and 1302. The highest correlation of the PC5 scores was with the total dissolved solids of the lakes, with a linear regression accounting for 35% of the variability (see Figure 3.12).

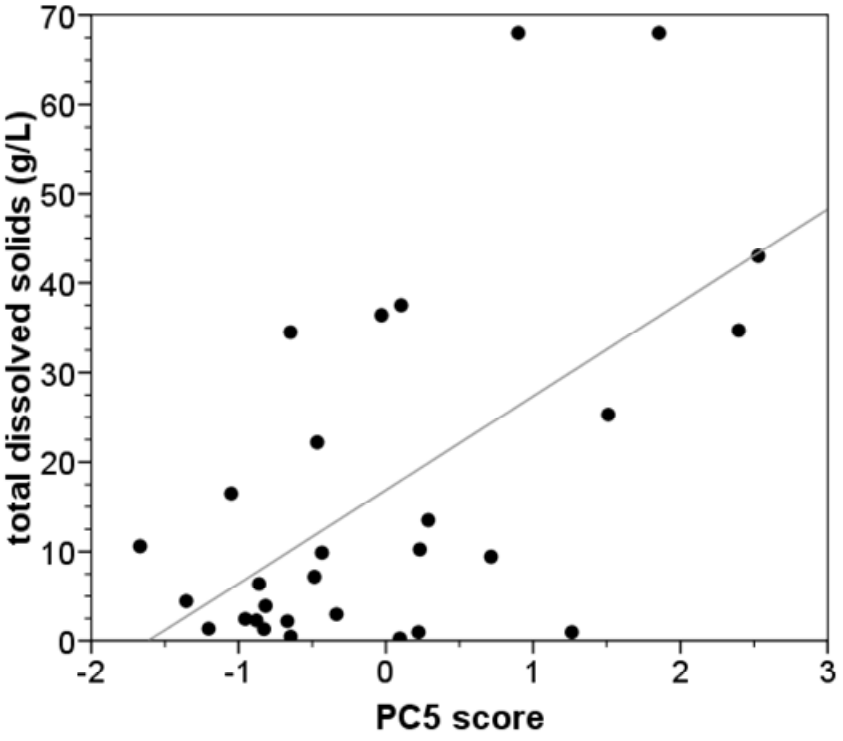

Figure 3.12 Correlation of total dissolved solids with principal component 5 scores. PC5 accounted for 10.8% of the total initial variance in the relative distribution of GDGTs. The linear regression has a determination coefficient of $R^2 = 0.35$ ($P = 0.001$).

As previously mentioned, in our data set of 38 lakes from the Iberian Peninsula, MBT and CBT together are able to explain 18.6% of the Digital Atlas instrumental mean annual temperature variability (multiple linear regression, $P = 0.024$), but CBT is not significant as a predictor variable ($P = 0.600$). We tested a multiple regression using PC2 and PC3, which are by definition independent of each other and have been shown to be correlated to CBT and MBT, respectively. The combination of both PCs is able to explain 37.6% of the Atlas MAT variability, and both predictor variables are significant. Table 3.3 shows the correlations that are obtained when all the extracted PCs are used and successively withdrawing the PCs with less significance.

Multiple regression of PCs with Atlas MAT			
Predictor variables	**R^2**	**Standard error of estimation**	**Significant variables**
PC1, PC2, PC3, PC4, PC5	0.56	1.9 ºC	all except PC 4
PC1, PC2, PC3, PC5	0.52	1.9 ºC	all
PC1, PC2, PC3	0.46	2.0 ºC	all
PC2, PC3	0.38	2.1 ºC	all
PC3	0.20	2.4 ºC	all

Table 3.3 Multiple regressions for estimating Atlas mean annual temperature (Atlas MAT) using the principal components as predictor variables. Each line is obtained withdrawing the PC with less significance from the previous regression. All regressions are significant at $P < 0.001$.

According to the results shown in Table 3.3, the four PCs that are significant predictor variables for estimating Atlas MAT can explain approximately half of the data variability. This suggests that temperature is not among the main factors influencing the distribution of GDGTs in the Iberian lakes surveyed. However, a certain degree of prediction can be achieved studying the degree of methylation (related to PC3), cyclization (related to PC2), and the relative abundances of branched vs isoprenoidal structures of the fossil GDGTs accumulated in the sediments (related to PC1). On the other hand, as the lakes surveyed have remarkably different characteristics (see Table 3.1) it is worth attempting to distinguish sites with favourable characteristics for GDGT-based climate studies. This objective is explored in the following section.

3.4.3. Results from Hierarchical Cluster Analysis

Our aim is to explore how the GDGTs distribution in lakes from Iberia can be used in order to reconstruct temperatures. Direct application of the published GDGT indices has proven to have a limited applicability in the set of studied lakes (section 3.4.1) and PCA analysis has shown that mean annual temperature can be better predicted using the principal components extracted from the normalised concentrations of the GDGTs (section 3.4.2). In order to see whether a set of lakes with common variables are more suitable to reconstruct temperatures, we performed a hierarchical cluster analysis (HCA) to group the lakes with similar characteristics and appraised their TEX_{86} and estimated

MAT distribution. Eight different cluster analyses were performed (see section 3.3.2), and between 4 and 8 clusters were produced in every analysis, depending on the dendrogram obtained (the complete suite of dendrograms can be found in Appendix 2). In cases when the value of the clustering criterion was not available for a lake, this was not included in the cluster analysis. Figure 3.13 shows the correlation of TEX_{86} vs Atlas MAT for the Iberian lakes grouped by clusters.

a) Chemical variables (single linkage)

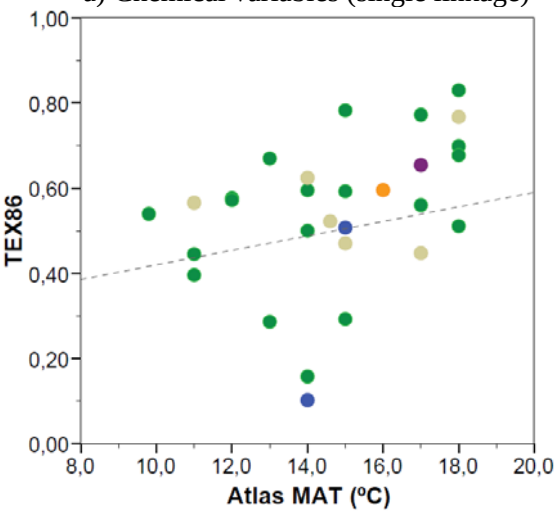

b) Chemical variables (complete linkage)

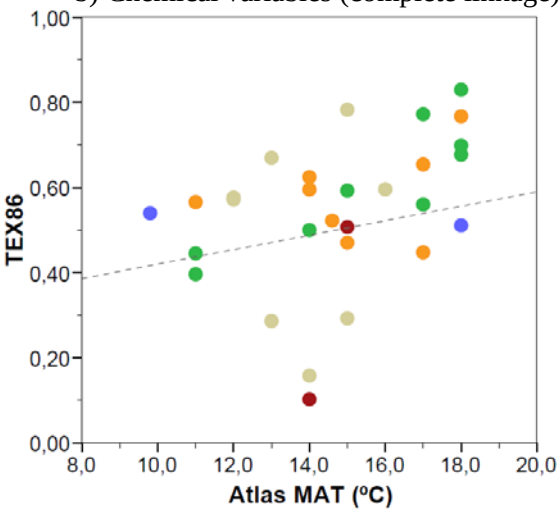

c) Morphological variables (single linkage)

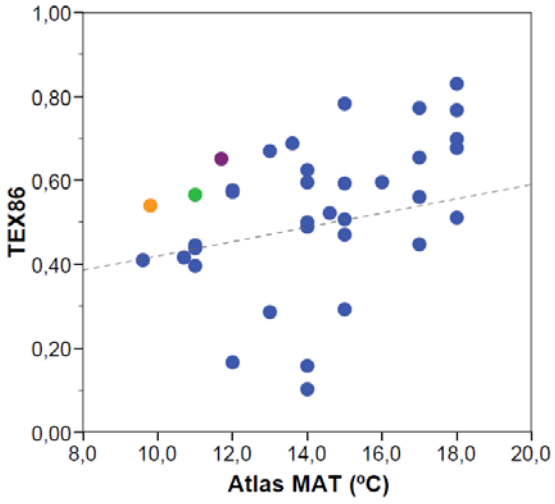

d) Morphological variables (complete linkage)

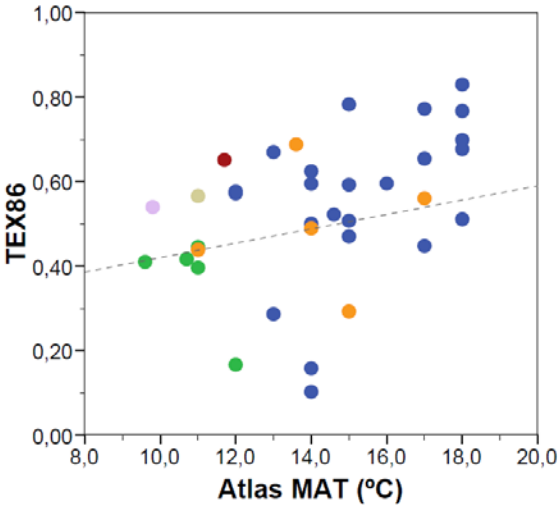

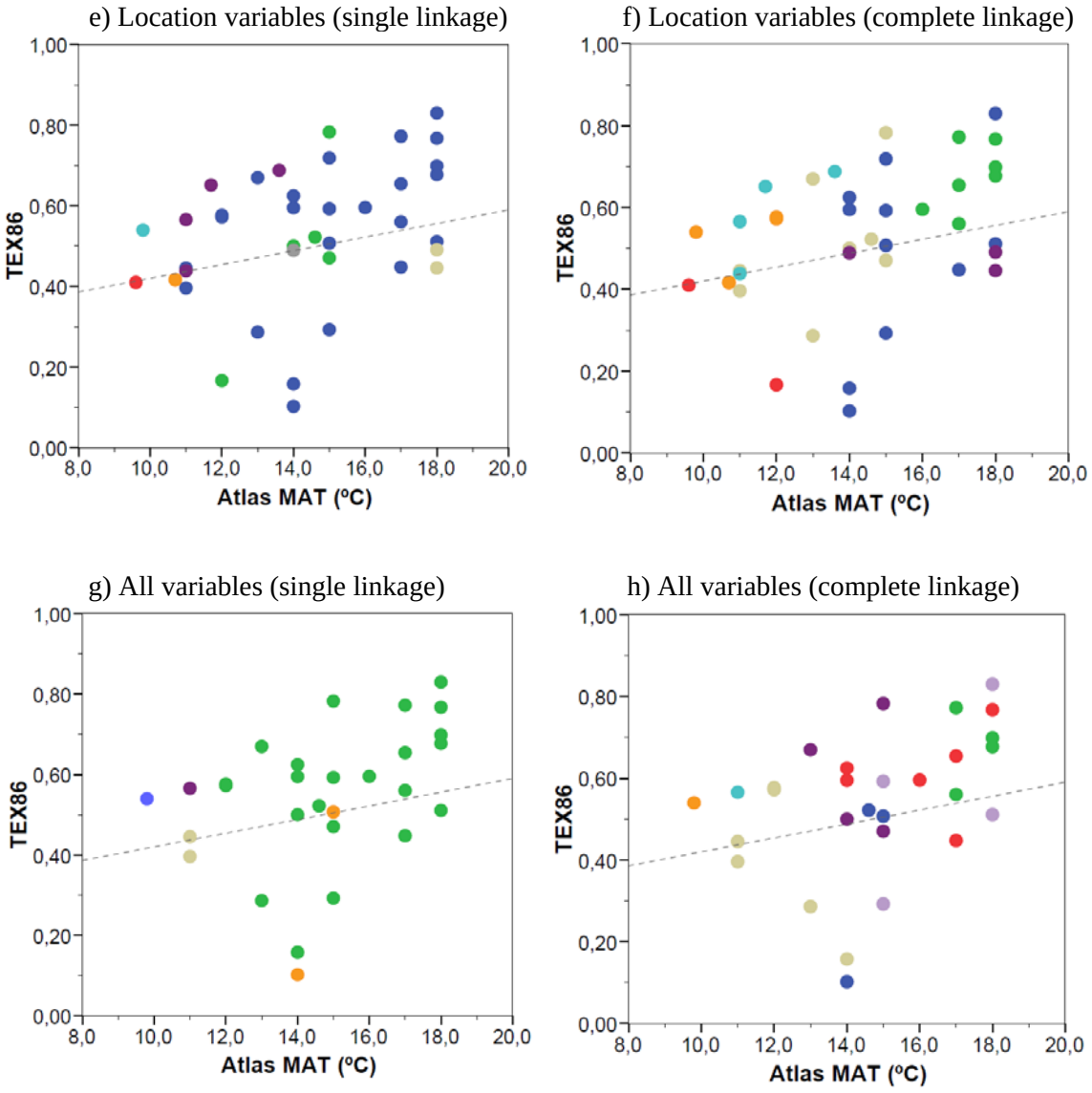

Figure 3.13 Correlations of TEX_{86} vs Atlas MAT for the Iberian lakes coloured according to the cluster they belong. Results are shown for eight different hierarchical cluster analyses performed: **a)** HCA, single linkage, chemical variables; **b)** HCA, complete linkage, chemical variables; **c)** HCA, single linkage, morphological variables; **d)** HCA, complete linkage, morphological variables; **e)** HCA, single linkage, location variables; **f)** HCA, complete linkage, location variables; **g)** HCA, single linkage, all variables; **h)** HCA, complete linkage, all variables. Dashed line is the lacustrine calibration by Powers et al. (2005) for reference.

Visually inspecting the plots does not reveal a particular cluster with lakes performing better in the correlation of TEX_{86} against Atlas MAT from which to derive a lacustrine calibration. Clustering using single linkage and chemical variables did not clearly differentiate groups with large/small residuals. Using complete linkage, however, there was one cluster that showed a rather high linear distribution (green dots, Figure 3.13b).

This cluster is comprised by lakes with relatively low conductivity values (<10 microS/cm), low total dissolved solids (< 7 g/L) and slightly basic pH (7-8.5). A linear regression with these 9 points gave a slope of 0.045 with a determination coefficient of R^2 = 0.77 (P = 0.002). These lakes are Amarga, Caicedo (2 samples), Estanca, Medina, Michos, Rincón, Zarracatín and Zóñar. In this plot it is also noticeable the different performance of two lakes clustered together (red dots, Figure 3.13b), which are the two most saline lakes, Salicor and Alcahozo, with the highest values of total dissolved solids (around 65 g/L) and conductivity (over 100 microS/cm). Salicor is close to the calibration line while Alcahozo plots far away. Chemical variables are the ones for which more missing values for lakes could be counted, and so several lakes were not considered in this analysis.

When morphological variables (depth and area) were used as clustering criteria, single linkage method produced one dominant cluster joining virtually all lakes. The only three exceptions are lakes that formed each one a cluster and correspond to Sanabria, the deepest lake, and Gallocanta and Villarquemado, which are the two largest lakes by far in the data set. Thus, the big cluster grouped relatively shallow and small lakes. This clustering suggests that the analysis is highly influenced by the extreme values in the depth and surface distribution. Complete linkage method with the same morphological variables produced a pattern in which two closely-related clusters contained the lakes with lowest residuals with the TEX_{86} calibration line (green and orange dots in Figure 3.13d). These two clusters comprise the 9 deepest lakes of our data set (except for Sanabria) with maximum depth values between 11 and 30 m: Caicedo, Enol, Estanya Gran, Montcortès, Grande, Taravilla, Tobar, Vilar, Zóñar. However, three of these lakes are not fitting the calibration line, namely Estanya Gran, Grande and Tobar.

When clustering was applied following geographical location criteria (latitude, longitude and altitude), single linkage produced several small clusters and one large cluster (Figure 3.13e). Only three individual clusters are on the calibration line (orange, red and gray dots) and correspond to lakes Enol, Montcortés and Vilar. Enol and Montcortés are mountain lakes and both located at high latitudes. El Vilar is also a lake of high latitude and located in the most eastern position among all lakes. Complete linkage method with the same location criteria gave again a pattern not easily related to

the distribution of residuals of TEX_{86} vs MAT (Figure 3.13f). Finally, including all the variables produced a large cluster using single linkage method. Only one cluster, comprising lake Caicedo (double sample, gray dots in Figure 3.13g) falls on the calibration line. This lake stands out for his depth after Sanabria. In this classification, again lakes Alcahozo and Salicor (orange dots) are grouped together due to their high conductivity and dissolved solids, but only Salicor fits the calibration, as previously mentioned. The complete linkage method using all variables aggregates la Playa lake with these two saline lakes, as it is the next lake with high values in conductivity and total dissolved solids, and is fitting quite well the calibration line. The other clusters have no apparent relationship with the residual distribution of TEX_{86} vs MAT.

Figure 3.14 shows the correlation between estimated MAT (MBT/CBT) and Digital Atlas MAT for the Iberian lakes, using the same clusters mentioned above. Several cluster analysis produced again one large cluster (see panels a, c, d, e and g in Figure 3.14). From these, the clustering using location variables and single linkage has an interest, since grouping 5 clusters together comprising only 9 points gives a slope similar to the 1:1 relationship between estimated and Atlas instrumental MAT (red, light blue, dark purple, light purple and orange dots in Figure 3.14e). These lakes are Gallocanta, Montcortès, Sanabria, Vilar, Taravilla, Villarquemado, Tobar, and Enol (2 smaples). It is worth mentioning that three of these lakes (Enol, Montcortès and Vilar) were the best-fitting to the TEX_{86} vs MAT regression when the same cluster classification was used (see Figure 3.13e). The most common feature in these 8 lakes is the high altitude (all except for lake Vilar are above 900 m), and several (Enol, Vilar, Montcortès and Sanabria) are located north of 42º N, and therefpre span a narrow range of mean annual temperatures, between 9.5 and 14 ºC.

Other classifications can reveal some structure on the controls on GDGT distribution. For instance, clustering for chemical variables using a complete linkage method (Figure 3.14b) yielded one cluster of 8 lakes roughly following a linear trend with a slope of 0.84 (green dots, linear regression $R^2 = 0.44$, $P = 0.05$). These lakes are the same ones selected as best-fitting the TEX_{86} *vs* MAT linear relationahip using the same clustering (see Figure 3.13b), and are characterized by low conductivity and total dissolved solids values. These lakes are Caicedo, Amarga, Estanca, Medina, Michos, Rincón, Zarracatín

and Zóñar. Clustering for location and employing the complete linkage method suggested no relationship between geographical location and response of estimated MAT (see Figure 3.14f). Finally, clustering with all variables and complete linkage gave again clouds of points with no suggested linear response to Atlas instrumental MAT. However, it is interesting to note that one cluster in this analysis has three of its four cases distributed in a nearly perfect linear trend (purple dots, Figure 3.14h). This cluster includes Carralogroño, Castillo, Chiprana and Estanca, all relatively shallow lakes from Ebro basin, with moderate basic pH (7.5-8.5) and all located below 500 m in altitude. Estanca is the lake which does not follow the linear trend, and the differences we can observe are that it is the largest lake and the one containing less dissolved solids and having lower conductivity values among the lakes of this cluster.

a) Chemical variables (single linkage)

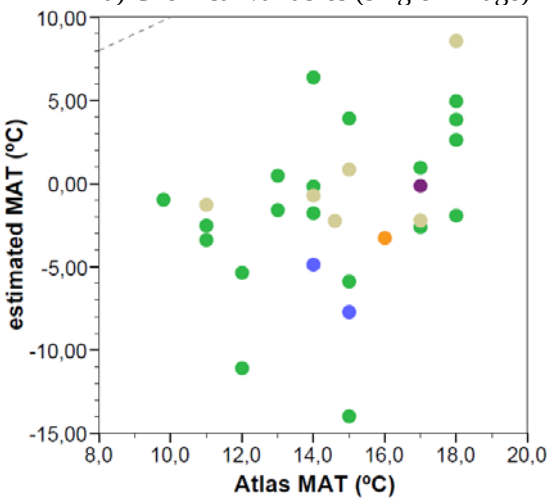

b) Chemical variables (complete linkage)

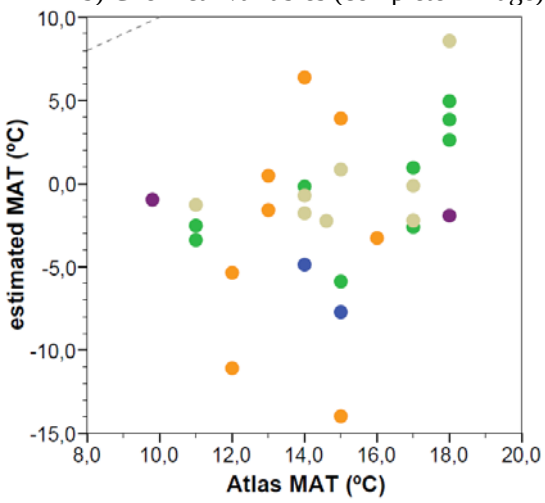

c) Morphological variables (single linkage)

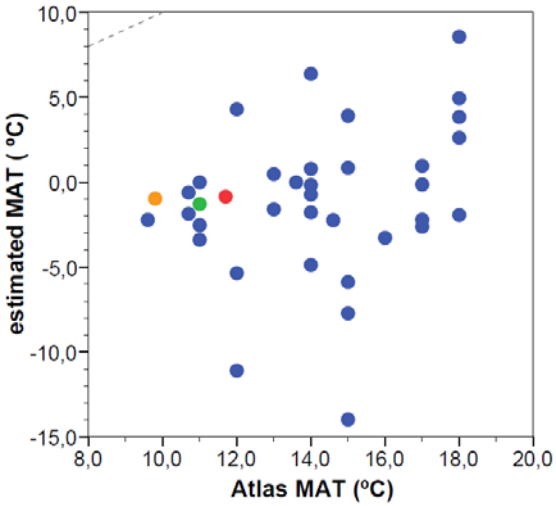

d) Morphological variables (complete linkage)

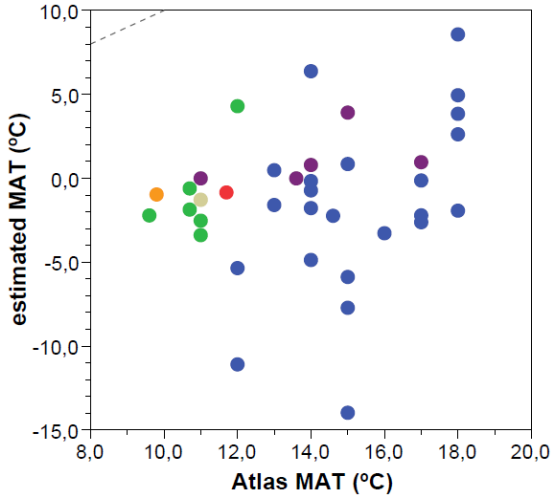

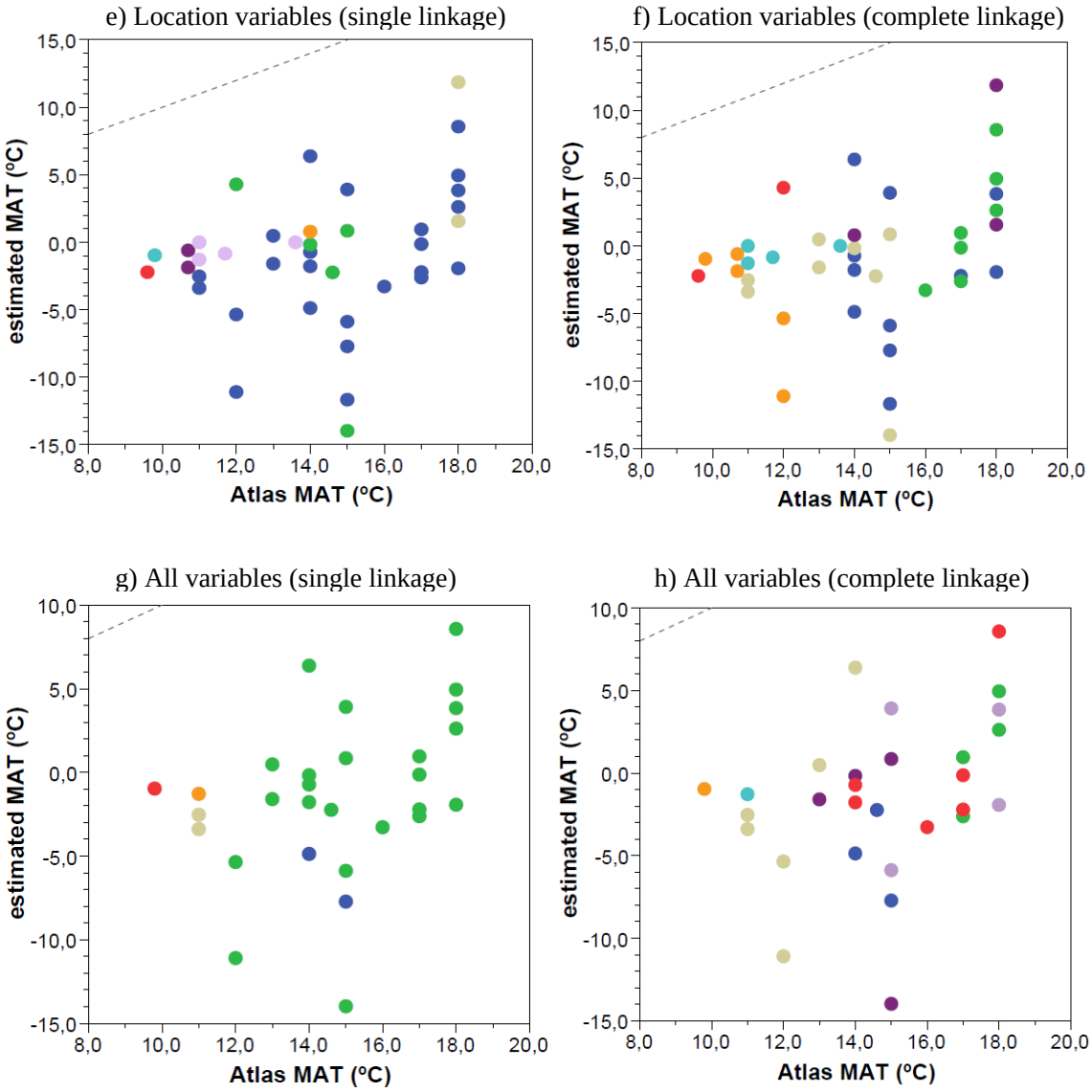

Figure 3.14 Correlations of estimated MAT (MBT/CBT) vs Atlas instrumental MAT for the Iberian lakes grouped according to the cluster they belong. Results are shown for eight different hierarchical cluster analyses performed: **a)** HCA, single linkage, chemical variables; **b)** HCA, complete linkage, chemical variables; **c)** HCA, single linkage, morphological variables; **d)** HCA, complete linkage, morphological variables; **e)** HCA, single linkage, location variables; **f)** HCA, complete linkage, location variables; **g)** HCA, single linkage, all variables; **h)** HCA, complete linkage, all variables. Dashed line is the 1:1 relationship and is shown for reference.

3.4.4. Comparison of Iberian lakes with other lacustrine sites

At present, TEX_{86} values combined with mean annual surface temperature have been published for 29 lakes (Powers, 2005; Blaga et al., 2009). Since this data set includes lakes with a worldwide distribution, the range of lake surface temperatures covered is large, from 2 ºC (Silsersee, Europe) to 28 ºC (Lake Turkana, Africa). We can add now the results of a regional data set from this study in the Iberian Peninsula (see Figure 3.15a), for which mean annual air temperatures (Atlas MAT) are available and cover the range 9 to 18 ºC.

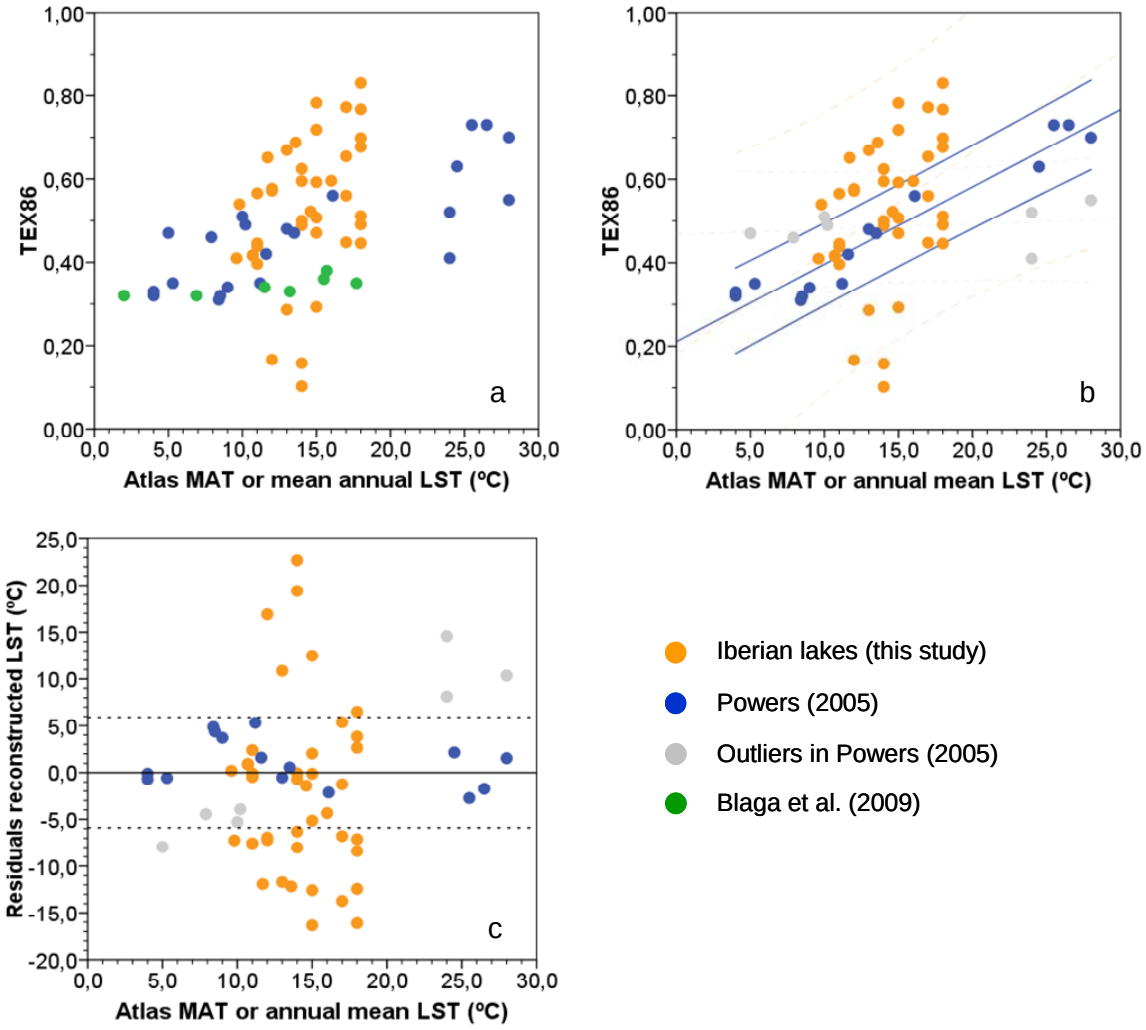

Figure 3.15 a) Comparison of TEX_{86} *vs* Atlas MAT for the Iberian lakes (this study, orange dots) and versus annual LST for lakes in Powers (2005) (blue dots) and in Blaga et al. (2009) (green dots); **b)** same plot without Blaga et al. (2009) distinguishing the outliers (gray dots) as considered in Powers (2005) and 95% confidence interval for the regression of accepted points in Powers study; **c)** residuals of all lakes referred to the calibration line in panel b, where dashed lines indicate 95% confidence interval as in panel b.

It is interesting to note that once the lakes are combined there is still a lack of data from 18 to 24 ºC. Furthermore, our lake data have a comparatively very large dispersion of TEX_{86} values given the narrow temperature window considered. However, the data available from Blaga et al. (2009) includes only those lakes that the authors considered suitable to include in the lake calibration because they had relatively low BIT values (<0.4) and a low probability of containing GDGTs of methanogenic source, which reduced the data set from 47 to 7 lakes. Conversely to our data from Iberian lakes, the lakes from Blaga et al. study show relatively invariable TEX_{86} despite the wide range of annual mean LST associated to the data set. Figure 3.15b further distinguishes the data points which were considered outliers in Powers (2005) (gray dots) due to unrealistic TEX_{86}-derived temperatures compared to the reference mean annual LST. This panel also shows the 95% confidence interval of the regression of the 16 accepted points in Powers study, which shows that the dispersion of results is relatively large, since it comprises a very wide range of residuals, i.e. ± 0.10 units of TEX_{86}, which is equivalent to ± 5.9 ºC. The lakes from our Iberian data set that fall into this confidence interval are the following ones: Montcortès, Enol, Caicedo, Taravilla, Fuentedepiedra, Salicor, Santa Pola, Chica, Chiprana, el Vilar, la Playa, Zóñar, Honda, Michos and Estanca (see Figure 3.15c).

3.5. Discussion and Conclusions

This chapter has explored the presence and relative abundances of the glycerol dialkyl glycerol tetraethers (GDGTs) in a set of 38 lakes in the Iberian Peninsula. Special attention has been given to the potential temperature influence on the distribution of these GDGTs. The indices TEX_{86} and MBT/CBT have been shown to have a limited applicability in predicting the surface air temperature (as an approximation to LST) when all the data set of lakes is considered. Principal Component Analysis has revealed that 67% of the variance in the GDGT distribution in lakes can be explained by three factors, i.e. isoprenoidal vs branched GDGTs (probably related to terrestrial vs lacustrine origin), combined with the degree of cyclization of GDGTs and the degree of methylation of the branched structures.. When two more factors are considered, which might relate to the length of the carbon chains and the water chemistry, 91% of the initial variance can be explained.

Using Hierarchical Cluster Analysis to group lakes with similar morphological, chemical and/or location characteristics has given some hints on the most suitable lakes that could be used for temperature reconstruction using GDGTs. Thus, lakes with low total dissolved solids and low conductivity showed a linear correlation of TEX_{86} vs MAT, and also of estimated MAT versus digital Atlas MAT (Figures 3.13b and 3.14b). Furthermore, lakes from northern latitudes and especially at high altitude had also a fairly good linear correlation of both proxies (TEX_{86} and MBT/CBT) vs Atlas MAT. Moreover, most deep lakes (with some exceptions) seem to have a linear relationship between their TEX_{86} value and Atlas MAT, although not for estimated MAT and Atlas MAT (Figures 3.13d and 3.14d). In addition, three lakes from Ebro basin seem to respond in a linear fashion to Atlas MAT when their MBT/CBT values are analysed (Figure 3.14h).

Following these findings, we can identify a set of lakes which show promise in terms of applying TEX_{86} index for temperature reconstruction (Caicedo, Enol, Estanca, Michos, Montcortès, Taravilla, el Vilar and Zóñar), mainly because they plot close to the Powers (2005) calibration line and are also selected in several clusters discussed in Section 3.4.3. Adding four lakes to this set, namely Amarga, Medina, Rincón and Zarracatín,

also supported by the cluster analysis but with higher residuals on Powers calibration, still give raise to a linear trend in TEX_{86} over Atlas MAT. Figures 3.16a and b show a proposed calibration of TEX_{86} and MBT/CBT including these selected Iberian lakes.

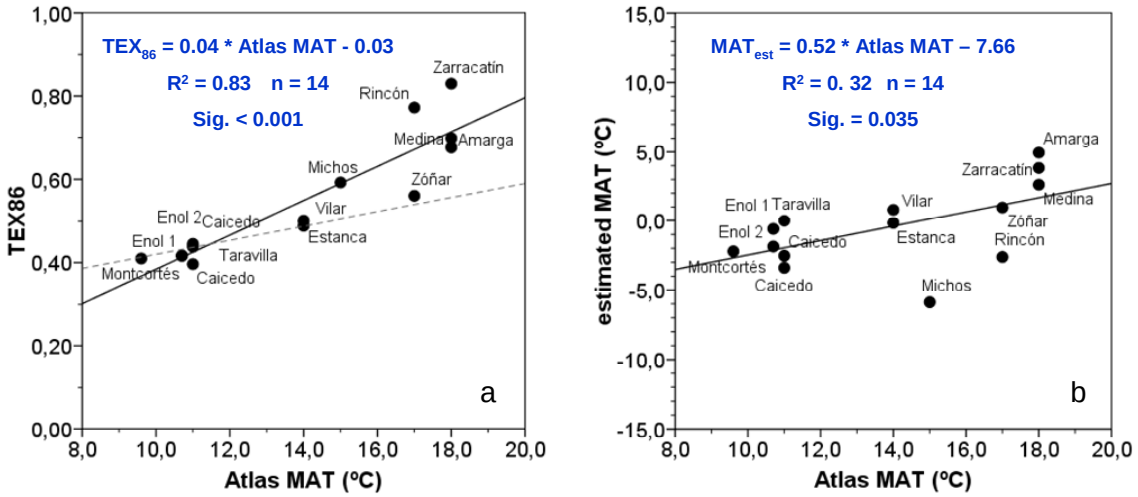

Figure 3.16 a) Calibration of TEX_{86} with Atlas MAT for the 12 selected lakes (14 values) from the Iberian Peninsula and **b)** calibration of estimated MAT with Atlas MAT for the same selected set.

A remarkable finding in this study is that when the complete Iberian lake data set is considered, the GDGT proxies show a low correlation with the Digital Atlas instrumental temperatures (TEX_{86} – Atlas MAT, $R^2 = 0.14$, Figure 3.5; estimated MAT – Atlas MAT, $R^2 = 0.09$, Figure 3.6). It is worth revising which factors can explain that:

- Reference temperatures have been taken from the Digital Climatic Atlas of the Iberian Peninsula. Even if this tool was carefully developed we can expect some differences between the actual air temperature in the lake environment and the Atlas temperature, due to the interpolation process between meteorological stations.
- There is at present no calibration of MBT and CBT in lakes, and so the soil calibration used to derive air temperature might not be suitable for lake sediments, for instance, due to preferential degradation of some branched GDGTs during their transport to the lakes.

- The seasonal variation of temperature for a single lake spans a range of values (minimum of 21 and maximum of 32 ºC) that is larger than the spatial temperature variation of the whole date set (Atlas mean annual temperatures range from 9.5 to 18.0 ºC). It is a possibility that GDGTs distributions in the different lakes may relate to temperatures from different seasons.
- The depth of the temperature signal: even if the lakes studied are relatively shallow, it could also be a relevant issue, since some lakes show a large temperature difference between surface and bottom waters at certain times of the year (e.g. a maximum of 22 ºC for lake Caicedo; Martín-Rubio et al., 2005).
- The presence of anoxic waters in some lakes is also probably influencing the depth distribution of different archaeal communities. For instance, it has been shown that different species inhabit the water masses separated by a clear chemocline (see Chapter 1). The presence of methanogenic archaea in anoxic lakes (e.g. Salicor) would hamper a reliable interpretation of TEX_{86} due to production of GDGTs with an unknown relationship with ambient temperature.
- An important confounding factor is probably the isoprenoidal GDGT signal advected from soils. Terrestrial input composition can differ widely from lake to lake, and thus it is difficult to know which lakes are more affected by the relative proportion of terrestrially-derived GDGTs. Catchment area information is not available for most of the lakes and thus it is not known whether there would be a relationship with the proportion of branched GDGT present in the lake sediments, and it is unknown which distribution of isoprenoidal GDGTs is arriving in the lake from surrounding soils. Analysing the soil GDGT composition in the catchment basins and comparing it to the lake sediment material would be of high interest. Further work should also include the study of the physico-chemical characteristics of the lake water column, ideally for a complete annual cycle, and presence of GDGTs in this water. This knowledge would help to understand the origin and significance of the GDGTs in sediments and better appraise the suitability of lakes for temperature reconstructions.

- The effect of air temperatures below 0 ºC and presence of surface ice on the archaeal synthesis of GDGTs. At least the following lakes experience air temperatures (monthly means from the Iberian Climatic Atlas) slightly below 0ºC: Estanya Gran, Gallocanta, Montcortès, Sanabria, Taravilla and Villarquemado.
- It is also still unknown, for most of the studied lakes located in karstic systems, which is the amplitude of the effect of colder groundwater input in the temperature of the lake. In fact, a great number of the surveyed lakes are located in karstic systems (see Table 3.1). Interestingly, many of the lakes that are known to occur in a karstic environment were selected as the best performing to apply GDGTs proxies.
- Salinity could also impinge an effect on the GDGT distribution. The fact that lakes with low conductivity values (related to low salinity) were shown to have less dispersion in the TEX_{86} – Atlas MAT regression (Figure 3.13b) supports this hypothesis. Although the two incubation studies performed so far suggested that salinity had no effect on GDGT distribution in the marine environment (Wuchter et al., 2004; Schouten et al., 2007), it could be that in lacustrine systems there is an effect. In fact, as molecular studies have shown, high salinity lakes embrace a diversity of Archaea with distinct ecology (e.g. Haloarchaea, see Chapter 1) and the GDGT production by these archea could differ from the expected distribution.

The range of conditions of the surveyed lakes, e.g. size of catchment, substrate rocks, amount and composition of terrestrial organic matter input, lake level and water chemistry, are probably more variable than the conditions experienced by a single lake in the last few millennia, or in some settings throughout the Quaternary. Consequently, we could anticipate that despite the high dispersion of results in the spatial dimension highlighted in this study, reconstructing down-core temperatures from GDGTs in one single lake might probably yield results which appear “to make sense” in terms of interpreting temperature relative changes. In fact we have shown that temperature reconstructions in relatively small and shallow lakes of the Iberian Peninsula using GDGT distribution in sediments is shown to have potential when lakes meet certain conditions for the application of these indices.

Chapter 4

Appraisal of GDGT proxies in Lake Baikal

4.1. Site description: Lake Baikal region

4.1.1. Location, geomorphology and hydrology

Lake Baikal is a very large temperate freshwater reservoir located in Central Asia (51º 28'- 55º 47' N and 103º 43' - 109º 58' E), in a rift zone that developed during the Tertiary, more than 30 Myr ago. This impressive lake lies at 455 m a.s.l., and extends over 600 km in length with an approximate surface of 31,700 km^2 and a maximum depth of 1,642 m. The volume of the lake is estimated in 23,600 km^3 and encloses ca. 20% of the global surface liquid freshwater resources (Kozhov, 1963). This unique ecosystem is also regarded to embrace the world's highest faunal and floral biodiversity of any lacustrine system.

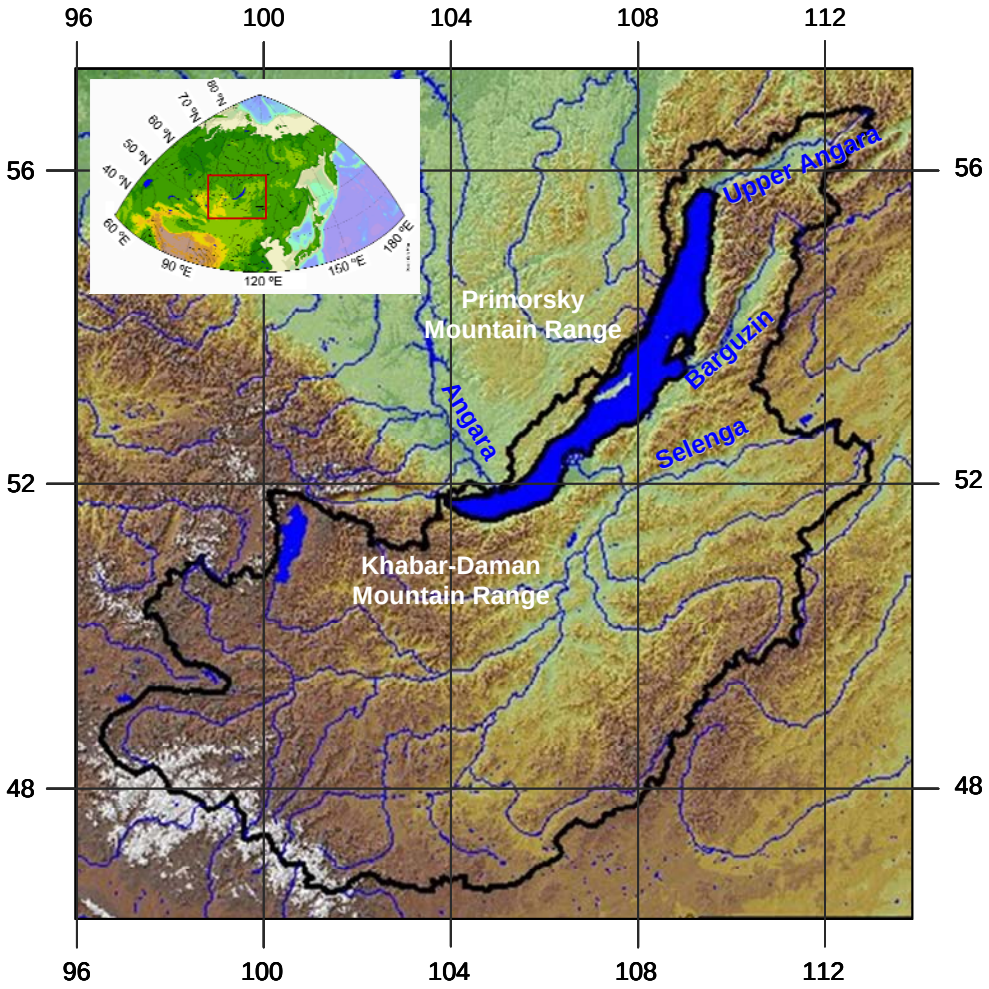

Figure 4.1 Location and physical geography of Lake Baikal in Central Asia.

Three main basins can be distinguished in Lake Baikal: the North (maximum sounded depth is 904 m), Central (1642 m) and South (1461 m) basins (see Figure 4.2). The Selenga River delta separates the Central and South basins, while an underwater mountain high, named Academician Ridge, serves as a natural division between the Central and North basins.

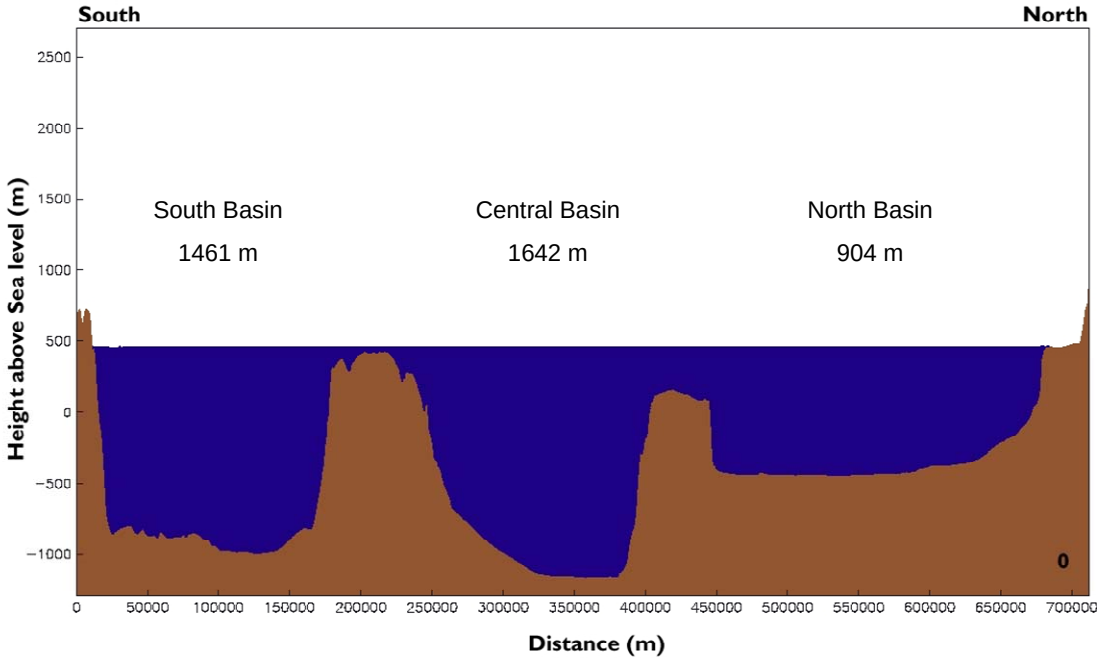

Figure 4.2 Bathymetry map of a SW-NE section along the Lake Baikal. Modified from INTAS Project 99-1669 Team (2002).

The Lake Baikal catchment area is estimated to be 541,000 km^2, thus the ratio of catchment: lake surface is ca. 17:1. The drainage basin extends south and east of the lake, mainly in the arid steppes of northern Mongolia. There are several mountain ridges surrounding the lake which rise to altitudes of 2,500-3,000 m, such as the Khamar-Daban mountain range south of the lake and the Primorsky range in the south west (see Figure 4.1).

The modern catchment area includes over 300 rivers and streams that drain through the boreal forests and the steppe landscapes of northern Mongolia (e.g. Williams et al., 2001). However, three main rivers account for more than two thirds of total riverine inflow: the Selenga River (47-61% inflow) is the largest tributary into the lake and has

developed a large delta in the eastern coast between Central and South Basins; the Upper Angara River enters the northern coast and accounts for 13-17 % of total inflow; and the Barguzin River (6% total inflow) flows through the eastern shore between Central and North basins (Morley et al. (2005), Mackay (2007) and references therein). The major outflow of Lake Baikal is the Angara River on the west coast of the South Basin.

At the bottom of the lake, a sedimentary archive has developed which is estimated to be up to 5 km thick in the Central and South basins, and the record estimated to span more than 20 Myr (e.g. Williams et al., 2001). This extraordinary geological repository has undergone the Quaternary glaciations which impacted on the lake sedimentology, chemistry and productivity but the sediments have remained well stratified as a result of continuous deposition undisturbed by growth/decay of high latitude ice sheets (ibid.).

Another interesting feature in the bottom sediments of Lake Baikal is the presence of **methane hydrates**, which are not known to occur in other freshwater bodies (Schmid et al., 2007). The sediment record is also punctuated by **turbidites**, although it is possible to retrieve undisturbed records from several sites in the lake (e.g. Charlet et al., 2005).

4.1.2. Climatology, hydrography and productivity

The south-eastern Siberian region, including Lake Baikal, is characterized by a remarkable continentality, with present mean daily temperatures ranging from 19 ºC in July to -25 ºC in January (Kozhova and Izmest'eva, 1998). Wet conditions are associated to the short summers, while during long, cold winters drier conditions prevail. The most prominent atmospheric feature is the Siberian High pressure system, which controls the moisture supply from the westerlies (see Figure 4.3). During its weak influence in spring, zonal (i.e. in the E-W direction) circulation intensifies and allows a westerly progression of cyclones moving through west Siberia to the Lake Baikal region. In summer, low-pressure systems form along the Asiatic polar front south of Lake Baikal, the westerly transport weakens and cyclonic activity and rainfall both

increase. In autumn, deep intrusions of cold arctic air from the Kara Sea in the north bring widespread cooling throughout eastern Siberia. This triggers the development of the Siberian High, which dominates this region of central Asia in winter (Mackay, 2007 and references therein). Periods of increased Siberian High intensity are thus associated with colder surface temperatures (Clark et al., 1999).

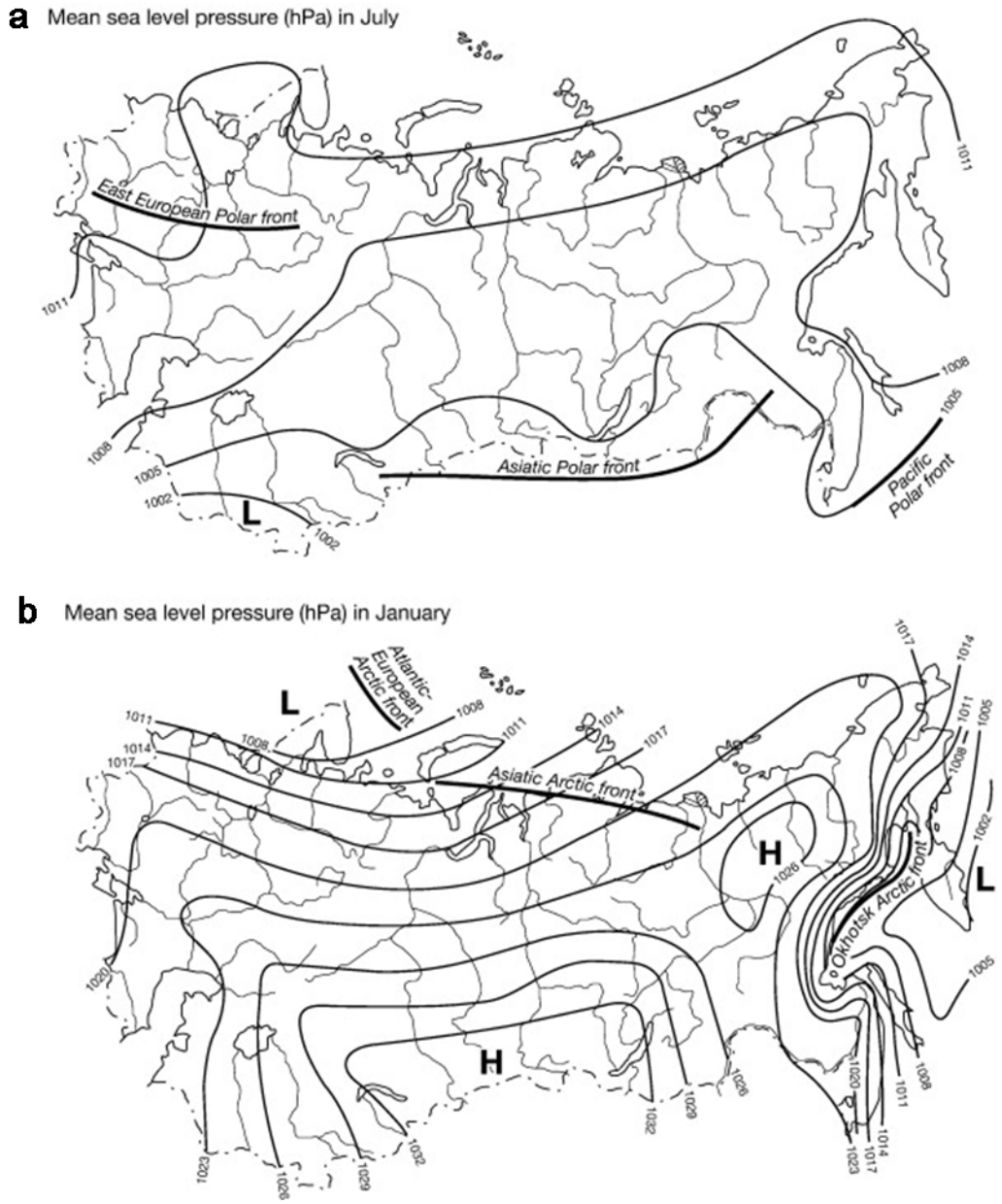

Figure 4.3 Mean sea-level pressure (hPa) across central Asia in (a) July and (b) January. L indicates low pressure system and H indicates high pressure systems. Source: Mackay (2007).

A prominent feature of the lake is the seasonal ice cover, which deeply influences the productivity patterns. Due to the lake length, which covers 4º in latitude, the surface of the North Basin freezes several weeks earlier than the South Basin and it also melts several weeks later (e.g. Kozhova and Izmest'eva, 1998). Thus, ice formation begins in late October in the north, and ice starts breaking in late May, although the basin does not become ice-free until mid-June. Conversely, in the South Basin ice forms in January and already starts breaking up late March, being usually completely melted by mid-May (Shimaraev et al., 1994). Ice thickness ranges from about 1 m in the north to about 80 cm in the south (e.g. Todd and Mackay, 2003). The formation and break-up of ice is complex: the end of freezing, for instance, is apparently relatively independent of air temperatures, occurring when air temperatures are still negative. The ensuing ice break-up is also thought to be a combination of air temperatures, the rate of heat flow through the ice into the lake, upwelling of warmer waters, riverine inflow and wind patterns (e.g. Magnuson et al., 2000; Todd and Mackay, 2003).

In a study reanalysing long term records in winter ice duration in Lake Baikal, Todd and Mackay (2003) found that the ice onset and break-up dates and ice thickness were strongly indicative of winter surface temperatures at a wide continental scale (northern Eurasia). Indeed, patterns of ice formation and break-up appear to be associated to large-scale atmospheric circulation features of the Northern Hemisphere, such as the North Atlantic Oscillation (NAO), Arctic Oscillation (AO) and Scandinavian (SCA) patterns (e.g. Livingstone, 1999; Todd and Mackay, 2003). This region in south-eastern Siberia has repeatedly shown to respond to north Atlantic climatic triggers via atmospheric teleconnections and for instance, increasing snow depths across eastern Siberia are connected to low SST in the mid and high latitudes of the North Atlantic (Ye, 2000, 2001).

Due to its sheer size and depth, Lake Baikal is characterised by a complex hydrography. Indeed, a fully oxygenated column of ca. 1640 m is not easy to explain (Kozhova and Izmest'eva, 1998). A first cause is the overturn occurring twice a year, in late spring and early winter (e.g. Wüest et al., 2005), a typical process of temperate lakes. However, this process cannot reach beneath ca. 300 m depth due to a physical decrease in the temperature of water maximum density with increasing pressure. The temperature of

maximum density is 4 ºC at surface but decreases 0.2 ºC per 100 m depth, and thus the colder than 4 ºC deep waters are weakly but permanently stratified by temperature (e.g. Weiss et al., 1991; Schmid et al., 2008). Deep-water renewal has thus been difficult to explain in Lake Baikal and several hypotheses have been proposed (e.g. Weiss et al., 1991; Shimaraev et al., 1993; Hohmann et al., 1997; Wüest et al., 2005). It has been recently demonstrated that wind stress on the lake surface induces coastal **Ekman transport**, which in turn results in downwelling of cold surface water, especially in periods of weak or reversed stratification, mainly June and December/January (Schmid et al., 2008). The cold plumes follow the steep slopes of the lake, in some cases reaching 400 m depth, where thermobaric instability can spontaneously plunge water deeper. This later process occurs when cold (< 4 ºC) surface water is pushed to a depth where its density (affected by increasing pressure) is higher than that of the surrounding (warmer) water at the same depth (Weiss et al., 1991). According to these observations and current December wind velocities in the three basins of Lake Baikal (Shimaraev et al., 1994), the Central Basin would have the most efficient deep-water renewal, followed by the South Basin and the least efficient process would occur in the North Basin (Schmid et al., 2008).

This vertical exchange is of primary importance for the biogeochemical processes in the lake by leading to efficient recycling of nutrients from the deep waters, which is on the same order of magnitude as the external nutrient inputs (Müller et al., 2005; Schmid et al., 2008). However, Lake Baikal is strongly oligotrophic compared to most lacustrine systems and therefore the proportion of allochthonous material in the lake is important (e.g. Brincat et al., 2000).

Diatoms are the dominant primary producers in the lake. Two blooms occur annually, coinciding with deeper mixing regime in spring and autumn (Popovskaya, 1987). The spring phytoplankton exhibits a phenomenon known as “melosira years”, or high-productive years during which planktonic algae blooms intensively in the interstitial water within the thawing ice and in the under-ice water (e.g. Bondarenko and Evstafyev, 2006). Due to the climatic gradient across the lake, there is a longer phytoplankton growing season in the South Basin compared to the North Basin. During summer

stratification, the diatom-dominated phytoplankton shifts to an autotrophic picoplankton dominance, with a high presence of cyanobacteria (e.g. Fietz et al., 2005).

The relative high oxygen content of the water column and surface sediments have profound implications on the organic matter preservation, since oxidation is occurring during vertical sinking of the particulate matter and its deposition in the first cm of the sediment. Furthermore, oxygen in bottom sediments supports an almost entirely endemic deep-water fauna (Fryer, 1991) and thus bioturbation, although this is minimal in the abyssal zones (Martin et al., 2005). Therefore only a few biological remains survive sinking and deposition (e.g. Russell and Rosell-Melé, 2005) and by being incorporated into the sediment record they become important proxies for past climate and environmental reconstruction studies. Higher productivity and preservation efficiency in the South compared to the North Basins has been detected by means of biomarker analysis (n-alkanes, total fatty acids and sterols) and carbon and nitrogen concentrations in sediment traps and surface sediments (Russell and Rosell-Melé, 2005; Müller et al., 2005).

4.2. Rationale for this study in Lake Baikal

Long continental paleoclimate records are relatively scarce compared to marine-derived records, especially those allowing quantitative reconstructions. In central Asia this lack of paleoclimate information is even more fundamental, with a very few continuous, high quality records spanning the Quaternary. Yet this region has likely experienced the largest increase in global warming in the last 150 yrs (IPCC, 2001) and future projections predict large disturbances associated to climate change. For instance, an increase of mean temperatures between 2 and 5 ºC is expected to occur during next century in Lake Baikal region, which would contribute to permafrost thawing and the release of a large amount of subsurface methane, a gas with a strong greenhouse effect, of global consequences (IPCC, 2001). It is therefore a relevant concern to investigate the processes that control climate variability in this region. The remoteness of this area (far from direct ice-sheet and oceanic influences) precludes direct extrapolation of climatic signals from the Atlantic and Pacific regions (e.g. Oberhänsli and Mackay, 2005); in this context, records integrating a regional signal in Central Asia are of primary interest. This background emphasises the outstanding relevance of Lake Baikal sediments as an archive of Quaternary climate changes. The lake location and a continuous, high resolution sedimentary record provide an excellent opportunity to study long-term trends as well as abrupt changes in regional climate, land-ocean interactions and teleconnections, as well as response to global processes.

A range of proxies for assessing past climate have been applied in Lake Baikal, among which diatom valve accumulation and diatom-related biogenic silica (e.g. Colman et al., 1995), pollen (e.g. Tarasov et al., 2005 , Demske et al., 2005) and biomarkers including pigments (e.g. Fietz et al., 2007) and n-alkanes (e.g. Brincat et al., 2000). Furthermore, isotopic measurements targeting the carbon ($\delta^{13}C$), oxygen ($\delta^{16}O$) and hydrogen (δD) have also been applied to characterize the organic matter remains and derive some climatic information (e.g. Seal and Shanks, 1998; Prokopenko et al., 2001a; Morley et al., 2005). Of all these proxies, diatoms are the most extensively studied in Lake Baikal sediments. Several studies have utilized these siliceous unicellular algae that respond rapidly to a changing environment and the biogenic silica (BioSi) derived from diatom frustules to reconstruct paleoclimates over a variety of timescales from the last 150

years to the last 12 million years (e.g., Granina et al. 1992; Colman et al. 1995; Williams et al. 1997; Mackay et al. 1998; Karabanov et al. 2000; Kashiwaya et al. 2001; Prokopenko et al., 2006). These studies have highlighted the sensitivity of the lake Baikal ecosystem to orbital forcing, with signals associated to the **precession**, **obliquity** and **eccentricity,** and to non-linear climate responses, as it is clear from regular oscillations of diatom records following the glacial-interglacial cycles.

The analysis of GDGTs in Lake Baikal is motivated by the fact that GDGTs can provide the first strictly quantitative temperature reconstruction in that region of Central Asia. Provided that GDGT-proxies are valid in this lake, the results can be compared to the estimations derived from former paleoclimate studies, to conform a multiproxy study in this unique ecosystem. Furthermore, GDGT temperature reconstructions are of high interest for climate model analysis, since they require quantitative input. As GDGTs allow in principle reconstruction of both lake surface and air surface temperature, a study in Lake Baikal potentially offers the opportunity to compare both temperatures and give some hints on the thermal inertia of this massive water body.

As shown in previous chapters, TEX_{86} and MBT/CBT proxies cannot be indiscriminately applied to every lake. TEX_{86} is usually more reliable in large lakes (Powers, 2005), of which Lake Baikal is one important exponent. In fact, the lacustrine calibration by Powers (2005) includes one surface sediment TEX_{86} value for Lake Baikal, which offers a first hint towards the validation of this proxy in this lake. However, given the large basin and complex hydrographical features present, it is worth an endeavour to validate GDGT proxies in this ecosystem.

To address this issue, GDGT fluxes and proxy indices are reported from annual sediment trap material collected in the North and the South basins of Lake Baikal. These results are complemented with surface sediments underlying the sediment trap moorings and from other sites of the lake and discussed in the framework of reliability of GDGT-based reconstructions. Second, two records for the last glacial-interglacial cycle obtained from cores retrieved in the North and South basins of the Lake Baikal are presented and discussed in comparison to global climatic signatures and proxy records from the Lake Baikal sedimentary archive.

4.3. Sediment traps and surface sediments

4.3.1. Sample description

Two mooring strings with an array of sediment traps consisting of open tubes (65 cm^2) were deployed over one year in the North Basin (NB, 12th March 2001 – 5th July 2002) and South Basin (SB, 5th July 2001 – 8th July 2002) of the Lake Baikal by the Continent project members (see location in Figure 4.7).

At the NB mooring (54º 27'N – 109º 00' E), 6 integrating sediment traps were exposed at 335, 445, 720, 775, 885 and 903 m and analysed for their GDGT content. The lake depth at this site is 920 m, and thus only ca. 20 m separated the deepest trap from the floor. At the same mooring, temperatures were recorded every hour with Richard Brancker TR-10000 temperature recorders at 16, 174, 227, 389, 550, 740, 795 and 868 m water depth.

At the SB mooring (51º 43'N – 105º 02' E), integrating sediment traps were analysed from the following depths: 40, 100, 255, 350, 455, 540, 635, 730, 825, 922, 1015, 1210 and 1396 m. The last trap was located at ca. 4 m from the lake floor, which is at 1400 m depth at this site. Temperatures were recorded every hour with VEMCO minilogs at 16, 41, 75, 100 and 195 m depth and with Richard Brancker TR-1000/1050 devices at 303, 350, 397, 445, 540, 825, 1015, 1210, 1305, 1352 and 1396 m depth.

Additionally, short gravity cores (EAWAG-63) were retrieved from the underlying sediments of both moorings and sampled at 1 cm intervals. Samples were stored at -20 ºC until freeze-dried. Results of the GDGT content for the first 10 cm of sediment are used to compare with the material in the sediment traps. Filtered samples from the sediment traps and sediments were extracted by MAE, saponified and analysed with HPLC/APCI-ion-trap-MS. The detailed methodological protocol can be found in Appendix 1.

Surface sediments (0-1 cm) analysed from Lake Baikal come from 6 sites from the NB and SB (see Figure 4.7). Table 4.1 shows the principal characteristics of the samples. Samples S3 and S6 are the surface sediments underlying the sediment trap moorings aforementioned.

	Sample code	Core (Continent Project)	Latitude ºN	Longitude ºE	Water depth (m)
North Basin	S1	CON01-415-6	53º 56'	108º 54'	390
	S2	CON01-603-4	53º 57'	108º 54'	386
	S3	Short core 9	54º 27'	109º 00'	915
South Basin	S4	CON01-431-4	52º 05'	105º 50'	632
	S5	CON01-605-3	51º 35'	104º 51'	675
	S6	Short core 3C	51º 43'	105º 02'	1487

Table 4.1 Surface sediments (0 - 1 cm) analysed for Lake Baikal.

4.3.2. Results and discussion

Reconstructed fluxes of GDGTs in the annual sediment traps are shown in Figure 4.4, together with reconstructed temperatures from TEX_{86} and BIT values for the particulate material recovered in each sediment trap. Temperatures are calculated using the surface-sediment calibration in Powers (2005), namely LST = (TEX_{86} – 0.21) / 0.019. This calibration includes more lakes and, more important, contains one sample from Lake Baikal, and is therefore preferred to the calibration by Powers et al. (2005).

A first observation is that fluxes are very similar in both basins, with slightly higher numbers for the SB (1.2 ± 0.2 to 62.4 ± 3.0 µg GDGT $m^{-2}\cdot d^{-1}$) than for the NB (4.3 ± 0.2 to 21.8 ± 1.2 µg GDGT $m^{-2}\cdot d^{-1}$). This is in agreement with results from total organic carbon, total nitrogen and other lipid fluxes assessed from samples in the same moorings, which found as well higher fluxes in the SB (Russell and Rosell-Melé, 2005;

Müller et al., 2005). The authors invoked higher productivity in the SB (due to longer growing season) and possibly greater degradation in the NB water column to explain the observed differences. Although primary productivity differences will not directly affect GDGT production, higher amounts of particles resulting from the primary productivity-based food web (e.g. algal remains, faecal pellets) are likely to induce efficient scavenging of the GDGTs and thus contribute to increased fluxes, as has been proposed to occur in the marine realm (e.g. Wuchter et al., 2005).

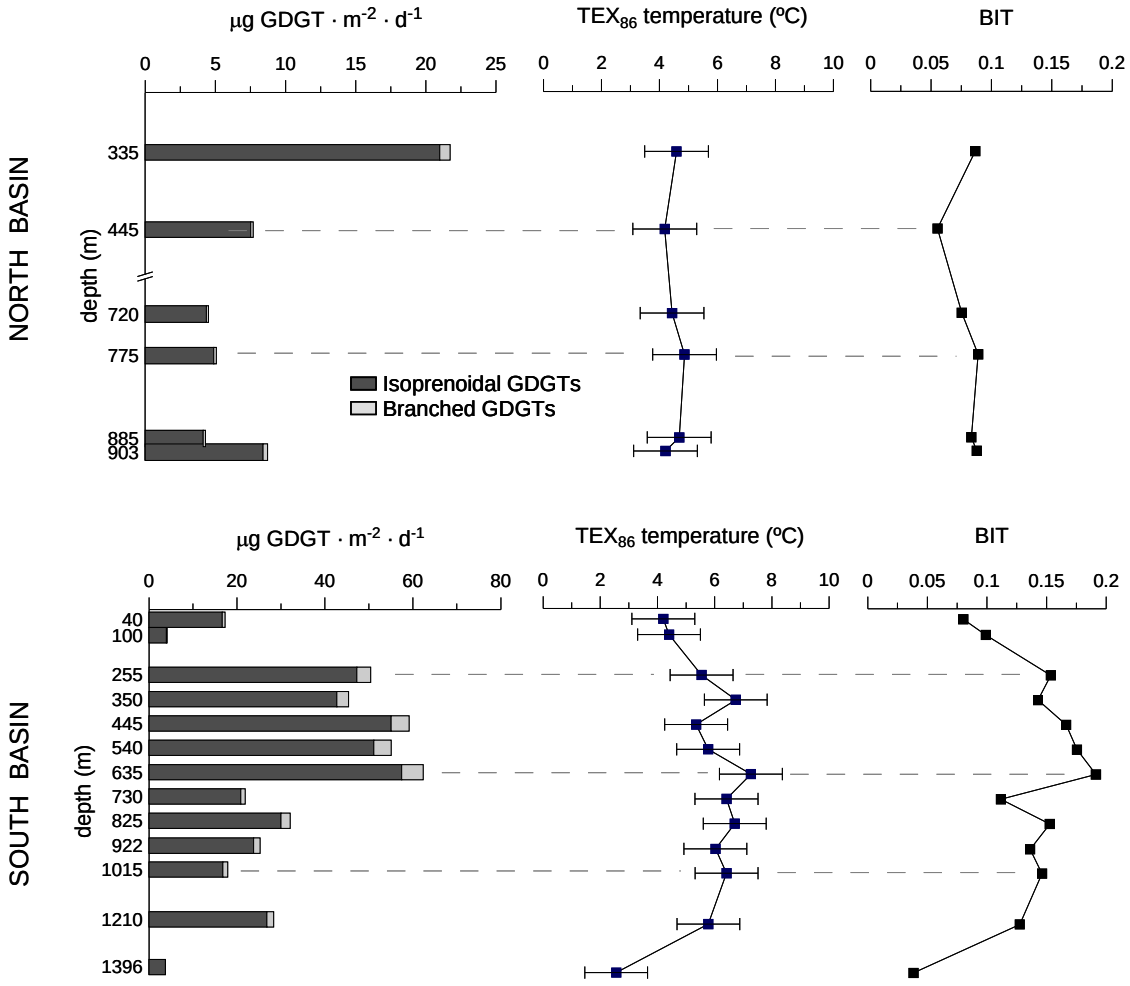

Figure 4.4 GDGT fluxes calculated from sediment traps deployed in (a) the North Basin mooring and (b) the South Basin mooring. TEX_{86} derived temperatures and BIT values analysed in the material from each sediment trap are shown. Error bars for TEX_{86} temperatures correspond to ±1σ associated to analytical precision.

There is no clear decrease of fluxes with depth in neither of the basins, thus suggesting either low degradation of GDGTs through the water column or new production of these lipids at depth. While no published GDGT values in traps deployed in lacustrine sites are available, this observation can be compared with marine data. Measured fluxes of GDGTs in two VERTEX stations from the Pacific ranged from 0.2 - 4 μg GDGT $m^{-2} \cdot d^{-1}$ in the oligotrophic waters and 5 - 97 μg GDGT $m^{-2} \cdot d^{-1}$ in an upwelling area (Wuchter et al., 2006), numbers which are very similar to those from Lake Baikal. Interestingly, fluxes in the VERTEX stations were shown to increase with depth. The authors proposed that this could be related to mid-depth production of GDGTs (given that Archaea are usually present all along the water column), accumulation in density discontinuities and/or zooplankton migration (Wuchter et al., 2006). All three hypotheses could apply for Lake Baikal as well. Thus, for instance, free-living with low sinking velocities Archaea could accumulate in density discontinuities and thus become an important source of GDGTs collected only in deeper traps. The GDGT flux profile of the mooring in the SB would support this idea, as there is an increase of flux between 100 and 255 m, which could be related to the density discontinuity associated to the thermocline in Lake Baikal (see Figure 4.6). For the NB mooring, conversely, the shallowest data is from 335 m depth, below the thermocline, and thus this question cannot be addressed.

Another common feature in both moorings is the low proportion of branched GDGTs to total GDGT flux (2 - 4 % in the NB and 0 - 8% in the SB) and the related remarkably low BIT values (0.06 - 0.09 for the NB and 0.04 - 0.19 for the SB). Assuming that branched GDGTs are exclusively of terrestrial origin, these results indicate that the GDGT modern fluxes in Lake Baikal are mainly of pelagic origin. However, comparison with BIT values measured in the underlying sediments suggests that it has not always been like this (see Figure 4.5). A surface value of 0.14 for the NB and 0.30 in the SB indicate higher proportion of branched GDGTs in sediments compared to the sediment traps. This could be due to several processes. A first interpretation is that past fluxes of branched GDGTs were higher than at present, given that the annual sediment trap represents only a snapshot observation contrasting with the integrative nature of the sediment. Alternatively, lower degradation of the deposited branched GDGTs compared to the isoprenoidal GDGTs could explain the differences. This hypothesis is supported

by findings in the Madeira Abyssal Plain, where soil-derived branched GDGTs were found to be better preserved than the isoprenoidal GDGTs in post-depositional oxidative conditions, which the authors associated to a likely enhanced protection provided by the soil matrix (Huguet et al., 2008). This would have profound implications for paleoclimate studies, in the sense that BIT values from the past would appear overestimated in those sediments that undergo significant oxidation. In particular, this could be a relevant concern in Lake Baikal sediments for the relatively high content of oxygen in the water column, although in sites with high sedimentation rates organic matter will be protected from oxidation by rapid burial. A third and more speculative hypothesis could be the *in situ* production of branched GDGTs by subsurface-dwelling Archaea, although there is at present no study supporting this idea.

Interestingly, the BIT profile, although showing low amplitude variation, resembles the flux profile in both basins (see Figure 4.4), and accordingly, higher percentages of branched GDGTs are associated with higher fluxes. A possible explanation for these parallel trends could be the Ekman-induced surface water plumes that have been observed in Lake Baikal (see Section 4.1). Because this downwelling occurs mostly near the lake shore and where most soil-derived branched GDGTs are expected, advective transport could convey these GDGTs into the basin at depth, thus bypassing the first traps. These water plumes have been observed to advance at ca. 1 km per day from the shore into the basin (Schmid et al., 2008), and it is thus plausible that they can reach the central part of the basin, where the moorings were deployed. The comparison of NB and SB profiles shows that BIT changes are larger in the SB, which would be in agreement with the SB having more efficient deep-water renewal processes associated to the downwelling described (see Section 4.1). Alternatively, the SB could receive soil-derived material from the Selenga river discharge by lateral transport at mid-depths, which would also explain the lower BIT in the shallowest traps.

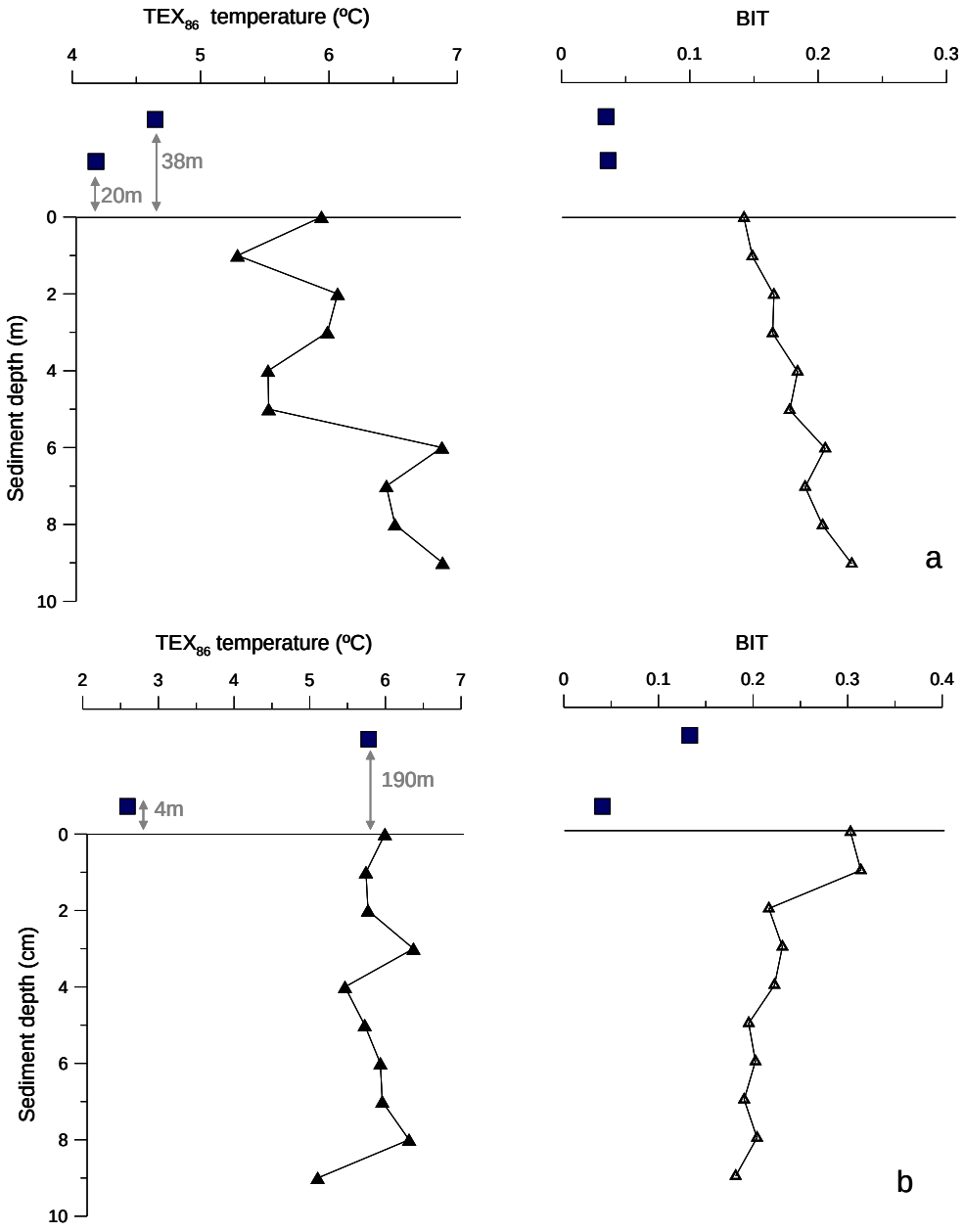

Figure 4.5 TEX_{86} reconstructed temperatures and BIT values for the two deepest sediment traps and the first 10 cm of the underlying sediments in the North Basin (a) and the South Basin (b).

Measured instrumental LST in the two deployed moorings range from 0.0 to 10.9 ºC in the NB and from 0.2 to 12.8 ºC in the SB, both recorded at 16 m depth. Deep-water temperature in both basins was fairly invariable, i.e. ca. 3.5 ºC. Figure 4.6 shows reconstructed monthly temperature profiles using the data form the Richard Bracking temperature recorders, together with the TEX_{86} derived temperature. Lake surface

temperatures (LST) estimated with TEX_{86} in sinking particles at all depths are in the range of measured LST during the year of deployment. However, differences are noted between the north and south water columns surveyed. In the NB, the temperatures reconstructed at 6 depths, from 335 to 903 m, are virtually invariable, averaging 4.5 ºC and with minimum and maximum values of 4.2 and 4.9 ºC. The BIT is also very stable in these samples (Figure 4.4). Conversely, in the SB, where 13 depths between 40 to 1396 m were analysed, reconstructed LST range from 2.6 to 7.3 ºC. Differences in LST along depth are thus negligible in the North Basin but significant in the South Basin, according to the analytical precision at the time of these analyses, i.e. ±1.1 ºC (1σ). TEX_{86} values are considered reliable due to low values of BIT in all sediment traps, which indicate no substantial contribution from soil GDGTs.

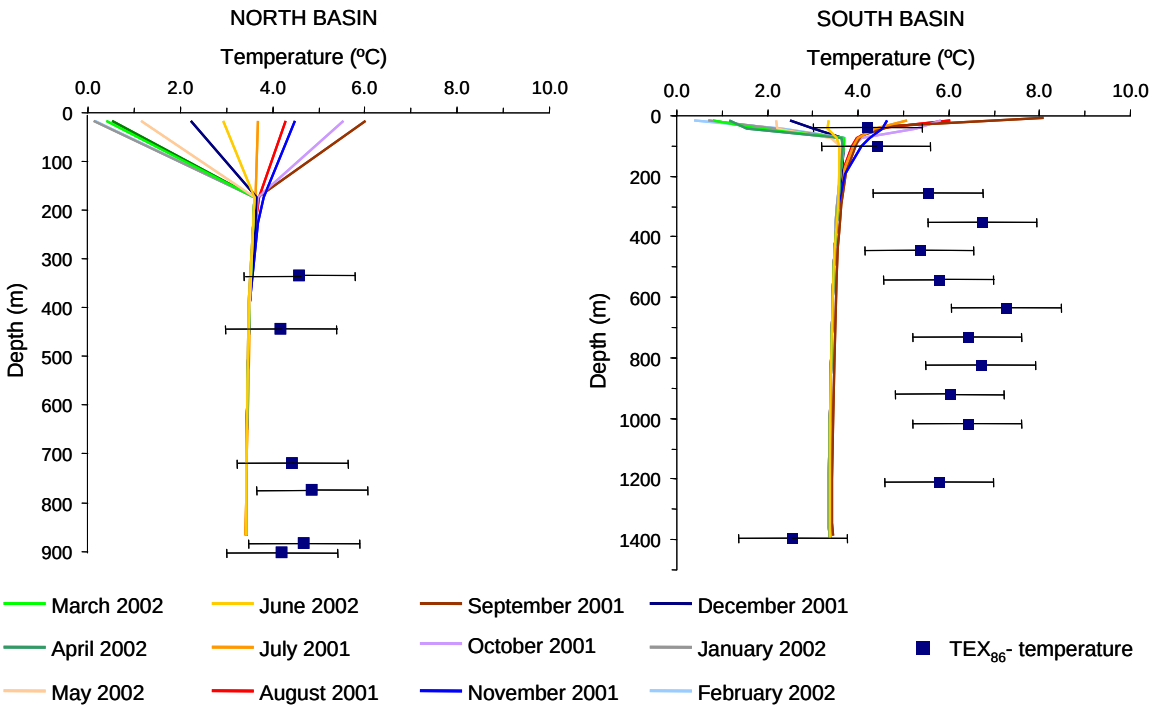

Figure 4.6 Monthly average temperature profiles reconstructed from measured temperatures in the moorings at the North and South Basins during deployment between March 2001 and July 2002. TEX_{86} reconstructed temperatures for the sediment traps and associated uncertainty (± 1σ) are shown at the collection depths.

Deep production of GDGTs cannot be ruled out but it is not suggested from the profiles, as almost all sediment trap reconstructed temperatures are higher than deep-water

temperature, especially in the SB. A common feature in both water columns is that TEX_{86} reconstructed temperatures are similar to LST from autumn months, i.e. from August to September (Figure 4.6). Although this is not conclusive, that observation would be in agreement with molecular studies indicating higher abundances of Archaea during autumn and winter in high-altitude and cold lakes (see Chapter 1) and better correlations of TEX_{86} with winter temperatures reported in Powers (2005) and Blaga et al. (2009). In that sense, enhanced production of GDGTs by an abundant archaeal population in autumn would bias the temperature signal towards these months. Alternatively, it could be that higher particle fluxes in autumn (consequence of the phytoplankton bloom) produce a more efficient scavenging of GDGTs, which would be more rapidly removed from the surface waters and prevented from further degradation, thus having a better representation in the sediments compared to GDGTs produced in other seasons.

In the more detailed particulate material profile of the SB, the surface samples and the deepest sample show significant TEX_{86} differences from the mid-depth samples. A possible explanation accounting for colder reconstructed temperatures in surface traps is that they collect particulate material from the coldest months that cannot reach greater depths because ice cover restricts productivity and thus particle production, thus decreasing the downward fluxes. Regarding the deepest trap sample in the SB, the TEX_{86} derived temperature is significantly colder than the above-lying reconstructed temperatures and, even being only 4 m above the sediment floor it is also not similar to the surface sediment value (see Figure 4.5). Instead, the surface sediment has nearly the same value than the second deepest trap, deployed at 190 m above the sediment floor, which indicates good agreement with TEX_{86} from collected particulate material during 2001-2002 and the integrated signal in the sediments. The deepest trap could perhaps be affected by *in situ* production of GDGTs, fuelled by the nutrient resuspension from the benthic boundary layer (e.g. Müller et al., 2005), which would explain a reconstructed temperature close to deep-water temperature.

Results for estimated LST, BIT and estimated MAT for surface sediments are shown in Figure 4.7. Estimated LST at the 6 sites explored are remarkably similar and average 6 ºC, except for sample S1 which appears as an outlier and has a value of 8.5 ºC. These

results are slightly lower but comparable within analytical uncertainty with the Lake Baikal TEX_{86} derived LST value reported by Powers (2005), which was 6.8 ºC using the same calibration. Furthermore, no differences in LST are suggested between the NB and SB. The annual mean subsurface water temperatures (16 m depth) indicated by the moorings discussed in the previous section are 2.6 ºC for the NB and 2.9 ºC for the SB, suggesting also no big differences in subsurface water temperature between both distant basins. BIT values in the 4 samples were it was measured are all below 0.3, which indicates relatively low recent contribution of soil-derived GDGTs.

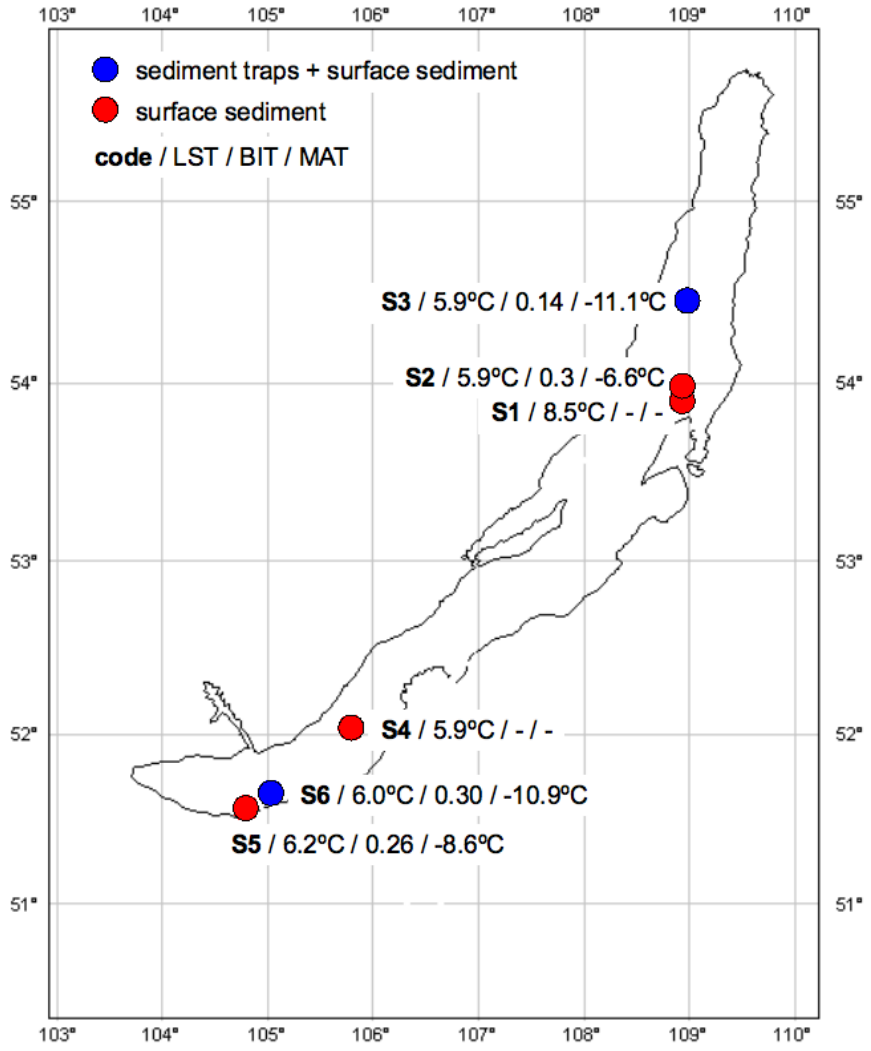

Figure 4.7 Location of sediment trap moorings and surface sediment sites in Lake Baikal. Labels for each site show sample code (see Table 4.1), reconstructed LST, BIT index and reconstructed MAT. BIT and MAT values are not available for samples analysed before branched GDGT measurements were set up.

The last value shown for the samples in Figure 4.7 corresponds to the MAT reconstructed from the MBT/CBT proxy. These indices have not yet been published for any lake and thus references for their applicability and interpretation are lacking. The reconstructed values range from - 6.6 ºC to - 11.1 ºC, show intra-basin variability and again there is no clear difference between the NB and the SB. Because the branched GDGTs used in the MBT and CBT indices are in principle originated in the soils of the Lake Baikal catchment basin, reference air temperatures from meteorological stations in this region were used for comparison. The catchment area was divided in two zones: one in the north, supposed to be the source of branched GDGTs collected in the samples S1 to S3 (NB) and one in the south, presumably the source of branched GDGTs found in the samples S4 to S6 (SB). The watershed between both zones is taken south of the Barguzin river (e.g. Karabanov et al., 2000). Thus, two reference air surface temperatures were obtained for the northern (taken as 53 - 57 ºN, 108 - 113 ºE) and southern (taken as 47 - 53 ºN, 98 – 112 ºE) catchment areas from the CRU TS 3, a 0.5° gridded global data set spanning 1901-2006 (Mitchell, 2003). The northern catchment annual mean air temperature has ranged in the last century from -9.0ºC to - 4.0ºC with a mean of -7.0 ºC. For the same period, the southern catchment annual mean air temperature has ranged from ca. - 5.0 ºC to -1.5 ºC, averaging -3.5 ºC. There is a clear difference between the two catchments of ca. 3 ºC, which is not represented in our data set. The reconstructed MAT values are colder than the measured air surface temperatures, except for sample S2, which shows good agreement with reference values for the northern catchment. A calibration of MBT/CBT in large lakes should be undertaken to assess whether this difference is a common feature in all lacustrine environments; for instance, a preferential degradation of some branched GDGTs during their transport could change the MBT/CBT values found in soils. Alternatively, assuming that the reconstructed MAT is reliable, soil material could be derived from high altitudes of the mountain ridges surrounding the lake, especially the Khamar Daban Range in the south, thus forcing a colder temperature signal of the MBT/CBT. That would be in agreement with the higher differences between measured and reconstructed air temperatures for the South Basin, surrounded by higher ranges.

4.4. GDGTs in Baikal sediment cores as climatic proxies

The long latitude range occupied by Lake Baikal and the complex hydrographical dynamics of the lake raised the question of whether the record of paleoclimate events in the sediments would be consistent along the lake. It was therefore deemed of high interest to analyse cores from different basins and compare the records. In this study, two cores were investigated located in the North and South basins of the Lake Baikal. The goal was to check the performance of the GDGT proxies for reconstructing the climate in the Baikal region, and general patterns of global climate. For this purpose, time series of GDGT parameters are examined for common trends observed in other climatic series, and absolute temperature values are also compared with various climate model outputs from the Paleoclimate Modelling Intercomparison Project (PMIP2, Braconnot et al., 2007) for the Lake Baikal region.

4.4.1. Sediment core description

The location of the two sediment cores studied coincides with S2 and S5 in the Baikal map of Figure 4.7. The core **CON01-603-2** (Continent Project) is located on the **Continent Ridge** in the north basin of Lake Baikal (53º 57’ N, 108º 54’ E), an “isolated high” with a steady accumulation of hemipelagic sediments and a variable terrigenous component. The detrital fraction represents around 30% of the cumulated thickness of the sediment and is probably transported from the Barguzin River (at 100 km) and/or local rivers along the southeastern coast of the North Baikal Basin (Charlet et al., 2005). In the south basin, core **CON01-605-3** was drilled at **Vydrino Shoulder** (51° 35' N, 104° 51' E). As revealed by seismic data, side-scan sonar mosaics and sedimentological data (Charlet et al., 2005), the core at this site comprises 90% of detrital material and the stratified seismic facies, which suggest a rather stable depositional environment. Both cores were selected at sites free of turbidites (ibid.) and because they were retrieved from the abyssal plains of the basins, the bioturbation is suggested to be minimal (Martin et al., 2005).

Fresh cores were subsampled in 1 cm slices. Core 603-2, with a mean sedimentation rate of 6.4 cm·kyr^{-1}(Demory et al., 2005) was sampled at every 5 cm, which gives a mean temporal resolution of 700 yr for the 334 cm long section analysed (~57 kyr). Core 605-3 displayed a higher sedimentation rate of about 17.3 cm·kyr^{-1} (ibid.) and was sampled at every 10 cm, which in turn yields a mean temporal resolution of 400 yr for the 498 cm long section analysed (~27 kyr).

The age models for cores 605-3 and 603-2 were developed by means of a paleomagnetic study by Demory et al. (2005). Down-core variations of normalised relative paleointensity were correlated to the equivalent record from ODP site 984 after removal of intervals affected by diagenesis. The average time resolution of this correlation was ~3.5 kyr for the core 603-2 and ~1.5 kyr for the core 605-3. Additionally, geomagnetic excursions such as Iceland Basin event were used as tie points and the topmost part (~1 m) of the sedimentary column was also dated by accelerator mass spectrometry (AMS) ^{14}C measurements performed on pollen concentrates (Piotrowska et al., 2004). Both magnetic and radiocarbon analyses were undertaken on the kasten cores retrieved at the two sites mentioned and dates were transferred to the pilot cores by correlation of down-core variations of high-resolution magnetic susceptibility (Demory et al., 2005). As can be seen in Figure 4.8 both methods show good agreement in both cores.

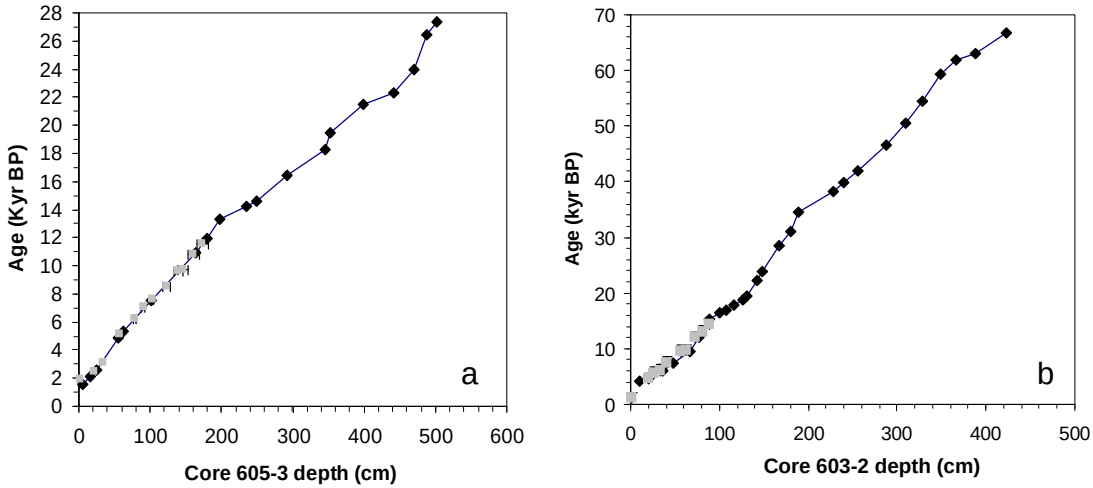

Figure 4.8 Diagrams of age versus depth for the two cores in **a)** South Basin (605-3) and **b)** North Basin (603-2) of Lake Baikal. Black dots are obtained from paleomagnetic intensity correlation with ODP site 984 (Demory et al., 2005) and grey squares are AMS ^{14}C dating performed on pollen concentrates (Piotrowska et al., 2004) including error bars.

4.4.2. Lake Baikal record of GDGT proxies for the last glacial-interglacial cycle

The reconstructed record of LST, MAT and BIT index is shown in Figure 4.9 and the following paragraphs offer a brief description of the observed trends.

Lake surface temperature (LST)

The longer record obtained from the north basin shows a decreasing trend in Baikal LST from 53 to 24 kyr BP. However, GDGTs concentrations were very low in the samples from cm 144 to 169 (~22.8 to ~28.9 kyr BP) and, although most GDGT chromatographic peaks were above the limit of detection, TEX_{86} is expected to be underestimated in this period. In fact, the LST record crosses the 0 ºC line only in this period, further supporting the idea of a temperature underestimation, since it is improbable that water temperatures go below 0 ºC. In the recent half of the studied period, a warming can be observed in both basins LST, but the trend is different. In the south basin there is a steady increase from ~4 ºC to ~7ºC in the last 27 kyr reconstructed. On the other hand, the record of the north basin shows a rapid increase between 24 and 18 kyr BP, afterwards indicates an important cold excursion centered around 16 kyr BP and for the last 15 kyr remains around 6 - 7 ºC. The cold excursion is also recorded in the south basin core, and although the minimum temperature occurs 1 kyr later, the resolution of sampling and uncertainties in the age model could account for this difference. LST records are remarkably similar in both basins for the last 11 kyr, with virtually equal present-day values, as already shown in previous section.

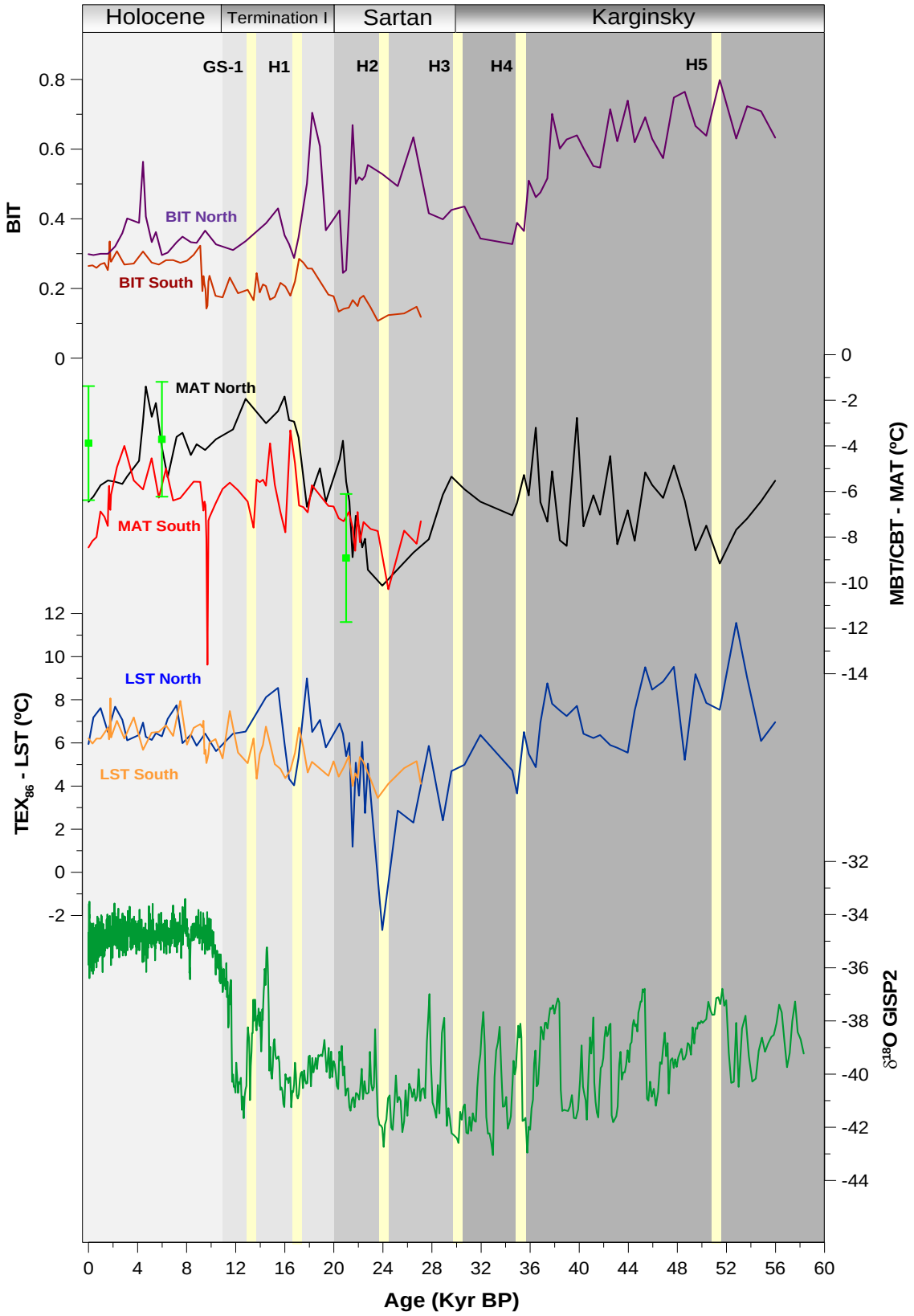

Figure 4.9 Lake Baikal records of TEX_{86} derived LST, MBT/CBT derived MAT and BIT, compared with $\delta^{18}O$ record from ice core GISP2 in Greenland (Stuiver et al., 1995), as indicative of global ice volume changes. Green dots in MAT record are results from global circulation models from the PMIP2 (error bars indicate 1σ of the range of model simulations). GS-1 and Heinrich events H2 to H5 indicate changes in Lake Baikal stratigraphy; Heinrich event H1 dating is from Hemming (2004).

Mean air temperature (MAT)

In the North Basin, MAT record shows a steady decrease between ~56 and ~52 kyr BP but this trend is truncated by a period of great variability and overall increasing values until ~34 kyr BP, afterwards warming steadily for 4 kyr. Between ~ 29 and ~23 kyr BP, the period of low GDGT concentrations and higher uncertainty associated to the reconstructions, the MAT in the North Basin experiences a cooling of ca. 5 ºC. A coeval but smaller cooling (~ 3 ºC) is recorded in the South Basin samples, free of the analytical problem mentioned. Because this temperature decrease is also recorded by LST in both basins, it is likely representing a regional temperature decrease, probably overestimated in the North Basin. MAT increases in both basins between 24 and 16 kyr BP. After this point, the trends diverge again. The north basin MAT declines until present values around - 6 ºC, punctuated only by a warm excursion between ~6 and ~4 kyr BP. Conversely, the South Basin MAT records a large cooling of about 4 ºC centred around 16 kyr BP, coeval with the LST cooling recorded n both basins. Interestingly, the North Basin MAT does not show this event. The South Basin suggests yet another abrupt cooling at ~ 9 kyr BP, this time with a decreasing of the reconstructed air temperatures of around 7 ºC and supported by more than one data point. The last 3 kyr in the South Basin suggest a decrease of MAT of more than 4 ºC, with a present-day value around – 8.6 ºC, colder than the – 6.6 ºC suggested for the North Basin.

BIT index

The BIT index has also different trends in the two basins of Lake Baikal. The southern record shows a firm increase for the whole record spanning the last 27 kyr, with rapid increases of about 0.1 - 0.2 between ~20 and ~17 kyr BP and between ~10 and ~9 kyr BP. On the other hand, the overall tendency of the North Basin record is a decrease of BIT values from 0.7-0.8 to 0.3-0.4 for the last 56 kyr. However, variability is also high in this record, with a sharp decrease between ~38 and ~34 kyr BP, and two others at ~21 and ~17 kyr BP, all of them characterized by a lowering of about 0.4 units of BIT and separated by a gradual increase between ~34 and ~21 kyr BP and an abrupt increase between ~21 and ~17 kyr BP. The recent part of the record shows a fairly stable BIT only disturbed by one rapid positive excursion at around 5 kyr BP.

4.4.3. Comparison with other proxies

The general warming in Lake Baikal from ca. 24 kyr BP onwards indicated by both LST and MAT records from the North and the South basins points to the transition from glacial to interglacial conditions. Comparison of this trend in Lake Baikal with the $\delta^{18}O$ record from the GISP2 ice core in Greenland (Stuiver et al., 1995), as indicative of global ice volume, highlights the climatic significance of the TEX_{86}, MBT/CBT proxies in Lake Baikal (see Figure 4.9) and further supports the sensitivity of this strongly continental and apparently isolated region to global climatic changes (e.g. Williams et al., 1997).

Comparison of the GDGT-proxies with other paleoclimatic proxies applied in Lake Baikal offers further evidence for their power to record climate changes in the region. The following paragraphs discuss this for a few periods identified within the last glacial-interglacial cycle.

Karginsky interstadial

Glacial periods are punctuated by short warming periods known as interstadials. The interstadial MIS 3 in the marine isotope record (ca. 59 to 29 cal kyr BP) is known in this region of Siberia as the Karginsky interstadial. The Karginsky is recorded in all three basins of Lake Baikal by an increase in diatom abundance and related biogenic silica (e.g. Karabanov et al., 1998; Khursevich et al., 2001; Prokopenko et al., 2001a; Swann et al., 2005). These two proxies are the most extensively studied in Baikal sediments and their changes in sediments reflect climate-induced phytoplankton productivity, with higher abundances related to warmer conditions (e.g. Bezrukova et al., 1991). The LST and MAT record in the North Basin of Lake Baikal, which cover part of the Karginsky interstadial period, shows indeed relatively warm temperatures for the surface water and air, which rapidly decline after ~30 kyr BP.

Sartan Glacial

The glacial period following the Karginsky is known in Siberia as the Sartan Glacial (e.g. Karabanov et al., 1998), spanning approximately from 30 to 20 kyr BP with obvious signals of cold conditions in Lake Baikal region. A high-resolution record

(ca. 1yr) of magnetic susceptibility, associated to changes in lake productivity, suggests that the coldest conditions for the last 50 kyr occurred during the Sartan Glacial, especially between 25 and 22 kyr BP (Boës et al., 2005). Remarkably, the GDGT proxies reconstruct the coldest temperatures in this period (excluding the rapid cold excursion at 9 kyr BP), although the LST and MAT in the North Basin are likely underestimated (see previous section).

Termination I

The Termination I refers to the last transition from glacial to interglacial conditions. Diatom abundances in Lake Baikal show an increase in all basins during Termination I (e.g. Karabanov et al., 2004). Other proxy evidences for the Termination in Lake Baikal encompass a general increase in phytoplankton and zooplankton remains including pigments (e.g. Soma et al., 1996; Tani et al., 2002), increase in accumulated total organic carbon (e.g. Karabanov et al., 2001; Prokopenko et al., 2001a,b) and gradual change from steppes to forest vegetation in the catchment basin (e.g. Velichko et al., 2002; Tarasov et al., 2005; Demske et al., 2005). Diatom records suggest that Termination I was a relatively rapid transition in Lake Baikal, lasting ca. 4 kyr (e.g. Boës et al. 2005; Mackay, 2007). The high-resolution diatom record of Boës et al. (2005) indicates a sharp warming in the North Basin starting from 18 kyr BP and stabilizing around 14 kyr BP. Only the North Basin MAT record suggests an abrupt warming in this period, but generally the paleotemperature proxies show a warming trend starting earlier, at ca. 22 kyr BP. In fact, at ca. 16 kyr BP northern LST experiences a cold excursion of about 4 ºC before increasing again. A possible interpretation for this cooling, also recorded by South Basin LST and MAT records and centred on 16 ka, is discussed in following paragraphs.

Abrupt changes

Studies by Prokopenko et al. (2001a, b) were the first to propose a link between abrupt changes in the lake Baikal ecosystem with ice-rafting pulses into the North Atlantic ocean from the Laurentide ice sheet (Heinrich events, Heinrich, 1988), associated with cooling cycles (Bond cycles, Bond et al., 1992). Further evidence of Heinrich events imprint in Central Asia climate is found in the Chinese loess sequences of deposited aeolian sediment (Porter and An, 1995). Prokopenko et al. and follow-up studies

suggest a lake-wide diatom abundance decline at the time of Heinrich events (e.g. Swann et al., 2005). Furthermore, Central Basin sediments record abrupt erosional processes (known as Kuzmin events) represented by deposition of mud layers; these are coeval high TOC values, strong positive excursions of $\delta^{13}C$ and maxima in C/N, associated with changes in the precipitation regime in the catchment area of Baikal and ensuing discharge changes of Selenga River (Prokopenko et al., 2001b). According to available AMS ^{14}C dates and stratigraphic position of the Kuzmin mud layers and diatom productivity drops, the Heinrich event signals in Lake Baikal were located at ~51 kyr BP (H5), ~35 kyr BP (H4), ~30 kyr BP (H3) and younger than ~24 kyr BP (H2), while for H6 and H7, although detected, it was not possible to derive and age (Prokopenko et al., 2001a,b; Swann et al., 2005). Although our core sampling resolution and chronological control precludes a detailed discussion of millennial-scale events, the LST and MAT records suggest cooling intervals at ca. 51, 35 and especially 24 kyr BP, which might correspond to the H5, H4 and H2. Additionally, compelling evidence for a cooling at ca. 16 kyr BP is derived from LST in both basins and MAT in the north, and could be related to H1, dated at 16.8 Kyr BP (Hemming, 2004).

Another abrupt change often discussed in the literature of Lake Baikal paleoclimatology is the GS-1 (Younger Dryas in the Blytt-Sernander terminology), indicating a rapid return to glacial conditions during Termination I (e.g. Dansgaard et al., 1993). The GS-1 was first claimed to impact the Lake Baikal as inferred from an abrupt drop in diatom productivity and BioSi (Colman et al., 1999; Karabanov et al., 2000) around 10-11 kyr ago. Concomitant with these changes, a decrease in total organic carbon, total chlorophyll *a* and total carotenoids between ca. 11 and 12 kyr BP were reported, indicating a decrease in primary productivity (Tani et al., 2002; Soma et al., 2007). Additionally, Morley et al. (2005) identified GS-1 in a Vydrino shoulder (South Basin) sediment core by means of a record of diatom concentrations and $\delta^{13}C_{ORG}$ changes at ca. 12.64 cal kyr BP, and Prokopenko and Williams (2004) suggested the occurrence of GS-1 interval starting at 12.89 kyr BP. These dates are significantly close to the one indicated in the record from GRIP ice core in Greenland (12.65 cal kyr BP; Lowe et al., 2008) and would indicate virtually no lag between the North Atlantic climatic trigger and Lake Baikal productivity response (Mackay, 2007). Pollen data also confirmed the cold nature of this period (Velichko et al., 2002) and subsequent studies support the idea

of cold and moist conditions of the GS-1 in the northern part of the lake (*Picea* forest development) contrasting with cold but arid conditions in the south (non arboreal pollen indicating widespread steppe vegetation) (Demske et al., 2005). The GDGT records show a rapid decrease in temperatures exclusively in the South Basin core, of about 2 ºC both in LST and MAT at ca. 13 kyr BP, a change that is larger than the analytical uncertainty and concomitant with the described proxy evidence within chronological uncertainty.

Holocene

The Holocene period, i.e. the present interglacial starting about 11 kyr ago, is thought to be a relatively stable period with generally warm conditions in Lake Baikal, as suggested by the diatom record (e.g. Karabanov et al., 2000). Indee, the last 11 kyr of the TEX_{86}-LST records in Lake Baikal are fairly stable and suggest similar temperatures in both basins. The MAT records, conversely, are distinguished by several oscillations. In the northern MAT there is a Holocene decrease of about 3 ºC, yet interrupted by a warming between ~4 and ~6 kyr BP, which could be related to a Holocene Optimum, as has been suggested to occur in Siberia, although the exact period is still under debate (e.g. 2.5-4.5 kyr BP in Karabanov et al., 2000; 4.6-6 kyr BP in Khotinsky et al., 1984). Boës et al. (2005) also found diatom productivity increases around this period, in particular at 6, 4.5 and 4 kyr BP, which could suggest temporal warming. On the other hand, the southern MAT shows a general increase of ca. 2 ºC until ~3 kyr BP with ensuing rapid cooling of about 4.5 ºC until present. Another important feature in the south is the remarkable cold excursion at ~9 kyr BP, although the short nature of the event precludes precise dating with the current age model. Productivity proxies in Lake Baikal suggest rapid fluctuations around 9 kyr BP; for instance, pigments and a high-resolution diatom record would indicate especially warm conditions close to 9 kyr BP (e.g. Fietz et al, 2007; Boës et al., 2005), while ca. 8 kyr BP the diatoms suggest an abrupt cooling (Boës et al., 2005).

BIT interpretation

In the South Basin the general increase of BIT could be related to the increase in moisture availability in the region. Pollen records in Lake Baikal sediments indicate low moisture availability at the beginning of the Holocene (Demske et al., 2005), but

subsequent development of taiga forest combined with positive shifts in $\delta^{18}O_{diatom}$ (Morley et al., 2005) reveal wetter climate well into the Holocene. The increased precipitation would translate into increased river discharge in the South and be the cause of the BIT raise. In the North Basin, BIT could be more related to fluxes of glacigenic clastics, supported by higher glacier presence in the north of the catchment basin. A mild decrease in the first part of the record could be related to deglaciations in the Karginsky interstadial diminishing the erosive force of melting glaciers, a process that looks especially important between ca. 38 and 35 kyr BP. The increase between 32 and 22 kyr BP could be related to the return to glacial conditions during the Sartan period, which could reinforce the glacier soil-erosion. Two extremely abrupt decreases of BIT in the north are coeval with rapid increases in MAT at ca. 21 kyr BP and 18 kyr BP. Conversely, a rapid but small increase before 4 kyr BP is concomitant with the warming suggested by north MAT. This provides more support to the hypothesis of soil erosion by glaciers, since the MAT increases at 21 and 18 kyr BP could have caused a brief decease of glacier erosive mechanisms, while the event at ca. 4 kyr BP could have induced an opposite trend.

4.4.4. Comparison with models

Comparison of the temperatures reconstructed with TEX_{86} and MBT/CBT is done here with simulated air temperature from global circulation models (GCM) from the Paleoclimate Modelling Intercomparison Project (PMIP2) provided by Dr Masa Kageyama. A summary of the models characteristics is shown in Table 4.2. The model simulations correspond to the region defined between latitudes 50-55°N and longitudes 105-110°E, including Lake Baikal. Control experiments are for the pre-industrial climate. Simulations are compared to the proxy data for two periods: the Holocene Optimum (6 kyr BP), for which 14 sensitivity experiments were used, and the Last Glacial Maximum (LGM, 21 kyr BP), for which 9 experiments were used. Model experiments use the following boundary conditions: Peltier (2004) ICE-5G ice-sheets, 21 kyr BP insolation (Berger, 1978) and greenhouse gas concentrations from ice-core data (CO_2=185 ppm, CH_4=350 ppb, N_2O=200 ppb).

Model	Points in the selected region	Control temperature (°C) (pre-industrial period)
CSIRO-Mk3L-1.0	1	-1.95
CSIRO-Mk3L-1.1	1	-1.73
FOAM	1	-7.48
MIROC3.2	4	-4.54
MIROC3.2.2	4	-4.69
CCSM	4	-5.31
GISSmodelE	2	0.4
ECHAM5-MPIOM1	4	-3.66
ECHAM53-MPIOM127-LPJ	4	-3.32
IPSL_CM4_MR	4	-7.49
FGOALS-1.0g	4	-5.24
ECBILTCLIO	1	-1.71
ECBILTCLIOVECODE	1	-0.38
MRI-CGCM2.3.4nfa	4	-7.06
MRI-CGCM2.3.4fa	4	-3.8
UBRIS-HADCM3M2	6	-2.71
HADCM3	6	-1.67
CNRM-CM33	4	-0.83

Table 4.2 Global circulation models from the Paleoclimate Modelling Intercomparison Project (PMIP2) and indication of the number of modelled cells in the selected region (50-55°N, 105-110°E) and temperatures from the control experiment (pre-industrial period).

Mean air temperature values for the control, Holocene Optimum (6 kyr BP) and LGM (21 kyr BP) model simulations are plotted in Figure 4.9 with the proxy-derived MAT. While the mean control temperature is higher than the estimated MAT, Holocene Optimum and LGM mean temperatures agree quite well with the proxy data. A closer comparison is shown in Figure 4.10, which provides the simulated and reconstructed temperature anomalies, i.e. the difference between the periods studied and control (models) or present-day (proxies) values.

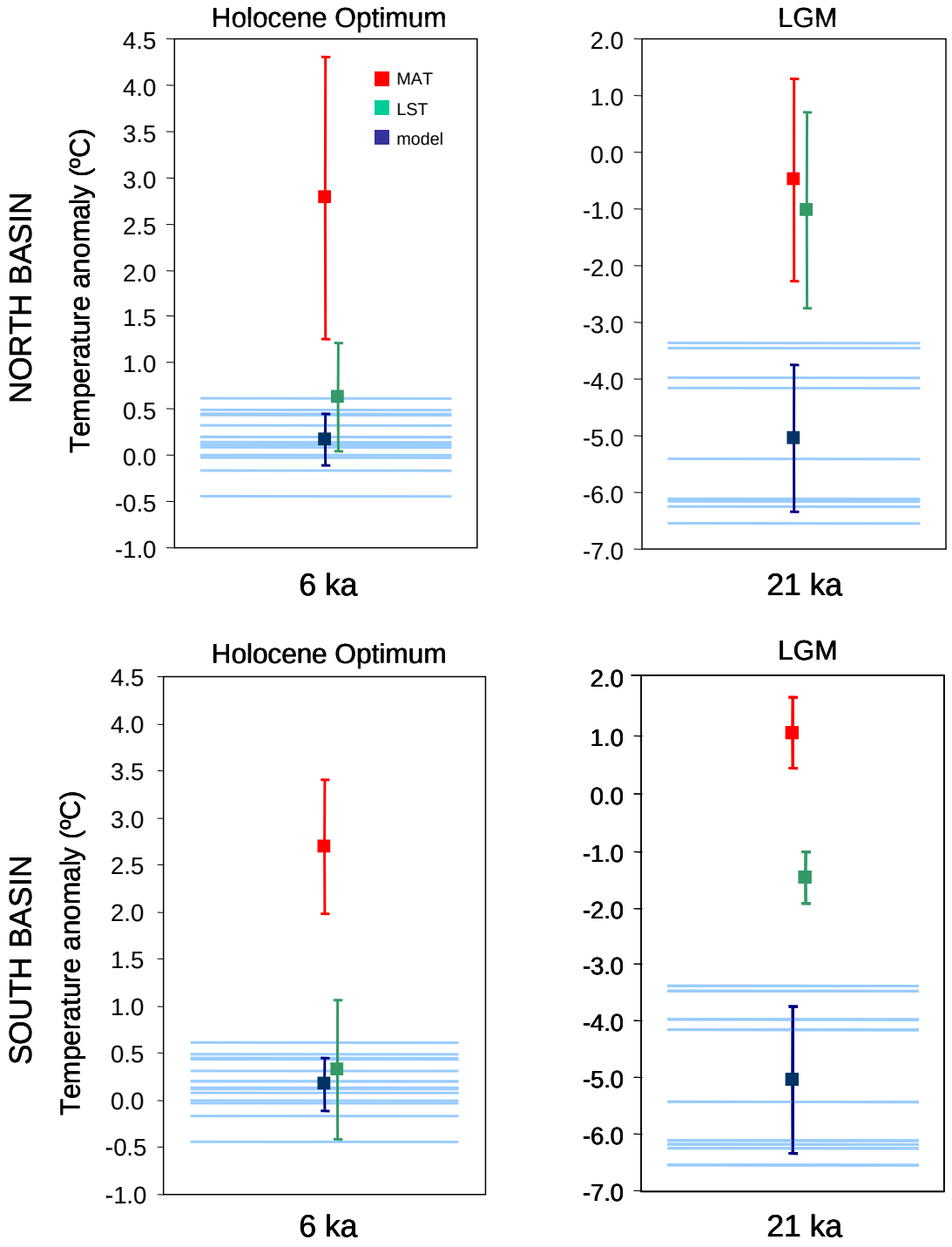

Figure 4.10 Comparison of temperature anomalies for the Holocene Optimum (6 kyr BP) and LGM (21 kyr BP) reconstructed by TEX_{86} (LST) and MBT/CBT (MAT) proxies and simulated by global circulation models from the PMIP2. Proxy values are an average of data from 4 - 8 kyr BP (Holocene Optimum) and from 19 -23 kyr BP (LGM). Horizontal light blue lines indicate simulations of the individual models used. Error bars indicate ± 1σ for the model and proxy data.

The model simulations suggest a small temperature anomaly for the Holocene Optimum (0.17 ºC) and relatively low dispersion (± 0.28 ºC, 1σ). A higher temperature anomaly of - 5.05 as well as higher dispersion (± 1.30 ºC, 1σ) are instead simulated for the LGM. Interestingly, reconstructed anomalies for LST are in all cases closer to the model simulations than the anomalies for reconstructed MAT, although models provide air and not water temperature. Indeed, the Holocene Optimum difference between MAT and simulated temperature anomalies is for both Baikal basins 2.5 ºC, while for the LGM these differences are higher, 4.6 ºC in the North Basin and 6.2 ºC in the South Basin, with reconstructed MAT being always higher than the simulated temperatures.

One of the possible explanations for this disagreement could be the set of the boundary conditions used in the GCMs of the PMIP2. For instance, lakes, dust input and vegetation changes are not considered in the model. The presence of lakes in the region could modulate the temperatures due to higher thermal inertia of water, and provide a buffer effect for cold incoming air; this effect would be especially important close to Lake Baikal given its large volume. In turn, vegetation changes would modify evapotranspiration and albedo in the region. On the other hand, the proxies studied could be influenced by several factors. For instance, during extended soil snow-cover in glacial periods, temperatures under the ice/snow could keep warmer than overlying air temperatures. In that sense, both pelagic GDGTs and soil branched GDGTs would record warmer temperatures. Alternatively, the rapid recent cooling suggested by MAT reconstructions (see Figure 4.9) could be originated by factors other than air temperature decline, which would in turn force the observed smaller than simulated anomalies for the Holocene Optimum and LGM, given that they are calculated with the most recent sample. Figure 4.9 suggests some support for this hypothesis, as the absolute reconstructed and simulated temperatures for the past are fairly similar.

4.5. Conclusions and outlook

Results shown for annual sediment traps and surface sediments in two distant basins of Lake Baikal indicate that TEX_{86} is able to reconstruct LST at this site. Although a certain bias towards autumn temperatures is suggested in the TEX_{86} signal, seasonal trap material would be necessary to derive a conclusive statement. Modern fluxes of branched GDGTs are shown to be low compared to pelagic isoprenoidal GDGTs and thus further suggest that TEX_{86} would be a reliable proxy for assessing LST, although past fluxes of GDGTs could have been higher than present-day ones. Furthermore, results of MBT/CBT proxy are reported for the first time for lake sediments and reconstructed MAT values are shown to be generally colder than measured temperatures in the catchment basin of Lake Baikal, which suggests a limited applicability of the MBT/CBT indices in this region, although the lack of a specific calibration for lake sediments could be the cause of the observed mismatch. Analysis of both isoprenoidal and branched GDGT distribution in soils around the lake would provide highly relevant information on the terrestrial sources of GDGTs and the potential impact of soil-derived isoprenoidal GDGTs in TEX_{86} from the lake.

Two records of LST, MAT and BIT index for the last climatic cycle are obtained from GDGT concentrations in sedimentary cores retrieved in the South Basin and North Basin of Lake Baikal. The reconstructed temperatures suggest that GDGT distributions document the transition from glacial to interglacial conditions in the lake region. Comparison of the obtained records with well-established proxies from the sedimentary archive of Lake Baikal further confirms the presence of a climatic signal in GDGTs. Furthermore, even if the chronological control and sampling resolution preclude a detailed discussion of events at submillennial scales, it is noted that GDGTs could be recording abrupt changes in Lake Baikal, such as Heinrich event signals and the GS-1 (Younger Dryas). A comparison of GDGT-proxy reconstructions and GCMs simulations from the PMIP2 for the Baikal region highlights close absolute temperature values for the Holocene Optimum and the LGM, but differences in control values lead to large differences in air temperature anomalies (2.5 to 6.2 ºC). Given the limitations of the model boundary conditions and the partial understanding of the GDGT proxy controls, these differences can potentially be reduced by addressing these issues.

Chapter 5

Archaeal lipids in new archives

5.1. Archaeal lipids in drill core samples from the Bosumtwi impact structure, Ghana

This section contains a reduced and modified version of a published manuscript (Escala et al., 2008) which can be found complete in the Appendix 3.

5.1.1. Introduction

The Bosumtwi impact structure, in Ghana, West Africa, was the subject of the ICDP Bosumtwi Crater Drilling Project in 2004 (e.g. Koeberl et al., 2007). This relatively young crater of 1.07 Myr age (Koeberl et al., 1997) was excavated in about 2.2 Ga metavolcanics and metasedimentary rocks and has a rim-to-rim diameter of about 10.5 km. The structure has a pronounced central uplift, presumably originating from the rebound of the target rocks (Scholz et al., 2002). It is almost completely filled with a lake that has a current maximum depth of 78 m. At present, underneath the lake there is a 150 to 310 m thick layer of post-impact lake sediments, with typical seismic velocity values of unconsolidated and water-saturated sediments (Scholz et al., 2007). The lake sediments, in turn, are underlain by about 200 m of various polymict and monomict impact breccias (see, e.g. Koeberl et al. 2007, for a summary). The velocities for the impact breccia are also relatively low, which suggests that the Bosumtwi impact structure is composed of highly-fractured material (e.g. Scholz et al., 2007).

The interest in such impact events is not restricted to the geological structures originating as a consequence of the collisions, but they also have important geochemical and biological implications. For instance, moderate-sized impacts and the subsequent hydrothermal systems generated can have profound effects on the organic matter abundance and composition, via processes including maturation, melting and irradiation (Parnell and Lindgren, 2006). Moreover, asteroid and comet impacts can have a profound effect on the availability and characteristics of habitats for the microorganisms living in the terrestrial surface and subsurface. Several estimates suggest that the biomass contained in microbial communities living at the terrestrial subsurface (terrestrial deep biosphere) is very large and that the total number of prokaryotes in this environment is close to the total number of microbial cells in the entire ocean (e.g.

Gold, 1992; Whitman et al., 1998; Karner et al., 2001). A common process associated to meteorite impacts is bulking, which increases the porosity of the shock rock lithologies and thus the surface area where lithophytic organisms can grow (e.g. Cockell et al., 2003, 2005). Furthermore, large impacts have the potential of locally sterilizing the soil, given high shock pressures and high temperatures that can persist in the hydrothermal systems generated. This issue has recently been discussed for the Chesapeake Bay impact structure at the east coast of North America (Cockell et al., 2007; Glamoclija and Schieber, 2007; Voytek et al., 2007). The Bosumtwi site, as it is a well-preserved and young impact structure, is an excellent site to explore the presence and structure of subsurface microbial life.

When searching for microbial life, the two prokaryotic domains of life, Archaea and Bacteria, are the usual targets of any molecular or geochemical survey. This preliminary study considers the presence of lipid biomarkers of prokaryotic life in the impact breccias. In particular, we focus on GDGTs, archaeal lipids that are very refractory and thus are preserved and accumulated in sediments and soils (e.g. Schouten et al., 2000). During the ICDP Bosumtwi Crater Drilling Project, several cores were retrieved from the geological structure. Here we report an exploratory survey of archaeal biomarkers in the impactite rocks recovered from a core drilled in the Bosumtwi crater.

5.1.2. Samples and methods

Impact breccia samples were recovered from underneath the lacustrine sediments in core LB08 drilled near the central uplift of the Bosumtwi impact structure (cf. Koeberl et al., 2007), at 235.77, 240.04, 280.30, 283.50, 353.95, 382.17 and 417.60 meters below the lake surface (water column depth at this site was 73 m). The outer layer of the rock pieces was discarded in order to avoid contamination from handling. The samples were then finely ground by means of mortar and pestle, and approximately 2 g of rock powder were extracted with MAE and saponified, and the GDGT content was analysed by HPLC/APCI-ion-trap-MS. The detailed analytical protocols are described in Appendix 1.

5.1.3. Results and discussion

Archaeal lipids were detected in four of the seven impactite rock samples analysed (i.e. at 235.77, 240.04, 283.50 and 382.17 m) and none of the target lipids was detected in the laboratory blank. The highest concentration of GDGT lipids was found at 382.17 m depth. By comparison with external standards we can estimate that the concentration of GDGTs in some samples is at most a few ng/g. Figure 5.1 shows the depth profile of total archaeal lipids (GDGTs) and specifically GDGT-I (caldarchaeaol, *m/z* 1302) concentrations, both normalized to the maximum concentration of total GDGTs. Archaeal lipid concentrations were dominated by GDGT-I in the four samples where GDGTs were detected. In two of these samples (240.04 and 382.17 m), GDGT-I was the only archaeal lipid detected, whereas for the other two samples (235.77 and 283.50 m depth), GDGT-I concentration was 81% and 38% of total GDGT concentration, respectively. The other GDGTs identified were those with *m/*z 1300, 1298, 1296 and 1292 (crenarchaeol), thus only isoprenoidal GDGTs were detected. These results show no trend of archaeal lipid concentration versus depth.

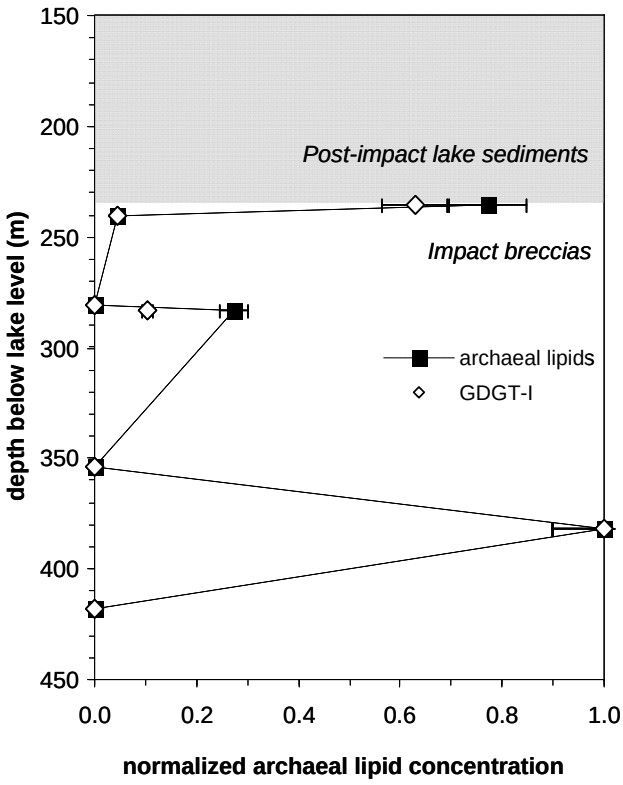

Figure 5.1 Depth profiles of normalised total archaeal lipid and GDGT-I concentrations in impactites from drill core LB08 from the Bosumtwi impact structure.

The rock samples analysed in the laboratory come from the inner part of the cores and we can also rule out laboratory contamination. Thus, we infer that archaeal presence in the Bosumtwi crater is revealed by the occurrence of typical biomarker lipids, GDGTs, in the impactite rocks of this geological structure. The origin of the archaeal community is however difficult to evaluate at this time given the available data. Little information can be derived from the distribution of the detected GDGTs: GDGTs with *m/*z 1300, 1298 and 1296 have been described in environmental samples including soils and lakes and ascribed to mesophilic Archaea (e.g. Powers et al., 2004; Weijers et al., 2004), but the same structures have been also observed in membranes from thermoacidophilic species (e.g. Shimada et al., 2002). Conversely, crenarchaeol is considered a marker for mesophilic Archaea, especially abundant in aquatic environments although it has also been observed, in less abundance, in soil samples (e.g. Weijers et al., 2004). However, branched bacterial GDGTs, which are ubiquitous in soils, were not detected. The relatively high abundance of GDGT-I in the studied Bosumtwi samples is more unusual and can provide more insights on the origin of the lipids, as discussed below.

We have considered three main pathways for the GDGTs to reach the breccia samples, which are not mutually exclusive and are discussed below: i) from soils and rocks pre-dating the impact event, ii) generation during the post-impact hydrothermal system, and iii) from hydrogeological activity.

Firstly, it can be considered that lipids found in the rocks are from pre-impact archaeal lipids, accumulated in surface soils older than 1.07 Myr that have survived the impact event originating the Bosumtwi crater. Archaeal lipids have been found in sedimentary rocks as old as 120 Myr (Kuypers et al., 2002) and therefore, it is plausible that the lipids detected are fossil remnants of the archaeal cells that dwelled in former soils. Signatures of fossil biological activity have been found in other impact craters. For instance, in the Haughton impact structure (Nunavut, Canada) several biomarkers were identified in the melt breccias and are considered to have survived the impact event and the ensuing relatively high temperatures (around 210ºC) that lasted for ~5 kyr (Parnell et al., 2005; Lindgren et al., 2006). However, temperature effects on GDGT stability should also be taken into account. There is evidence from pyrrhotite deformation in the impact rocks of Bosumtwi suggesting peak shock temperatures at the drilling site

around 250ºC (Kontny et al., 2007). There is also evidence of a moderately high-temperature post-impact hydrothermal alteration event near the central uplift, with calculated temperatures not higher than 300-350ºC (Petersen et al., 2007), although geochemical analysis suggests that this did not produce a particularly severe alteration or involved a limited volume of fluid percolating through the impacted breccias (Ferriere et al., 2007). Thus we might consider the possibility that Archaea were present in the impact target soils and they were in contact with high-temperature fluids during a relatively long time, of a few thousand years. Schouten et al. (2004) investigated the thermal maturation of GDGTs using hydrous pyrolysis and found that GDGTs exposed to temperatures above 240ºC for 72 hours decreased rapidly and they were virtually completely degraded at 300ºC. Given that these values seem to be the peak temperatures reached during the impact event and post-impact hydrothermal processes, it is difficult to ascertain whether GDGTs were able to survive the thermal conditions in the recent Bosumtwi impact structure. However, it is interesting to note that Schouten et al. (2004) also found that GDGT-I seemed more thermally stable than the other GDGTs investigated, which is consistent with our results, where lipid distribution in rock samples is dominated by GDGT-I. The distribution of GDGTs in the sample from 283.50 m could just reflect the lipid distribution in pre-impact soils, in accordance with soil samples investigated so far (e.g. Weijers et al. 2006a). But the clear dominance of GDGT-I in the other samples, including the one at 235.77 m where little amounts of other lipids were detected, suggests an additional source for this lipid. Thus, a third explanation for the dominance of GDGT-I within the set of investigated archaeal lipids is a large contribution of methanogenic Archaea, which are known to contain high amounts of GDGT-I in their membranes (Koga et al., 1993).

Alternatively, the GDGTs could be of post-impact origin. Although the process of biological recovery after an impact is unique for each event and site, Cockell and Lee (2002) proposed a generalized sequence of post-impact succession. The three stages the authors distinguish after an impact event, which can include partial sterilization of the area, are: (i) phase of thermal biology, characterized by thermal activity and associated microbial ecology, (ii) phase of impact succession and climax, when greater colonization of the impact crater takes place, and (iii) phase of ecological assimilation, which culminates with the erosion or burial of the impact structure. Based on studies of

Haughton impact crater (about 24 km wide), the duration of the phase of thermal biology would be of the order of several thousands of years, although this will scale with the dimension of the event (Cockell and Lee, 2002). Although there is a lack of global data on biological signatures which can be unequivocally associated with this phase of development of any impact crater, it can be reasonably argued that at this stage at Bosumtwi crater, the transient hydrothermal system generated provided an ideal habitat for thermophilic Archaea. Thus, the GDGTs could be remnants of this relatively recent hydrothermal system.

Otherwise, the GDGTs could be of even more recent origin. During the second phase of succession and climax proposed by Cockell and Lee (2002), crater-lakes typically develop in the impact craters. In this scenario, recolonization of crater surface rocks and crater lakes can take place very rapidly, in some cases within a few months (see Cockell and Lee (2002), and references therein), with organisms that can be wind-borne, for instance. Since the meteorite impact took place (1.07 Ma), arguably enough time has passed by for prokaryotic communities (Bacteria and Archaea) to have developed in the surface of former air-exposed breccias and the lake filling the crater. The GDGTs present in the deep rocks of the Bosumtwi structure could have been carried by the water percolating from the sediments and of the lake above. In fact, mesophilic Archaea occur ubiquitously in the water column and sediments of lakes (e.g. Powers, 2005; this thesis), and seismic reflection data from Bosumtwi structure suggest highly fractured impact material and water-saturated lake sediments (Scholz et al., 2007). In the same context, post-impact soils from the crater rim could be a likely source for the archaeal lipids, given that there is hydrological contact between the brecciated crater-rim rocks and the sub-lake breccias. However, the surface of the crater rim is very small compared to the size of the lake and thus the contribution of these soils in comparison to the production of GDGTs in the lake is probably not very significant. Furthermore, those GDGTs typically present in soils (Weijers et al., 2006a) were not detected in the samples. If the lake waters are indeed the source of the archaeal lipids in the breccias, the high relative abundance of GDGT-I could be explained by the presence of archaeal methanogens in sediments, which could produce the CH_4 observed in surface sediments and deep water in the Bosumtwi lake (Koeberl et al., 2007).

The lack of correlation of GDGTs concentration with depth could be explained in this case by the vertical heterogeneity in lithology and grain size that has been reported for this core (Ferriere et al., 2007). For instance, high concentrations of GDGTs in the shallowest sample (235.77 m) just below the lake sediment can be connected to the presence of carbon-rich shale clasts in the upper metres of the impactite rocks. The depth-independent concentration of archaeal lipids is also consistent with the reported vertical structure in microbial distribution in the Chesapeake Bay impact structure, which is attributed to processes of sterilization and microbial recolonization linked to the impact cratering (Cockell et al., 2007).

5.1.4. Summary and conclusions

Seven samples of impact breccia from the central uplift of the Bosumtwi crater were analyzed for the presence of typical archaeal membrane-lipids (GDGTs). These have been detected in four of the samples, at a maximum depth of 382 m below lake level, and the distribution of the analyzed GDGTs is dominated by GDGT-I. The origin of these lipids is discussed and three hypotheses are considered as possible explanations: (i) pre-impact lipids in soil that survived the impact event, (ii) lipids synthesized by hyperthermofilic Archaea in the post-impact hydrothermal system, and (iii) lipids synthesized by Archaea thriving in the lake and/or crater-rim rocks that have percolated into the impactites. Additional data are needed to discriminate between these possible modes of origin for these lipids, but our preliminary results suggest that studies on the microbial community in the deep interior of the Bosumtwi structure would be rewarding.

Chapter 6

Conclusions and outlook

Advantages and pitfalls of GDGT proxies and outlook for future studies

This thesis has addressed some of the analytical methodology and validation issues of the paleoclimatic proxies TEX_{86}, BIT and MBT/CBT, first proposed in 2002, 2004 and 2007, respectively.

Several analytical questions were addressed in Chapter 2 of the present thesis. First, a rapid method for the screening of GDGTs in sediment samples using HPLC-MS was described; this method increases the throughput of samples, which is an advantage for high-resolution, long-term paleoclimatic studies that result in a great number of samples to analyse. Second, the standard cleanup method for GDGTs (alumina fractionation) was compared to a widely used cleanup in biomarker analysis (alkaline hydrolysis); the results demonstrated that TEX_{86} and BIT indices obtained through both methods are statistically comparable. Therefore, alkaline hydrolysis can be used confidently for GDGT analysis, a method that is especially convenient for samples with high amounts of fresh labile organic matter. However, the liquid extraction using a water phase should be avoided during hydrolysis because it was shown to lead to massive losses of GDGTs; this water extraction is not a key step during the process and can be therefore omitted if necessary. Additionally, the effect on TEX_{86} and BIT of using different adsorbents (silica and alumina) and degree of activation (activated and 5% deactivated) for GDGT fractionation was tested; results indicated virtually no effect on TEX_{86} but slight differences in BIT raised from using different degrees of activation, which poses some doubt on the comparability of published results.

Regarding the analytical instrumentation, a reduction of flow in the HPLC system and concomitant change of the HPLC column was proved to be effective for saving solvent volume without loss of chromatographic peak resolution. Concerning the identification and quantification of GDGTs, the comparability of TEX_{86} and BIT measurements undertaken with two different designs of mass spectrometer, i.e. a quadrupole and an ion-trap, was confirmed. This increases the reliability on these proxies, since nowadays both designs are used by several laboratories that perform GDGT analysis. Furthermore, the branched GDGTs included in the BIT index were shown to be highly sensitive to

mass spectrometer tuning, in contrast to the isoprenoidal GDGTs. This is a key finding, since it has a vital influence on the BIT index because it comprises both isoprenoidal and branched GDGTs. Accordingly, the results of the laboratory intercomparison study (Schouten et al., 2009) including TEX_{86} and BIT values from 15 laboratories indeed show a large dispersion of BIT values among laboratories. This effect poses BIT on the centre of attention of future investigations and the isolation of branched GDGTs to perform MS tuning experiments will be a critical step on the development of this proxy. A follow-up of the intercomparison study is now under way to examine among other issues the MS tuning effect on the individual GDGTs and the resulting dispersion of calculated indices (S.Schouten, pers. comm.).

The results from the laboratory intercomparison also underlined the high dispersion of TEX_{86} values from different laboratories. This is another drawback worth addressing in future studies, since the comparability of results undertaken by different laboratories is obliged for a reliable use of a proxy, especially a quantitative one. In particular, this is of great importance for the inclusion of TEX_{86} in multiproxy studies and for its use in climate models requiring a quantitative input. Regarding the analytical development of the proxies, the results of this thesis and previous analytical studies suggest that the analytical instrumentation issues are the ones that need more attention in the future. Indeed, the sample extraction techniques (Schouten et al., 2007b) and sample cleanup (this study) appear to be quite less influent on the final indices values.

In relation to the application interpretation of the proxies, the GDGT distributions in surface sediments from 38 lakes of the Iberian Peninsula were examined in Chapter 3. A principal component analysis was undertaken to uncover the main factors influencing the relative abundances of the detected GDGTs; the results indicated that the origin of the lipids (terrestrial versus aquatic), combined with the degree of cyclization and methylation of the lipids were the principal components. The indices BIT, TEX_{86} and MBT were found to be associated to some degree with these principal factors. None of the factors extracted from the principal component analysis was found to be connected to temperature; that is probably due to the complexity of factors that configure the final relative abundances of isoprenoidal and branched GDGTs in the lake sediments. TEX_{86}

and MBT/CBT had thus a limited applicability for reconstructing the lake surface temperatures (LST). In fact, Powers (2005) already emphasized that TEX_{86} is probably easier to apply in large lakes and in that sense, the small size of the lakes surveyed in Iberia was a challenge for the interpretation of this proxy. The high diversity of the lakes studied and significant inputs of soil-derived GDGTs might be two important factors masking the temperature signal.

A cluster analysis was then undertaken in order to seek a subset of lakes with similar characteristics that made them suitable for the application of TEX_{86} and MBT as temperature proxies. The lakes were clustered according to their morphological, chemical and geographical location characteristics and subset calibrations of the TEX_{86} and MBT were tested. Eventually, a group of lakes was identified that showed a fairly linear relationship of these proxies with temperature, comprising mostly deep, low-conductivity lakes, mainly located at high altitude and latitude. These results suggest that GDGT proxies are more successful in lakes that experience the most stable conditions throughout the year, i.e. lakes from high latitudes where hydrological stress is minimized and with sufficient water depth to avoid seasonal desiccation and to buffer changes in chemical input from runoff.

Temperature estimations in the Iberian lakes could likely improve by inspecting the reliability of the Digital Climatic Atlas temperatures at the lakes locations. Aditionally, analysing the MBT and CBT values in the soils of the catchment area of the lakes would be of high interest to compare them with the values in the lake sediments. In fact, this is the first report of MBT and CBT results for lacustrine environments. Further investigation is under way for the delimitation of the catchment basins of the Iberian lakes using GIS tools, which is intended to include the catchment area as a new parameter in the principal component analysis and to indicate the region where soil studies could be undertaken to complement the results presented here.

The validity of TEX_{86}, MBT/CBT and BIT was investigated in Lake Baikal ecosystem (Chapter 4) by means of (i) examining modern fluxes of GDGTs in the lake water column, (ii) inspecting surface sediment proxy values and comparing them with

instrumental temperatures, and (iii) by obtaining two records of the proxies for the last climatic cycle and assessing the agreement with global climatic trends and with other proxy reconstructions within the lake sedimentary archive.

Fluxes of GDGTs were shown to be higher in the South Basin compared to the North Basin of Lake Baikal, consistent with previous studies using other biomarkers. The TEX_{86} values of the collected particulate material in both basins of Lake Baikal were in the range of annual lake surface temperatures (LST). Even a slight bias towards autumn LST was suggested, but seasonal traps would be required to test this hypothesis. Because deep-water GDGT production could not be ruled out, molecular studies targeting the viable archaeal cells in the water column would be very useful in improving the interpretation of the sediment trap material. BIT values were relatively low in both basins, providing some evidence that recent TEX_{86} values are not highly influenced by soil input.

The GDGT signal integrated in the sediment surface also indicated that TEX_{86} was in the range of measured annual LST and that BIT values were relatively low. MBT/CBT proxy was conversely suggesting colder than measured temperatures in the catchment basin of the Lake Baikal. The two records of the GDGT indices in the North and South basins of the lake indicated a climatic control on the TEX_{86} and MBT/CBT indices; this was clear from the reconstructed transition from glacial to interglacial conditions and the partial agreement with reconstructed changes in Lake Baikal region derived from other proxies applied in the sediments. Furthermore, some hints point out that GDGTs could be recording abrupt changes in Lake Baikal, such as Heinrich event signals and the GS-1, and clearly increasing the resolution of the two records is an essential step for future studies. Another critical concern in the outlook is the refinement of the age model for the Lake Baikal sediment cores. This could be further addressed by means of compound-specific radiocarbon analysis (CSRA) on the individual GDGTs. Although this would require isolation of relatively high amounts of GDGTs, performing CSRA could potentially provide a better chronological constraint and at the same time help to resolve the age difference between soil-derived branched GDGTs and mostly pelagic (e.g. crenarchaeol) GDGTs. In any case, the results from Lake Baikal support the idea

that validation of the proxies that want to be used in an ecosystem is extremely useful before climatic reconstructions are undertaken, especially given the limited knowledge of the controls on the GDGT proxies.

Regarding the BIT index, although a relationship between its value and TEX_{86} reliability has been observed, efforts to derive a BIT limit value for the application of TEX_{86} have not yet succeeded. This is probably because BIT is not designed to reflect the amount and distribution of soil-derived isoprenoidal GDGTs. To some extent, the BIT and TEX_{86} values from the Iberian Peninsula lakes reinforce this disconnection, as the final selected lakes considered more adequate for climatic reconstructions using GDGTs have BIT values as high as 0.98 in a scale from 0 to 1. A study of soil composition in terms of isoprenoidal GDGTs and controls on their composition, as well as more investigations of TEX_{86} fluctuations at increasing amounts of soil material following the pioneer study by Weijers et al. (2006b) would surely contribute to a better understanding of BIT-TEX_{86} relationship and to derive additional information from this index.

Furthermore, results from the Lake Baikal survey foresee a possible new application of BIT index, as a proxy of glacier retreat and advance. The preliminary results of two records in Lake Baikal suggest that both river discharge changes associated to moisture availability in the drainage basin and glacier advance and retreat could be the main causes of the BIT oscillations in the sedimentary archive of the lake. More detailed comparison of the obtained records with atmospheric and glacier dynamics reconstructed for the Lake Baikal region are clearly required to confirm this hypothesis. However, the previous use of BIT to recreate the history of reactivation of the hydrological system in Europe during the last deglaciation (Ménot et al., 2006) and the BIT oscillations in sediments from the North Atlantic associated to iceberg discharges during Heinrich events (Schouten et al., 2007d) already provide some support for this hypothesis.

GDGT findings in the impact structure of Bosumtwi in Africa showed the potential of archaeal membrane lipid analysis as indicators of microbial change processes associated

to the evolution of impacted areas. The hypotheses discussed regarding the origin of the GDGTs should be further examined at the light of future intact polar lipid and isotopic analysis on the GDGTs, results that would indicate recent versus ancient GDGT composition and main metabolic processes associated to the source archaea. The recent advances achieved in intact polar GDGT analysis (e.g. Pitcher et al., 2008), guarantee that this technique is going to be of widespread use both in water column studies and especially in sediment records, where it can be applied to distinguish ancient GDGTs bringing past climate information from recent GDGTs synthesized by the subsurface archaea.

The results presented in this thesis have expanded the range of environments where TEX_{86}, MBT, CBT and BIT proxies have been applied, and have strengthened the reliability of the proxy measurements by discussing several analytical methodology advances and performing validation and calibration exercises in Iberian and Siberian lacustrine systems.

Glossary

Branched applied to chemical structures that are composed of a methylated carbon chain. Branched GDGT synthesis is attributed to bacteria.

Eccentricity Earth orbital parameter defined by the shape of the orbit around the sun.

Ekman transport net motion of a fluid resulting from the interaction between Coriolis effect an stress by surface wind.

Isoprenoidal applied to chemical structures that are based on the isoprene unit (isoterpene or 2-methyl-1,3-butadiene). Isoprenoidal GDGTs are ascribed to archaea.

Mesophile an organism with moderate optimum growth temperatures, typically between 15 and 40 ºC.

Methane hydrate solid form of water that encloses a large amount of methane in the crystal structure.

Methanogen organism whose metabolism is characterized by production of methane under anoxic conditions.

Normal phase applied to chromatography that involves a polar stationary phase and a less polar mobile phase.

Obliquity Earth orbital parameter related to the angle of the Earth axis with respect to the plane of revolution around the sun.

Precession Earth orbital parameter related to the direction of the Earth axis in a specific moment of its revolution around the sun.

Thermophile an organism with relatively high optimum growth temperatures, between 45 and 80 °C.

Turbidite sedimentary deposit at the base of the continental slope or on the abyssal plain resulting from an underwater avalanche.

Index of figures and tables

FIGURES

Chapter 1

Chapter 2

Chapter 3

Chapter 4

Chapter 5

TABLES

Chapter 1

Chapter 2

Chapter 3

Chapter 4

References

Albers S. V., van de Vossenberg J., Driessen A. J. M., and Konings W. N. (2000) Adaptations of the archaeal cell membrane to heat stress. *Frontiers In Bioscience* 5, D813-D820.

Aloisi G., Bouloubassi I., Heijs S. K., Pancost R. D., Pierre C., Sinninghe Damsté J. S., Gottschal J. C., Forney L. J., and Rouchy J. M. (2002) CH_4-consuming microorganisms and the formation of carbonate crusts at cold seeps. *Earth and Planetary Science Letters* 203(1), PII S0012-821X(02)00878-6.

Auguet J. C. and Casamayor E. O. (2008) A hotspot for cold Crenarchaeota in the neuston of high mountain lakes. *Environmental Microbiology* 10(4), 1080-1086.

Barns S. M., Delwiche C. F., Palmer J. D., and Pace N. R. (1996) Perspectives on archaeal diversity, thermophily and monophyly from environmental rRNA sequences. *Proceedings of the National Academy of Sciences of the United States of America* 93(17), 9188-9193.

Bendle J. A., Pancost R. D., Weijers J. W. H., Maslin M. A., Sinninghe Damsté J. S., Schouten S., Hopmans E. C., and Boot C. (in prep.) Major changes in Last Glacial and Holocene terrestrial temperatures and sources of organic carbon recorded in the Amazon Fan by the MBT/CBT continental paleothermometer.

Berger A. L. (1978) Long-term variations of caloric insolation resulting from Earth's orbital elements. *Quaternary Research* 9(2), 139-167.

Bezrukova Y. V., Bogdanov Y. A., Williams D. F., Granina L. Z., Grachev M. A., Ignatova N. V., Karabanov Y. B., Kuptsov V. M., Kurylev A. V., Letunova P. P., Likhoshway Y. V., Chernyayeva G. P., Shimarayeva M. K., and Yakushin A. O. (1991) A dramatic change of the ecological-system of Lake Baikal in Holocene. *Doklady Akademii Nauk Sssr* 321(5), 1032-1037.

Biddle J. F., Lipp J. S., Lever M. A., Lloyd K. G., Sorensen K. B., Anderson R., Fredricks H. F., Elvert M., Kelly T. J., Schrag D. P., Sogin M. L., Brenchley J. E., Teske A., House C. H., and Hinrichs K. U. (2006) Heterotrophic archaea dominate sedimentary subsurface ecosystems off Peru. *Proceedings of the National Academy of Sciences of the United States of America* 103(10), 3846-3851.

Blaga C. I., Reichart G. J., Heiri O., and Sinninghe Damsté J. S. (2009) Tetraether membrane lipid distributions in water-column particulate matter and sediments: A study of 47 European lakes along a north-south transect. *Journal of Paleolimnology* 41(3), 523-540.

Bligh E. G. and Dyer W. J. (1959) A rapid method of total lipid extraction and purification. *Canadian Journal Of Biochemistry And Physiology* 37(8), 911-917.

Boës X., Piotrowska N., and Fagel N. (2005) High-resolution diatom/clay record in Lake Baikal from grey scale, and magnetic susceptibility over Holocene and Termination I. *Global and Planetary Change* 46(1-4), 299.

Bolgrien D. W., Granin N. G., and Levin L. (1995) Surface-temperature dynamics of Lake Baikal observed from AVHRR images. *Photogrammetric Engineering And Remote Sensing* 61(2), 211-216.

Bond G., Heinrich H., Broecker W., Labeyrie L., McManus J., Andrews J., Huon S., Jantschik R., Clasen S., Simet C., Tedesco K., Klas M., Bonani G., and Ivy S. (1992) Evidence for massive discharges of icebergs into the North-Atlantic Ocean during the Last Glacial period. *Nature* 360(6401), 245-249.

Bondarenko N. A. and Evstafyev V. K. (2006) Eleven- and ten-year basic cycles of Lake Baikal spring phytoplankton conformed to solar activity cycles. *Hydrobiologia* 568, 19-24.

Bouloubassi I., Aloisi G., Pancost R. D., Hopmans E., Pierre C., and Sinninghe Damsté J. S. (2006) Archaeal and bacterial lipids in authigenic carbonate crusts from Eastern Mediterranean mud volcanoes. *Organic Geochemistry* 37(4), 484-500.

Braconnot P., Otto-Bliesner B., Harrison S., Joussaume S., Peterchmitt J. Y., Abe-Ouchi A., Crucifix M., Driesschaert E., Fichefet T., Hewitt C. D., Kageyama M., Kitoh A., Laine A., Loutre M. F., Marti O., Merkel U., Ramstein G., Valdes P., Weber S. L., Yu Y., and Zhao Y. (2007) Results of PMIP2 coupled simulations of the mid-Holocene and Last Glacial Maximum - part 1: Experiments and large-scale features. *Climate of the Past* 3(2), 261-277.

Brassell S. C., Eglinton G., Marlowe I. T., Pflaumann U., and Sarnthein M. (1986) Molecular stratigraphy: a new tool for climatic assessment. *Nature* 320(13), 129-133.

Brincat D., Yamada K., Ishiwatari R., Uemura H., and Naraoka H. (2000) Molecular-isotopic stratigraphy of long-chain n-alkanes in Lake Baikal Holocene and Glacial Age sediments. *Organic Geochemistry* 31(4), 287-294.

Brochier-Armanet C., Boussau B., Gribaldo S., and Forterre P. (2008) Mesophilic Crenarchaeota: proposal for a third archaeal phylum, the Thaumarchaeota. *Nature Reviews Microbiology* 6(3), 245-252.

Casamayor E. O. and Borrego C. M. (2009) Archaea. In *Encyclopedia of inland waters*, Vol. 3 (ed. G. E. Likens), pp. 167-181. Oxford: Elsevier.

Casamayor E. O., Muyzer G., and Pedros-Alio C. (2001) Composition and temporal dynamics of planktonic archaeal assemblages from anaerobic sulfurous environments studied by 16s rDNA denaturing gradient gel electrophoresis and sequencing. *Aquatic Microbial Ecology* 25(3), 237-246.

Cattell R. B. (1966) The scree test for the number of factors. *Multivariate Behav Res* 1((2)), 245-276.

Cavicchioli R. (2006) Cold-adapted Archaea. *Nature Reviews Microbiology* 4, 331-343.

Cockell C. S. and Lee P. (2002) The biology of impact craters - a review. *Biological Reviews* 77(3), 279-310.

Cockell C. S., Lee P., Broady P., Lim D. S. S., Osinski G. R., Parnell J., Koeberl C., Pesonen L., and Salminen J. (2005) Effects of asteroid and comet impacts on habitats for lithophytic organisms - a synthesis. *Meteoritics & Planetary Science* 40(12), 1901-1914.

Cockell C. S., Osinski G. R., and Lee P. (2003) The impact crater as a habitat: effects of impact processing of target materials. *Astrobiology* 3(1), 181-191.

Cockell C. S., Voytek M. A., Gronstal A. L., Kirshtein J., Finster K., Schippers A., Reysenback A., Gohn G., Sanford W. E., and Horton J. W. (2007) Influence of impacts on the deep subsurface biosphere- preliminary results from the ICDP-USGS Chesapeake Bay impact structure drilling project. *GSA Denver Annual Meeting*, 534.

Colman S. M., Peck J. A., Hatton J., Karabanov E. B., and King J. W. (1999) Biogenic silica records from the BDP93 drill site and adjacent areas of the Selenga Delta, Lake Baikal, Siberia. *Journal of Paleolimnology* 21(1), 9-17.

Colman S. M., Peck J. A., Karabanov E. B., Carter S. J., Bradbury J. P., King J. W., and Williams D. F. (1995) Continental climate response to orbital forcing from biogenic silica records in Lake Baikal. *Nature* 378(6559), 769-771.

Cytryn E., Minz D., Oremland R. S., and Cohen Y. (2000) Distribution and diversity of Archaea corresponding to the limnological cycle of a hypersaline stratified lake (Solar Lake, Sinai, Egypt). *Applied and Environmental Microbiology* 66(8), 3269-3276.

Charlet F., Fagel N., De Batist M., Hauregard F., Minnebo B., and Meischner D. (2005) Sedimentary dynamics on isolated highs in Lake Baikal: Evidence from detailed high-resolution geophysical data and sediment cores. *Global and Planetary Change* 46(1-4), 125.

Chave K. E. (1954a) Aspects of the biogeochemistry of Magnesium .1. Calcareous marine organisms. *Journal of Geology* 62(3), 266-283.

Chave K. E. (1954b) Aspects of the biogeochemistry of Magnesium .2. Calcareous sediments and rocks. *Journal of Geology* 62(6), 587-599.

D'Hondt S., Rutherford S., and Spivack A. J. (2002) Metabolic activity of subsurface life in deep-sea sediments. *Science* 295(5562), 2067-2070.

Dansgaard W., Johnsen S. J., Clausen H. B., Dahljensen D., Gundestrup N. S., Hammer C. U., Hvidberg C. S., Steffensen J. P., Sveinbjornsdottir A. E., Jouzel J., and Bond G. (1993) Evidence for general instability of past climate from a 250-kyr ice-core record. *Nature* 364(6434), 218-220.

Davis B., Brewer S., Stevenson A. C., and Guiot J. (2003) The temperature of Europe during the Holocene reconstructed from pollen data. *Quaternary Science Reviews* 22(15-17), 1701-1716.

de la Torre J. R., Walker C. B., Ingalls A. E., Konneke M., and Stahl D. A. (2008) Cultivation of a thermophilic ammonia oxidizing archaeon synthesizing crenarchaeol. *Environmental Microbiology* 10(3), 810-818.

De Long E. F., King L. L., Massana R., Cittone H., Murray A., Schleper C., and Wakeham S. G. (1998) Dibiphytanyl ether lipids in nonthermophilic crenarchaeotes. *Applied and Environmental Microbiology* 64(3), 1133-1138.

Demory F., Nowaczyk N. R., Witt A., and Oberhansli H. (2005) High-resolution magnetostratigraphy of late Quaternary sediments from Lake Baikal, Siberia: Timing of intracontinental paleoclimatic responses. *Global and Planetary Change* 46(1-4), 167-186.

Demske D., Heumann G., Granoszewski W., Nita M., Mamakowa K., Tarasov P. E., and Oberhansli H. (2005) Late Glacial and Holocene vegetation and regional climate variability evidenced in high-resolution pollen records from Lake Baikal. *Global and Planetary Change* 46(1-4), 255-279.

De Rosa M. and Gambacorta A. (1988) The lipids of Archaebacteria. *Progress In Lipid Research* 27(3), 153-175.

Dong H. L., Zhang G. X., Jiang H. C., Yu B. S., Chapman L. R., Lucas C. R., and Fields M. W. (2006) Microbial diversity in sediments of saline Qinghai Lake, China: linking geochemical controls to microbial ecology. *Microbial Ecology* 51(1), 65-82.

Downing J. A., Prairie Y. T., Cole J. J., Duarte C. M., Tranvik L. J., Striegl R. G., McDowell W. H., Kortelainen P., Caraco N. F., Melack J. M., and Middelburg J. J. (2006) The global abundance and size distribution of lakes, ponds, and impoundments. *Limnology and Oceanography* 51(5), 2388-2397.

Emiliani C. (1955) Pleistocene temperatures. *Journal of Geology* 63(6), 538-578.

Erez J. and Luz B. (1983) Experimental paleotemperature equation for planktonic-foraminifera. *Geochimica et Cosmochimica Acta* 47(6), 1025-1031.

Escala M., Fietz S., Rueda G., and Rosell-Melé A. (in press) Analytical considerations for the use of the paleothermometer Tetraether indEX and the Branched vs. Isoprenoid Tetraether index regarding the choice of cleanup and instrumental conditions. *Analytical Chemistry*.

Escala M., Rosell-Melé A., Fietz S., and Koeberl C. (2008) Archaeabacterial lipids in drill core samples from the Bosumtwi impact structure, Ghana. *Meteoritics and Planetary Science* 43(11), 1777-1782.

Escala M., Rosell-Melé A., and Masqué P. (2007) Rapid screening of glycerol dialkyl glycerol tetraethers in continental Eurasia samples using HPLC/APCI-Ion Trap Mass Spectrometry. *Organic Geochemistry* 38(1), 161-164.

Fang J. S. and Barcelona M. J. (1998) Structural determination and quantitative analysis of bacterial phospholipids using Liquid Chromatography Electrospray Ionisation Mass Spectrometry. *Journal of Microbiological Methods* 33(1), 23-35.

Ferriere L., Koeberl C., and Reimold W. U. (2007) Drill core LB-08a, Bosumtwi impact structure, Ghana: petrographic and shock metamorphic studies of material from the central uplift. *Meteoritics & Planetary Science* 42(4-5), 611-633.

Fietz S., Nicklisch A., and Oberhansli H. (2007) Phytoplankton response to climate changes in Lake Baikal during the Holocene and Kazantsevo interglacials assessed from sedimentary pigments. *Journal of Paleolimnology* 37, 177-203.

Fietz S., Sturm M., and Nicklisch A. (2005) Flux of lipophilic photosynthetic pigments to the surface sediments of Lake Baikal. *Global and Planetary Change* 46(1-4), 29-44.

Forster A., Schouten S., Moriya K., Wilson P. A., and Sinninghe Damsté J. S. (2007) Tropical warming and intermittent cooling during the Cenomanian/Turonian Oceanic Anoxic Event 2: sea surface temperature records from the equatorial Atlantic. *Paleoceanography* 22(1).

Franzmann P. D., Stackebrandt E., Sanderson K., Volkman J. K., Cameron D. E., Stevenson P. L., McMeekin T. A., and Burton H. R. (1988) Halobacterium-lacusprofundi sp-nov, a halophilic bacterium isolated from Deep Lake, Antarctica. *Systematic and Applied Microbiology* 11(1), 20-27.

Fryer G. (1991) Comparative aspects of adaptive radiation and speciation in Lake Baikal and the Great Rift lakes of Africa. *Hydrobiologia* 211(2), 137-146.

Gattinger A., Schloter M., and Munch J. C. (2002) Phospholipid etherlipid and phospholipid fatty acid fingerprints in selected euryarchaeotal monocultures for taxonomic profiling. *FEMS Microbiology Letters* 213(1), PII S0378-1097(02)00794-2.

Glamoclija M. and Schieber J. (2007) Fossil microbial signatures from impact induced hydrothermal settings; preliminary SEM results from the ICDP-USGS Chesapeake Bay impact structure Drilling Project. *GSA Denver Annual Meeting*, 316.

Gliozzi A., Paoli G., Derosa M., and Gambacorta A. (1983) Effect of isoprenoid cyclization on the transition-temperature of lipids in thermophilic Archaebacteria. *Biochimica et Biophysica Acta* 735(2), 234-242.

Gold T. (1992) The deep, hot biosphere. *Proceedings of the National Academy of Sciences of the United States of America* 89(13), 6045-6049.

Guckert J. B., Antworth C. P., Nichols P. D., and White D. C. (1985) Phospholipid, ester-linked fatty-acid profiles as reproducible assays for changes in prokaryotic community structure of estuarine sediments. *Fems Microbiology Ecology* 31(3), 147-158.

Hallam S. J., Konstantinidis K. T., Putnam N., Schleper C., Watanabe Y., Sugahara J., Preston C., de la Torre J., Richardson P. M., and DeLong E. F. (2006) Genomic analysis of the uncultivated marine crenarchaeota Cenarchaeum symbiosum. *Proceedings of the National Academy of Sciences of the United States of America* 103(48), 18296-18301.

Harvey H. R., Fallon R. D., and Patton J. S. (1986) The effect of organic-matter and oxygen on the degradation of bacterial-membrane lipids in marine-sediments. *Geochimica et Cosmochimica Acta* 50(5), 795-804.

Hays J. D., Imbrie J., and Shackleton N. J. (1976) Variations in Earth's orbit - pacemaker of ice ages. *Science* 194(4270), 1121-1132.

Heinrich H. (1988) Origin and consequences of cyclic ice rafting in the northeast Atlantic-Ocean during the past 130,000 years. *Quaternary Research* 29(2), 142-152.

Hemming S. R. (2004) Heinrich events: massive late Pleistocene detritus layers of the North Atlantic and their global climate imprint. *Reviews of Geophysics* 42(1).

Herfort L., Schouten S., Boon J. P., and Sinninghe Damsté J. S. (2006a) Application of the TEX_{86} temperature proxy to the southern North Sea. *Organic Geochemistry* 37(12), 1715-1726.

Herfort L., Schouten S., Boon J. P., Woltering M., Baas M., Weiers J. W. H., and Sinninghe Damsté J. S. (2006b) Characterization of transport and deposition of terrestrial organic matter in the southern North Sea using the BIT index. *Limnology and Oceanography* 51(5), 2196-2205.

Herndl G. J., Reinthaler T., Teira E., van Aken H., Veth C., Pernthaler A., and Pernthaler J. (2005) Contribution of archaea to total prokaryotic production in the deep Atlantic Ocean. *Applied and Environmental Microbiology* 71(5), 2303-2309.

Hershberger K. L., Barns S. M., Reysenbach A. L., Dawson S. C., and Pace N. R. (1996) Wide diversity of Crenarchaeota. *Nature* 384(6608), 420.

Hoefs M. J. L., Schouten S., de Leeuw J. W., King L. L., Wakeham S. G., and Sinnninghe Damsté J. S. (1997) Ether lipids of planktonic Archaea in the marine water column. *Applied and Environmental Microbiology* 63(8), 3090-3095.

Hohmann R., Kipfer R., Peeters F., Piepke G., Imboden D. M., and Shimaraev M. N. (1997) Deep-water renewal in Lake Baikal. *Limnology and Oceanography* 42(5), 841-855.

Hopmans E. C., Schouten S., Pancost R. D., Van der Meer M. T. J., and Sinninghe Damsté J. S. (2000) Analysis of intact tetraether lipids in archaeal cell material and sediments by High Performance Liquid Chromatography/Atmospheric Pressure Chemical Ionization Mass Spectrometry. *Rapid Communications in Mass Spectrometry* 14(7), 585-589.

Hopmans E. C., Weijers J. W. H., Schefuss E., Herfort L., Sinninghe Damsté J. S., and Schouten S. (2004) A novel proxy for terrestrial organic matter in sediments based on branched and isoprenoid tetraether lipids. *Earth and Planetary Science Letters* 224(1-2), 107-116.

Huber H., Hohn M. J., Rachel R., Fuchs T., Wimmer V. C., and Stetter K. O. (2002) A new phylum of Archaea represented by a nanosized hyperthermophilic symbiont. *Nature* 417(6884), 63-67.

Huguet C., de Lange G. J., Gustafsson O., Middelburg J. J., Sinninghe Damsté J. S., and Schouten S. (2008) Selective preservation of soil organic matter in oxidized marine sediments (Madeira Abyssal Plain). *Geochimica et Cosmochimica Acta* 72(24), 6061-6068.

Huguet C., Kim J., Sinninghe Damsté J. S., and Schouten S. (2006) Reconstruction of sea surface temperature variations in the Arabian Sea over the last 23 kyr using organic proxies (TEX_{86} and $U_k^{37'}$). *Paleoceanography* 21(3), PA3003, doi: 10.1029/2005PA001215.

Huguet C., Schimmelmann A., Thunell R., Lourens L. J., Sinninghe Damsté J. S., and Schouten S. (2007a) A study of the TEX_{86} paleothermometer in the water column and sediments of the Santa Barbara Basin, California. *Paleoceanography* 22(3).

Huguet C., Smittenberg R. H., Boer W., Sinninghe Damsté J. S., and Schouten S. (2007b) Twentieth century proxy records of temperature and soil organic matter input in the Drammensfjord, southern Norway. *Organic Geochemistry* 38, 1838-1849.

Ingalls A. E., Shah S. R., Hansman R. L., Aluwihare L. I., Santos G. M., Druffel E. R. M., and Pearson A. (2006) Quantifying archaeal community autotrophy in the mesopelagic ocean using natural radiocarbon. *Proceedings of the National Academy of Sciences of the United States of America* 103(17), 6442-6447.

INTAS Project 99-1669 Team. (2002) A new bathymetric map of Lake Baikal. CD-ROM.

IPCC. (2001) Climate change 2001: The scientific basis. Contribution of working group I to the Third Assessment Report of the Intergovernmental Panel on Climate Change (ed. J. T. Houghton, Y. Ding, D.J. Griggs, M. Noguer, P.J. van der Linden, X. Dai, K. Maskell, and C.A. Johnson), 881 pp.

IPCC. (2007) Climate change 2007: The physical science basis. Contribution of working group I to the Fourth Assessment Report of the Intergovernmental Panel on Climate Change (ed. S. Solomon, D. Qin, M. Manning, Z. Chen, M. Marquis, K.B. Averyt, M. Tignor and H.L. Miller), 996 pp.

Itoh Y. H., Sugai A., Uda I., and Itoh T. (2001) The evolution of lipids. *Space Life Sciences: Living Organisms, Biological Processes and the Limits of Life* 28(4), 719-724.

Jurgens G., Glockner F. O., Amann R., Saano A., Montonen L., Likolammi M., and Munster U. (2000) Identification of novel Archaea in bacterioplankton of a boreal forest lake by phylogenetic analysis and fluorescent in situ hybridization. *FEMS Microbiology Ecology* 34(1), 45-56.

Kaiser H. F. (1958) The Varimax criterion for analytic rotation in factor-analysis. *Psychometrika* 23(3), 187-200.

Kaiser H. F. (1960) The application of electronic-computers to factor-analysis. *Educational and Psychological Measurement* 20(1), 141-151.

Karabanov E., Williams D., Kuzmin M., Sideleva V., Khursevich G., Prokopenko A., Solotchina E., Tkachenko L., Fedenya S., Kerber E., Gvozdkov A., Khlustov O., Bezrukova E., Letunova P., and Krapivina S. (2004) Ecological collapse of Lake Baikal and Lake Hovsgol ecosystems during the Last Glacial and consequences

for aquatic species diversity. *Palaeogeography Palaeoclimatology Palaeoecology* 209(1-4), 227-243.

Karabanov E. B., Prokopenko A. A., Kuz'min M. I., Williams D. F., Gvozdkov A. N., and Kerber E. V. (2001) Glacial and interglacial periods of Siberia: paleoclimate record of Lake Baikal and correlation with west Siberian stratigraphic scheme (the Brunhes Chron). *Geologiya i Geofizika* 42(1-2), 48-63.

Karabanov E. B., Prokopenko A. A., Williams D. F., and Colman S. M. (1998) Evidence from Lake Baikal for Siberian glaciation during oxygen-isotope substage 5d. *Quaternary Research* 50(1), 46-55.

Karabanov E. B., Prokopenko A. A., Williams D. F., and Khursevich G. K. (2000) A new record of Holocene climate change from the bottom sediments of Lake Baikal. *Palaeogeography Palaeoclimatology Palaeoecology* 156(3-4), 211-224.

Karner M. B., DeLong E. F., and Karl D. M. (2001) Archaeal dominance in the mesopelagic zone of the Pacific Ocean. *Nature* 409(25), 507-510.

Kashiwaya K., Ochiai S., Sakai H., and Kawai T. (2001) Orbit-related long-term climate cycles revealed in a 12-Myr continental record from Lake Baikal. *Nature* 410(6824), 71-74.

Kates M., Stanacev N. Z., and Chan T. H. (1963) Aliphatic diether analogs of glyceride-derived lipids .1. Synthesis of d-alpha,beta-dialkyl glyceryl ethers. *Biochemistry* 2(2), 394-&.

Keough B. P., Schmidt T. M., and Hicks R. E. (2003) Archaeal nucleic acids in picoplankton from great lakes on three continents. *Microbial Ecology* 46(2), 238-248.

Khursevich G. K., Karabanov E. B., Prokopenko A. A., Williams D. F., Kuzmin M. I., Fedenya S. A., and Gvozdkov A. A. (2001) Insolation regime in Siberia as a major factor controlling diatom production in Lake Baikal during the past 800,000 years. *Quaternary International* 80-1, 47-58.

Kim J. H., Ludwig W., Schouten S., Kerherve P., Herfort L., Bonnin J., and Sinninghe Damsté J. S. (2007) Impact of flood events on the transport of terrestrial organic matter to the ocean: A study of the Tet River (SW France) using the BIT index. *Organic Geochemistry* 38, 1593-1606.

Kim J. H., Schouten S., Buscail R., Ludwig W., Bonnin J., Sinninghe Damsté J. S., and Bourrin F. (2006) Origin and distribution of terrestrial organic matter in the NW Mediterranean (Gulf of Lions): exploring the newly developed BIT index. *Geochemistry Geophysics Geosystems* 7.

Kim J. H., Schouten S., Hopmans E. C., Donner B., and Sinninghe Damsté J. S. (2008) Global sediment core-top calibration of the TEX_{86} paleothermometer in the ocean. *Geochimica et Cosmochimica Acta* 72, 1154-1173.

King L. L., Pease T. K., and Wakeham S. G. (1998) Archaea in Black Sea water column particulate matter and sediments - evidence from ether lipid derivatives. *Organic Geochemistry* 28(11), 677-688.

Koeberl C., Bottomley R., Glass B. P., and Storzer D. (1997) Geochemistry and age of Ivory Coast tektites and microtektites. *Geochimica et Cosmochimica Acta* 61(8), 1745-1772.

Koeberl C., Milkereit B., Overpeck J. T., Scholz C. A., Amoako P. Y. O., Boamah D., Danuor S., Karp T., Kueck J., Hecky R. E., King J. W., and Peck J. A. (2007) An international and multidisciplinary drilling project into a young complex impact structure: The 2004 ICDP Bosumtwi Crater Drilling Project - an overview. *Meteoritics & Planetary Science* 42(4-5), 483-511.

Koga Y. and Morii H. (2006) Special methods for the analysis of ether lipid structure and metabolism in Archaea. *Analytical Biochemistry* 348(1), 1-14.

Koga Y., Morii H., Akagawa-Matsushita M., and Ohga I. (1998) Correlation of polar lipid composition with 16S rRNA phylogeny in methanogens. Further analysis of lipid component parts. *Bioscience Biotechnology and Biochemistry* 62(2), 230-236.

Koga Y., Nishihara M., Morii H., and Akagawamatsushita M. (1993) Ether polar lipids of methanogenic bacteria - structures, comparative aspects, and biosyntheses. *Microbiological Reviews* 57(1), 164-182.

Könneke M., Bernhard A. E., de la Torre J. R., Walker C. B., Waterbury J. B., and Stahl D. A. (2005) Isolation of an autotrophic ammonia-oxidizing marine archaeon. *Nature* 437(7058), 543-546.

Kontny A., Elbra T., Just J., Pesonen L. J., Schleicher A. M., and Zolk J. (2007) Petrography and shock-related remagnetization of pyrrhotite in drill cores from the Bosumtwi Impact Crater Drilling Project, Ghana. *Meteoritics & Planetary Science* 42(4-5), 811-827.

Kozhov M. (1963) Lake Baikal and its life. *Monographiae Biologicae. Vol. XL*, VI+344p. Illus. Maps.

Kozhova O. M. and Izmest'eva L. R. (1998) *Lake Baikal: Evolution and biodiversity*. Backhuys Publishers.

Kuypers M. M. M., Blokker P., Hopmans E. C., Kinkel H., Pancost R. D., Schouten S., and Sinninghe Damsté J. S. (2002) Archaeal remains dominate marine organic matter from the early Albian Oceanic Anoxic Event 1b. *Palaeogeography Palaeoclimatology Palaeoecology* 185(1-2), PII S0031-0182(02)00301-2.

Le Treut H., Somerville R., Cubasch U., Ding Y., Mauritzen C., Mokssit A., Peterson T., and Prather M. (2007) Historical overview of climate change. In *Climate change 2007: The physical science basis. Contribution of working group I to the Fourth*

Assessment Report of the Intergovernmental Panel on Climate Change (ed. S. Solomon, D. Qin, M. Manning, Z. Chen, M. Marquis, K.B. Averyt, M. Tignor and H.L. Miller). Cambridge University Press, Cambridge, United Kingdom and New York.

Lea D. W. (2003) Elemental and isotopic proxies of past ocean temperatures. In *The oceans and marine geochemistry* (ed. H. Elderfield), pp. 365-390. Elsevier.

Leininger S., Urich T., Schloter M., Schwark L., Qi J., Nicol G. W., Prosser J. I., Schuster S. C., and Schleper C. (2006) Archaea predominate among ammonia-oxidizing prokaryotes in soils. *Nature* 442, 806-809.

Li J. G., Philp R. P., Pu F., and Allen J. (1996) Long-chain alkenones in Qinghai Lake sediments. *Geochimica et Cosmochimica Acta* 60(2), 235-241.

Lindgren P., Parnell J., Bowden S. A., Taylor C., Osinski G. R., and Lee P. (2006) Preservation of biological signature within impact melt breccias, Haughton Impact Structure. In *Lunar and Planetary Science 37* Vol. Abstract 1028, Lunar and Planetary Institute, Houston. Lunar and Planetary Institute, Houston (CD-ROM).

Lipp J. S., Morono Y., Inagaki F., and Hinrichs K. U. (2008) Significant contribution of Archaea to extant biomass in marine subsurface sediments. *Nature* 454(7207), 991-994.

Livingstone D. M. (1999) Ice break-up on southern Lake Baikal and its relationship to local and regional air temperatures in Siberia and to the North Atlantic Oscillation. *Limnology and Oceanography* 44(6), 1486-1497.

Lowe J. J., Rasmussen S. O., Bjorck S., Hoek W. Z., Steffensen J. P., Walker M. J. C., Yu Z. C., and Grp I. (2008) Synchronisation of palaeoenvironmental events in the North Atlantic region during the last Termination: a revised protocol recommended by the INTIMATE group. *Quaternary Science Reviews* 27(1-2), 6-17.

MacGregor B. J., Moser, D.P., Alm, E.W., Nealson, K.H., Stahl, D.A. (1997) Crenarchaeota in Lake Michigan sediment. *Applied and Environmental Microbiology* 63(3), 1178-1181.

Mackay A. W. (2007) The paleoclimatology of Lake Baikal: a diatom synthesis and prospectus. *Earth-Science Reviews* 82(3-4), 181-215.

Magnuson J. J., Robertson D. M., Benson B. J., Wynne R. H., Livingstone D. M., Arai T., Assel R. A., Barry R. G., Card V., Kuusisto E., Granin N. G., Prowse T. D., Stewart K. M., and Vuglinski V. S. (2000) Historical trends in lake and river ice cover in the Northern Hemisphere. *Science* 289(5485), 1743-1746.

Mancuso C. A., Nichols P. D., and White D. C. (1986) A method for the separation and characterization of archaebacterial signature ether lipids. *Journal of Lipid Research* 27(1), 49-56.

Martín-Rubio M., Rodríguez-Lázaro J., Anadon P., Robles F., Utrilla R., and Vázquez A. (2005) Factors affecting the distribution of recent lacustrine ostracoda from the Caicedo de Yuso-Arreo Lake (Western Ebro Basin, Spain). *Palaeogeography Palaeoclimatology Palaeoecology* 225(1-4), 118-133.

Martin P., Boes X., Goddeeris B., and Fagel N. (2005) A qualitative assessment of the influence of bioturbation in Lake Baikal sediments. *Global and Planetary Change* 46(1-4), 87-99.

Ménot G., Bard E., Rostek F., Weijers J. W. H., Hopmans E. C., Schouten S., and Sinninghe Damsté J. S. (2006) Early reactivation of European rivers during the Last Deglaciation. *Science* 313(5793), 1623-1625.

Mighall T. M., Martínez Cortizas A., Biester H., and Turner S. E. (2006) Proxy climate and vegetation changes during the last five millennia in NW Iberia: pollen and non-pollen palynomorph data from two ombrotrophic peat bogs in the north western Iberian Peninsula. *Review of Palaeobotany and Palynology* 141(1-2), 203-223.

Milligan G. W. (1980) An examination of the effect of six types of error perturbation on fifteen clustering algorithms. *Psycometrika* 45(3), 325-342.

Mitchell T. D. (2003) A comprehensive set of climate scenarios for Europe and the globe. Tyndall centre working paper 55.

Moreno A., Valero-Garcés B. L., González-Sampériz P., and Rico M. (2008) Flood response to rainfall variability during the last 2000 years inferred from the Taravilla Lake record (Central Iberian Range, Spain). *Journal of Paleolimnology* 40(3), 943-961.

Morley D. W., Leng M. J., Mackay A. W., and Sloane H. J. (2005) Late Glacial and Holocene environmental change in the Lake Baikal region documented by oxygen isotopes from diatom silica. *Global and Planetary Change* 46(1-4), 221-233.

Müller B., Maerki M., Schmid M., Vologina E. G., Wehrli B., Wüest A., and Sturm M. (2005) Internal carbon and nutrient cycling in Lake Baikal: sedimentation, upwelling, and early diagenesis. *Global and Planetary Change* 46(1-4), 101-124.

Naughton F., Goni M. F. S., Desprat S., Turon J. L., Duprat J., Malaize B., Joli C., Cortijo E., Drago T., and Freitas M. C. (2007) Present-day and past (last 25 000 years) marine pollen signal off western Iberia. *Marine Micropaleontology* 62(2), 91-114.

Nicault A., Alleaume S., Brewer S., Carrer M., Nola P., and Guiot J. (2008) Mediterranean drought fluctuation during the last 500 years based on tree-ring data. *Climate Dynamics* 31(2-3), 227-245.

Ninyerola M., Pons X., and Roure J. M. (2005) Atlas climático digital de la Península Ibérica. Metodología y aplicaciones en bioclimatología y geobotánica. Universitat Autònoma de Barcelona, Bellaterra.

Nishihara M. and Koga Y. (1987) Extraction and composition of polar lipids from the archaebacterium Methanobacterium-thermoautotrophicum - effective extraction of tetraether lipids by an acidified solvent. *Journal Of Biochemistry* 101(4), 997-1005.

Oberhänsli H. and Mackay A. W. (2005) Introduction to "Progress towards reconstructing past climate in central Eurasia, with special emphasis on Lake Baikal". *Global and Planetary Change* 46(1-4), 1-7.

Øvreås L., Forney L., Daae F. L., and Torsvik V. (1997) Distribution of bacterioplankton in meromictic Lake Saelenvannet, as determined by denaturing gradient gel electrophoresis of pcr-amplified gene fragments coding for 16S rRNA. *Applied and Environmental Microbiology* 63(9), 3367-3373.

Paillard D. (2001) Glacial cycles: toward a new paradigm. *Reviews of Geophysics* 39(3), 325-346.

Pancost R. D., Hopmans E. C., Sinninghe Damsté J. S., and Party M. S. S. (2001) Archaeal lipids in Mediterranean cold seeps: molecular proxies for anaerobic methane oxidation. *Geochimica et Cosmochimica Acta* 65(10), 1611-1627.

Parkes R. J., Cragg B. A., Bale S. J., Getliff J. M., Goodman K., Rochelle P. A., Fry J. C., Weightman A. J., and Harvey S. M. (1994) Deep bacterial biosphere in Pacific-Ocean sediments. *Nature* 371(6496), 410-413.

Parnell J. and Lindgren P. (2006) The processing of organic matter in impact craters. In *First International Conference on Impact Cratering in the Solar System*. European Space Agency.

Parnell J., Osinski G. R., Lee P., Green P. F., and Baron M. J. (2005) Thermal alteration of organic matter in an impact crater and the duration of postimpact heating. *Geology* 33(5), 373-376.

Pearson E. J., Farrimond P., and Juggins S. (2007) Lipid geochemistry of lake sediments from semi-arid Spain: relationships with source inputs and environmental factors. *Organic Geochemistry* 38(7), 1169-1195.

Peltier W. R. (2004) Global glacial isostasy and the surface of the Ice-Age Earth: the ICE-5G (VM2) model and grace. *Annual Review of Earth and Planetary Sciences* 32, 111-149.

Peñalba M. C., Arnold M., Guiot J., Duplessy J. C., and de Beaulieu J. L. (1997) Termination of the Last Glaciation in the Iberian Peninsula inferred from the pollen sequence of Quintanar de la Sierra. *Quaternary Research* 48(2), 205-214.

Pernthaler J., Glockner F. O., Unterholzner S., Alfreider A., Psenner R., and Amann R. (1998) Seasonal community and population dynamics of pelagic bacteria and archaea in a high mountain lake. *Applied and Environmental Microbiology* 64(11), 4299-4306.

Peterse F., Schouten S., van der Meer J., van der Meer M. T. J., and Sinninghe Damsté J. S. (2009) Distribution of branched tetraether lipids in geothermally heated soils: implications for the MBT/CBT temperature proxy. *Organic Geochemistry* 40(2), 201-205.

Petersen M. T., Newsom H. E., Nelson M. J., and Moore D. M. (2007) Hydrothermal alteration in the Bosumtwi Impact Structure: evidence from 2m(1)-muscovite, alteration veins, and fracture fillings. *Meteoritics & Planetary Science* 42(4-5), 655-666.

Pichon J. J., Labracherie M., Labeyrie L. D., and Duprat J. (1987) Transfer-functions between diatom assemblages and surface hydrology in the Southern-Ocean. *Palaeogeography Palaeoclimatology Palaeoecology* 61(1-2), 79-95.

Piotrowska N., Bluszcz A., Demske D., Granoszewski W., and Heumann G. (2004) Extraction and AMS radiocarbon dating of pollen from Lake Baikal sediments. *Radiocarbon* 46(1), 181-187.

Pitcher A., Hopmans E. C., Schouten S., and Sinninghe Damsté J. S. (2009) Separation of core and intact polar archaeal tetraether lipids using silica columns: insights into living and fossil biomass contributions. *Organic Geochemistry* 40(1), 12-19.

Poole C. F. (2003) *The essence of chromatography*. Elsevier: Amsterdam. 925 pp.

Popovskaya G. I. (1987) Phytoplankton of the world's deepest lake. *Proceedings of the Zoological Institute of USSR Academy of Sciences* 172, 107-116, (in Russian).

Porter S. C. and An Z. S. (1995) Correlation between climate events in the North-Atlantic and China during the Last Glaciation. *Nature* 375(6529), 305-308.

Powers L. A. (2005) Calibration and applicaton of a new paleotemperature tool in lacustrine systems: TEX_{86} for continental paleoclimate reconstruction. PhD thesis, University of Minnesota.

Powers L. A., Johnson T. C., Werne J. P., Castañeda I. S., Hopmans E. C., Sinninghe Damsté J. S., and Schouten S. (2005) Large temperature variability in the Southern African Tropics since the Last Glacial Maximum. *Geophysical Research Letters* 32(8), doi:10.1029/2004GL022014.

Powers L. A., Werne J. P., Johnson T. C., Hopmans E. C., Sinninghe Damsté J. S., and Schouten S. (2004) Crenarchaeotal membrane lipids in lake sediments: a new paleotemperature proxy for continental paleoclimate reconstruction? *Geology* 32(7), 613-616.

Prahl F. G. and Wakeham S. G. (1987) Calibration of unsaturation patterns in long-chain ketone compositions for palaeotemperature assessment. *Nature* 330(26), 367-369.

Preston C. M., Wu K. Y., Molinski T. F., and DeLong E. F. (1996) A psychrophilic crenarchaeon inhabits a marine sponge: Cenarchaeum symbiosum gen nov, sp, nov. *Proceedings of the National Academy of Sciences of the United States of America* 93(13), 6241-6246.

Prokopenko A. A., Hinnov L. A., Williams D. F., and Kuzmin M. I. (2006) Orbital forcing of continental climate during the Pleistocene: a complete astronomically tuned climatic record from Lake Baikal, se Siberia. *Quaternary Science Reviews* 25(23-24), 3431-3457.

Prokopenko A. A., Karabanov E. B., Williams D. F., Kuzmin M. I., Khursevich G. K., and Gvozdkov A. A. (2001a) The detailed record of climatic events during the past 75,000 yrs BP from the Lake Baikal drill core BDP-93-2. *Quaternary International* 80-1, 59-68.

Prokopenko A. A. and Williams D. F. (2004) Deglacial methane emission signals in the carbon isotopic record of Lake Baikal. *Earth and Planetary Science Letters* 218(1-2), 135-147.

Prokopenko A. A., Williams D. F., Karabanov E. B., and Khursevich G. K. (2001b) Continental response to Heinrich events and Bond cycles in sedimentary record of Lake Baikal, Siberia. *Global and Planetary Change* 28(1-4), 217-226.

Réthoré G., Montier T., Le Gall T., Delepine P., Cammas-Marion S., Lemiegre L., Lehn P., and Benvegnu T. (2007) Archaeosomes based on synthetic tetraether-like lipids as novel versatile gene delivery systems. *Chemical Communications*(20), 2054-2056.

Riera S., Wansard G., and Julia R. (2004) 2000-year environmental history of a karstic lake in the Mediterranean Pre-Pyrenees: the Estanya Lakes (Spain). *Catena* 55(3), 293-324.

Rosell-Melé A. (2003) Biomarkers as proxies of climate change. In *Global change in the Holocene* (ed. A. W. Mackay, R. W. Battarbee, J. B. Birks, and F. Oldfield), pp. 358-372.

Rossel P. E., Lipp J. S., Fredricks H. F., Arnds J., Boetius A., Elvert M., and Hinrichs K. U. (2008) Intact polar lipids of anaerobic methanotrophic archaea and associated bacteria. *Organic Geochemistry* 39(8), 992-999.

Rueda G., Rosell-Melé A., Escala M., Gyllencreutz R., and Backman J. (2009) Comparison of instrumental and GDGT-based estimates of sea surface and air temperatures from the Skagerrak. *Organic Geochemistry* 40(2), 287-291.

Russell M. and Rosell-Melé A. (2005) Preliminary study of fluxes of major lipid biomarker classes in the water column and sediments of Lake Baikal, Russia. *Global and Planetary Change* 46(1-4), 45-56.

Schleper C., DeLong E. F., Preston C. M., Feldman R. A., Wu K. Y., and Swanson R. V. (1998) Genomic analysis reveals chromosomal variation in natural populations of the uncultured psychrophilic archaeon Cenarchaeum symbiosum. *Journal of Bacteriology* 180(19), 5003-5009.

Schleper C., Holben W., Klenk H.P. (1997a) Recovery of crenarchaeotal ribosomal DNA sequences from freshwater-lake sediments. *Applied and Environmental Microbiology* 63 (1), 321-323.

Schleper C., Swanson R. V., Mathur E. J., and DeLong E. F. (1997b) Characterization of a DNA polymerase from the uncultivated psychrophilic archaeon Cenarchaeum symbiosum. *Journal of Bacteriology* 179(24), 7803-7811.

Schmid M., Budnev N. M., Granin N. G., Sturm M., Schurter M., and Wüest A. (2008) Lake Baikal deepwater renewal mystery solved. *Geophysical Research Letters* 35(9).

Schmid M., De Batist M., Granin N. G., Kapitanov V. A., McGinnis D. F., Mizandrontsev I. B., Obzhirov A. I., and Wüest A. (2007) Sources and sinks of methane in Lake Baikal: A synthesis of measurements and modeling. *Limnology and Oceanography* 52(5), 1824-1837.

Scholz C. A., Karp T., Brooks K. M., Milkereit B., Amoako P. Y. O., and Arko J. A. (2002) Pronounced central uplift identified in the Bosumtwi Impact Structure, Ghana, using multichannel seismic reflection data. *Geology* 30(10), 939-942.

Scholz C. A., Karp T., and Lyons R. P. (2007) Structure and morphology of the Bosumtwi Impact Structure from seismic reflection data. *Meteoritics & Planetary Science* 42(4-5), 549-560.

Schouten S., Forster A., Panoto F. E., and Sinninghe Damsté J. S. (2007a) Towards calibration of the TEX_{86} palaeothermometer for tropical sea surface temperatures in ancient greenhouse worlds. *Organic Geochemistry* 38, 1537-1546.

Schouten S., Hoefs M. J. L., Koopmans M. P., Bosch H. J., and Damsté J. S. S. (1998) Structural characterization, occurrence and fate of archaeal ether-bound acyclic and cyclic biphytanes and corresponding diols in sediments. *Organic Geochemistry* 29(5-7), 1305-1319.

Schouten S., Hopmans E. C., Baas M., Boumann H., Standfest S., Konneke M., Stahl D. A., and Sinnnghe Damsté J. S. (2008a) Intact membrane lipids of "Candidatus nitrosopumilus maritimus," A cultivated representative of the cosmopolitan mesophilic group I Crenarchaeota. *Applied and Environmental Microbiology* 74(8), 2433-2440.

Schouten S., Hopmans E. C., and Sinninghe Damsté J. S. (2004) The effect of maturity and depositional redox conditions on archaeal tetraether lipid palaeothermometry. *Organic Geochemistry* 35(5), 567-571.

Schouten S., Hopmans E. C., Pancost R. D., and Sinninghe Damsté J. S. (2000) Widespread occurrence of structurally diverse tetraether membrane lipids: evidence for the ubiquitous presence of low-temperature relatives of hyperthermophiles. *Proceedings of the National Academy of Sciences of the United States of America* 97(26), 14421-14426.

Schouten S., Hopmans E. C., Schefuss E., and Sinninghe Damsté J. S. (2002) Distributional variations in marine crenarchaeotal membrane lipids: A new tool for reconstructing ancient sea water temperatures?. *Earth and Planetary Science Letters* 204(1-2), 265-274.

Schouten S., Hopmans E. C., van der Meer J., Mets A., Bard E., Bianchi T. S., Diefendorf A., Escala M., Freeman K. H., Furukawa Y., Huguet C., Ingalls A., Menot-Combes G., Nederbragt A. J., Oba M., Pearson A., Pearson E. J., Rosell-Melé A., Schaeffer P., Shah S. R., Shanahan T. M., Smith R. W., Smittenberg R., Talbot H. M., Uchida M., Van Mooy B. A. S., Yamamoto M., Zhang Z. H., and Sinninghe Damsté J. S. (2009) An interlaboratory study of TEX_{86} and BIT analysis using High-Performance Liquid Chromatography-Mass Spectrometry. *Geochemistry Geophysics Geosystems* 10.

Schouten S., Huguet C., Hopmans E. C., Kienhuis M. V. M., and Sinninghe Damsté J. S. (2007b) Analytical methodology for TEX_{86} paleothermometry by High-Performance Liquid Chromatography/Atmospheric Pressure Chemical Ionization-Mass Spectrometry. *Analytical Chemistry* 79(7), 2940-2944.

Schouten S., Ossebaar J., Brummer G. J., Elderfield H., and Sinninghe Damsté J. S. (2007c) Transport of terrestrial organic matter to the deep North Atlantic Ocean by ice rafting. *Organic Geochemistry* 38(7), 1161-1168.

Schouten S., van der Meer M. T. J., Hopmans E. C., and Sinninghe Damsté J. S. (2008b) Comment on "Lipids of marine archaea: patterns and provenance in the water column and sediments" By Turich et al. (2007). *Geochimica et Cosmochimica Acta* 72(21), 5342-5346.

Schouten S., van der Meer M. T. J., Hopmans E. C., Rijpstra W. I. C., Reysenbach A. L., Ward D. M., and Sinninghe Damsté J. S. (2007d) Archaeal and bacterial glycerol dialkyl glycerol tetraether lipids in hot springs of Yellowstone National Park. *Applied and Environmental Microbiology* 73, 6181-6191.

Seal R. R. and Shanks W. C. (1998) Oxygen and hydrogen isotope systematics of Lake Baikal, Siberia: Implications for paleoclimate studies. *Limnology and Oceanography* 43(6), 1251-1261.

Shimada H., Nemoto N., Shida Y., Oshima T., and Yamagishi A. (2002) Complete polar lipid composition of thermoplasma acidophilum HO-62 determined by High-Performance Liquid Chromatography with Evaporative Light-Scattering Detection. *Journal of Bacteriology* 184(2), 556-563.

Shimaraev M. N., Granin N. G., and Zhdanov A. A. (1993) Deep ventilation of Lake Baikal waters due to spring thermal bars. *Limnology and Oceanography* 38(5), 1068-1072.

Shimaraev M. N., Verbolov V. I., Granin N. G., and Sherstayankin P. P. (1994) *Physical limnology of Lake Baikal: A review*.

Sinninghe Damsté J. S., Hopmans E. C., Pancost R. D., Schouten S., and Geenevasen J. A. J. (2000) Newly discovered non-isoprenoid glycerol dialkyl glycerol tetraether lipids in sediments. *Chemical Communications*(17), 1683-1684.

Sinninghe Damsté J. S., Ossebaar J., Schouten S., and Verschuren D. (2006) A new palaeoproxy for lake temperatures based on crenarchaeotal lipids: Application in Lake Challa, East Africa. *EGU General Assembly*, abstract 05784.

Sinninghe Damsté J. S., Rijpstra W. I. C., Hopmans E. C., Prahl F. G., Wakeham S. G., and Schouten S. (2002a) Distribution of membrane lipids of planktonic Crenarchaeota in the Arabian Sea water column. *Applied and Environmental Microbiology* 68(6), 2997-3002.

Sinninghe Damsté J. S., Schouten S., Hopmans E. C., van Duin A. C. T., and Geenevasen J. A. J. (2002b) Crenarchaeol: the characteristic core glycerol dibiphytanyl glycerol tetraether membrane lipid of cosmopolitan pelagic Crenarchaeota. *Journal of Lipid Research* 43(10), 1641-1651.

Soma Y., Tanaka A., Soma M., and Kawai T. (1996) Photosynthetic pigments and perylene in the sediments of southern basin of Lake Baikal. *Organic Geochemistry* 24(5), 553-561.

Soma Y., Tani Y., Soma M., Mitake H., Kurihara R., Hashomoto S., Watanabe T., and Nakamura T. (2007) Sedimentary steryl chlorin esters (SCES) and other photosynthetic pigments as indicators of paleolimnological change over the last 28,000 years from the Buguldeika Saddle of Lake Baikal. *Journal of Paleolimnology* 37, 163-175.

Stuiver M., Grootes P. M., and Braziunas T. F. (1995) The GISP2 delta O-18 climate record of the past 16,500 years and the role of the sun, ocean, and volcanoes. *Quaternary Research* 44(3), 341-354.

Sturt H. F., Summons R. E., Smith K., Elvert M., and Hinrichs K. U. (2004) Intact polar membrane lipids in prokaryotes and sediments deciphered by High-Performance Liquid Chromatography/Electrospray Ionization Multistage Mass Spectrometry - new biomarkers for biogeochemistry and microbial ecology. *Rapid Communications in Mass Spectrometry* 18(6), 617-628.

Swann G. E. A., Mackay A. W., Leng M. J., and Demory F. (2005) Climatic change in Central Asia during MIS 3/2: a case study using biological responses from Lake Baikal. *Global and Planetary Change* 46(1-4), 235-253.

Tague C., Farrell M., Grant G., Lewis S., and Rey S. (2007) Hydrogeologic controls on summer stream temperatures in the Mackenzie river basin, Oregon. *Hydrological Processes* 21(24), 3288-3300.

Tani Y., Kurihara K., Nara F., Itoh N., Soma M., Soma Y., Tanaka A., Yoneda M., Hirota M., and Shibata Y. (2002) Temporal changes in the phytoplankton community of the southern basin of Lake Baikal over the last 24,000 years recorded by photosynthetic pigments in a sediment core. *Organic Geochemistry* 33(12), 1621-1634.

Tarasov P., Granoszewski W., Bezrukova E., Brewer S., Nita M., Abzaeva A., and Oberhansli H. (2005) Quantitative reconstruction of the Last Interglacial vegetation and climate based on the pollen record from Lake Baikal, Russia. *Climate Dynamics* 25(6), 625-637.

Tierney J. E., Russell J. M., Huang Y. S., Sinninghe Damsté J. S., Hopmans E. C., and Cohen A. S. (2008) Northern hemisphere controls on tropical Southeast African climate during the past 60,000 years. *Science* 322(5899), 252-255.

Todd M. C. and Mackay A. W. (2003) Large-scale climatic controls on Lake Baikal ice cover. *Journal of Climate* 16(19), 3186-3199.

Tornabene T. G. and Langworthy T. A. (1979) Diphytanyl and dibiphytanyl glycerol ether lipids of methanogenic archaeabacteria. *Science* 203(4375), 51-53.

Turich C., Freeman K. H., Bruns M. A., Conte M., Daniel Jones A., and Wakeham S. G. (2007) Lipids of marine archaea: patterns and provenance in the water-column and sediments. *Geochimica et Cosmochimica Acta* 71, 3272-3291.

Turich C., Freeman K. H., Jones A. D., Bruns M. A., Conte M., and Wakeham S. G. (2008) Reply to the comment by S. Schouten, M. Van der Meer, E. Hopmans, and J.S. Sinninghe Damsté on "Lipids of marine archaea: patterns and provenance in the water column". *Geochimica et Cosmochimica Acta* 72(21), 5347-5349.

Uda I., Sugai A., Itoh Y. H., and Itoh T. (2001) Variation in molecular species of polar lipids from thermoplasma acidophilum depends on growth temperature. *Lipids* 36(1), 103-105.

Urbach E., Vergin K. L., Young L., Morse A., Larson G. L., and Giovannoni S. J. (2001) Unusual bacterioplankton community structure in ultra-oligotrophic crater lake. *Limnology and Oceanography* 46(3), 557-572.

Valero-Garcés B. L., Moreno A., Navas A., Mata P., Machín J., Huertas A. D., Sampériz P. G., Schwalb A., Morellón M., Cheng H., and Edwards R. L. (2008) The Taravilla Lake and tufa deposits (Central Iberian Range, Spain) as palaeohydrological and palaeoclimatic indicators. *Palaeogeography Palaeoclimatology Palaeoecology* 259(2-3), 136-156.

van Dongen B. E., Semiletov I., Weijers J. W. H., and Gustafsson O. R. (2008) Contrasting lipid biomarker composition of terrestrial organic matter exported from across the Eurasian Arctic by the five great Russian Arctic rivers. *Global Biogeochemical Cycles* 22.

van deVossenberg J., UbbinkKok T., Elferink M. G. L., Driessen A. J. M., and Konings W. N. (1995) Ion permeability of the cytoplasmic membrane limits the maximum growth temperature of Bacteria and Archaea. *Molecular Microbiology* 18(5), 925-932.

Velichko A. A., Catto N., Drenova A. N., Klimanov V. A., Kremenetski K. V., and Nechaev V. P. (2002) Climate changes in east Europe and Siberia at the late glacial-Holocene transition. *Quaternary International* 91(1), 75.

Voytek M. A., Amirbahman A., Cockell C. S., Jones E. J. P., Kirshtein J. D., Ohno T., and Sanford W. E. (2007) Biogeochemical evidence for in situ microbial metabolism in the Chesapeake Bay impact structure. *GSA Denver Annual Meeting*, 535.

Walker I. R., Smol J. P., Engstrom D. R., and Birks H. J. B. (1991) An assessment of chironomidae as quantitative indicators of past climatic-change. *Canadian Journal of Fisheries and Aquatic Sciences* 48(6), 975-987.

Webb B. W. and Nobilis F. (1997) Long-term perspective on the nature of the air-water temperature relationship: A case study. *Hydrological Processes* 11(2), 137-147.

Wefer G., Berger W. H., Bijma J., and Fischer G. (1999) Clues to ocean history: a brief overview of proxies. In *Use of proxies in paleoceanography: examples from the South Atlantic* (ed. G. Fischer and G. Wefer), pp. 734.

Weijers J. W. H., Schefuss E., Schouten S., and Sinninghe Damsté J. S. (2007a) Coupled thermal and hydrological evolution of tropical Africa over the last deglaciation. *Science* 315(5819), 1701-1704.

Weijers J. W. H., Schouten S., Hopmans E. C., Geenevasen J. A. J., David O. R. P., Coleman J. M., Pancost R. D., and Sinninghe Damsté J. S. (2006a) Membrane lipids of mesophilic anaerobic bacteria thriving in peats have typical archaeal traits. *Environmental Microbiology* 8(4), 648-657.

Weijers J. W. H., Schouten S., Spaargaren O. C., and Sinninghe Damsté J. S. (2006b) Occurrence and distribution of tetraether membrane lipids in soils: implications for the use of the TEX_{86} proxy and the BIT index. *Organic Geochemistry* 37(12), 1680-1693.

Weijers J. W. H., Schouten S., van den Donker J. C., Hopmans E. C., and Sinninghe Damsté J. S. (2007b) Environmental controls on bacterial tetraether membrane lipid distribution in soils. *Geochimica et Cosmochimica Acta* 71(3), 703-713.

Weijers J. W. H., Schouten S., van der Linden M., van Geel B., and Sinnninghe Damsté J. S. (2004) Water table related variations in the abundance of intact archaeal membrane lipids in a Swedish peat bog. *FEMS Microbiology Letters* 239(1), 51-56.

Weiss R. F., Carmack E. C., and Koropalov V. M. (1991) Deep-water renewal and biological production in Lake Baikal. *Nature* 349(6311), 665-669.

Wetzel R. G. (2001) *Limnology: Lake and river ecosystems*. London, UK, Academic Press. 1006 pp.

White D. C., Davis W. M., Nickels J. S., King J. D., and Bobbie R. J. (1979) Determination of the sedimentary microbial biomass by extractable lipid phosphate. *Oecologia* 40(1), 51-62.

Whitman W. B., Coleman D. C., and Wiebe W. J. (1998) Prokaryotes: The unseen majority. *Proceedings of the National Academy of Sciences of the United States of America* 95(12), 6578-6583.

Williams D. F., Kuzmin M. I., Prokopenko A. A., Karabanov E. B., Khursevich G. K., and Bezrukova E. V. (2001) The Lake Baikal drilling projects in the context of a global lake drilling initiative. *Quaternary International* 80-1, 3-18.

Williams D. F., Peck J., Karabanov E. B., Prokopenko A. A., Kravchinsky V., King J., and Kuzmin M. I. (1997) Lake Baikal record of continental climate response to orbital insolation during the past 5 million years. *Science* 278(5340), 1114-1117.

Woese C. R., Balch W. E., Magrum L. J., Fox G. E., and Wolfe R. S. (1977) Ancient divergence among Bacteria. *Journal of Molecular Evolution* 9(4), 305-311.

Woese C. R., Kandler O., and Wheelis M. L. (1990) Towards a natural system of organisms - proposal for the domains Archaea, Bacteria and Eukarya. *Proceedings of the National Academy of Sciences of the United States of America* 87(12), 4576-4579.

Wuchter C., Schouten S., Coolen M. J. L., and Sinninghe Damsté J. S. (2004) Temperature-dependent variation in the distribution of tetraether membrane lipids of marine crenarchaeota: implications for TEX_{86} paleothermometry. *Paleoceanography* 19(4), PA4028 10.1029/2004PA001041.

Wuchter C., Schouten S., Wakeham S. G., and Sinninghe Damsté J. S. (2005) Temporal and spatial variation in tetraether membrane lipids of marine Crenarchaeota in particulate organic matter: Implications for TEX_{86} paleothermometry. *Paleoceanography* 20(3), PA3013 10.1029/2004PA001110

Wuchter C., Schouten S., Wakeham S. G., and Sinninghe Damsté J. S. (2006) Archaeal tetraether membrane lipid fluxes in the northeastern Pacific and the Arabian Sea: implications for TEX_{86} paleothermometry. *Paleoceanography* 21(4).

Wüest A., Ravens T. M., Granin N. G., Kocsis O., Schurter M., and Sturm M. (2005) Cold intrusions in Lake Baikal: Direct observational evidence for deep-water renewal. *Limnology and Oceanography* 50(1), 184-196.

Ye H. C. (2000) Decadal variability of Russian winter snow accumulation and its associations with Atlantic sea surface temperature anomalies. *International Journal of Climatology* 20(14), 1709-1728.

Ye H. C. (2001) Quasi-biennial and quasi-decadal variations in snow accumulation over northern Eurasia and their connections to the Atlantic and Pacific Oceans. *Journal of Climate* 14(24), 4573-4584.

Zink K. G., Leythaeuser D., Melkonian M., and Schwark L. (2001) Temperature dependency of long-chain alkenone distributions in recent to fossil limnic sediments and in lake waters. *Geochimica et Cosmochimica Acta* 65(2), 253-265.

Zink K. G., Mangelsdorf K., Granina L., and Horsfield B. (2008) Estimation of bacterial biomass in subsurface sediments by quantifying intact membrane phospholipids. *Analytical and Bioanalytical Chemistry* 390(3), 885-896.

Appendices

Appendix 1

ANALYTICAL PROTOCOLS

1. FREEZE-DRYING

1.1. Sediment or glass fibre filter samples were frozen at -20 ºC.

1.2. The samples were freeze-dried for 24 h (filters) or 48 h (sediments) using a Cryodos freeze-dryer (Telstar).

2. MICROWAVE ASSISTED EXTRACTION (MAE)

2.1. The sediment samples were finely ground by means of mortar and pestle. The glass fibre filter samples were cut into pieces.

2.2. 1g of sediment was weighted into a microwave vessel. Alternatively, one filter was cut in four pieces and inserted into the microwave vessel. 12 out of 14 vessels were filled with samples, while one vessel was kept empty as a blank and another vessel was filled with 1g of sediment previously extracted and combusted at 450 ºC for one night.

2.3. 50 μL of standard (GDGT-0 in hexane:acetone, 0.84 ± 0.02 μg $\cdot mL^{-1}$) were added as external standard to the vessel containing the pre-combusted sediment.

2.4. 10 mL of dicholormethane:methanol (3:1) were added to each vessel together with a magnetic stirrer. The vessels were closed and screwed tightly and loaded into the microwave. The temperature and pressure probes were connected to the blank vessel.

2.5. The microwave extraction was performed. The temperature program was as follows**:**

Time (min)	Temperature
0	room temperature
0 - 2.5	ramp to 70ºC
2.5 - 7.5	70ºC maintained
7.5 – 37.5	*cooling*

Appendix 1. Table 1. Microwave temperature program for biomarker extraction.

2.6. The content of the vessels was transferred to Pyrex test tubes by means of glass funnels. To ensure maximum recovery of the sample, 0.5 mL of extraction solvent were used twice to rinse the microwave vessels.

2.7. Test tubes were centrifuged at 2200 rpm for 5 minutes and the supernatant was transferred into new tubes.

3. CLEAN-UP: ALKALINE HYDROLYSIS (SAPONIFICATION)

3.1. Liquid extracted samples were concentrated by vacuum rotary evaporation to 1.5 mL.

3.2. 3 ml of potassium hydroxide (KOH, 8% in methanol) were added. To prepare this reagent, the weighted KOH pellets were ultrasonicated for 15 minutes three times with hexane and subsequently dissolved in the methanol by ultrasonication during 15 minutes.

3.3. The mixture was homogenised and kept for 24 h in a dark place for the reaction to take place.

3.4. The sample was concentrated by vacuum rotary evaporation to 1 mL.

3.5. The neutral fraction was recovered by a liquid-liquid extraction with 3 mL of hexane four times. Intermediate evaporations were needed. The sample was finally brought to 3 mL volume.

The following steps were only performed until the realization that water led to massive losses of GDGTs (see Section 2.4):

3.6. The hexane was twice rinsed with 3 mL of Milli-Q water in order to remove the remaining salts in the organic solvent.

3.7. The water volume was rinsed three times with 0.5 mL of hexane to recover the lipids that were potentially transferred to water in the previous step.

4. CLEAN-UP: PREPARATIVE COLUMN FRACTIONATION

4.1. Liquid extracted samples were brought to dryness by vacuum rotary evaporation.

4.2. Alumina (Merck) was activated by furnacing it at 450 ºC for a minimum of 5h.

4.3. Glass Pasteur pipettes were filled with the activated alumina.

4.4. The extracts were loaded on the column and eluted with 3 mL of a mixture of hexane/dichloromethane (9:1, v/v) and 3 mL of a mixture of dichloromethane/methanol (1:1, v/v).

4.5. The later fraction contained the GDGTs and was evaporated by vacuum rotary evaporation and under a stream of N_2.

For comparison purposes, activated silica and deactivated alumina and silica were used for GDGT column fractionation (see Section 2.4), which included the following changes to the protocol:

4.2b Silica (Acröss) was activated by furnacig it at 120 ºC for a minimum of 5h.

4.4b The extracts were eluted in silica with 4 mL of the aforementioned solvent mixtures.

4.2c Activated alumina and silica were deactivated by addition of Milli-Q water (5% dry weight), thoroughly mixed for 20 min and stored in dessicator overnight.

5. INSTRUMENTAL ANALYSIS BY HPLC/APCI-MS WITH AN ION-TRAP SYSTEM

Analyses were performed using an Agilent 1100 HPLC coupled to a Bruker ion trap Esquire 3000 MS with an APCI interface.

5.1. Dry samples were redissolved in 200 μL of hexane/n-propanol (99:1, v/v).

5.2. The samples were filtered through 0.45 μm Millipore PVDF filter and usually 10 μL were injected.

5.3. Sample extracts were eluted using a Nucleosil CN column (4 x 150 mm, 5 μm; Tracer) at 30.0ºC equipped with a precolumn filter, in isocratic mode using hexane/*n*-propanol (98:2) at a flow rate of 1 $mL \cdot min^{-1}$. For a comparison study (see Section 2.4) samples were eluted with a Prevail CN column in the ion-trap system with the conditions described in line 6.3 below.

5.4. The parameters of the APCI were set as follows to generate positive ion spectra: corona voltage 5000 V, nebulizer gas pressure 60 psi and dry gas flow 6 L/min, capillary voltage 4200 V, vaporizer temperature 300ºC and dry N_2 flux at 250ºC.

5.5. For the monitoring of the complete array of GDGTs, two m/z ranges were recorded to include all the GDGTs, namely *m/z* 1010-1060 (for branched GDGTs) and *m/z* 1285-1310 (for isoprenoidal GDGTs).

5.6. The integration of the relevant GDGTs was undertaken on the individual extracted chromatograms of $[M+H]^+ \pm 0.5$ m/z units.

INSTRUMENTAL ANALYSIS BY HPLC/APCI-MS WITH A QUADRUPOLE SYSTEM

Analyses were performed using an Dionex P680 HPLC system coupled to a Thermo Finnigan TSQ Quantum Discovery Max quadrupole MS via an APCI interface.

5.7. Dry samples were redissolved in 200 μL of hexane/n-propanol (99:1, v/v).

5.8. The samples were filtered through 0.45 μm Millipore PVDF filter and usually 10 μL injected.

5.9. Sample extracts were eluted using a Prevail CN column (2.1 x 150 mm, 3 μm; Alltech) at 30.0ºC equipped with a precolumn filter and a guard column. Flow rate was 3 $mL \cdot min^{-1}$. Samples were eluted with hexane/ n-propanol following this gradient elution:

Time (min)	% propanol
0	1.5
4	1.5
15	5.0
16	10.0
20	10.0
21	1.5
30	1.5

Appendix 1. Table 2. Gradient elution in the Dionex HPLC.

5.10. The parameters of the APCI were set as follows to generate positive ion spectra: corona discharge 3 μA, vaporizer temperature 400ºC, sheath gas pressure 49 mTorr, auxiliary gas (N_2) pressure 5 mTorr and capillary temperature 200ºC.

5.11. GDGTs were detected in selected ion monitoring (SIM) mode of $[M+H]^+$ ± 0.5 *m/z* units .

5.12. The integration of the relevant GDGTs was undertaken on the individual chromatograms of $[M+H]^+$.

Appendix 2

DATA COMPILATION

1. Analytical considerations for the use of the paleothermometer Tetraether Index$_{86}$ and the Branched vs Isoprenoid Tetraether index regarding the choice of clean-up and instrumental conditions (***Section 2.4***).

	Control	Activated alumina	Deactivated alumina (5%)	Activated silica	Deactivated silica (5%)
TEX$_{86}$ (1)	0.563	0.572	0.588	0.563	0.581
TEX$_{86}$ (2)	0.584	0.582	0.580	0.569	0.592
TEX$_{86}$ (3)	0.584	0.567	0.574	0.555	0.575
Average TEX$_{86}$	0.577	0.574	0.581	0.562	0.582
BIT (1)	0.506	0.457	0.495	0.455	0.469
BIT (2)	0.499	0.463	0.496	0.460	0.479
BIT (3)	0.509	0.445	0.506	0.451	0.484
Average BIT	0.505	0.455	0.499	0.455	0.477

Appendix 2. Table 1. Comparison of TEX$_{86}$ and BIT values obtained with different adsorbents and degree of activation for the fractionation of GDGTs.

Sample	TEX_{86} Alumina fractionation	TEX_{86} Alkaline hydrolysis	BIT Alumina fractionation	BIT Alkaline hydrolysis
Lake Caicedo	0.388	0.365	0.843	0.818
Lake Tobar	0.709	0.707	0.319	0.299
Lake Estanya Gran	0.158	0.160	0.817	0.819
Lake Zóñar	0.643	0.629	0.502	0.522
Lake La Playa	0.673	0.659	-	-
Lake Baikal	0.300	0.287	-	-
Lake Baikal	0.193	0.178	0.373	0.330
Lake Baikal	0.249	0.224	0.365	0.311
Lake El Vilar	0.490	0.482	0.675	0.634
Lake El Vilar	-	-	0.503	0.456
Lake El Vilar	-	-	0.738	0.671
Lake Villarquemado	0.603	0.596	0.080	0.067
North Atlantic	0.503	0.481	0.395	0.303
Skagerrak	0.377	0.355	0.017	0.017
Skagerrak	0.389	0.300	0.018	0.019
Skagerrak	0.382	0.396	0.014	0.028
Skagerrak	0.375	0.359	0.019	0.027
Skagerrak	0.364	0.380	0.020	0.023
Skagerrak	0.364	0.371	0.023	0.026
Skagerrak	0.372	0.378	0.015	0.018
Skagerrak	0.366	0.371	0.016	0.016
Skagerrak	0.364	0.369	0.018	0.020
Skagerrak	0.380	0.376	0.021	0.018
Skagerrak	0.368	0,364	0,021	0,017
Skagerrak	0.374	0,372	0,024	0,031

Appendix 2. Table 2. Comparison of TEX_{86} and BIT obtained with two clean-up methods: alumina fractionation and alkaline hydrolysis.

Sample	TEX_{86} Tracer (1 mL/min)	TEX_{86} Prevail (0.3 mL/min)	BIT Tracer (1 mL/min)	BIT Prevail (0.3 mL/min)
Lake Estanya Gran	0.206	0.224	0.930	0.947
Lake Baikal	0.317	0.314	0.526	0.496
Lake Baikal	0.350	0.325	0.478	0.472
Lake Baikal	0.527	0.502	0.013	0.012
Lake Baikal	0.522	0.484	0.009	0.009
Lake Baikal	0.473	0.447	0.018	0.016
Lake Baikal	0.485	0.426	0.018	0.020
Lake Caicedo	0.465	0.409	0.893	0.920
Lake El Vilar	0.489	0.513	0.851	0.892
Lake Zóñar	0.660	0.666	0.866	0.799
Lake Villarquemado	0.616	0.628	0.247	0.168
Lake La Playa	0.735	0.732	-	-
Lake El Tobar	0.643	0.732	0.524	0.421
Skagerrak	0.369	0.339	0.120	0.075
Skagerrak	0.291	0.318	0.052	0.062
Skagerrak	0.423	0.383	0.215	0.158
Skagerrak	0.378	0.337	0.133	0.134
Drammensfjord	0.411	0.382	0.479	0.457
Arabian Sea	0.724	0.700	0.030	0.029

Appendix 2. Table 3. Comparison of TEX_{86} and BIT values analysed with two HPLC columns: Tracer Nucleosil (flow: 1 mL/min) and Prevail (flow: 0.3 mL/min).

Sample	TEX_{86} Ion-trap	TEX_{86} quadrupole	BIT Ion-trap	BIT quadrupole
Lake Estanya Gran	0.224	0.158	0.947	0.817
Lake Caicedo	0.409	0.388	0.920	0.843
Lake El Vilar	0.513	0.490	0.892	0.675
Lake Zóñar	0.666	0.643	0.799	0.502
Lake Villarquemado	0.628	0.603	0.168	0.080
Lake La Playa	0.732	0.673	-	-
Lake Tobar	0.732	0.709	0.421	0.319
Lake Baikal	0.314	0.193	0.496	0.373
Lake Baikal	0.325	0.249	0.472	0.365
Lake Baikal	0.502	0.481	-	-
Lake Baikal	0.484	0.485	0.008	0.004
Lake Baikal	0.447	0.446	-	-
Lake Baikal	0.426	0.424	0.020	0.004
Lake Baikal	0.299	0.302	0.501	0.327
Lake Baikal	0.287	0.283	0.451	0.307
Lake Baikal	0.301	0.306	0.423	0.288
Skagerrak	0.339	0.371	0.076	0.016
Skagerrak	0.318	0.300	0.062	0.019
Skagerrak	0.383	0.389	0.160	0.018
Skagerrak	0.337	0.366	0.134	0.016
Drammensfjord	0.382	0.400	0.457	0.143
Arabian Sea	0.700	0.704	0.029	0.003

Appendix 2. Table 4. Comparison of TEX_{86} and BIT values measured with two mass spectrometers: an ion-trap and a quadrupole system.

		Response of GDGTs						
		m/z 1300	m/z 1298	m/z 1296	m/z 1292	m/z 1050	m/z 1036	m/z 1022
Capillary Temperature (ºC)	**100**	1,32E+07	6,85E+06	1,43E+06	9,39E+07	5,87E+05	3,37E+05	1,97E+05
	150	1,23E+07	6,41E+06	1,33E+06	8,70E+07	4,59E+05	2,28E+05	1,21E+05
	200	1,22E+07	6,04E+06	1,26E+06	8,14E+07	1,78E+05	1,00E+05	4,68E+04
	250	8,85E+06	4,47E+06	9,61E+05	6,65E+07	2,68E+04	1,33E+04	1,28E+04
Vaporizer temperature (ºC)	**300**	8,20E+06	4,84E+06	1,01E+06	3,55E+07	1,50E+05	7,50E+04	3,66E+04
	350	1,15E+07	6,79E+06	1,36E+06	6,82E+07	1,65E+05	8,31E+04	3,22E+04
	400	1,36E+07	7,51E+06	1,49E+06	9,98E+07	1,71E+05	8,23E+04	2,87E+04
	450	1,15E+07	6,63E+06	1,34E+06	9,16E+07	1,39E+05	7,67E+04	2,35E+04
	500	9,65E+06	5,36E+06	1,05E+06	7,39E+07	1,06E+05	5,50E+04	2,47E+04
Corona current (µA)	**3**	1,31E+07	6,60E+06	1,39E+06	9,71E+07	1,68E+05	8,67E+04	4,47E+04
	4	1,19E+07	6,33E+06	1,36E+06	9,14E+07	1,87E+05	8,16E+04	3,70E+04
	5	1,31E+07	6,70E+06	1,42E+06	9,52E+07	1,94E+05	9,13E+04	5,52E+04
	6	1,12E+08	1,39E+07	7,00E+06	1,54E+06	1,89E+05	8,78E+04	3,92E+04
	8	1,11E+08	1,50E+07	7,49E+06	1,63E+06	2,11E+05	1,08E+05	4,90E+04
	10	1,14E+08	1,46E+07	7,40E+06	1,52E+06	1,63E+05	9,78E+04	3,69E+04
	15	1,03E+08	1,34E+07	6,93E+06	1,41E+06	1,84E+05	8,65E+04	3,75E+04
	25	6,02E+07	8,03E+06	3,71E+06	8,08E+05	9,05E+04	4,57E+04	3,01E+04
	50	4,86E+07	6,64E+06	2,69E+06	5,07E+05	7,33E+04	3,05E+04	2,10E+04
	75	4,92E+07	5,70E+06	2,60E+06	5,07E+05	7,65E+04	2,82E+04	1,93E+04

Appendix 2. Table 5. GDGTs response (area in arbitrary units) at different settings of the APCI-MS parameters.

2. Exploration of GDGT distribution in Iberian lakes and their potential for climate reconstruction ***(Chapter 3).***

Lake	References
Caicedo	Martín-Rubio M., Rodríguez-Lázaro J., Anadon P., Robles F., Utrilla R., and Vázquez A. (2005) Factors affecting the distribution of recent lacustrine ostracoda from the caicedo de yuso-arreo lake (western ebro basin, spain). *Palaeogeography Palaeoclimatology Palaeoecology* 225(1-4), 118-133.
Chiprana	Valero-Garcés B. L., Navas A., Machín J., Stevenson T., and Davis B. (2000) Responses of a saline lake ecosystem in a semiarid region to irrigation and climate variability - the history of Salada Chiprana, central Ebro Basin, Spain. *Ambio* 29(6), 344-350.
El Vilar	Casamayor E. O., Schafer H., Baneras L., Pedros-Alio C., and Muyzer G. (2000) Identification of and spatio-temporal differences between microbial assemblages from two neighboring sulfurous lakes: Comparison by microscopy and denaturing gradient gel electrophoresis. *Applied and Environmental Microbiology* 66(2), 499-508.
Estanya Gran	Riera S., Wansard G., and Julia R. (2004) 2000-year environmental history of a karstic lake in the Mediterranean Pre-Pyrenees: The Estanya lakes (Spain). *Catena* 55(3), 293-324.
Gallocanta	Luzón A., Pérez A., Mayayo M. J., Soria A. R., Goñi M. F. S., and Roc A. C. (2007) Holocene environmental changes in the Gallocanta lacustrine basin, Iberian Range, NE Spain. *Holocene* 17(5), 649-663.
Honda	Castro M.C., Rivera M., Crespo M., Martín-García J.M. and Guerrero F. (2003) Morphological and sedimentological characterization of Honda temporary lake (southern Spain). *Limnetica* 22(3-4), 147-154.
Montcortès	Serra T., Colomer J., Soler M., and Vila X. (2003) Spatio-temporal heterogeneity in a planktonic Thiocystis minor population, studied by laser in situ particle analysis. *Freshwater Biology* 48(4), 698-708.
Sanabria	de Hoyos C. and Comín F. A. (1999) The importance of inter-annual variability for management. *Hydrobiologia* 395, 281-291.
Tobar	Boronat M. D. and Miracle M. R. (1997) Size distribution of Daphnia longispina in the vertical profile. *Hydrobiologia* 360, 187-196.
Taravilla	Valero-Garcés B. L., Moreno A., Navas A., Mata P., Machín J., Huertas A. D., Samperiz P. G., Schwalb A., Morellón M., Cheng H., and Edwards R. L. (2008) The Taravilla lake and tufa deposits (central Iberian Range, Spain) as palaeohydrological and palaeoclimatic indicators. *Palaeogeography Palaeoclimatology Palaeoecology* 259(2-3), 136-156. Moreno A., Valero-Garcés B. L., González-Sampériz P., and Rico M. (2008) Flood response to rainfall variability during the last 2000 years inferred from the Taravilla lake record (central Iberian Range, Spain). *Journal of Paleolimnology* 40(3), 943-961.
Villarquemado	Rubio-Dobón J. C. and Valle-Melendo J. (2005) Estudio de la evolución del régimen hidrológico en zonas húmedas drenadas: los humedales del Cañizar (Provincia de Teruel, España). *Investigaciones Geográficas* 38, 47-64.

Continued

Lake	References
Zóñar	Valero-Garcés B. L., González-Sampériz P., Navas A., Machín J., Mata P., Delgado-Huertas A., Bao R., Moreno A., Carrión J. S., Schwalb A., and González-Barrios A. (2006) Human impact since medieval times and recent ecological restorationin a Mediterranean Lake: the Laguna Zonar, southern Spain. *Journal of Paleolimnology* 35(3), 441-465.
several lakes	Pearson E. J., Farrimond P., and Juggins S. (2007) Lipid geochemistry of lake sediments from semi-arid Spain: relationships with source inputs and environmental factors. *Organic Geochemistry* 38(7), 1169-1195.
several lakes	Pearson E. J. (2003) Lipid biomarkers in Spanish saline lake sediments: indicators of organic inputs and environmental change. PhD thesis, University of Newcastle, UK.

Appendix 2. Table 6. References for the Iberian Peninsula lakes.

Lake	TEX_{86}	BIT	MBT	CBT	LST (TEX_{86})	MAT_{est} (MBT/CBT)	Atlas MAT
Alcahozo	0.102	0.984	0.235	1.127	-8.7	-4.9	14.0
Amarga	0.699	0.556	0.274	0.285	26.4	5.0	18.0
Caicedo	0.396	0.944	0.156	0.545	8.6	-3.4	11.0
Caicedo	0.445	0.921	0.182	0.591	11.5	-2.5	11.0
Carralogroño	0.670	0.726	0.187	0.519	24.7	-1.6	13.0
Carravalseca	0.286	0.906	0.241	0.588	2.1	0.5	13.0
Castillo	0.783	0.927	0.065	1.190	31.3	-14.0	15.0
Chica	0.511	0.973	0.182	0.529	15.4	-1.9	18.0
Chiprana	0.470	0.521	0.259	0.643	13.0	0.8	15.0
El Pinet	0.446	0.907	0.466	0.569	11.5	11.9	18.0
Enol 1	0.417	0.921	0.172	0.331	9.8	-0.6	10.7
Enol 2	0.416	0.921	0.157	0.385	9.8	-1.9	10.7
Eras	0.577	0.889	0.091	1.021	19.2	-11.1	12.0
Estanca	0.500	0.881	0.193	0.397	14.7	-0.2	14.0
Estanya Gran	0.166	0.955	0.289	0.434	-4.9	4.3	12.0
Fuentedepiedra	0.448	0.739	0.214	0.729	11.6	-2.2	17.0
Gallocanta	0.566	0.839	0.230	0.717	18.6	-1.3	11.0
Gosque	0.654	0.704	0.222	0.548	23.8	-0.1	17.0
Grande	0.293	0.987	0.253	0.285	2.5	3.9	15.0
Honda	0.596	0.838	0.166	0.587	20.3	-3.3	16.0
Iglesia	0.572	0.838	0.109	0.502	18.9	-5.4	12.0
Manjavacas	0.624	0.211	0.207	0.534	22.0	-0.7	14.0
Medina	0.677	0.853	0.250	0.404	25.1	2.6	18.0
Michos	0.593	0.978	0.288	1.518	20.1	-5.9	15.0
Montcortés	0.410	0.910	0.172	0.505	9.4	-2.2	9.6
Navagrande	0.595	0.951	0.191	0.557	20.3	-1.8	14.0
Pajares	0.719	0.554	0.074	0.989	27.6	-11.7	15.0
Playa	0.522	0.383	0.180	0.551	16.0	-2.2	14.6
Rincón	0.772	0.443	0.157	0.465	30.7	-2.6	17.0
Salicor	0.507	0.495	0.176	1.112	15.1	-7.7	15.0
Sanabria	0.540	0.987	0.257	0.824	17.0	-1.0	9.8

Continued

Lake	TEX_{86}	BIT	MBT	CBT	LST (TEX_{86})	MAT_{est} (MBT/CBT)	Atlas MAT
Santa Pola	0.491	0.825	0.337	0.981	14.2	1.6	18.0
Taravilla	0.438	0.873	0.161	0.208	11.1	0.0	11.0
Taray	0.158	0.984	0.310	0.321	-5.4	6.4	14.0
Tiscar	0.767	0.538	0.349	0.297	30.4	8.6	18.0
Tobar	0.688	0.509	0.155	0.180	25.8	0.0	13.6
Vilar	0.489	0.851	0.219	0.434	14.1	0.8	14.0
Villarquemado	0.651	0.209	0.123	0.094	23.6	-0.8	11.7
Zarracatín	0.830	0.484	0.279	0.429	34.1	3.8	18.0
Zóñar	0.560	0.774	0.200	0.315	18.2	1.0	17.0

Appendix 2. Table 7. Proxy indices, reconstructed lake surface temperature (LST) and mean annual air temperature (MAT_{est}) and Digital Climatic Atlas mean annual air temperature (Atlas MAT) for lakes from the Iberian Peninsula.

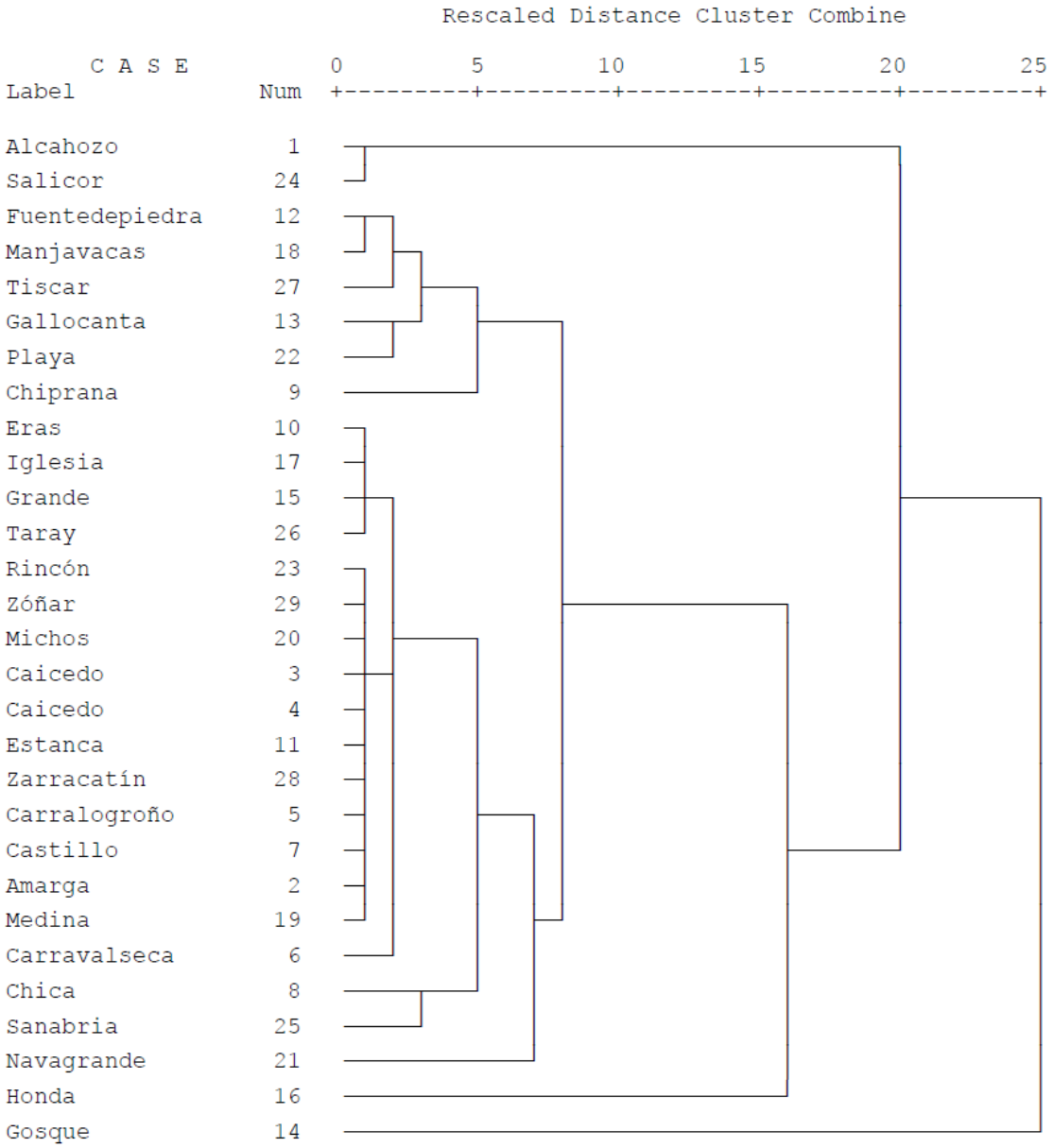

Appendix 2. Figure 1. Dendrogram of the Hierarchical Cluster Analysis of the Iberian lakes, clustering for chemical variables (total dissolved solids, pH and conductivity) and using single linkage method. According to it, 5 clusters were considered.

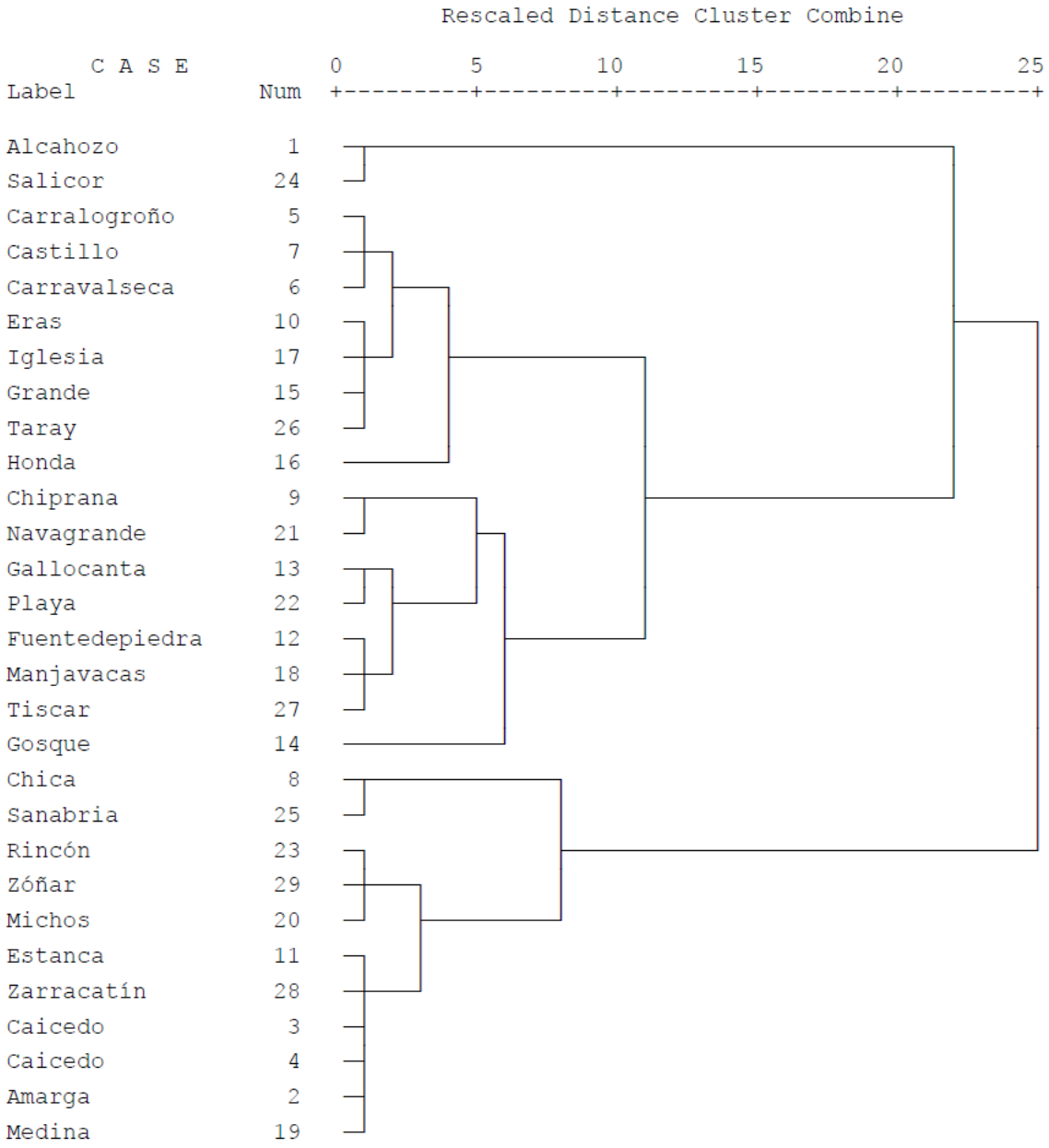

Appendix 2. Figure 2. Dendrogram of the Hierarchical Cluster Analysis of the Iberian lakes, clustering for chemical variables (total dissolved solids, pH and conductivity) and using complete linkage method. According to it, 5 clusters were considered.

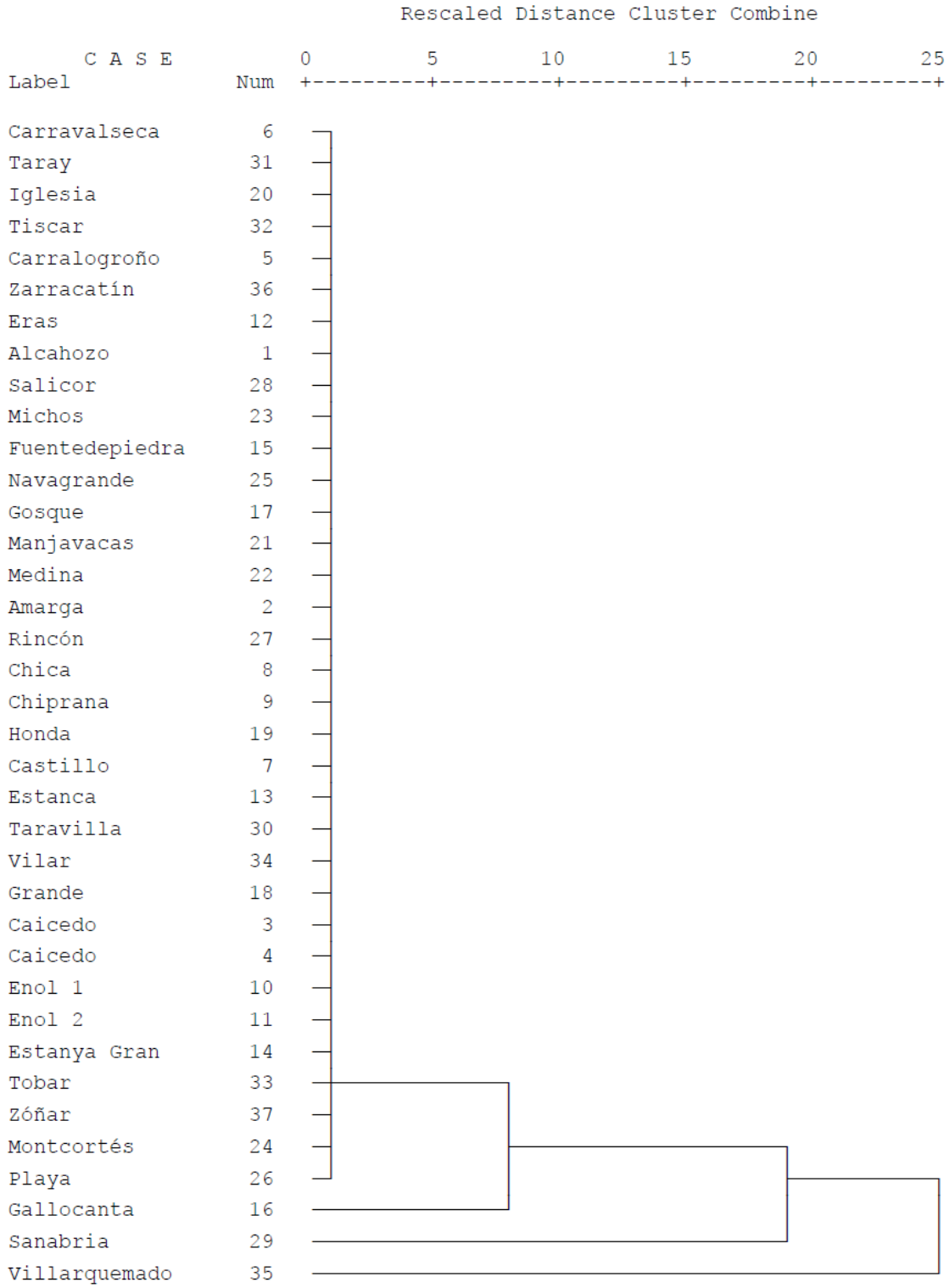

Appendix 2. Figure 3. Dendrogram of the Hierarchical Cluster Analysis of the Iberian lakes, clustering for morphological variables (maximum depth and area) and using single linkage method. According to it, 4 clusters were considered.

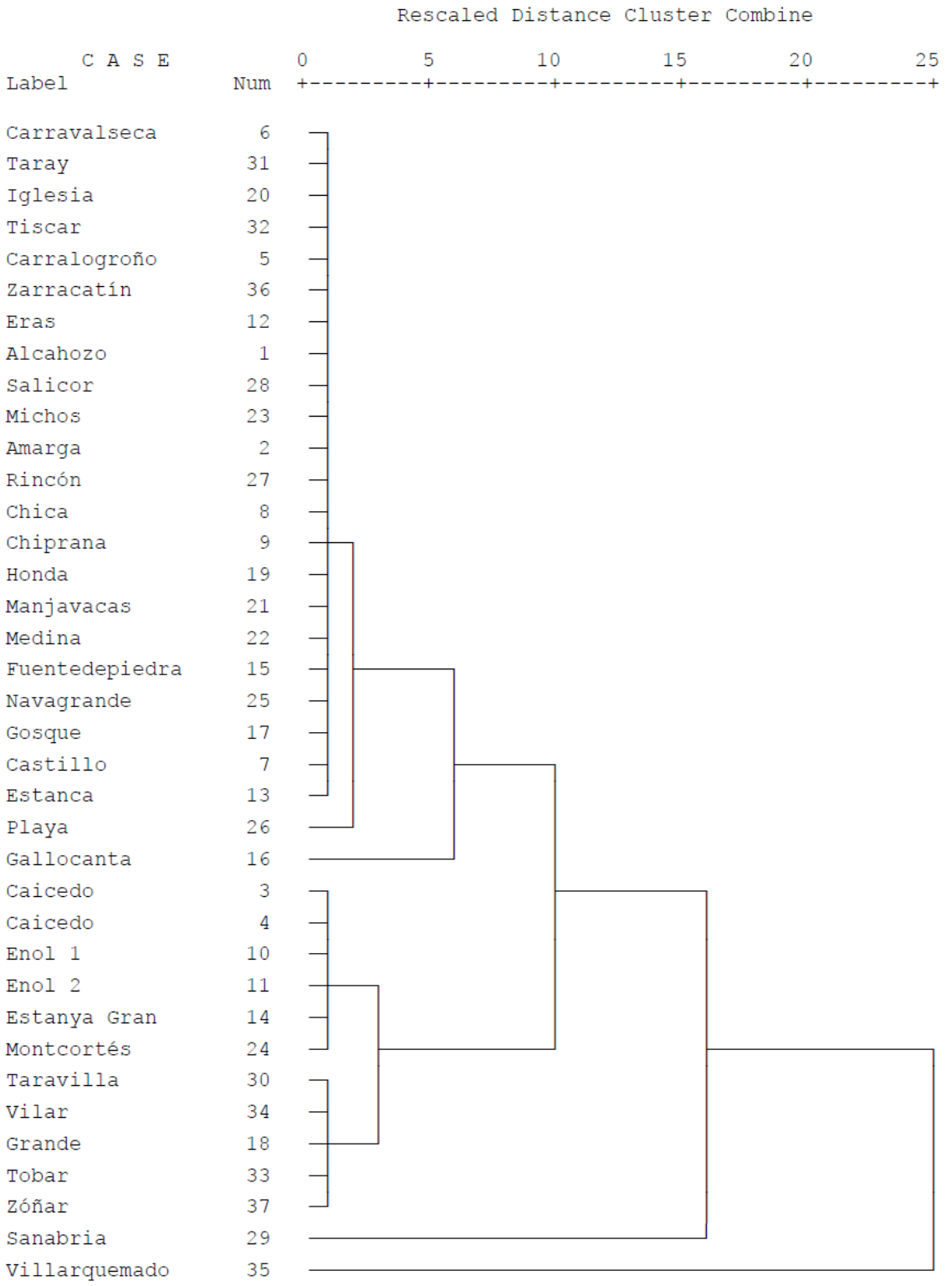

Appendix 2. Figure 4. Dendrogram of the Hierarchical Cluster Analysis of the Iberian lakes, clustering for morphological variables (maximum depth and area) and using complete linkage method. According to it, 6 clusters were considered.

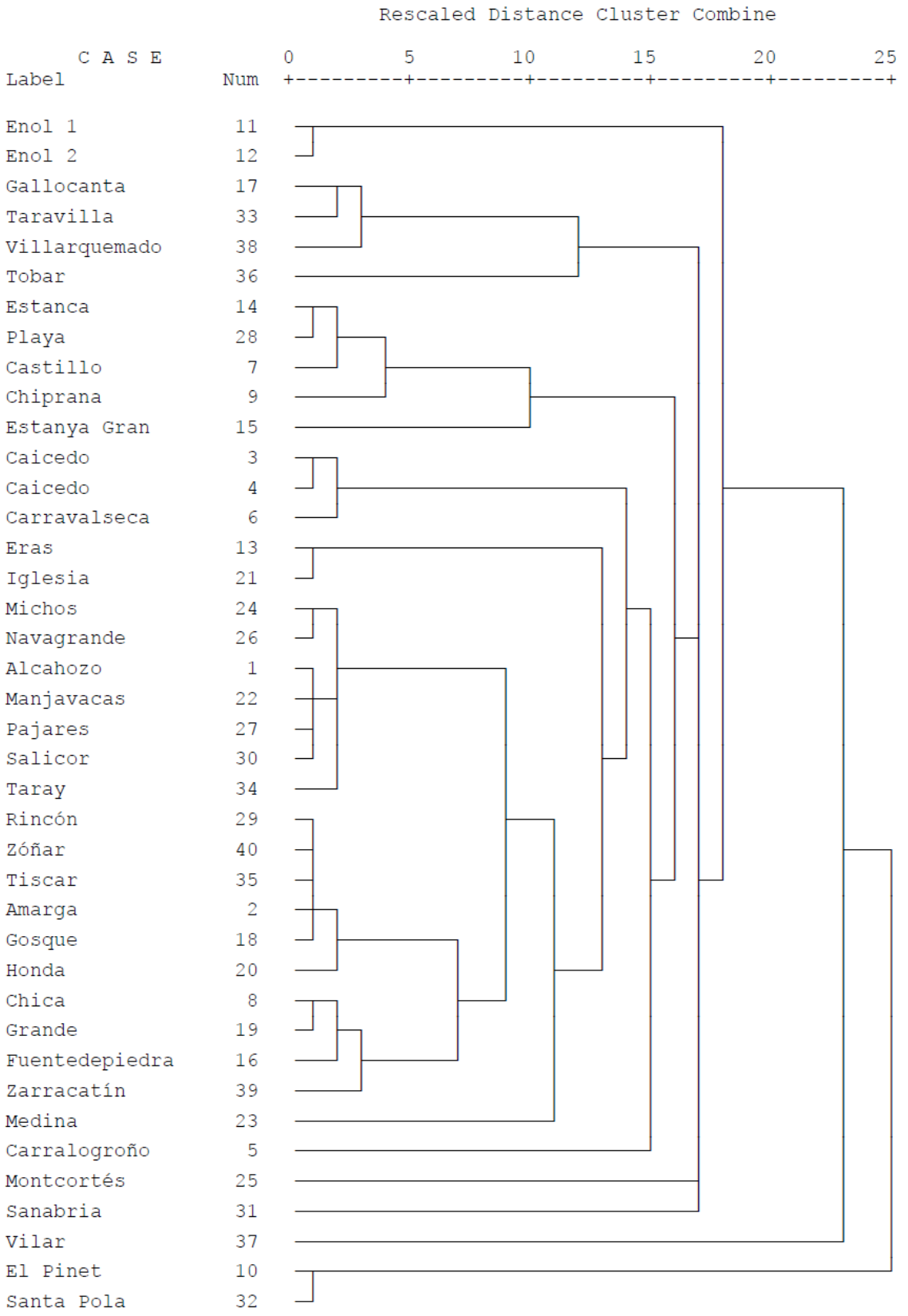

Appendix 2. Figure 5. Dendrogram of the Hierarchical Cluster Analysis of the Iberian lakes, clustering for geographical location variables (latitude, longitude, elevation) and using single linkage method. According to it, 8 clusters were considered.

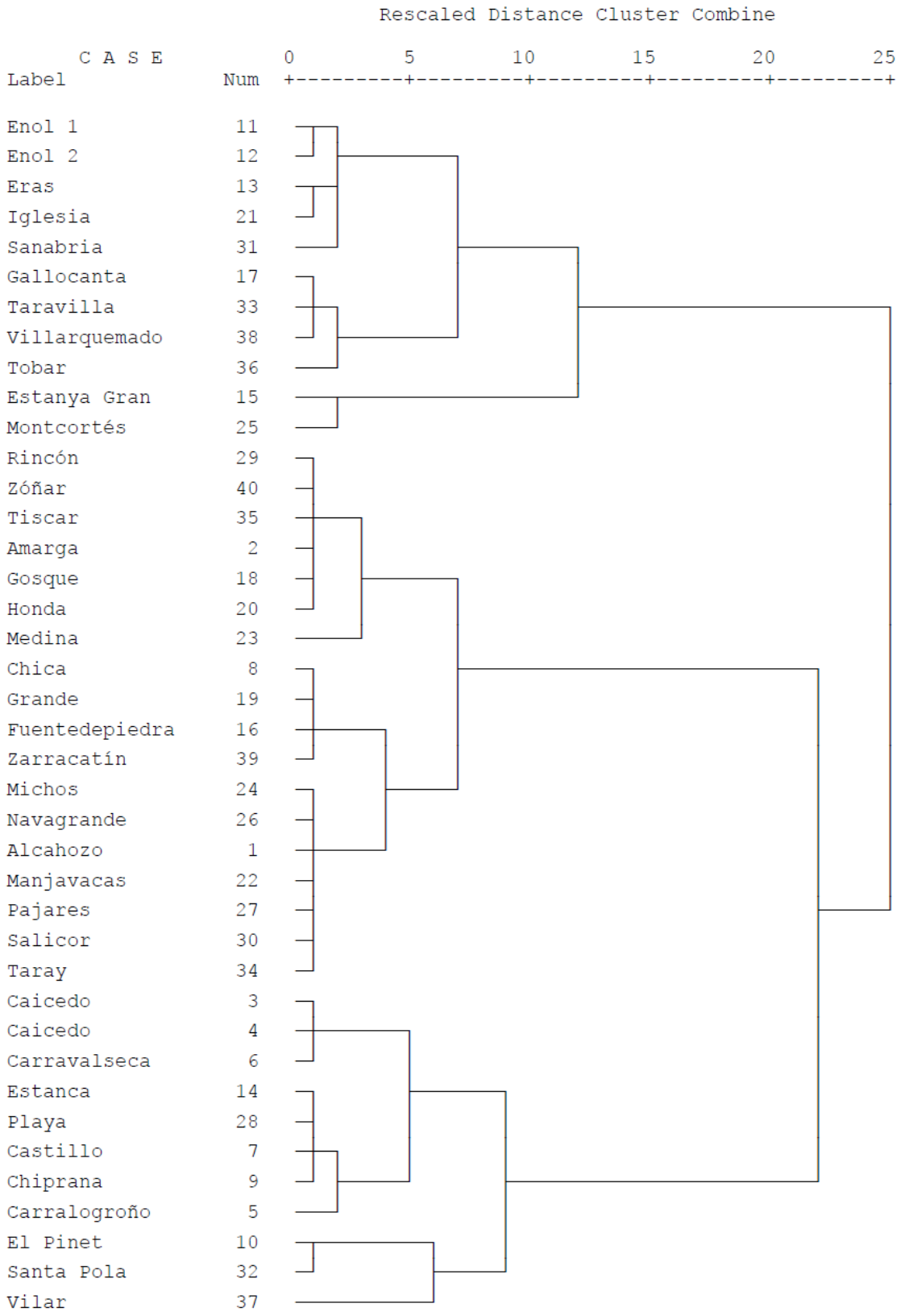

Appendix 2. Figure 6. Dendrogram of the Hierarchical Cluster Analysis of the Iberian lakes, clustering for geographical location variables (latitude, longitude, elevation) and using complete linkage method. According to it, 8 clusters were considered.

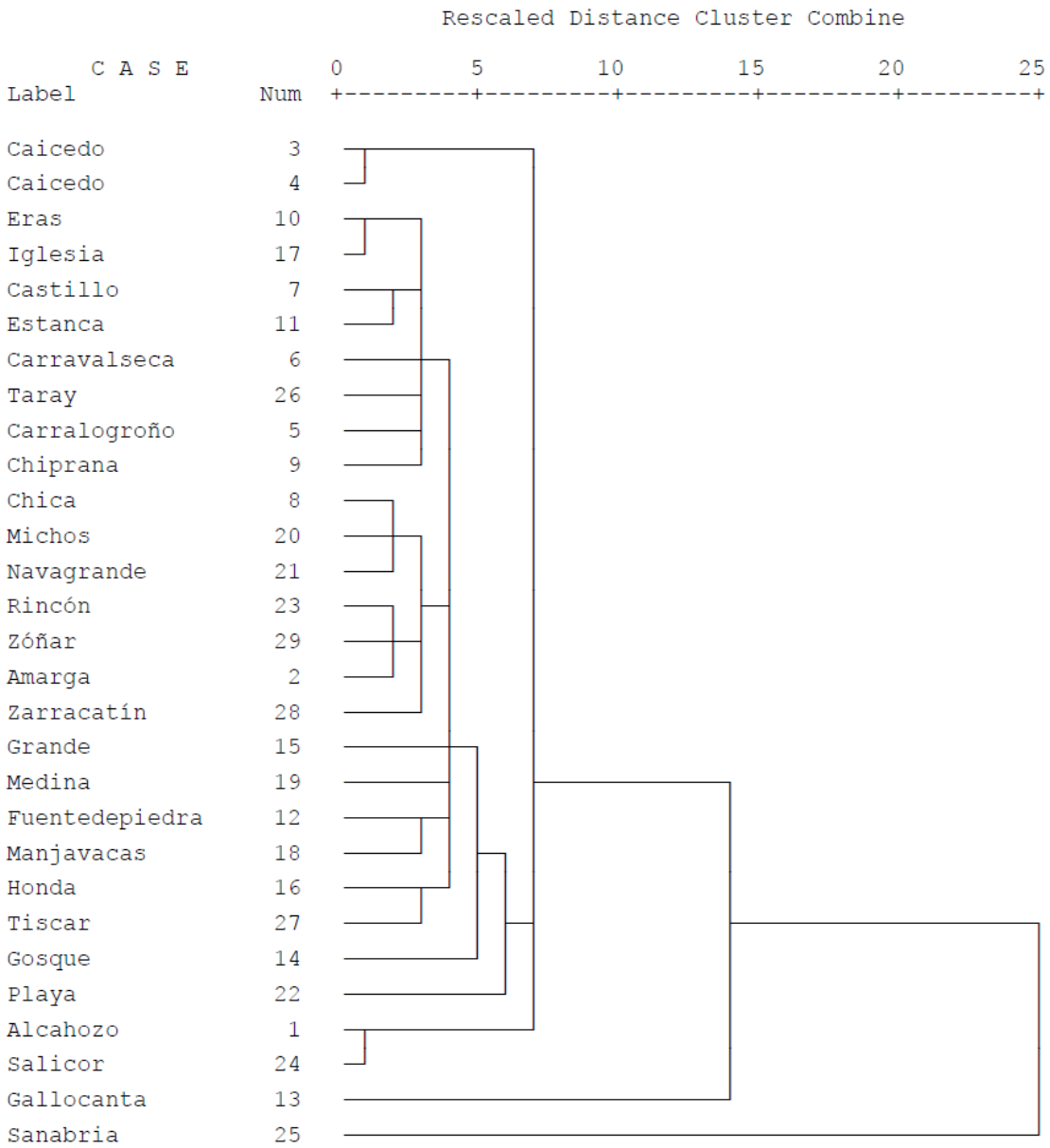

Appendix 2. Figure 7. Dendrogram of the Hierarchical Cluster Analysis of the Iberian lakes, clustering for chemical (total dissolved solids, conductivity and pH), morphological (area and maximum depth) and geographical location (latitude, longitude, elevation) variables, and using single linkage method. According to it, 5 clusters were considered.

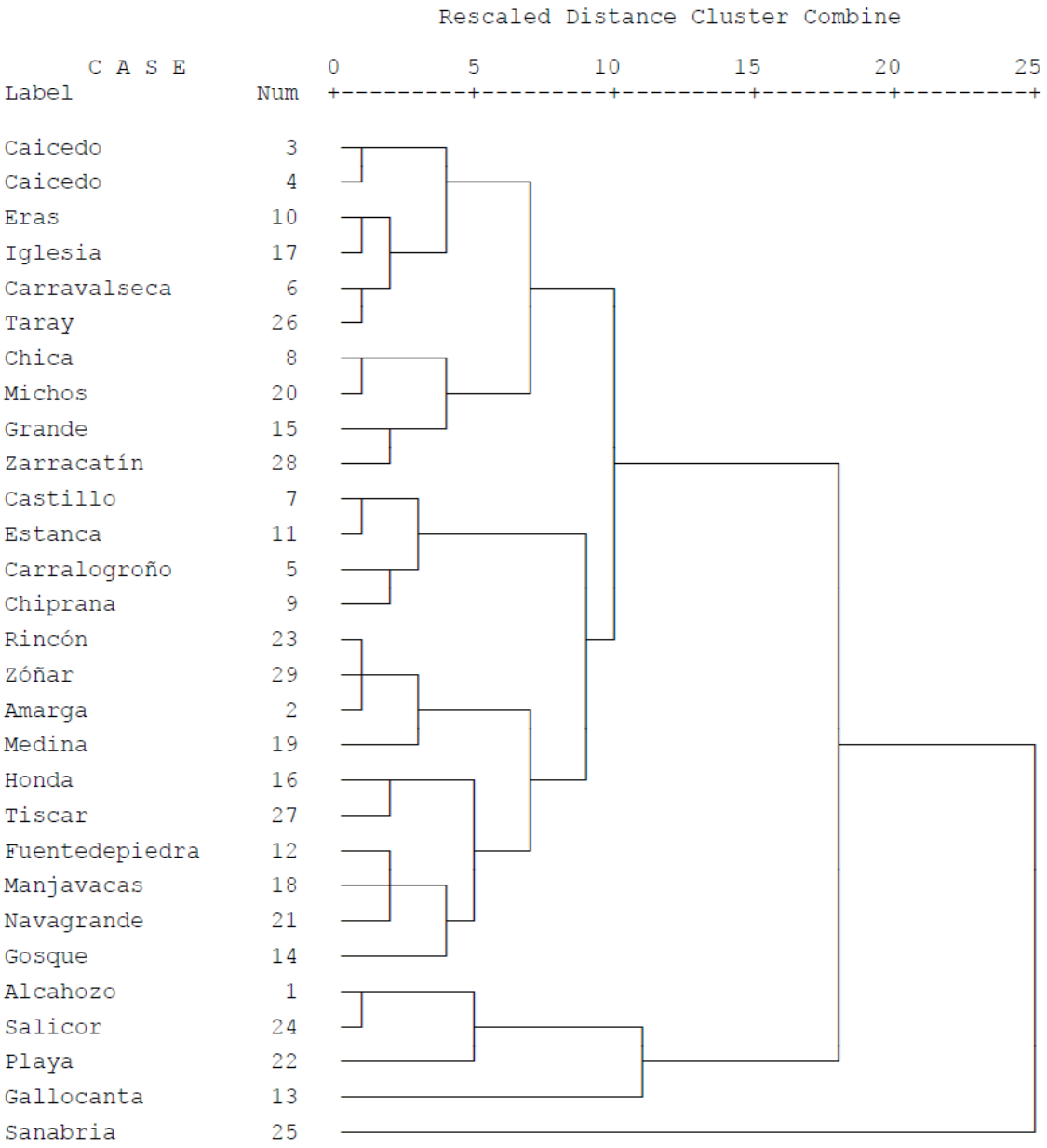

Appendix 2. Figure 8. Dendrogram of the Hierarchical Cluster Analysis of the Iberian lakes, clustering for chemical (total dissolved solids, conductivity and pH), morphological (area and maximum depth) and geographical location (latitude, longitude, elevation) variables, and using complete linkage method. According to it, 5 clusters were considered.

3. Appraisal of GDGT proxies in Lake Baikal ***(Chapter 4)***.

Water depth (m)	Flux isoprenoidal GDGTs*	Flux branched GDGTs	Total flux GDGTs	BIT	TEX_{86}	LST ºC (TEX_{86})
South Basin						
40	16.7 ± 0.8	0.6 ± 0.03	17.3 ± 0.8	0.080	0.290	4.2
100	3.9 ± 0.2	0.2 ± 0.1	4.1 ± 0.2	0.099	0.294	4.4
255	47.3 ± 2.5	3.1 ± 0.2	50.5 ± 2.5	0.154	0.315	5.5
350	42.7 ± 2.2	2.7 ± 0.1	45.5 ± 2.3	0.143	0.338	6.7
445	55.0 ± 2.9	4.1 ± 0.2	59.2 ± 2.9	0.166	0.312	5.3
540	51.1 ± 2.6	3.9 ± 0.2	55.2 ± 2.6	0.176	0.320	5.8
635	57.5 ± 3.0	4.9 ± 0.3	62.4 ± 3.0	0.191	0.348	7.3
730	20.9 ± 1.1	1.0 ± 0.1	22.0 ± 1.1	0.112	0.332	6.4
825	30.0 ± 1.6	2.1 ± 0.1	32.2 ± 1.6	0.153	0.337	6.7
922	23.8 ± 1.3	1.5 ± 0.1	25.3 ± 1.3	0.136	0.325	6.0
1015	16.8 ± 0.9	1.1 ± 0.1	17.9 ± 0.9	0.146	0.332	6.4
1210	26.8 ± 1.4	1.5 ± 0.1	28.4 ± 0.5	0.128	0.320	5.8
1396	3.7 ± 0.2	0.0 ± 0.1	1.2 ± 0.2	0.038	0.259	2.6
North Basin						
335	21.0 ± 1.1	0.7 ± 0.1	21.8 ± 1.2	0.087	0.297	4.6
445	7.5 ± 0.3	0.2 ± 0.1	7.7 ± 0.3	0.055	0.289	4.2
720	4.4 ± 0.2	0.1 ± 0.1	4.5 ± 0.2	0.075	0.294	4.4
775	4.9 ± 0.2	0.2 ± 0.1	5.1 ± 0.2	0.089	0.302	4.9
885	4.1 ± 0.2	0.2 ± 0.1	4.3 ± 0.2	0.083	0.299	4.7
903	8.4 ± 0.4	0.3 ± 0.1	8.7 ± 0.4	0.088	0.290	4.2

Appendix 2. Table 8. Fluxes of GDGTs, BIT, TEX_{86} and reconstructed LST values for the collected particulate material in the sediment traps at Lake Baikal. *Fluxes are in $\mu g \cdot m^{-2} \cdot day^{-1}$.

Sediment depth (cm)	BIT	TEX_{86}	LST - ºC (TEX_{86})
North Basin			
0 - 1	0.303	0.324	6.0
1 - 2	0.314	0.319	5.7
2 - 3	0.217	0.320	5.8
3 - 4	0.231	0.331	6.4
4 - 5	0.223	0.314	5.5
5 - 6	0.195	0.319	5.7
6 - 7	0.203	0.323	5.9
7 - 8	0.191	0.323	6.0
8 - 9	0.204	0.330	6.3
9 - 10	0.182	0.307	5.1
South Basin			
0 - 1	0.142	0.323	5.9
1 - 2	0.149	0.310	5.3
2 - 3	0.165	0.325	6.1
3 - 4	0.165	0.324	6.0
4 - 5	0.184	0.315	5.5
5 - 6	0.178	0.315	5.5
6 - 7	0.206	0.341	6.9
7 - 8	0.190	0.333	6.4
8 - 9	0.203	0.334	6.5
9 - 10	0.226	0.341	6.9

Appendix 2. Table 9. BIT, TEX_{86} and reconstructed LST values for the sediments underlying the sediment trap moorings in Lake Baikal.

Sample	BIT	TEX_{86}	MBT	CBT	LST - ºC (TEX_{86})	MAT_{est} - ºC (MBT/CBT)
S1	-	0.371	-	-	8.5	-
S2	0.298	0.323	0.095	0.558	5.9	-6.6
S3	0.142	0.323	0.064	0.875	5.9	-11.1
S4	-	0.322	-	-	5.9	-
S5	0.265	0.328	0.093	0.764	6.2	-8.6
S6	0.303	0.324	0.063	0.847	6.0	-10.9

Appendix 2. Table 10. BIT, TEX_{86}, MBT, CBT and reconstructed lake surface temperature (LST) and mean annual air temperature (MAT_{est}) for the surface sediments analysed in Lake Baikal.

Depth (cm)	Age (kyr BP)	BIT	TEX_{86}	MBT	CBT	LST - ºC (TEX_{86})	MAT_{est} - ºC (MBT/CBT)
0	0.00	0.265	0.328	0.093	0.764	6.2	-8.5
1	0.32	0.266	0.324	0.088	0.708	6.0	-8.2
2	0.65	0.260	0.328	0.095	0.727	6.2	-8.0
3	0.97	0.269	0.328	0.111	0.686	6.2	-6.9
4	1.29	0.274	0.333	0.115	0.737	6.5	-7.1
5	1.57	0.253	0.337	0.107	0.738	6.7	-7.5
6	1.62	0.264	0.334	0.127	0.736	6.5	-6.5
7	1.67	0.291	0.327	0.131	0.675	6.2	-5.8
8	1.73	0.335	0.333	0.114	0.690	6.5	-6.7
9	1.78	0.287	0.363	0.112	0.689	8.1	-6.8
10	1.83	0.277	0.329	0.118	0.644	6.3	-6.1
20	2.32	0.307	0.344	0.123	0.541	7.0	-4.9
30	2.92	0.269	0.328	0.133	0.496	6.2	-4.0
40	3.68	0.271	0.346	0.108	0.524	7.2	-5.5
50	4.44	0.306	0.318	0.116	0.608	5.7	-5.9
60	5.14	0.275	0.333	0.132	0.545	6.5	-4.5
70	5.73	0.269	0.334	0.095	0.536	6.5	-6.3
80	6.32	0.281	0.340	0.119	0.529	6.8	-5.0
90	6.90	0.282	0.330	0.095	0.551	6.3	-6.4
100	7.48	0.274	0.361	0.094	0.536	8.0	-6.3
110	8.03	0.280	0.323	0.100	0.527	5.9	-5.9
120	8.57	0.297	0.337	0.106	0.521	6.7	-5.6
130	9.11	0.323	0.341	0.110	0.540	6.9	-5.6
133.3	9.29	0.193	0.338	0.104	0.608	6.7	-6.5
134.8	9.37	0.236	0.344	0.093	0.589	7.0	-6.8
136.3	9.45	0.212	0.314	0.100	0.581	5.5	-6.4
137.8	9.53	0.198	0.318	0.098	0.587	5.7	-6.6
139.3	9.61	0.142	0.306	0.085	0.679	5.1	-8.1
140.8	9.69	0.150	0.310	0.087	1.291	5.2	-13.6
142.3	9.77	0.221	0.314	0.080	0.568	5.5	-7.3
143.8	9.85	0.236	0.324	0.079	0.546	6.0	-7.1
153.1	10.36	0.179	0.327	0.106	0.624	6.2	-6.5
163.6	10.93	0.174	0.310	0.130	0.683	5.3	-5.9
172.8	11.52	0.231	0.352	0.118	0.592	7.5	-5.6
182.8	12.19	0.187	0.315	0.116	0.612	5.6	-5.9
193.3	12.97	0.196	0.306	0.109	0.629	5.1	-6.4

Continued

Depth (cm)	Age (kyr BP)	BIT	TEX_{86}	MBT	CBT	LST - ºC (TEX_{86})	MAT_{est} - ºC (MBT/CBT)
203.3	13.45	0.166	0.328	0.093	0.672	6.2	-7.6
213.3	13.70	0.244	0.292	0.130	0.638	4.3	-5.5
222.9	13.95	0.189	0.314	0.115	0.570	5.5	-5.6
233.8	14.23	0.212	0.322	0.095	0.450	5.9	-5.5
243.2	14.46	0.207	0.338	0.110	0.560	6.8	-5.7
253.5	14.79	0.168	0.323	0.115	0.386	6.0	-3.9
262.8	15.19	0.175	0.305	0.113	0.572	5.0	-5.7
273.5	15.65	0.216	0.301	0.116	0.716	4.8	-6.9
282.7	16.04	0.206	0.293	0.097	0.714	4.4	-7.8
292.4	16.45	0.180	0.300	0.034	-0.108	4.7	-3.3
303.3	16.83	0.220	0.315	0.037	0.066	5.5	-4.8
313.3	17.17	0.286	0.338	0.101	0.607	6.7	-6.6
323.3	17.52	0.274	0.320	0.110	0.665	5.8	-6.7
333.3	17.86	0.257	0.298	0.113	0.705	4.6	-6.9
343.3	18.21	0.257	0.307	0.128	0.656	5.1	-5.7
353.3	19.56	0.182	0.295	0.118	0.698	4.5	-6.6
363.3	19.98	0.178	0.308	0.095	0.578	5.1	-6.7
373.3	20.39	0.134	0.294	0.097	0.649	4.4	-7.2
383.3	20.80	0.142	0.302	0.088	0.611	4.9	-7.3
393.3	21.22	0.145	0.312	0.102	0.643	5.4	-6.9
403.3	21.53	0.167	0.286	0.085	0.624	4.0	-7.6
413.3	21.73	0.158	0.297	0.061	0.607	4.6	-8.6
423.3	21.93	0.150	0.293	0.077	0.509	4.4	-6.9
433.3	22.12	0.172	0.312	0.064	0.586	5.3	-8.2
443.3	22.42	0.179	0.307	0.085	0.600	5.1	-7.3
453.3	23.00	0.146	0.292	0.076	0.583	4.3	-7.6
463.3	23.58	0.107	0.275	0.075	0.588	3.4	-7.7
473.3	24.44	0.124	0.288	0.064	0.808	4.1	-10.3
483.3	25.72	0.128	0.302	0.070	0.561	4.8	-7.7
493.3	26.74	0.148	0.308	0.051	0.523	5.2	-8.3
498.3	27.09	0.118	0.288	0.063	0.476	4.1	-7.3

Appendix 2. Table 11. BIT, TEX_{86}, MBT, CBT and reconstructed lake surface temperature (LST) and mean annual air temperature (MAT_{est}) for sediment samples analysed from core CON01-605-3 in the South Basin of Lake Baikal. Sediment depth refers to the upper depth of the section analysed.

Depth (cm)	Age (kyr BP)	BIT	TEX_{86}	MBT	CBT	LST - ºC (TEX_{86})	MAT_{est} - ºC (MBT/CBT)
0.0	0.00	0.298	0.323	0.095	0.558	5.9	-6.5
1.0	0.39	0.296	0.346	0.103	0.573	7.2	-6.2
3.5	0.98	0.300	0.355	0.126	0.644	7.6	-5.7
4.0	1.58	0.300	0.333	0.127	0.627	6.5	-5.5
6.5	2.17	0.321	0.356	0.132	0.659	7.7	-5.6
7.0	2.76	0.359	0.344	0.133	0.673	7.1	-5.7
8.0	3.15	0.401	0.326	0.170	0.834	6.1	-5.3
10.0	4.11	0.388	0.331	0.151	0.663	6.4	-4.7
16.0	4.44	0.564	0.342	0.155	0.493	6.9	-2.9
20.0	4.67	0.407	0.329	0.176	0.440	6.3	-1.4
26.0	5.16	0.333	0.327	0.141	0.396	6.1	-2.7
30.0	5.49	0.362	0.333	0.163	0.449	6.5	-2.1
36.0	5.98	0.296	0.330	0.121	0.438	6.3	-4.1
40.0	6.46	0.303	0.345	0.107	0.504	7.1	-5.4
46.0	7.19	0.332	0.357	0.134	0.457	7.7	-3.6
50.0	7.66	0.349	0.324	0.133	0.434	6.0	-3.4
56.0	8.35	0.333	0.331	0.107	0.398	6.4	-4.4
60.0	8.81	0.331	0.321	0.107	0.347	5.9	-3.9
66.0	9.50	0.366	0.332	0.117	0.428	6.4	-4.2
70.0	10.40	0.326	0.317	0.119	0.387	5.6	-3.7
76.0	11.77	0.310	0.332	0.119	0.340	6.4	-3.3
80.0	12.80	0.336	0.334	0.139	0.301	6.5	-1.9
86.0	14.47	0.387	0.364	0.143	0.438	8.1	-3.0
90.0	15.44	0.430	0.373	0.143	0.382	8.6	-2.5
96.0	15.98	0.353	0.323	0.134	0.264	6.0	-1.8
100.0	16.34	0.327	0.292	0.121	0.309	4.3	-2.9
106.0	16.75	0.288	0.287	0.113	0.273	4.0	-2.9
110.0	17.12	0.347	0.311	0.135	0.463	5.3	-3.6
116.0	17.81	0.501	0.381	0.079	0.497	9.0	-6.7
120.0	18.23	0.704	0.334	0.073	0.388	6.5	-6.0
126.0	18.87	0.608	0.344	0.093	0.386	7.1	-5.0
130.0	19.34	0.367	0.320	0.099	0.579	5.8	-6.5
134.9	20.47	0.424	0.341	0.104	0.401	6.9	-4.6
135.9	20.73	0.245	0.332	0.117	0.384	6.4	-3.8
136.9	21.00	0.253	0.312	0.096	0.468	5.4	-5.6
137.9	21.26	0.435	0.324	0.102	0.593	6.0	-6.4

Continued

Depth (cm)	Age (kyr BP)	BIT	TEX_{86}	MBT	CBT	LST - ºC (TEX_{86})	MAT_{est} - ºC (MBT/CBT)
138.9	21.52	0.669	0.233	0.048	0.572	1.2	-8.9
139.9	21.78	0.501	0.307	0.074	0.512	5.1	-7.1
140.9	22.05	0.520	0.277	0.076	0.573	3.5	-7.6
141.9	22.30	0.511	0.325	0.074	0.664	6.1	-8.5
142.9	22.54	0.523	0.262	0.069	0.595	2.8	-8.1
143.9	22.77	0.555	0.306	0.066	0.726	5.0	-9.4
148.9	23.95	0.528	0.159	0.079	0.870	-2.7	-10.1
153.9	25.21	0.494	0.264	0.091	-	2.9	-
158.9	26.48	0.634	0.254	0.065	0.638	2.3	-8.7
163.9	27.74	0.416	0.321	0.065	0.576	5.9	-8.1
168.9	28.88	0.398	0.256	0.100	0.549	2.4	-6.1
172.9	29.59	0.426	0.299	0.117	0.553	4.7	-5.3
178.9	30.64	0.435	0.305	0.111	0.581	5.0	-5.9
182.9	31.94	0.344	0.331	0.121	0.694	6.4	-6.4
188.9	34.54	0.327	0.300	0.093	0.610	4.7	-7.1
192.9	34.92	0.389	0.279	0.126	0.727	3.7	-6.5
198.9	35.50	0.365	0.334	0.107	0.492	6.5	-5.3
202.9	35.88	0.510	0.314	0.122	0.673	5.5	-6.2
208.9	36.45	0.462	0.303	0.130	0.389	4.9	-3.2
212.9	36.84	0.476	0.342	0.095	0.556	6.9	-6.5
218.9	37.41	0.516	0.377	0.081	0.575	8.8	-7.3
222.9	37.79	0.701	0.359	0.091	0.390	7.8	-5.1
228.9	38.42	0.601	0.353	0.098	0.754	7.5	-8.1
232.9	38.97	0.628	0.348	0.088	0.732	7.2	-8.4
238.9	39.81	0.639	0.357	0.121	0.295	7.7	-2.8
242.9	40.35	0.602	0.332	0.085	0.620	6.4	-7.5
248.9	41.16	0.551	0.328	0.093	0.515	6.2	-6.2
252.9	41.70	0.547	0.331	0.088	0.580	6.4	-7.0
258.9	42.54	0.714	0.322	0.106	0.400	5.9	-4.4
262.9	43.10	0.623	0.320	0.079	0.672	5.8	-8.3
268.9	43.95	0.739	0.315	0.069	0.459	5.5	-6.8
272.9	44.52	0.620	0.352	0.083	0.680	7.5	-8.2
278.9	45.37	0.692	0.391	0.087	0.372	9.5	-5.2
282.9	45.94	0.630	0.371	0.093	0.466	8.5	-5.7
288.9	46.84	0.574	0.378	0.078	0.446	8.8	-6.3

Continued

Depth (cm)	Age (kyr BP)	BIT	TEX_{86}	MBT	CBT	LST - ºC (TEX_{86})	MAT_{est} - ºC (MBT/CBT)
293.9	47.72	0.748	0.391	0.084	0.327	9.5	-4.9
298.9	48.60	0.765	0.309	0.103	0.594	5.2	-6.4
303.9	49.48	0.666	0.385	0.076	0.689	9.2	-8.6
308.9	50.36	0.639	0.359	0.090	0.645	7.9	-7.5
313.9	51.45	0.798	0.353	0.050	0.609	7.5	-9.2
319.9	52.80	0.630	0.430	0.067	0.540	11.6	-7.7
323.9	53.70	0.723	0.381	0.088	0.598	9.0	-7.2
328.9	54.82	0.709	0.326	0.096	0.562	6.1	-6.4
333.9	55.98	0.633	0.342	0.099	0.480	7.0	-5.5
338.9	57.13	0.538	0.229	0.101	0.534	1.0	-5.9

Appendix 2. Table 12. BIT, TEX_{86}, MBT, CBT and reconstructed lake surface temperature (LST) and mean annual air temperature (MAT_{est}) for sediment samples analysed from core CON01-603-2 in the North Basin of Lake Baikal. Underlined indices and reconstructions are from samples with very low concentrations of GDGTs.

4. Archaeal lipids in the Bosumtwi impact structure ***(Chapter 5)***.

Sample code	Depth (m)	GDGT I m/z 1302	GDGT II m/z 1300	GDGT III m/z 1298	GDGT IV m/z 1296	GDGT V m/z 1292	GDGT V' m/z 1292
Bosumtwi KR8-66	353.95	0	0	0	0	0	0
Bosumtwi KR8-37	283.59	404163	120749	144979	27785	89086	0
Bosumtwi KR8-01	235.77	1588308	146519	75396	19415	81462	0
Bosumtwi KR8-35	280.39	71107	0	0	0	82958	0
Bosumtwi KR8-05	240.04	272270	0	0	0	0	0
Bosumtwi KR8-78	382.17	2427557	0	0	0	0	0

Appendix 2. Table 13. Response (area in arbitrary units) of the isoprenoidal GDGTs found in Bosumtwi impacted rocks. Branched GDGTs were not detected. Depth is taken from the lake surface.

Appendix 3

PUBLISHED MANUSCRIPTS

Geochemistry Geophysics Geosystems G3
AN ELECTRONIC JOURNAL OF THE EARTH SCIENCES
Published by AGU and the Geochemical Society

Article
Volume 10, Number 3
20 March 2009
Q03012, doi:10.1029/2008GC002221
ISSN: 1525-2027

An interlaboratory study of TEX_{86} and BIT analysis using high-performance liquid chromatography–mass spectrometry

Stefan Schouten, Ellen C. Hopmans, Jaap van der Meer, and Anchelique Mets
Departments of Marine Organic Biogeochemistry and Marine Ecology, Royal Netherlands Institute for Sea Research, P.O. Box 59, NL-1790 AB Den Burg, Texel, Netherlands (stefan.schouten@nioz.nl)

Edouard Bard
CEREGE, UMR6635, Aix-Marseille Université, IRD, Collège de France, CNRS, Europole de l'Arbois, BP80, F-13545 Aix-en-Provence, France

Thomas S. Bianchi
Department of Oceanography, Texas A&M University, 3146 TAMU, College Station, Texas 77843, USA

Aaron Diefendorf
Stable Isotope Biogeochemistry Group, Department of Geosciences, Pennsylvania State University, 218 Deike Building, University Park, Pennsylvania 16802, USA

Marina Escala
Institute of Environmental Science and Technology, Universitat Autònoma de Barcelona, Edifici Cn, Campus UAB, E-08193 Barcelona, Spain

Katharine H. Freeman
Stable Isotope Biogeochemistry Group, Department of Geosciences, Pennsylvania State University, 218 Deike Building, University Park, Pennsylvania 16802, USA

Yoshihiro Furukawa
Department of Earth and Planetary Materials Science, Graduate School of Science, Tohoku University, 6-3 Aoba, Aramaki, Sendai 980-8578, Japan

Carme Huguet and Anitra Ingalls
School of Oceanography, University of Washington, Box 355351, Seattle, Washington 98195-5351, USA

Guillemette Ménot-Combes
CEREGE, UMR6635, Aix-Marseille Université, IRD, Collège de France, CNRS, Europole de l'Arbois, BP80, F-13545 Aix-en-Provence, France

Alexandra J. Nederbragt
Department of Earth Sciences, University College London, Gower Street, London WC1E 6BT, UK

Masahiro Oba
Institute of Geology and Paleontology, Tohoku University, 6-3 Aoba, Aramaki, Sendai 980-8578, Japan

Ann Pearson
Department of Earth and Planetary Sciences, Harvard University, Hoffman 303, Cambridge, Massachusetts 02138, USA

Emma J. Pearson
School of Geography, Politics and Sociology, Newcastle University, Daysh Building, Newcastle upon Tyne NE1 7RU, UK

Antoni Rosell-Melé
ICREA, Passeig Lluís Companys 23, E-09010 Barcelona, Spain

Also at Institute of Environmental Science and Technology, Universitat Autònoma de Barcelona, Barcelona, Spain

Philippe Schaeffer
Laboratoire de Géochimie Bioorganique, UMR7177, ECPM, Institut de Chimie de Strasbourg, Université Louis Pasteur, CNRS, 25 rue Becquerel, F-67200 Strasbourg, France

Sunita R. Shah
Department of Earth and Planetary Sciences, Harvard University, Hoffman 303, Cambridge, Massachusetts 02138, USA

Timothy M. Shanahan
Department of Marine Chemistry and Geochemistry, Woods Hole Oceanographic Institution, MS #4, Fye 117, 266 Woods Hole Road, Woods Hole, Massachusetts 02543, USA

Richard W. Smith
Department of Oceanography, Texas A&M University, 3146 TAMU, College Station, Texas 77843, USA

Rienk Smittenberg
Geology Department, ETH Zurich, Sonneggstrasse 5, CH-8092 Zürich, Switzerland

Helen M. Talbot
School of Civil Engineering and Geosciences, University of Newcastle, Drummond Building, Newcastle upon Tyne NE1 7RU, UK

Masao Uchida
AMS Facility, Environmental Chemistry Division, National Institute for Environmental Studies, 16-2 Onogawa, Tsukuba 305-8506, Japan

Benjamin A. S. Van Mooy
Department of Marine Chemistry and Geochemistry, Woods Hole Oceanographic Institution, MS #4, Fye 117, 266 Woods Hole Road, Woods Hole, Massachusetts 02543, USA

Masanobu Yamamoto
Faculty of Environmental Earth Science, Hokkaido University, Kita-10, Nishi-5, Kita-ku, Sapporo 060-0810, Japan

Zhaohui Zhang
Department of Geosciences, University of Massachusetts, 611 North Pleasant Street, Amherst, Massachusetts 01003, USA

Jaap S. Sinninghe Damsté
Departments of Marine Organic Biogeochemistry and Marine Ecology, Royal Netherlands Institute for Sea Research, P.O. Box 59, NL-1790 AB Den Burg, Texel, Netherlands

[1] Recently, two new proxies based on the distribution of glycerol dialkyl glycerol tetraethers (GDGTs) were proposed, i.e., the TEX_{86} proxy for sea surface temperature reconstructions and the BIT index for reconstructing soil organic matter input to the ocean. In this study, fifteen laboratories participated in a round robin study of two sediment extracts with a range of TEX_{86} and BIT values to test the analytical reproducibility and repeatability in analyzing these proxies. For TEX_{86} the repeatability, indicating intralaboratory variation, was 0.028 and 0.017 for the two sediment extracts or ±1–2°C when translated to temperature. The reproducibility, indicating among-laboratory variation, of TEX_{86} measurements was substantially higher, i.e., 0.050 and 0.067 or ±3–4°C when translated to temperature. The latter values are

higher than those obtained in round robin studies of Mg/Ca and $U^{k'}_{37}$ paleothermometers, suggesting the need to primarily improve compatibility between labs. The repeatability of BIT measurements for the sediment with substantial amounts of soil organic matter input was relatively small, 0.029, but reproducibility was large, 0.410. This large variance could not be attributed to specific equipment used or a particular data treatment. We suggest that this may be caused by the large difference in the molecular weight in the GDGTs used in the BIT index, i.e., crenarchaeol versus the branched GDGTs. Potentially, this difference gives rise to variable responses in the different mass spectrometers used. Calibration using authentic standards is needed to establish compatibility between labs performing BIT measurements.

Components: 6500 words, 5 figures, 5 tables.

Keywords: TEX_{86}; BIT; round robin; HPLC/MS.

Index Terms: 4954 Paleoceanography: Sea surface temperature; 0424 Biogeosciences: Biosignatures and proxies; 0452 Biogeosciences: Instruments and techniques.

Received 27 August 2008; **Revised** 3 February 2009; **Accepted** 12 February 2009; **Published** 20 March 2009.

Schouten S., et al. (2009), An interlaboratory study of TEX_{86} and BIT analysis using high-performance liquid chromatography–mass spectrometry, *Geochem. Geophys. Geosyst.*, *10*, Q03012, doi:10.1029/2008GC002221.

1. Introduction

[2] Reconstruction of ancient seawater temperatures is of considerable importance in understanding past climate changes. Over the last decades several temperature proxies have been developed and used to reconstruct past seawater temperatures on the basis of inorganic or organic fossil remains. Two of the most popular tools are presently the Mg/Ca ratio of planktonic foraminifera [*Nürnberg et al.*, 1996; *Elderfield and Ganssen*, 2000] and the $U^{K'}_{37}$ ratio based on long-chain C_{37} alkenones derived from haptophyte algae [*Brassell et al.*, 1986; *Prahl and Wakeham*, 1987].

[3] Recently, a second organic seawater temperature proxy based on archaeal glycerol dibiphytanyl glycerol tetraether (GDGT) lipids, the TEX_{86}, was proposed [*Schouten et al.*, 2002]. These lipids are biosynthesized by marine Crenarchaeota which are ubiquitous in marine environments and are among the dominant prokaryotes in today's oceans [*Karner et al.*, 2001; *Herndl et al.*, 2005]. Marine Crenarchaeota biosynthesize different types of GDGTs, i.e., GDGTs containing 0 to 3 cyclopentyl moieties (GDGT-0 to GDGT-3; see structures in Figure 1) and crenarchaeol which, in addition to four cyclopentyl moieties, has a cyclohexyl moiety (GDGT-4). Finally, they also biosynthesize small quantities of a crenarchaeol regio-isomer (GDGT-4'). A study of marine surface sediments showed that higher overlying sea surface temperatures result in an increase in the relative amounts of GDGTs with two or more cyclopentyl moieties. The TEX_{86} ratio was proposed as a means to quantify the relative abundance of GDGTs [*Schouten et al.*, 2002]:

$$TEX_{86} = \frac{[GDGT-2] + [GDGT-3] + [GDGT-4']}{[GDGT-1] + [GDGT-2] + [GDGT-3] + [GDGT-4']} \quad (1)$$

The TEX_{86} has recently been calibrated with annual mean sea surface temperature using marine sediment core tops with the following resulting equation [*Kim et al.*, 2008]:

$$T = -10.78 + 56.2 * TEX_{86} (r^2 = 0.935, n = 223) \quad (2)$$

Studies have shown that this proxy can be analyzed in a range of sediments up to 120 My old and applied to the reconstruction of ancient sea surface water temperatures [e.g., *Schouten et al.*, 2003; *Forster et al.*, 2007]. TEX_{86} values in modern sediments range typically from 0.3 to 0.7 [e.g., *Kim et al.*, 2008], while in ancient sediments they can be as high as 0.96 [e.g., *Forster et al.*, 2007].

[4] In addition to archaeal GDGTs, bacterial GDGTs with nonisoprenoidal carbon skeletons also are encountered frequently in marine sediments (GDGT-I to GDGT-III, Figure 1). Several studies have now shown that they are especially abundant in soils and peats [*Weijers et al.*, 2006] and progressively decrease in concentration from coastal sediments to open marine sediments, suggesting a terrestrial origin [*Hopmans et al.*, 2004; *Herfort et al.*, 2006; *Kim et al.*, 2006]. *Hopmans et al.* [2004] proposed the BIT index to quantify the relative abundance of these bacterial GDGTs ver-

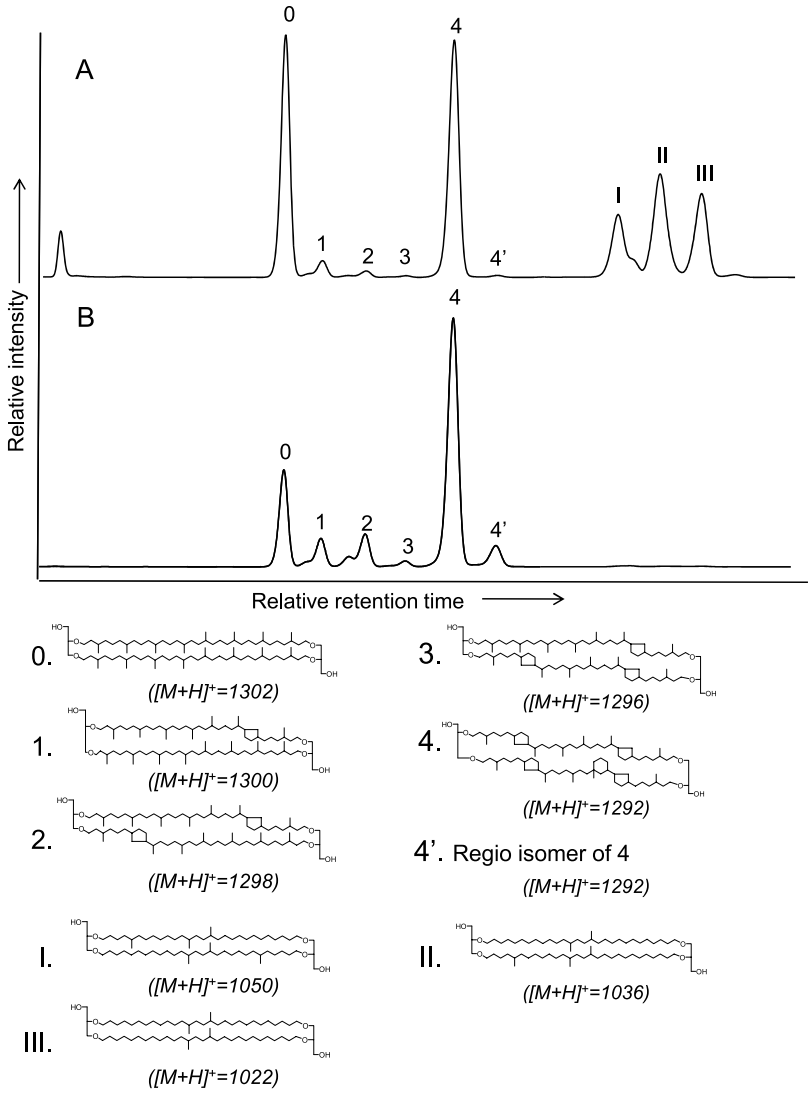

Figure 1. HPLC base peak chromatogram of interlaboratory standards (a) S1 and (b) S2. Numbers in italics with the structures of GDGTs indicate the masses of the $[M+H]^+$ ions of the GDGTs. Samples were run at the Royal NIOZ under conditions described by *Schouten et al.* [2007].

sus crenarchaeol as a proxy for the input of terrestrial organic matter into marine sediments:

$$\mathrm{BIT} = \frac{[\mathrm{GDGT-I}] + [\mathrm{GDGT-II}] + [\mathrm{GDGT-III}]}{[\mathrm{GDGT-4}] + [\mathrm{GDGT-I}] + [\mathrm{GDGT-II}] + [\mathrm{GDGT-III}]} \quad (3)$$

Several studies have now shown that this proxy can be applied to trace the relative importance of soil organic matter in coastal marine environments [e.g., *Herfort et al.*, 2006; *Kim et al.*, 2006; *Huguet et al.*, 2007; *Walsh et al.*, 2008]. Furthermore, *Weijers et al.* [2006] found that high input of soil organic matter in marine sediments can potentially bias TEX_{86} values as it can also contain GDGTs 1–3. They recommended simultaneous reporting of BIT indices in order to monitor for this effect. BIT values can range from 0.01 in open marine sediments up to 1 in some soils [e.g., *Hopmans et al.*, 2004; *Kim et al.*, 2006; *Huguet et al.*, 2007; *Walsh et al.*, 2008].

[5] A prerequisite for the wider application of these proxies is the robustness and analytical reproducibility of their analysis. This is especially important with these proxies as they are analyzed by high-performance liquid chromatography (HPLC) coupled to mass spectrometry (MS) [*Hopmans et al.*, 2000; *Schouten et al.*, 2007; *Escala et al.*, 2007], a technique that was, until recently, not commonly used in many paleoceanographic and organic geochemical laboratories. A

Table 1. HPLC/MS Methods Used by Participants in the Round Robin Study[a]

Lab	HPLC Column	HPLC Gradient	MS Type	MS Method	Integration
1	Prevail Cyano	Hex:IPA	Ion trap	Mass scanning	$[M+H]^+$ ions
2	Prevail Cyano	Hex:IPA	Single quad	SIM	$[M+H]^+$ ions
4	Prevail Cyano	Hex:IPA	Single quad	SIM	$[M+H]^+$ ions
5	Teknokroma Cyano	Hex:IPA	Ion trap	na	$[M+H]^+$ ions
6	Prevail Cyano	Hex:IPA	Single quad	SIM	$[M+H]^+$ + $[M+H+1]^+$ ions
7	Prevail Cyano	Hex:IPA	Ion trap	na	Mass ranges
11	Prevail Cyano	Hex:IPA	Ion trap	na	$[M+H]^+$ ions
12	Prevail Cyano	Hex:IPA	Ion trap	na	$[M+H]^+$ ions
13	Prevail Cyano	Hex:IPA	Single quad	SIM	$[M+H]^+$ ions
14	Prevail Cyano	Hex:IPA	Single quad	SIM	$[M+H]^+$ ions
15	Prevail Cyano	Hex:IPA	Single quad	SIM	$[M+H]^+$ ions
16	Prevail Cyano	Hex:IPA	TOF	Mass scanning	$[M+H]^+$ ions
17	Prevail Cyano	Hex:IPA	Single quad	SIM	$[M+H]^+$ ions
18	Prevail Cyano	Hex:IPA	Ion trap	na	Mass ranges
19	Prevail Cyano	Hex:IPA	Single quad	SIM	$[M+H]^+$ ions
20	Prevail Cyano	Hex:IPA	Single quad	Mass scanning	$[M+H]^+$ ions

[a] Hex, hexane; IPA, isopropanol; SIM, selected ion monitoring; TOF, time of flight; na, not applicable.

common procedure to establish the robustness and reproducibility of an analytical method is a round robin study, as has been done for the $U^{K'}_{37}$ ratio of long-chain C_{37} alkenones [*Rosell-Melé et al.*, 2001] and for the Mg/Ca ratio of (foraminiferal) carbonates [*Rosenthal et al.*, 2004; *Greaves et al.*, 2008]. To assess the reproducibility of the HPLC/MS technique for TEX_{86} and BIT analysis, we performed an anonymous round robin study on filtered polar fractions obtained from extracts of two sediments, following the general outline and methods as in previous paleoceanographic proxy round robin studies by *Rosell-Melé et al.* [2001] and *Rosenthal et al.* [2004].

2. Materials and Methods

[6] A general invitation was sent to a large number of laboratories to participate in an anonymous round robin study, to which 21 labs responded positively. To assess systematic errors in TEX_{86} and BIT analysis these labs received two vials, each containing 1 mg of a polar fraction of a sediment extract labeled S1 and S2, prepared at the NIOZ Royal Netherlands Institute for Sea Research. Labs were requested to analyze the samples when their HPLC/MS set up was performing well according to their criteria and to inject sufficient enough amounts to be above the limit of quantification [cf. *Schouten et al.*, 2007]. The vials were distributed by the end of August 2007 and results reported here are those of the fifteen labs which reported their results before 1 January 2008. One lab (14) reported their results for S1 after this deadline. Their results are included in Tables 1–4 but are not considered further in this study.

2.1. Sediment Origin and Extraction Procedure

[7] The standards comprised filtered polar fractions of sediment extracts labeled S1 and S2. Sediment S1 was derived from a piston core taken

Table 2. Reported Results of TEX_{86} Analysis[a]

Lab	TEX_{86} S1	SD	n	TEX_{86} S2	SD	n
1	0.423	0.014	10	0.697	0.007	5
2	0.401	0.009	16	0.701	0.010	10
4	*0.479*[b]	*0.007*	5	0.745	0.007	7
5	*0.472*[b]	*0.036*[c]	6	*0.675*	*0.044*[c]	6
6	0.414	0.008	15	0.713	0.004	16
7	*0.348*[b]	*0.018*	3	0.660	0.006	3
11	0.410	0.004	3	0.718	0.004	3
12	0.393	0.013	5	0.694	0.005	5
13	0.420	0.012	8	0.699	0.007	8
14[d]	0.84	0.02	4			
15	0.414	0.016	4	0.673	0.008	6
16	0.410	0.007	5	0.711	0.003	5
17	0.433	0.008	6	0.697	0.004	6
18	0.378	0.005	5	0.666	0.007	5
19	*0.480*[b]	*0.003*	7	0.739	0.004	7
20	0.381		2	0.680	0.004	3

[a] Values in italics were rejected and not further considered in the statistical treatment of the data.
[b] Outliers based on visual inspection of normal probability plots of laboratory means.
[c] Outliers based on visual inspection of chi-squared probability plots of laboratory variances.
[d] Result submitted after passing of the deadline and not included further in this study.

Table 3. Reported Results of BIT Index Analysis[a]

Lab	BIT S1	SD	n	BIT S2	SD	n
1	*0.489*	*0.069*[b]	6	0.016	0.0005	4
2	0.582	0.013	16	0.017	0.0005	4
4	0.739	0.006	5	0.040	0.0008	7
5	*0.652*	*0.065*[b]	6	*0.118*[c]	*0.0184*	6
6	0.455	0.008	15	0.015	0.0005	16
7	0.668	0.008	3	0.035	0.0020	3
11	0.338	0.014	3	*0.009*[c]	*0.0028*	3
12	0.658	0.002	5	0.029	0.0021	5
13	0.595	0.010	8	0.019	0.0005	8
14[d]	0.34	0.01	4			
15	0.821	0.011	4	*0.055*[c]	*0.0094*[b]	6
16	0.447	0.014	5	0.012	0.0008	5
17	0.664	0.005	6	0.031	0.0014	6
18	0.250	0.011	5	0.012	0.0012	5
19	*0.476*[c]	*0.031*[b]	7	0.025	0.0023	7
20	0.626	0.015	3	*0.030*	*0.0070*[b]	3

[a] Values in italics were rejected and not further considered in the statistical treatment of the data.
[b] Outliers based on visual inspection of chi-squared probability plots of laboratory variances.
[c] Outliers based on visual inspection of normal probability plots of laboratory means.
[d] Result submitted after passing of the deadline and not included further in this study.

in the Drammensfjord, Norway (D2-H; 59 40.11 N, 10 23.76 E; water depth 113 m; sediment depth 746–797 cm). Sediment S2 was derived from a gravity core (TY92–310G; 16 03 N, 52 71 E; 880 m water depth; 0–42 cm depth) taken in the Arabian Sea. The reason to choose these two sediments is that they were expected to cover a large range of TEX_{86} (temperate versus tropical) and BIT (coastal versus open ocean) values.

[8] The sediments were freeze-dried and Soxhlet extracted for 24 h using a mixture of dichloromethane (DCM) and methanol (7:1, v/v). The combined extracts were separated over a column filled with alumina oxide into an apolar and polar fraction using hexane: DCM (9:1, v/v) and DCM:methanol (1:1, v/v), respectively. The resulting pooled polar fraction was condensed by rotary evaporation and further dried under a stream of nitrogen. The polar fraction was weighed and dissolved in hexane/isopropanol (99:1, v/v) in a concentration of 2 mg/ml. Aliquots of 1 mg were filtered using a PTFE 0.4 μm filter, dried under a stream of nitrogen and distributed to the different labs.

2.2. TEX_{86} and BIT Analysis

[9] All labs used HPLC/Atmospheric Pressure Chemical Ionization (APCI)/MS to analyze GDGTs. The HPLC methods used by the different labs are listed in Table 1 and generally followed that of *Schouten et al.* [2007], i.e., a cyano column with a hexane-isopropanol gradient as the mobile phase. Injected sample sizes ranged from 3 to 300 μg of filtered polar fraction. Base peak chromatograms of HPLC/MS analyses of S1 and S2 are shown in Figure 1.

2.3. Statistical Analysis

[10] Statistical analysis was based on the international standard ISO 5725 for interlaboratory tests [*International Organization for Standardization*, 1986]. Repeatability (r) and reproducibility (R)

Table 4. Reported Results of TEX_{86} and BIT Index Analysis After Adopting a Common Integration Style[a]

Lab	TEX_{86} S1	BIT S1	TEX_{86} S2	BIT S2
1	0.423 (0.000)	0.489 (0.000)	0.697 (0.000)	0.016 (0.000)
2	0.401 (0.000)	0.581 (0.000)	0.701 (0.000)	0.017 (0.000)
4	0.436 (0.043)	0.721(0.018)	0.745 (0.000)	0.031 (0.009)
5				
6	0.439 (0.025)	0.459 (0.004)	0.713 (0.000)	0.013 (0.002)
7	0.348 (0.000)	0.674 (0.006)	0.662 (0.002)	0.030 (0.006)
11	0.413 (0.004)	0.337 (0.002)	0.717 (0.001)	0.009 (0.000)
12	0.390 (0.003)	0.636 (0.022)	0.691 (0.003)	0.022 (0.007)
13	0.414 (0.006)	0.584 (0.010)	0.703 (0.004)	0.013 (0.006)
14[b]		0.590 (0.250)		
15	0.408 (0.006)	0.811 (0.011)	0.704 (0.031)	0.039 (0.016)
16	0.410 (0.000)	0.447 (0.000)	0.711 (0.000)	0.012 (0.000)
17	0.432 (0.001)	0.665 (0.001)	0.698 (0.001)	0.030 (0.001)
18	0.378 (0.000)	0.250 (0.000)	0.666 (0.000)	0.012 (0.000)
19	0.479 (0.001)	0.453 (0.031)	0.738 (0.001)	0.022 (0.003)
20				

[a] Numbers in parentheses indicate absolute difference with previously reported values in Tables 2 and 3.
[b] Result submitted after passing of the deadline and not included further in this study.

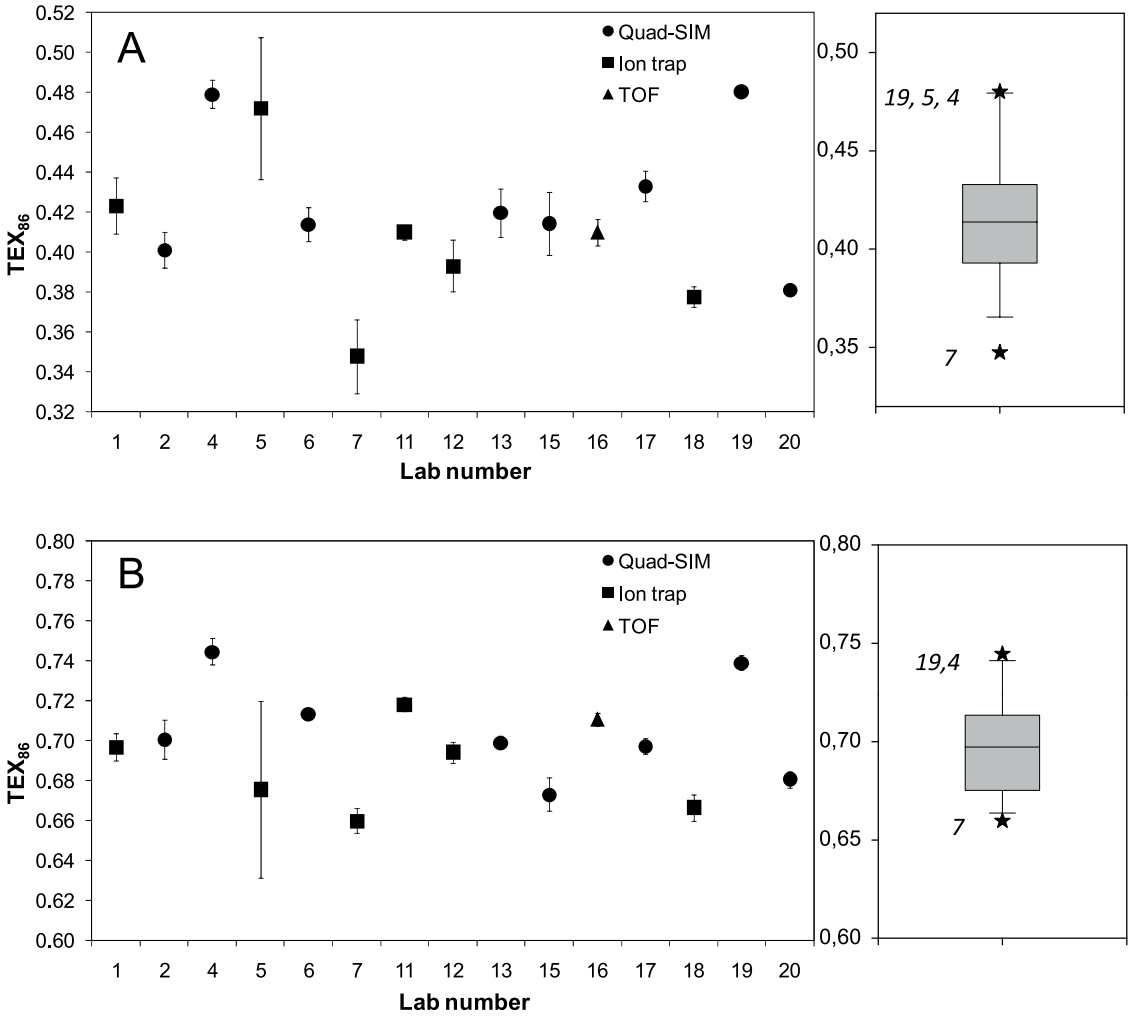

Figure 2. Graph of reported average TEX_{86} values of individual labs for (a) sample S1 from Arabian Sea sediment and (b) sample S2 from Drammensfjord sediment. Error bars indicate standard deviations (SD) of measurements. Next to the graphs, box plots are shown for each sample. Box indicates lower 25% and upper 75% percentile, and bars indicate lower 10% and upper 90% percentile. Numbers in box plot indicate lab numbers.

values were estimated. The repeatability r should be interpreted as the value below which the difference between two single test results obtained by the same method on identical test material under the same test conditions (same operator, same apparatus, same laboratory and within a short interval of time) may be expected to lie with a probability of 95%. The reproducibility R should be interpreted as the value below which the difference between two single test results obtained by the same method on identical test material but under different test conditions (different operators, different apparatus, different laboratory and not necessarily within a short interval of time) may be expected to lie with a probability of 95%. Under these definitions, all laboratories are considered to be using the "same method," and R refers to interlaboratory results, while r refers to intralaboratory results. Outlying data and labs were detected by visual inspection of normal probability plots of laboratory means, chi-square probability plots of laboratory variances and Bartlett's test for homogeneity of variances.

3. Results and Discussion

[11] The results discussed here of the anonymous round robin study of two sediment extracts, labeled S1 and S2, are based on the fifteen labs which reported their results before the deadline of 1 January 2008. The results of the TEX_{86} and BIT analyses of the different labs are listed in Tables 2 and 3 and plotted in Figures 2 and 3, while the methods used are summarized in Table 1. All labs used almost identical LC conditions (solvent gradients, column

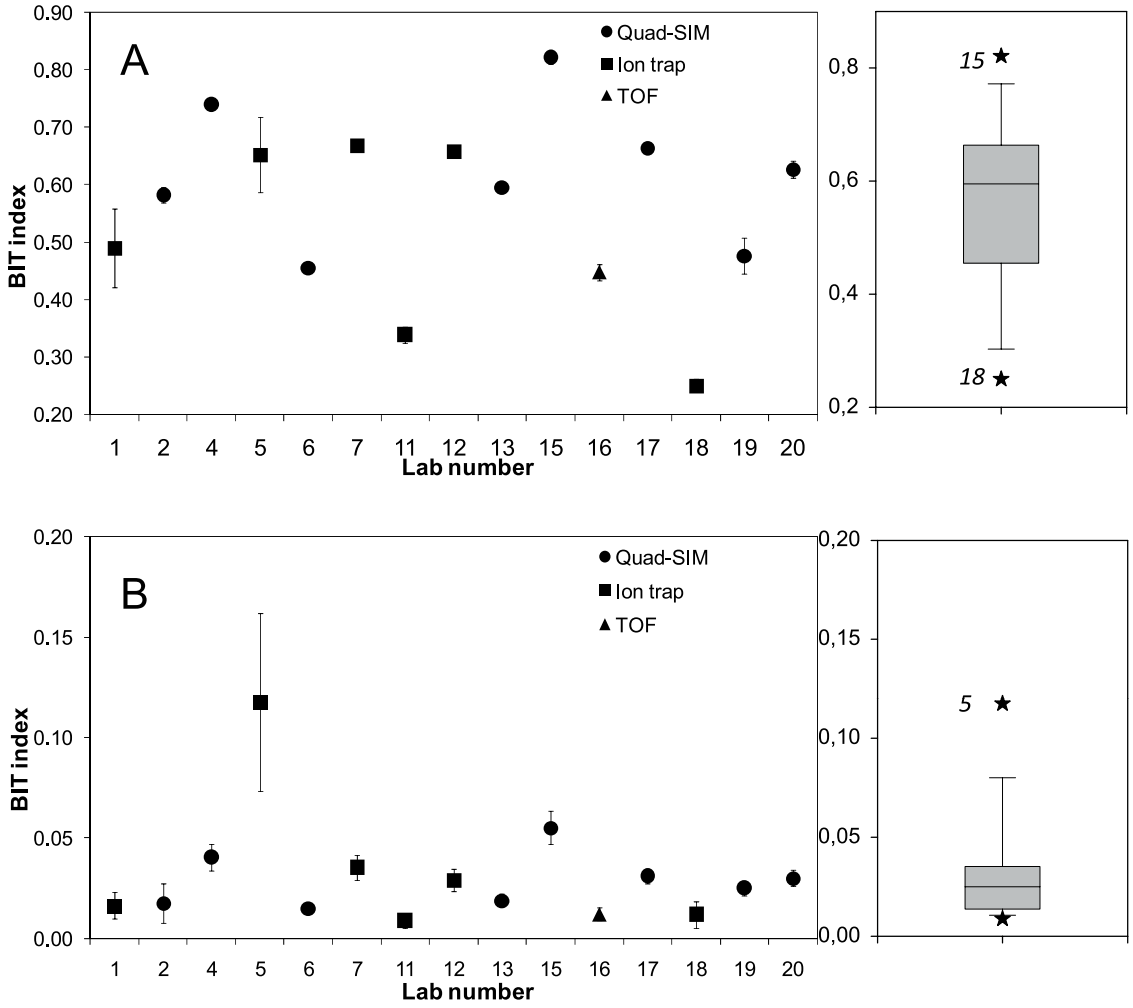

Figure 3. Graph of reported average BIT values of individual labs for (a) sample S1 from Arabian Sea sediment and (b) sample S2 from Drammensfjord sediment. Error bars indicate standard deviations (SD) of measurements. Next to the graphs, box plots are shown for each sample. Box indicates lower 25% and upper 75% percentile, and bars indicate lower 10% and upper 90% percentile. Numbers in box plot indicate lab numbers.

type) but a variety of mass spectrometry techniques, i.e., eight labs used quadrupole MS, six labs used ion trap MS and one lab used time-of-flight MS (TOF). Note that most labs analyzed the samples within 1–2 days and thus standard deviations listed do not represent long-term reproducibility. Furthermore, since labs received "ready-to-inject" polar fractions, the results do not allow evaluation of the effects of individual sample work up procedures as was done for the $U^{K'}_{37}$ ratio of long-chain C_{37} alkenones [*Rosell-Melé et al.*, 2001] and for the Mg/Ca ratio of (foraminiferal) carbonates [*Rosenthal et al.*, 2004].

3.1. TEX_{86} Analysis

[12] The results of the TEX_{86} analysis are listed in Table 2 and shown in Figure 2. In Figure 4a we plotted the distribution of TEX_{86} values for both samples S1 and S2. The results have a reasonably Gaussian-like distribution with a broader range for sample S1. We then statistically identified (see section 2.3) four outliers for S1 (labs 4,5,7,19) and one outlier for S2 (lab 5) which were removed from subsequent statistical treatment. These anomalous results cannot be attributed to a particular mass spectrometric technique since the outliers were from two labs using a quadrupole MS and two labs using an ion trap MS (Table 1 and Figure 2).

[13] The estimated repeatability for TEX_{86}, after removal of the outliers, was 0.028 and 0.017 for S1 and S2, respectively (Table 5). The reproducibility, however, was slightly higher for S2, i.e., 0.067 compared to 0.050 for S1. However, the variance estimate for S1 was made after removal of four

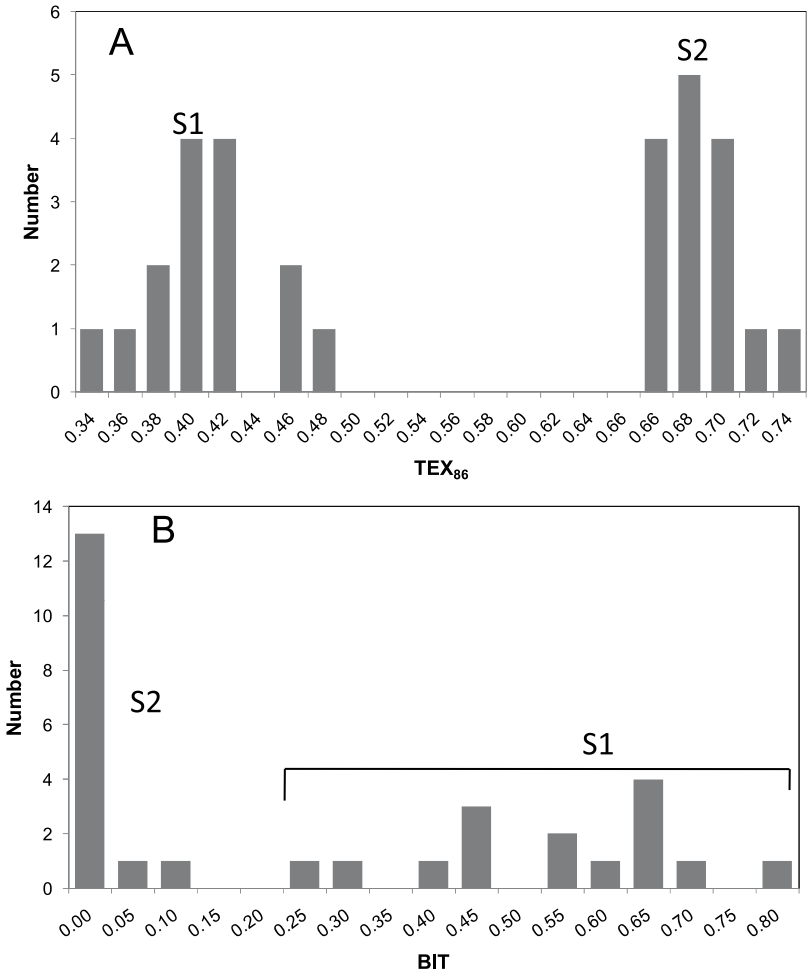

Figure 4. Distribution of (a) TEX_{86} and (b) BIT values.

outliers. Removal of only the most severe outlier (lab 5) would have resulted in a reproducibility of 0.092. If we convert these TEX_{86} values to temperatures [*Kim et al.*, 2008] then the repeatability of TEX_{86} analysis corresponds to 1.9 and 1.1°C for S1 and S2, respectively, while the reproducibility corresponds to 3.3 and 4.5°C for S1 and S2, respectively (Table 5). The better repeatability and, when taking account of the number of outliers removed from S1, reproducibility of sample S2 likely is due to the higher abundances of the minor GDGTs, GDGTs 1–3 and GDGT-4', relative to GDGT-0 and crenarchaeol (GDGT-4). This is likely to have enabled a more reliable quantification, as amounts were not only above the limit of detection but also above the limit of quantification which is likely to be an order of magnitude higher for TEX_{86} analysis [cf. *Schouten et al.*, 2007].

[14] To investigate potential causes for outliers and differences between labs, we plotted the TEX_{86} values of S1 against S2 (Figure 5a). This reveals that, in general, there is a tendency toward some systematic difference. For example, outliers in TEX_{86} measurements of S1 also tend to be outliers in TEX_{86} measurements of S2. This suggests that the differences between labs are not caused by inhomogeneity between individual vials of the standards. Another potential cause for the differences may be the "integration style" used, i.e., which criteria were used to define peak starts and ends. The latter can be important because coelutions occur between the GDGTs of interest and other minor isomers. Therefore, labs were asked to reintegrate the peak areas in their chromatogram according to a prescribed format and preferably by a person not aware of the previous results. Twelve labs reported the results of this exercise which showed that with only a few exceptions, the changes in TEX_{86} were relatively minor (Table 4) and unlikely to account for the observed differences. The results of lab 5 are, for both samples, outliers. Examination of their LC/MS equipment

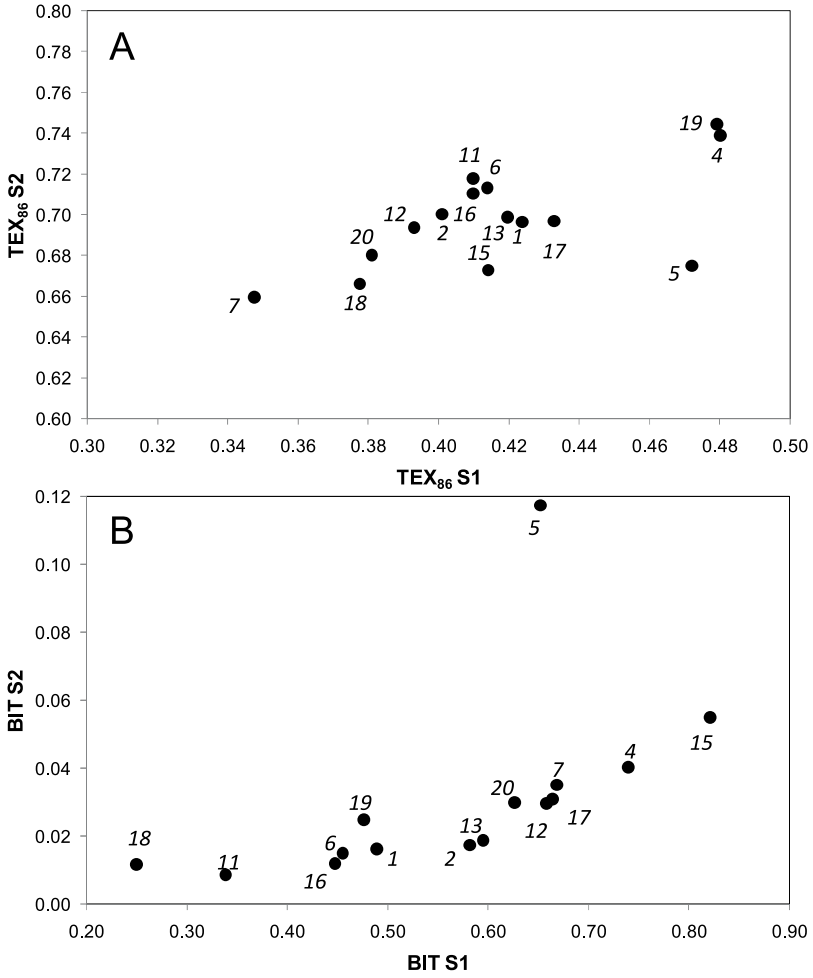

Figure 5. Crossplots of (a) TEX_{86} and (b) BIT index for sample S1 against S2. Numbers in italics indicate lab numbers.

revealed that the cone of the nebulizer was not well aligned with the ion source, and the inner surfaces of the interface had some chemical residues. This highlights the fact that maintenance of the APCI interface is of prime importance to obtain consistent and robust results.

[15] The results obtained for TEX_{86} analysis compared reasonably well to those obtained for other paleothermometers, especially considering the relatively recent development of the proxy. *Rosell-Melé et al.* [2001] found for $U^{k'}_{37}$ analyses of several sediments a repeatability of 1.6°C, but their reproducibility of 2.1°C was substantially better than obtained in our study. *Rosenthal et al.* [2004] reported a repeatability of 1–2°C and a reproducibility of 2–3°C for Mg/Ca analysis of foraminifera, also numbers that are similar to our study. These estimates also already contained biases induced by work up procedures, something which is not applicable in our study. In fact, the reproducibility of standard mixtures, which does not include biases by sample work up, is even better at 0.5 and 1.3°C for Mg/Ca and $U^{k'}_{37}$, respectively. Thus, our interlaboratory study suggests that repeatability (r) of TEX_{86} temperatures is similar to those of other paleothermometers but that the reproducibility (R) among labs is significantly higher. Hence, there is a need to improve reproducibility between labs using standards or calibrations. It also should be noted, however, that a large number of the participating labs had relatively little experience in analyzing GDGTs using HPLC/APCI/MS at this point. Presumably, the robustness of these analyses will improve with increasing experience.

3.2. BIT Analysis

[16] The results of the analysis of samples S1 and S2 for BIT are displayed in Table 3 and Figures 3 and 4. Sample S2 is from an open marine sediment with a small contribution of soil organic matter,

Table 5. Summary Statistics of All Measurements Made by the Different Laboratories

	Mean[a]	Mean	Median	Mode	SD[a]	SD	r	R	$\%RSD_r$	$\%RSD_R$
TEX_{86} S1	0.420	0.409	0.410	0.380	0.034	0.017	0.028	0.050	6.8	12
TEX_{86} S2	0.702	0.704	0.701	0.690	0.026	0.023	0.017	0.067	2.4	9.5
BIT S1	0.554	0.558	0.583	0.738	0.131	0.138	0.029	0.410	5.2	74
BIT S2	0.032	0.022	0.018	0.040	0.027	0.009	0.004	0.028	16	127

[a] Including outliers.

and thus values are nearly all below 0.1 (Figure 3b and Table 3). On the basis of the Bartlett's test four outliers were removed (labs 5,11,15,20) but the variability remained inhomogeneous even after removal of these four outliers. The repeatability was 0.004, while the reproducibility was much larger at 0.028. Sample S1 is from a Norwegian fjord, which likely contains substantial amounts of soil organic carbon [e.g., *Huguet et al.*, 2007]. Indeed substantially higher BIT indices were measured for this sample than for S2. However, a large spread in BIT values ranging from 0.25 to 0.82 (on a scale from 0 to 1; Figure 3a and Table 3) and a broad nonuniform distribution were found (Figure 4b), quite different from that observed for the TEX_{86} measurements. For BIT measurements of S1, the repeatability estimate is 0.029 while the reproducibility estimate is high at 0.410 even after removing three outliers on the basis of Bartlett's test (Table 5).

[17] The large reproducibility estimate for sample S1 and the inhomogeneity in variances between different BIT measurements is striking. It suggests that the BIT index can be determined by most labs fairly reproducibly but that there are considerable differences between labs. This suggests that there is some major underlying problem in determining the BIT index which is not apparent for TEX_{86} analysis, even though both parameters are measured in a single analysis. A similar reintegration exercise was performed for the BIT measurements as with the TEX_{86} measurements but again this did not result in substantial changes in the reported results (Table 4). Plotting the results of BIT measurements of S1 against S2 shows that the differences are systematic (Figure 5b) and thus again cannot be due to inhomogeneity between the distributed vials. Furthermore, there is no particular distinction in BIT values based on the type of mass spectrometer used (Figure 3), nor do similar clusters form among laboratories as those found for the TEX_{86} results (Figure 5a).

[18] There may be several reasons for this large spread in BIT indices. First, branched GDGTs have a later elution time. Most chromatographic programs made use of a hexane-isopropanol gradient and thus, depending on the elution time, a varying percentage of isopropanol may have been present in the APCI chamber during the ionization of the branched GDGTs compared to the amount present during the ionization of crenarchaeol (GDGT-4). This may have given rise to differences in the ionization efficiency of the GDGTs in the APCI and thus variation in the BIT index may depend on the chromatographic behavior of the GDGTs on the LC column. However, at the NIOZ lab similar BIT values were obtained for S1 despite variations in retention time of up to 5 min or when using an isocratic elution program, suggesting that varying isopropanol concentrations does not have a major effect on the indices measured. Second, and likely more importantly, there is a large mass difference between branched GDGTs (*m/z* 1022–1050) and crenarchaeol (*m/z* 1292). Thus, the BIT index will be more affected by the mass calibration and tuning of the mass spectrometer used, in contrast to the TEX_{86}, where mass differences of the GDGTs used are much smaller (*m/z* 1300 to *m/z* 1292). This difference does not depend on the type of mass spectrometer (Figure 3). To solve this problem unequivocally, mixtures of authentic standards of crenarchaeol and a branched GDGT in known ratios are required, something which needs to be considered in future round robin studies. Until then, it is clear that the BIT index can only be used as a crude qualitative measure for the relative input of soil organic matter in coastal systems. The results also have consequences for assessing biases in TEX_{86} using an absolute BIT value [cf. *Weijers et al.*, 2006]. Instead, it may be possible to assess this bias by correlating BIT values with TEX_{86} values, i.e., large changes in soil organic matter input, and thus in the BIT index, will likely lead to changes in the TEX_{86}.

4. Conclusions

[19] An anonymous interlaboratory study of TEX_{86} and BIT analysis of two sediment extracts was

carried out by fifteen different laboratories around the world and revealed relatively large variances between the different labs, especially for BIT analysis. Repeatability of TEX_{86} analysis was, in terms of temperature, similar to the work-up and analytical repeatability of other paleothermometers (±1–2°C) but the reproducibility between labs was larger (±3–4°C), indicating the need for improved analytical protocols. Paleotemperature reconstructions based on TEX_{86} therefore are likely to perform as well as other proxies for determining magnitudes and rates of climatic changes, based on the generally good laboratory repeatability. The poor reproducibility will only impact the reconstruction of absolute temperatures. For BIT values the reproducibility was large (0.410), potentially because of differences in mass calibration and tuning of the mass spectrometers used. Our results suggest that there is a clear need for further round robin studies which should include the use of mixtures of authentic standards, constraining the effects of mass calibrations and tuning set ups, evaluation of sample work up procedures and the monitoring of long-term reproducibility.

References

Brassell, S. C., G. Eglinton, I. T. Marlowe, U. Pflaumann, and M. Sarnthein (1986), Molecular stratigraphy: A new tool for climatic assessment, *Nature*, *320*, 129–133, doi:10.1038/320129a0.

Elderfield, H., and G. Ganssen (2000), Past temperature and $\delta^{18}O$ of surface ocean waters inferred from foraminiferal Mg/Ca ratios, *Nature*, *405*, 442–445, doi:10.1038/35013033.

Escala, M., A. Rosell-Melé, and P. Masqué (2007), Rapid screening of glycerol dialkyl glycerol tetraethers in continental Eurasia samples using HPLC/APCI-ion trap mass spectrometry, *Org. Geochem.*, *38*, 161–164, doi:10.1016/j.orggeochem.2006.08.013.

Forster, A., S. Schouten, K. Moriya, P. A. Wilson, and J. S. Sinninghe Damsté (2007), Tropical warming and intermittent cooling during the Cenomanian/Turonian oceanic anoxic event 2: Sea surface temperature records from the equatorial Atlantic, *Paleoceanography*, *22*, PA1219, doi:10.1029/2006PA001349.

Greaves, M., et al. (2008), Interlaboratory comparison study of calibration standards for foraminiferal Mg/Ca thermometry, *Geochem. Geophys. Geosyst.*, *9*, Q08010, doi:10.1029/2008GC001974.

Herfort, L., S. Schouten, J. P. Boon, M. Woltering, M. Baas, J. W. H. Weijers, and J. S. Sinninghe Damsté (2006), Characterization of transport and deposition of terrestrial organic matter in the southern North Sea using the BIT index, *Limnol. Oceanogr.*, *51*, 2196–2205.

Herndl, G. J., T. Reinthaler, E. Teira, H. van Aken, C. Veth, A. Pernthaler, and J. Pernthaler (2005), Contribution of Archaea to total prokaryotic production in the deep Atlantic Ocean, *Appl. Environ. Microbiol.*, *71*, 2303–2309, doi:10.1128/AEM.71.5.2303-2309.2005.

Hopmans, E. C., S. Schouten, R. D. Pancost, M. T. J. Van Der Merr, and J. S. Sinninghe Damsté (2000), Analysis of intact tetraether lipids in archaeal cell material and sediments using high performance liquid chromatography/atmospheric pressure ionization mass spectrometry, *Rapid Commun. Mass Spectrom.*, *14*, 585–589, doi:10.1002/(SICI)1097-0231(20000415)14:7<585::AID-RCM913>3.0.CO;2-N.

Hopmans, E. C., J. W. H. Weijers, E. Schefuß, L. Herfort, J. S. Sinninghe Damsté, and S. Schouten (2004), A novel proxy for terrestrial organic matter in sediments based on branched and isoprenoid tetraether lipids, *Earth Planet. Sci. Lett.*, *224*, 107–116, doi:10.1016/j.epsl.2004.05.012.

Huguet, C., R. H. Smittenberg, W. Boer, J. S. Sinninghe Damsté, and S. Schouten (2007), Twentieth century proxy records of temperature and soil organic matter input in the Drammensfjord, southern Norway, *Org. Geochem.*, *38*, 1838–1849, doi:10.1016/j.orggeochem.2007.06.015.

International Organization for Standardization (1986), Determination of repeatability and reproducibility for a standard test method by interlaboratory tests, *ISO 5725*, 2nd ed., Geneva, Switzerland.

Karner, M., E. F. DeLong, and D. M. Karl (2001), Archaeal dominance in the mesopelagic zone of the Pacific Ocean, *Nature*, *409*, 507–510, doi:10.1038/35054051.

Kim, J.-H., S. Schouten, R. Buscail, W. Ludwig, J. Bonnin, J. S. Sinninghe Damsté, and F. Bourrin (2006), Origin and distribution of terrestrial organic matter in the NW Mediterranean (Gulf of Lions): Exploring the newly developed BIT index, *Geochem. Geophys. Geosyst.*, *7*, Q11017, doi:10.1029/2006GC001306.

Kim, J.-H., S. Schouten, E. C. Hopmans, B. Donner, and J. S. Sinninghe Damsté (2008), Global sediment core-top calibration of the TEX_{86} paleothermometer in the ocean, *Geochim. Cosmochim. Acta*, *72*, 1154–1173, doi:10.1016/j.gca.2007.12.010.

Nürnberg, D., J. Bijma, and C. Hemleben (1996), Assessing the reliability of magnesium in foraminiferal calcite as a proxy for water mass temperatures, *Geochim. Cosmochim. Acta*, *60*, 803–814, doi:10.1016/0016-7037(95)00446-7.

Prahl, F. G., and S. G. Wakeham (1987), Calibration of unsaturation patterns in long-chain ketone compositions for paleotemperature assessment, *Nature*, *330*, 367–369, doi:10.1038/330367a0.

Rosell-Melé, A., et al. (2001), Precision of the current methods to measure the alkenone proxy U^{K}_{37} and absolute alkenone abundance in sediments: Results of an interlaboratory comparison study, *Geochem. Geophys. Geosyst.*, *2*(7), 1046, doi:10.1029/2000GC000141.

Rosenthal, Y., et al. (2004), Interlaboratory comparison study of Mg/Ca and Sr/Ca measurements in planktonic foraminifera for paleoceanographic research, *Geochem. Geophys. Geosyst.*, *5*, Q04D09, doi:10.1029/2003GC000650.

Schouten, S., E. C. Hopmans, and J. S. Sinninghe Damsté (2002), Distributional variations in marine crenarchaeotal membrane lipids: A new organic proxy for reconstructing ancient sea water temperatures?, *Earth Planet. Sci. Lett.*, *204*, 265–274, doi:10.1016/S0012-821X(02)00979-2.

Schouten, S., E. C. Hopmans, M. M. M. Kuypers, Y. Van Breugel, A. Forster, and J. S. Sinninghe Damsté (2003), Extremely high sea water temperatures at low latitudes during the middle Cretaceous as revealed by archaeal membrane lipids, *Geology*, *31*, 1069–1072, doi:10.1130/G19876.1.

Schouten, S., C. Huguet, E. C. Hopmans, M. V. M. Kienhuis, and J. S. Sinninghe Damsté (2007), Improved analytical methodology and constraints on analysis of the TEX_{86} paleothermometer by high performance liquid chromatography/

atmospheric pressure chemical ionization-mass spectrometry, *Anal. Chem.*, *79*, 2940–2944, doi:10.1021/ac062339v.

Walsh, E. M., A. E. Ingalls, and R. G. Keil (2008), Sources and transport of terrestrial organic matter in Vancouver Island fjords and the Vancouver-Washington Margin: A multiproxy approach using δ^{13}Corg, lignin phenols, and the ether lipid BIT index, *Limnol. Oceanogr.*, *53*, 1054–1063.

Weijers, J. W. H., S. Schouten, O. C. Spaargaren, and J. S. Sinninghe Damsté (2006), Occurrence and distribution of tetraether membrane in soils: Implications for the use of the BIT index and the TEX_{86} SST proxy, *Org. Geochem.*, *37*, 1680–1693, doi:10.1016/j.orggeochem.2006.07.018.

Available online at www.sciencedirect.com
ScienceDirect
Organic Geochemistry 38 (2007) 161–164
Organic Geochemistry
www.elsevier.com/locate/orggeochem

Note

Rapid screening of glycerol dialkyl glycerol tetraethers in continental Eurasia samples using HPLC/APCI-ion trap mass spectrometry

Marina Escala [a,*], Antoni Rosell-Melé [a,b], Pere Masqué [a,c]

[a] *ICTA, Autonomous University of Barcelona, Bellaterra 08193, Catalonia, Spain*
[b] *ICREA, Passeig Lluís Companys, 23, Barcelona 09010, Catalonia, Spain*
[c] *Physics Department, Autonomous University of Barcelona, Bellaterra 08193, Catalonia, Spain*

Received 2 December 2005; received in revised form 11 August 2006; accepted 25 August 2006
Available online 31 October 2006

Abstract

The TEX_{86} ratio has been proposed as a palaeotemperature proxy for reconstructing surface water temperatures in aquatic environments. It is based on measuring the relative abundance of membrane lipids of marine Crenarchaeota, namely glycerol dialkyl glycerol tetraethers (GDGTs). Here we describe the rapid screening of GDGTs in sediments and water particulate matter with an optimized method using HPLC coupled to an ion trap mass spectrometer. The reproducibility of the analysis is as good as 0.012 (RSD 2.2%) for TEX_{86}, thus providing a reproducible method for GDGT analysis. Preliminary results are shown for sediments from small as well as large lakes and for sediment trap material from Lake Baikal. GDGTs are present in most of the samples and TEX_{86} values are presented along with estimated temperatures.

1. Introduction

In 2002, a novel sea surface temperature (SST) proxy for estimating past sea or lake surface temperature (SST or LST) based on biomarkers was proposed, named TEX_{86} (Schouten et al., 2002). This index reflects the relative abundance of different membrane lipids of marine Crenarchaeota, namely glycerol dialkyl glycerol tetraethers (GDGTs), which are currently analyzed using high performance liquid chromatography-atmospheric pressure chemical ionization mass spectrometry (HPLC/APCI-MS) (Hopmans et al., 2000). In palaeoclimate studies high throughput methods are needed to allow analysis of large arrays of samples extending back in time with the maximum resolution available. Here, we describe an optimized method which allows rapid screening of GDGTs in extracts of different samples. The method is appraised through analysis of lacustrine sediments and water particulate matter from lakes located at different latitudes.

2. Experimental

Optimization of HPLC/APCI-MS conditions was carried out using a purified sample of GDGT-0 (I) provided by Dr H. Morii (UOEH, Kitakyushu,

* Corresponding author.
E-mail address: marina.escala@uab.es (M. Escala).

0146-6380/$ - see front matter © 2006 Elsevier Ltd. All rights reserved.
doi:10.1016/j.orggeochem.2006.08.013

Japan). Late Holocene sediment samples from Iberian Peninsula lakes were provided by Dr B. Valero-Garcés (IPE-CSIC, Zaragoza, Spain). Core top sediments, water column particulate material obtained from sediment traps (one year integrated signal) and discrete near-surface water samples (2 l filtered through 0.7 μm glass microfibre filters) from the north and south basins of Lake Baikal were sampled in summer 2001 (Russell and Rosell-Melé, 2005).

Filters or sediments were freeze-dried and extracted with CH_2Cl_2/MeOH (3:1, v/v) using microwave-assisted extraction (Kornilova and Rosell-Melé, 2003) and extracts were hydrolyzed overnight with 8% KOH in MeOH. The neutral fraction was recovered with hexane and residual KOH was removed by liquid extraction with Milli-Q water. The solvent was removed (vacuum rotatory evaporation and N_2 stream) and the samples were redissolved in hexane/propanol (99:1, v/v). Prior to injection, they were filtered through a 0.45 μm Millipore PVDF filter.

Analysis was performed using an Agilent 1100 HPLC instrument coupled to a Bruker ion trap Esquire 3000 mass spectrometer with an APCI interface. Extracts were separated at 30.0 °C with an Econosphere NH_2 column (4.6 × 150 mm, 5 μm; Alltech) equipped with a precolumn filter, in isocratic mode using hexane/*n*-propanol (98:2). Flow rate was 1 ml min^{-1} and 10 μl of sample were injected. The sensitivity of the mass spectrometer was optimized by infusion of a solution of GDGT-0 via a direct probe and monitoring the area in the mass chromatogram of the protonated molecule $[M + H]^+$ of GDGT-0 (*m*/*z* 1302). The parameters optimized to generate positive ion spectra were the corona voltage (5000 V), the capillary voltage (4200 V) and the temperature of the desolvation chamber (vaporizer temperature 300 °C) and the dry N_2 flux (drying temperature 250 °C). The GDGTs relevant to TEX_{86} were monitored at *m*/*z* 1302 (I), 1300 (II), 1298 (III), 1296 (IV) and 1292 (regioisomers V and VI).

3. Results and discussion

Using our HPLC conditions, GDGT-0 eluted at 4.5 min, prior to the other tetraethers. GDGTs were identified from their mass spectra and the elution order reported elsewhere (e.g. Schouten et al., 2002). Elution of the relevant compounds was complete in 7 min (Fig. 1a). After every 4 runs, the column was flushed with a gradient elution programme, increasing the *n*-propanol% in hexane from 2 to 8% to avoid peak retention time shifts due to possible system contamination. This enabled four samples to be analyzed

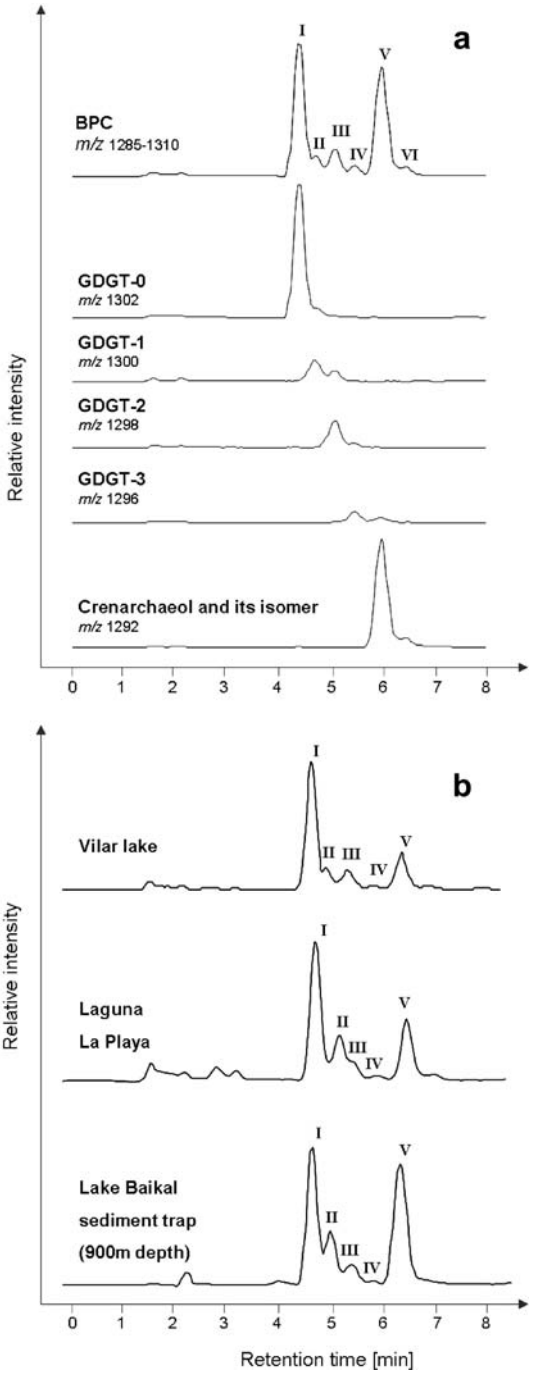

Fig. 1. (a) Base peak chromatogram and extracted ion chromatograms for GDGTs in sediments from Lake Villarquemado (Teruel, Spain). (b) Base peak chromatograms for sediments analyzed with the rapid screening method: sediment from lake El Vilar; sediment from Laguna La Playa; material from a sediment trap deployed at 900 m depth in the north basin of Lake Baikal.

every hour. Currently, TEX_{86} measurements in a sample are reported to take one hour (Hopmans et al., 2000), so that the method presented here increases fourfold the sample throughput.

The repeatability was assessed with three consecutive injections of a standard solution of 45 ppb GDGT-0 in hexane/propanol (99:1, v/v) and the relative standard deviation (RSD) was determined to be 2.0%. Two lake sediment extracts were injected on three different days in order to estimate the reproducibility of the analysis. For samples from Lake Vilar, the precision (1σ) for TEX_{86} was 0.012 (RSD 2.2%), which is equivalent to 0.8 °C. For Laguna La Playa, the precision (1σ) was 0.055 (RSD 7.8%), which corresponds to 3.7 °C. The Laguna La Playa sample produced an extremely low signal, which hampered integration and might have been the cause of the relatively low reproducibility. The optimized method enabled detection of the target GDGTs in most of the samples from the Iberian lakes and Lake Baikal (Fig. 1b). A comparison of the estimated temperatures based on the TEX_{86} measurements and reference temperatures is shown in Table 1. For Lake Baikal sediment trap material and sediment samples, GDGT-0 (I) and crenarchaeol (V) were the predominant GDGTs, in agreement with the typical GDGT distribution found at cold sites and in low temperature incubations (Schouten et al., 2002; Wuchter et al., 2004). The estimated temperatures for Lake Baikal are similar to those reported for surface water (e.g. Bolgrien et al., 1995). The results

Table 1
TEX_{86} values and estimated temperatures (Wuchter et al., 2005) using the rapid screening method

Sample		TEX_{86}	Estimated temperature (°C)	Reference temperature (°C)[a]
Lake Baikal (north basin)				
Sediment trap (300 m depth)		0.312	1.4	Ice-covered Dec–May; <4 °C end of June;
Sediment trap (900 m depth)		0.342	3.5	6 °C early July; 12–14 °C early Aug
Filter (10 m depth)		n.d.		
Surface sediment (390 m depth)		0.371	5.4	
Lake Baikal (south basin)				
Sediment trap (40 m depth)		0.411	8.1	Ice-covered Jan–April; <4 °C end of June;
Sediment trap (1396 m depth)		0.393	6.8	8–12 °C early July
Filter (10 m depth)		n.d.		
Surface sediment (632 m depth)		0.322	2.1	
Iberian Peninsula lakes				
Villarquemado	1°02′W, 40°03′N	0.683	26.2	Min. −1.7 Max. 30.6 Av. 11.7
Caicedo (litoral sample)	2°06′W, 42°47′N	0.520	15.3	Min. 0.4 Max. 26.0 Av. 11.0
La Playa (1)	0°11′W, 41°25′N	0.652	24.1	Min. 1.4 Max. 31.9 Av. 14.6
La Playa (2)		0.762	31.4	
La Playa (3)		0.705	27.7	
El Tobar	3°57′W, 40°33′N	0.360	4.7	Min. 1.8 Max. 31.8 Av. 13.6
Sanabria	6°42′W, 42°07′N	0.549	17.2	Min. −1.7 Max. 26.1 Av. 9.8
Caicedo	2°06′W, 42°47′N	0.471	12.0	Min. 0.4 Max. 26.0 Av. 11.0
Montcortés	1°00′E, 42°20′N	0.542	16.8	Min. −3.3 Max. 26.9 Av. 9.6
Enol	4°09′W, 43°11′N	0.470	12.0	Min. 0.8 Max. 23.7 Av. 10.7
Taravilla	1°59′W, 40° 39′N	0.486	13.1	Min. −1.7 Max. 30.3 Av. 11.0
Zoñar	4°41′W, 37°29′N	0.557	17.8	Min. 4.0 Max. 18.0 Av. 16.1
Estaña Grande	0°32′E, 42°02′N	0.205	−5.6	Min. −1.6 Max. 29.7 Av. 12.0
El Vilar (1)	2°45′E, 42°07′N	0.540	16.7	Min. 2.0 Max. 27.8 Av. 14.1
El Vilar (2)		0.562	18.1	
El Vilar (3)		0.547	17.1	

n.d., GDGTs not detected.

[a] Present day temperatures are reported for the sampling sites for comparison with estimated temperatures. Lake Baikal reference temperatures from Bolgrien et al. (1995). Iberian Peninsula lakes minimum (Min.), maximum (Max.) and average (Av.) annual present day temperatures correspond to air temperatures from Digital Climatic Atlas of the Iberian Peninsula (www.opengis.uab.es/wms/iberia/index.htm).

point to considerably lower temperatures for the northern than for the southern basin. None of the GDGTs were detected in filtered particulate matter from Lake Baikal, which may be due to the small amount of water filtered (2 l). As for the Iberian lakes, estimated Late Holocene temperatures are in the range for present day temperatures, as would be expected because of the similar temperatures in southwestern Europe throughout the Holocene (e.g. Davis et al., 2003). A discussion on the significance of the temperatures based on TEX_{86} measurements is beyond the scope of the present note.

Our results show that the optimized method allows reproducible and rapid screening of GDGTs in different samples, significantly reducing the time required per analysis and thereby enhancing the potential for TEX_{86} use in palaeoclimate studies.

Acknowledgements

The authors thank E. Hopmans and A. Eustaquio for advice on method development. M. Russell, B. Valero-Garcés, A. Moreno and H. Morii are acknowledged for provision of samples. The Generalitat de Catalunya is also acknowledged for a FI Grant. S. Schouten and C.A. Lewis are thanked for their reviews.

Associate Editor—**S. Schouten**

References

Bolgrien, D.W., Granin, N.G., Levin, L., 1995. Surface-temperature dynamics of Lake Baikal observed from Avhrr images. Photogrammetric Engineering And Remote Sensing 61, 211–216.

Davis, B., Brewer, S., Stevenson, A.C., Guiot, J., 2003. The temperature of Europe during the Holocene reconstructed from pollen data. Quaternary Science Reviews 22, 1701–1716.

Hopmans, E.C., Schouten, S., Pancost, R.D., Van der Meer, M.T.J., Sinninghe Damsté, J.S., 2000. Analysis of intact tetraether lipids in archaeal cell material and sediments by high performance liquid chromatography/atmospheric pressure chemical ionization mass spectrometry. Rapid Communications in Mass Spectrometry 14, 585–589.

Kornilova, O., Rosell-Melé, A., 2003. Application of microwave-assisted extraction to the analysis of biomarker climate proxies in marine sediments. Organic Geochemistry 34, 1517–1523.

Russell, M., Rosell-Melé, A., 2005. Preliminary study of fluxes of major lipid biomarker classes in the water column and sediments of Lake Baikal, Russia. Global and Planetary Change 46, 45–56.

Schouten, S., Hopmans, E.C., Schefuss, E., Sinninghe Damsté, J.S., 2002. Distributional variations in marine crenarchaeotal membrane lipids: a new tool for reconstructing ancient sea water temperatures? Earth and Planetary Science Letters 204, 265–274.

Wuchter, C., Schouten, S., Coolen, M.J.L., Sinninghe Damsté, J.S., 2004. Temperature-dependent variation in the distribution of tetraether membrane lipids of marine Crenarchaeota: implications for TEX86 paleothermometry. Paleoceanography 19, PA4028. doi:10.1029/2004PA001041.

Wuchter, C., Schouten, S., Wakeham, S.G., Sinninghe Damsté, J.S., 2005. Temporal and spatial variation in tetraether membrane lipids of marine Crenarchaeota in particulate organic matter: Implications for TEX86 paleothermometry. Paleoceanography 20, PA3013. doi:10.1029/2004PA001110.

Appendix A. Structures of glycerol dialkyl glycerol tetraethers

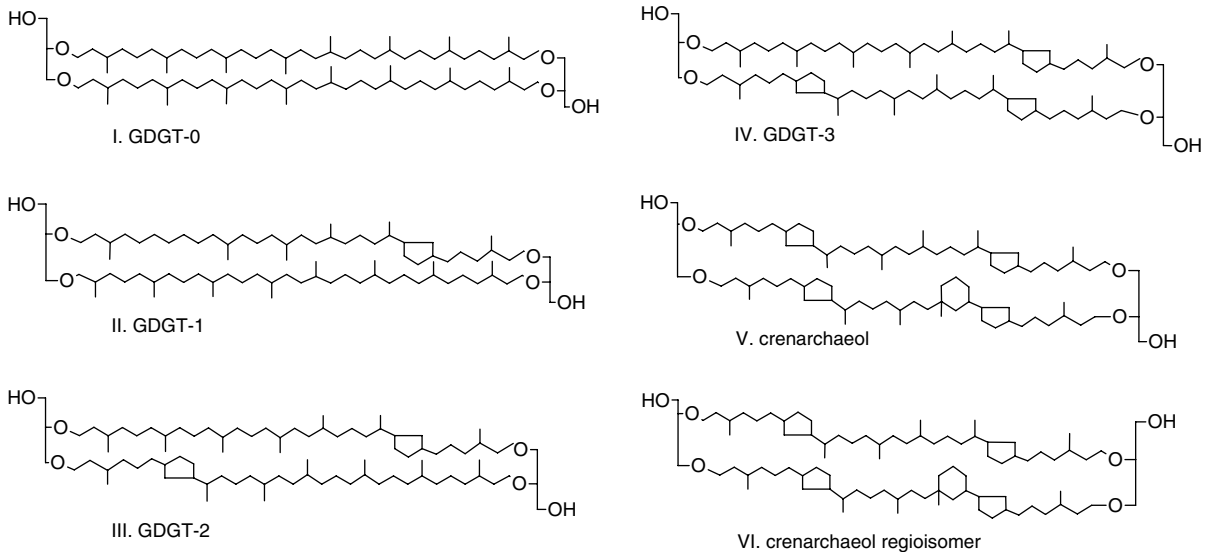

Arabic numbers are indicative of cyclopentane rings. Roman numeration is used to identify structures. $TEX^{86} = (III + IV + VI)/(II + III + IV + VI)$.

Anal. Chem. **XXXX,** *xxx,* 000–000

Analytical Considerations for the Use of the Paleothermometer Tetraether Index$_{86}$ and the Branched vs Isoprenoid Tetraether Index Regarding the Choice of Cleanup and Instrumental Conditions

Marina Escala,[†] Susanne Fietz,[†] Gemma Rueda,[†] and Antoni Rosell-Melé*[,†,‡]

Institute of Environmental Science and Technology, Faculty of Sciences, Universitat Autònoma de Barcelona, Cerdanyola del Vallès 08193, Catalonia, Spain, and ICREA, Passeig Lluís Companys 23, Barcelona 08010, Catalonia, Spain

The tetraether index of tetraethers consisting of 86 carbons (TEX$_{86}$) is a novel proxy applied to obtain paleotemperature reconstructions from marine and lacustrine settings. It is usually applied alongside the branched vs isoprenoid tetraether (BIT) index, which provides paleoenvironmental information as well as information on the reliability of TEX$_{86}$. Both indices are calculated via the analysis of glycerol dialkyl glycerol tetraethers or GDGTs by means of high-performance liquid chromatography/atmospheric pressure chemical ionization-mass spectrometry (HPLC/APCI-MS). Here we test the performance of alternative methods for sample cleanup and instrumental analysis. In particular, we evaluate using alkaline hydrolysis as an alternative cleanup step to alumina column fractionation and show that the resulting TEX$_{86}$ and BIT are statistically equivalent. We also test two different adsorbents in the activated or deactivated state for preparative column fractionation and show that any of them can be used to measure TEX$_{86}$ but that a certain discrimination between GDGTs used in the BIT index can occur. Regarding the mass spectrometer design, an ion-trap is shown to be as precise as a quadrupole mass spectrometer for GDGT analysis. Some differences are observed for TEX$_{86}$ and especially for BIT values obtained from both MS designs. We provide evidence that the APCI conditions are at least partly responsible for these differences. We recommend caution when comparing BIT values among laboratories as this index seems to be especially sensitive to analytical conditions.

Quantitative reconstruction of past sea surface temperature (SST) is of primary importance to understand the mechanisms responsible for natural climate variability. Geochemical proxies developed to estimate past SST based on organic molecules or trace elements have proven invaluable for such a purpose.[1−3] One of the most novel approaches is based on the relative concentrations of membrane lipids synthesized by aquatic Archaea, the glycerol dialkyl glycerol tetraethers or GDGTs[4] (Figure 1, structures 0−4′). These lipids with an isoprenoidal structure are ubiquitous in the marine water column and eventually accumulate in the ocean floor sediments. Their internal cyclization has been found to be mainly determined by water temperature,[5,6] which has been expressed as the TEX$_{86}$ (tetraether index of tetraethers consisting of 86 carbons) to derive a proxy to estimate past SST;[7]

$$\mathrm{TEX}_{86} = \frac{[\text{GDGT-2}] + [\text{GDGT-3}] + [\text{GDGT-4}']}{[\text{GDGT-1}] + [\text{GDGT-2}] + [\text{GDGT-3}] + [\text{GDGT-4}']} \quad (1)$$

Its calibration to derive quantitative past temperature reconstructions has been undertaken using a suite of 223 core-top sediments with a worldwide distribution, resulting in the following equation:[8]

$$\mathrm{SST} = -10.78 + 56.2(\mathrm{TEX}_{86}) \quad (2)$$

TEX$_{86}$ has been applied to reconstruct SST in diverse oceanic environments.[9−12] A remarkable advantage of TEX$_{86}$ over other

* To whom correspondence should be addressed. E-mail: antoni.rosell@uab.cat. Fax +34 93 581 33 31.

† Universitat Autònoma de Barcelona.

‡ ICREA.

(1) Brassell, S. C.; Eglinton, G.; Marlowe, I. T.; Pflaumann, U.; Sarnthein, M. *Nature* **1986**, *320*, 129–133.
(2) Chave, K. E. *J. Geol.* **1954**, *62*, 266–283.
(3) Chave, K. E. *J. Geol.* **1954**, *62*, 587–599.
(4) Schouten, S.; Hopmans, E. C.; Pancost, R. D.; Sinninghe Damsté, J. S. *Proc. Natl. Acad. Sci. U.S.A.* **2000**, *97*, 14421–14426.
(5) Schouten, S.; Forster, A.; Panoto, F. E.; Sinninghe Damsté, J. S. *Org. Geochem.* **2007**, *38*, 1537–1546.
(6) Wuchter, C.; Schouten, S.; Coolen, M. J. L.; Sinninghe Damsté, J. S. *Paleoceanography* **2004**, *19*, PA4028, DOI: 10.1029/2004PA001041.
(7) Schouten, S.; Hopmans, E. C.; Schefuss, E.; Sinninghe Damsté, J. S. *Earth Planet. Sci. Lett.* **2002**, *204*, 265–274.
(8) Kim, J. H.; Schouten, S.; Hopmans, E. C.; Donner, B.; Sinninghe Damsté, J. S. *Geochim. Cosmochim. Acta* **2008**, *72*, 1154–1173.
(9) Dumitrescu, M.; Brassell, S. C.; Schouten, S.; Hopmans, E. C.; Sinninghe Damsté, J. S. *Geology* **2006**, *34*, 833–836.
(10) Huguet, C.; Kim, J.; Sinninghe Damsté, J. S.; Schouten, S. *Paleoceanography* **2006**, *21*, PA3003, DOI: 10.1029/2005PA001215.
(11) Schouten, S.; Eldrett, J.; Greenwood, D. R.; Harding, I.; Baas, M.; Sinninghe Damsté, J. S. *Geology* **2008**, *36*, 147–150.

10.1021/ac8027678 CCC: $40.75

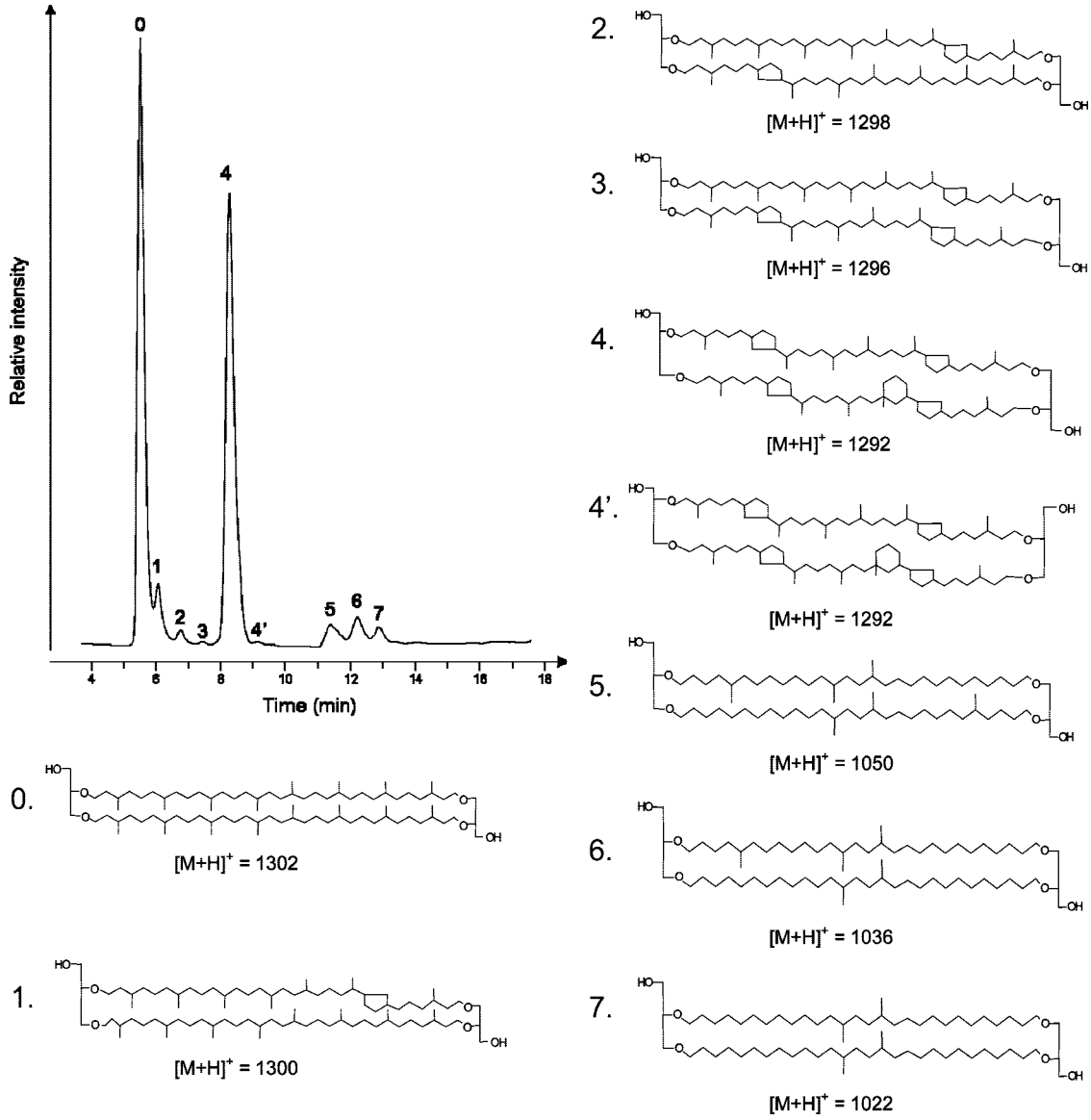

Figure 1. Base peak chromatogram and structures of glycerol dialkyl glycerol tetraethers or GDGTs and the corresponding masses of the protonated molecules. Note that structure 4′ is a regioisomer of structure 4 (crenarchaeol).

proxies is that it can also be applied to lake sediments to reconstruct past surface lake water temperature, albeit with a different calibration equation than in eq 2.[13−15] In fact, TEX_{86} is the only method available to paleoclimatologists to quantify past surface water temperatures in lakes. Because of the thermal stability of the GDGTs, TEX_{86} can be applied in marine environments beyond the temporal range of most conventional proxies.

Another group of GDGTs which are ubiquitous in aquatic sediments have the characteristic feature that they present branched instead of isoprenoidal structures (Figure 1, structures 5−7). The branched GDGTs have a terrestrial origin,[16] and in paleo-studies their presence in aquatic settings is used to assess the relative changes in fluvial or runoff input of soil organic matter, which can be used to gain information on the past hydrological cycle. This information is derived from the branched vs isoprenoid tetraether (BIT) index[17] (eq 3), which quantifies the relative abundance of the soil-originated branched GDGTs versus the isoprenoidal crenarchaeol (GDGT-4), which is predominantly derived from aquatic Archaea.

$$\mathrm{BIT} = \frac{[\text{GDGT-5}] + [\text{GDGT-6}] + [\text{GDGT-7}]}{[\text{GDGT-4}] + [\text{GDGT-5}] + [\text{GDGT-6}] + [\text{GDGT-7}]} \quad (3)$$

Thus, typical values for BIT in soils are around 0.90, while open marine sediments display values close to 0.01, and coastal

(12) Sluijs, A.; Schouten, S.; Pagani, M.; Woltering, M.; Brinkhuis, H.; Sinninghe Damsté, J. S.; Dickens, G. R.; Huber, M.; Reichart, G. J.; Stein, R.; Matthiessen, J.; Lourens, L. J.; Pedentchouk, N.; Backman, J.; Moran, K. *Nature* **2006**, *441*, 610–613.

(13) Powers, L. A.; Johnson, T. C.; Werne, J. P.; Castaneda, I. S.; Hopmans, E. C.; Sinninghe Damsté, J. S.; Schouten, S. *Geophys. Res. Lett.* **2005**, *32*, DOI: 10.1029/2004GL022014.

(14) Powers, L. A.; Werne, J. P.; Johnson, T. C.; Hopmans, E. C.; Sinninghe Damsté, J. S.; Schouten, S. *Geology* **2004**, *32*, 613–616.

(15) Tierney, J. E.; Russell, J. M.; Huang, Y. S.; Sinninghe Damsté, J. S.; Hopmans, E. C.; Cohen, A. S. *Science* **2008**, *322*, 252–255.

(16) Sinninghe Damsté, J. S.; Hopmans, E. C.; Pancost, R. D.; Schouten, S.; Geenevasen, J. A. J. *Chem. Commun.* **2000**, 1683−1684.

(17) Hopmans, E. C.; Weijers, J. W. H.; Schefuss, E.; Herfort, L.; Sinninghe Damsté, J. S.; Schouten, S. *Earth Planet. Sci. Lett.* **2004**, *224*, 107–116.

sediments usually have BIT values in between those two extremes.[17−20] This index is used to assess the reliability of TEX_{86} as this is compromised as a SST proxy if the sediment sample contains significant amounts of terrestrial GDGTs.[21] The value of the BIT index as a climate proxy has also been demonstrated in several recent multiproxy studies focusing on the abundance and distribution of terrestrial organic matter in continental margins,[18,19,22−24] for instance tracing the reactivation of the European hydrological system at the onset of the last deglaciation.[25] Consequently, as both TEX_{86} and BIT are being increasingly used worldwide as climate proxies, there is much interest to clarify any constrains regarding their measurement. Given their novelty, very few reports address the robustness of the analytical methodology employed to quantify the relative abundance of GDGTs in environmental samples.

The most common analytical method used to measure both GDGTs indices in a sediment sample includes the organic solvent extraction of the organic matter, followed by a fractionation of the extract in apolar and polar fractions with activated aluminum oxide (alumina).[26,27] The polar fraction containing the GDGTs is then analyzed by high-performance liquid chromatography−mass spectrometry (HPLC−MS) with an atmospheric pressure chemical ionization interface (APCI) and a quadrupole detector.[26,27] Several methods for the extraction of the organic matter from sediment samples were compared in a recent paper by Schouten et al.[27] The authors showed that there was no significant difference between Soxhlet, ultrasonic, and accelerated solvent extraction methods. They also compared two analytical columns and two mass spectrometers with quadrupole design and evaluated the advantages of full scan vs single ion monitoring (SIM) mode. In this study, the reproducibility for the TEX_{86} index was ±0.004, which translates into a temperature uncertainty of ±0.3 °C.[27]

The aim here is to discuss the comparability of alternative analytical methods to measure the TEX_{86} and BIT, using procedures and equipment which are not employed commonly to measure the GDGT proxies but are nonetheless frequently used by organic geochemists. For instance, it might be desirable in some cases to remove certain compounds in samples with a rich organic content in order to facilitate the detection of compounds such as the GDGTs. For this purpose, we tested alkaline hydrolysis (saponification) as an alternative option to column fractionation for the cleanup of organic extracts. We also tested different adsorbents and their degree of activation for the fractionation of the extracts. In addition we explored different analytical instrumental configurations, in particular, to measure TEX_{86} and BIT with an ion trap mass spectrometer as an alternative to using a quadrupole mass spectrometer.

EXPERIMENTAL SECTION

Sediment Extraction. A set of 23 marine and lacustrine sediments, including both organic-rich ocean sediment surface and below-surface sediment samples were freeze-dried and homogenized by mortar and pestle. Between 1−2 g of the freeze-dried sediments were extracted by microwave assisted extraction (MAE) using a mixture of dichloromethane (DCM)/methanol (3:1, v/v).[28] All extracts were dried by vacuum rotary evaporation, and half of each extract was subject to alkaline hydrolysis whereas the other half was fractionated with preparative column chromatography.

Additionally, approximately 15 g of freeze-dried sediment from Lake Banyoles (Catalonia, Spain) were ground before ultrasonic extraction with a mixture of DCM/methanol (3:1, v/v). This extract was split in several aliquots to test different adsorbents in preparative column chromatography.

Comparison of Cleanup Procedures. For alkaline hydrolysis, the extracts were redissolved in 1.5 mL of methanol and 3 mL of 8% potassium hydroxide in methanol and left overnight. The samples were concentrated to 1 mL by vacuum rotary evaporation, and the neutral compounds were recovered by liquid extraction with hexane (3 × 3 mL).

To assess the recovery of GDGTs when water is used to remove remaining salts from the hexane fraction, eight aliquots of a GDGT-0 standard solution were saponified and extracted with hexane, and four of them were further extracted with water (2 × 1 mL). A nonsaponified aliquot was used as a control.

For preparative column chromatography, glass Pasteur pipets were filled with activated alumina (Merck; placed for a minimum of 5 h at 450 °C) and the extracts were eluted with 3 mL of a mixture of hexane/DCM (9:1, v/v) and 3 mL of DCM/methanol (1:1, v/v). The last polar fraction contained the GDGTs.

Previous to the injection in the HPLC−MS, all extracts were evaporated, redissolved in hexane/*n*-propanol (99:1, v/v), and filtered through 0.45 μm PVDF filters.

Comparison of Adsorbents in Preparative Column Chromatography. Aliquots of Banyoles extract were fractionated with glass Pasteur pipets filled with the different adsorbents. These were activated alumina (placed for a minimum of 5 h at 450 °C), activated silica (up to 5 h at 120 °C), and their deactivated homologues (5% dry weight with Milli-Q water, thoroughly mixed for 20 min and stored in a desiccator overnight). In the alumina columns, the extracts were eluted with 3 mL of solvent, whereas for silica the elution volume was 4 mL, the apolar and polar solvents being the mixtures indicated above for column chromatography. Triplicates of the experiments and a blank control were performed. The polar fraction was evaporated and redissolved in hexane/*n*-propanol (99:1, v/v) and filtered through 0.45 μm PVDF filters. An analysis of variance was undertaken with the results using the SPSS statistical software.

(18) Huguet, C.; Smittenberg, R. H.; Boer, W.; Sinninghe Damsté, J. S.; Schouten, S. *Org. Geochem.* **2007**, *38*, 1838–1849.

(19) Kim, J. H.; Schouten, S.; Buscail, R.; Ludwig, W.; Bonnin, J.; Sinninghe Damsté, J. S.; Bourrin, F. *Geochem. Geophys., Geosyst.* **2006**, 7, DOI: 10.1029/2006GC001306.

(20) Walsh, E. M.; Ingalls, A. E.; Keil, R. G. *Limnol. Oceanogr.* **2008**, *53*, 1054–1063.

(21) Weijers, J. W. H.; Schouten, S.; Spaargaren, O. C.; Sinninghe Damsté, J. S. *Org. Geochem.* **2006**, *37*, 1680–1693.

(22) Herfort, L.; Schouten, S.; Boon, J. P.; Sinninghe Damsté, J. S. *Org. Geochem.* **2006**, *37*, 1715–1726.

(23) Kim, J. H.; Ludwig, W.; Schouten, S.; Kerherve, P.; Herfort, L.; Bonnin, J.; Sinninghe Damsté, J. S. *Org. Geochem.* **2007**, *38*, 1593–1606.

(24) van Dongen, B. E.; Semiletov, I.; Weijers, J. W. H.; Gustafsson, O. R. *Global Biogeochem. Cycles* **2008**, *22*, DOI: 10.1029/2007GB002974.

(25) Ménot, G.; Bard, E.; Rostek, F.; Weijers, J. W. H.; Hopmans, E. C.; Schouten, S.; Sinninghe Damsté, J. S. *Science* **2006**, *313*, 1623–1625.

(26) Hopmans, E. C.; Schouten, S.; Pancost, R. D.; Van der Meer, M. T. J.; Sinninghe Damsté, J. S. *Rapid Commun. Mass Spectrom.* **2000**, *14*, 585–589.

(27) Schouten, S.; Huguet, C.; Hopmans, E. C.; Kienhuis, M. V. M.; Sinninghe Damsté, J. S. *Anal. Chem.* **2007**, *79*, 2940–2944.

(28) Kornilova, O.; Rosell-Melé, A. *Org. Geochem.* **2003**, *34*, 1517–1523.

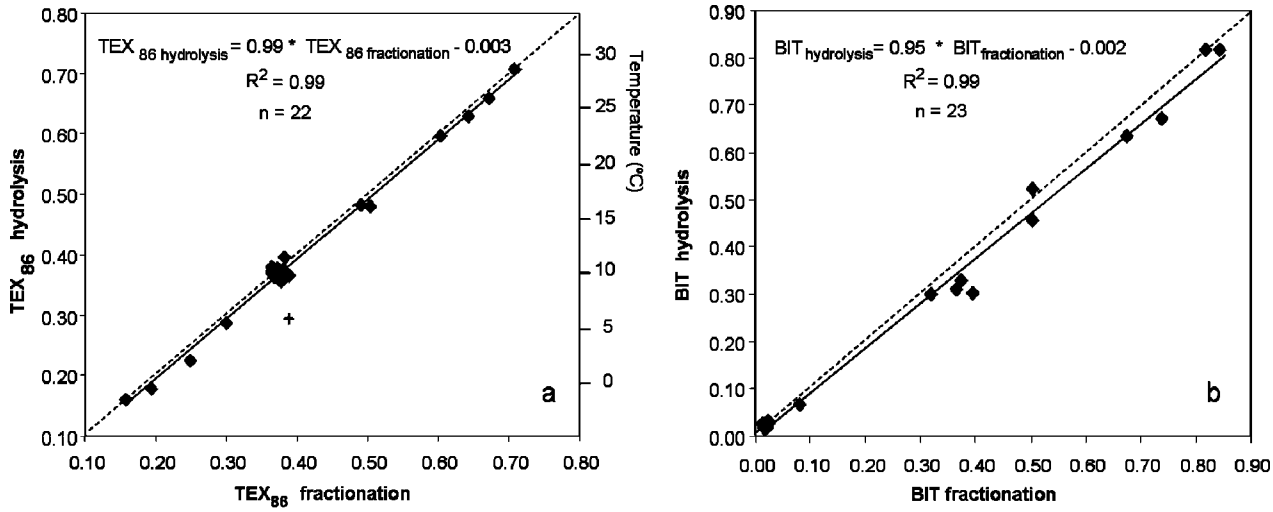

Figure 2. Cross-plots of TEX_{86} (a) and BIT values (b) obtained with the two cleanup methods tested: activated alumina column fractionation and alkaline hydrolysis (saponification). The cross symbol indicates an outlier data point. The standard deviation of the injections is not represented as it is smaller than the dot sizes. The dashed line indicates the 1:1 correspondence and is drawn only for illustration purposes.

HPLC−APCI-MS Systems. The equipment used included a Dionex P680 HPLC system coupled to a Thermo Finnigan TSQ Quantum Discovery Max quadrupole mass spectrometer with an APCI interface, hereafter referred to as the quadrupole system. The APCI was used in the positive mode, and the main parameters were optimized by infusion of a GDGT-0 solution (kindly provided by Dr. H. Morii, UOEH, Kitakyushu, Japan) and set as follows: vaporizer temperature 400 °C, corona discharge 3 μA, sheath gas pressure 6.5 Pa, auxiliary gas (N_2) pressure 0.7 Pa, and capillary temperature 200 °C. GDGTs were detected in SIM mode and quantified by the integration of their protonated molecule ($[M + H]^+$, see Figure 1). A second system, composed of an Agilent HPLC 1100 series coupled to a Bruker 3000 ion-trap mass spectrometer with an APCI interface, hereafter referred to as the ion-trap system, was also used for comparison. The positive mode in the APCI interface coupled to the ion-trap was set with the following parameters: vaporizer temperature 300 °C, dry temperature 250 °C, corona discharge 5 kV, capillary voltage 4200 V, nebulizer gas pressure 60 psi, and dry gas flow 6 L/min. Two m/z ranges were recorded to include the BIT and TEX_{86} GDGTs, namely, m/z 1010−1060 and m/z 1285−1310, respectively. The integration of the relevant GDGTs was done on the individual extracted chromatograms of $[M + H]^+ \pm 0.5$ m/z units. The TEX_{86} and BIT indices were calculated using eqs 1 and 3, and TEX_{86} was converted to temperature values using eq 2.

HPLC Columns and Conditions. The samples were eluted in a Prevail CN column (150 mm × 2.1 mm, 3 μm; Alltech) starting with an isocratic mixture of 98.5% hexane and 1.5% *n*-propanol for 4 min; afterward, the *n*-propanol was increased to 5% in 11 min and to 10% in 1 min; this proportion was held for 4 min and followed by a return to 1.5% *n*-propanol in 1 min and a stabilization period of 9 min. The solvent program is derived and modified from Schouten et al.[27] The flow rate was 0.3 mL/min, and the injection volume was 10 μL. The analysis of a large number of samples in paleoclimatology studies requires detailed consideration on cost and waste management issues during the analysis, and in particular for the GDGTs analysis, the volume of organic solvents used in the HPLC is a relevant concern. We tested an HPLC flow reduction with the aim to observe the change impinged on the stability of the GDGTs indices, given the resulting change in GDGTs peak shape and resolution. Alongside flow reduction, we used a smaller-particle size column to keep a comparable head pressure in the HPLC system. Thus, the Tracer Nucleosil CN column (4 mm × 150 mm, 5 μm; Teknokroma), which had been used in our laboratory for previous analysis at a flow rate of 1 mL/min, was compared to the aforementioned Prevail CN column (150 mm × 2.1 mm, 3 μm; Alltech) at a flow rate of 0.3 mL/min. The elution program with the Tracer Nucleosil CN column started with an isocratic mixture at 99% hexane and 1% *n*-propanol; after 12 min, *n*-propanol was increased to 10% in 1 min and these conditions were held for 3 min; *n*-propanol was returned to 1% in 1 min and held until the end of the run at 22 min. The flow rate was 1 mL/min and only increased to 2 mL/min between 13−16 min for column cleaning. This flow reduction and column comparison was tested on the ion-trap system.

Comparison of Mass Spectrometers. To investigate the reproducibility of the analysis using different designs of mass spectrometer, we compared the TEX_{86} and BIT values for 22 samples obtained with the ion-trap and the quadrupole spectrometers using the Prevail CN column and respective APCI interfaces with the aforementioned parameters.

RESULTS AND DISCUSSION

Cleanup Methods: Saponification vs Alumina Fractionation. A set of sediment extracts were subjected to two different cleanup methods, alkaline hydrolysis and fractionation through activated alumina columns, and their GDGT distribution was analyzed by means of an HPLC−APCI-quadrupole MS. The resulting TEX_{86} and BIT values obtained with the two procedures are plotted in Figure 2, which shows no sign of systematic difference between the two methods. We identified and discarded outliers for TEX_{86} if any point fell beyond 3 standard deviations of the linear regression between saponified vs fractionated extracts (see Figure 2). A paired *t* test of the remaining 22 TEX_{86} values indicated that the alkaline hydrolysis and alumina fractionation cleanup methods did not result in significantly different TEX_{86} values (t critical value = 2.83, t empirical value = 2.41, $P = 0.01$). The standard deviation of the regression

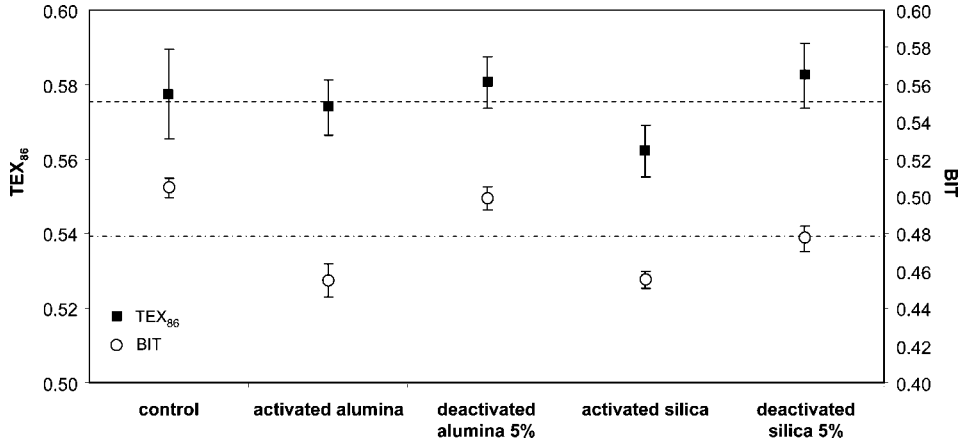

Figure 3. Comparison of the effect of the adsorbent type in column fractionation on TEX_{86} and BIT values for a sediment from Lake Banyoles. Error bars indicate $\pm 1\sigma$ ($n = 3$), and the dashed lines show the average index value.

including the 22 values is 0.013 or ~0.7 °C. This was half the precision we routinely obtain with the HPLC−quadrupole-MS, 1σ being 0.006 or ~0.3 °C. Regarding the BIT, a paired t test based on the 23 values also points at a nonsignificant difference between alkaline hydrolysis and alumina fractionation (t critical value = 2.82, t empirical value = 2.50, $P = 0.01$). Therefore, both methods are in principle comparable in terms of TEX_{86} and BIT measurement in lake and ocean sediment samples with different contents of organic matter. However, the saponification step may have a critical drawback if in the extraction process after saponification water is used to remove excess salt in the hexane extracts. We used a standard solution of GDGT-0 to calculate recoveries of the procedure. When the water extraction step was removed, the recovery of GDGT-0 of four replicate analyses was on average 104.6% ($\sigma = 4.5\%$, $n = 4$), which dropped to 6.1% ($\sigma = 4.1\%$, $n = 4$) when water extraction after hydrolysis was undertaken. This could lead to a massive underestimation of the amounts of GDGTs in the samples and clearly should be avoided.

Cleanup Methods: Comparison of Adsorbents. Four different adsorbents were tested in preparative chromatography. The resulting TEX_{86} and BIT values obtained from triplicate analyses are compared in Figure 3. We confirmed the normal distribution of the data sets with a Kolmogorov−Smirnov test ($P = 0.925$ for TEX_{86} and $P = 0.765$ for BIT) and the homogeneity of variance ($P = 0.600$ for TEX_{86} and $P = 0.626$ for BIT) previous to the analysis of variance (one-way ANOVA test). According to the ANOVA, the five methods tested (four adsorbents and a control) yielded significantly different results in terms of BIT ($P < 0.001$) but not for TEX_{86} ($P = 0.105$). There was a maximum TEX_{86} difference between methods of 0.020 or 1.1 °C (activated silica vs deactivated silica) and a minimum difference of 0.002 or 0.1 °C (deactivated silica vs deactivated alumina). Thus, it seems that the fractionation with the compared adsorbents is not discriminating between the isoprenoidal GDGTs related to TEX_{86}. On the other hand, the maximum difference between the average BIT values of the tested methods is 0.050 (control vs activated alumina and silica). It can be argued that for the qualitative nature of the proxy and its range of possible values (0−1) this difference raises no restriction for the selection of the cleanup method. However, results shown in Figure 3 suggest that the values of BIT in the hitherto published studies[17,18,21,22] might contain a certain degree of bias if activated alumina was used for the cleanup of samples, and this hampers the comparability of the published results.

HPLC Column Effects. The indices TEX_{86} and BIT were calculated for a set of 19 samples injected in two different HPLC columns operated at 0.3 and 1 mL/min. The columns had the same stationary phase but were different in terms of particle size, column diameter, and manufacturer. Given that the efficiency of a column is inversely proportional to the squared diameter and to the particle size, theoretically this gives a maximum increase of efficiency of ~6 times in changing columns from the Tracer Nucleosil CN to the Prevail CN. As the root square of column efficiency is proportional to the resolution it can provide, theoretically the resolution could be increased more than 2-fold with the Prevail CN in comparison to the Tracer CN tested. However this is compensated by the flow reduction, which was the final objective of the experiment. Column head pressure was comparable for both columns: in the Tracer Nucleosil CN column at 1 mL/min it was 59 bar, while a similar pressure (56 bar) was reached with the Prevail CN at 0.3 mL/min. The tested chromatographies did not produce significantly different TEX_{86} results (paired t test; $n = 19$, t critical value = 2.88, t empirical value = 1.43, $P = 0.01$). However, there is a certain degree of dispersion of the TEX_{86} results, indicated by a standard deviation of Tracer Nucleosil CN over Prevail CN results of 0.041 equivalent to 2.1 °C. Some samples show important differences in TEX_{86} values calculated with the two HPLC columns (six samples show a difference larger than 1.7 °C, which is the current error of the TEX_{86} calibration with SST[8]). At present, we have no explanation for the cause of the divergent TEX_{86} values with the two columns, but generally, the high correlation between both sets of results allows the intercomparability of the TEX_{86} values. The tested columns did also not significantly produce different BIT values (paired t test; $n = 18$, t critical value = 2.90, t empirical value = 1.92, $P = 0.01$), and only one sample shows a difference larger than 0.10. An important advantage of the Prevail CN column is that the narrower and smaller particle size column requires about 3 times less solvent volume compared to the

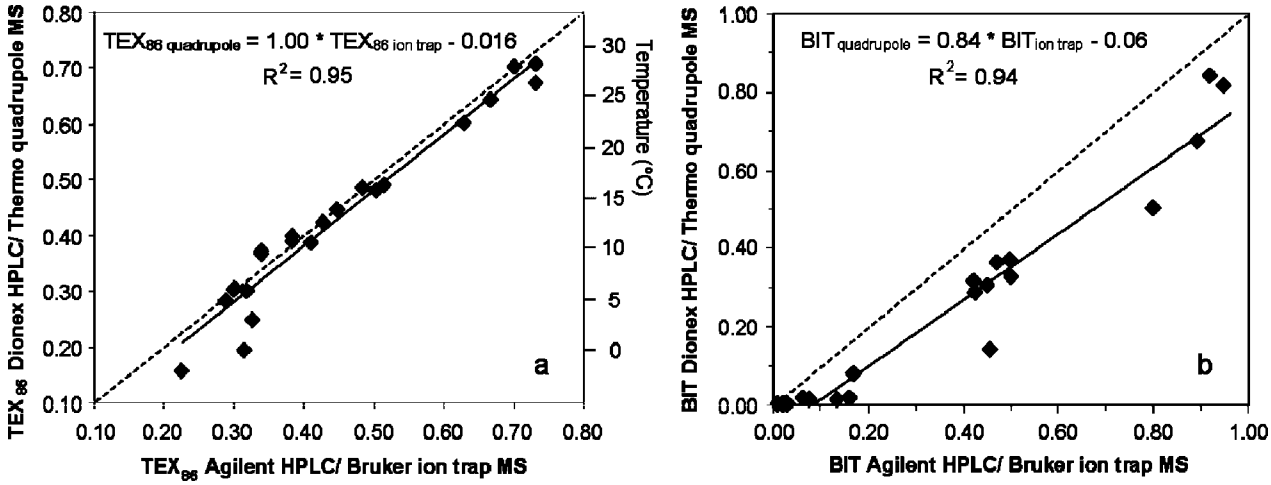

Figure 4. Cross-plots of TEX_{86} and BIT values obtained using the Dionex HPLC−Thermo quadrupole MS and the Agilent HPLC−Bruker ion-trap MS. The standard deviation of the injections is not represented as it is smaller than the dot sizes. The dashed line indicates the 1:1 correspondence and is drawn only for illustration purposes.

Trace CN, a significant cost and environmental advantage even if the run is lengthened by 7 min.

Comparison of Mass Spectrometers. With the aim of verifying whether BIT and TEX_{86} values obtained with the ion-trap MS are comparable to and as precise as the ones obtained with the quadrupole MS, a set of 22 sample extracts were injected in both systems using the same chromatographic conditions. The ion-trap system yielded a standard deviation of TEX_{86} from a triplicate injection of 0.007 or ~0.4 °C, while for the quadrupole system the standard deviation was 0.006 or ~0.3 °C. The BIT values from the same injections yielded a standard deviation of 0.002 for the ion-trap and 0.009 for the quadrupole system. Thus, no apparent difference in precision was obtained using both systems.

The cross-plot for TEX_{86} values (Figure 4a) suggests little systematic bias between the two HPLC−MS systems tested. The differences in TEX_{86} values for 18 out of the 22 samples range between 0.1 and 1.7 °C. However, four samples show differences of >3 °C. They have in common that the GDGT-2 was slightly overestimated, and the GDGT-1 slightly underestimated in the ion-trap MS compared to the quadrupole MS. Furthermore, three of these samples belong to the lower range of the TEX_{86} index, below 0.3. However, at present the cause of this difference is not clear to us. A systematic difference between both systems is clearly observed for BIT, as the quadrupole yielded lower values than the ion-trap MS (Figure 4b). This could be related to the different analytical conditions employed in the MS system and a different response or ionization efficiency of isoprenoidal vs branched GDGTs, given that conditions in both systems were optimized with the isoprenoidal GDGT-0 but not with a branched GDGT.

To further appraise the effects of the MS conditions on the TEX_{86} and BIT, we investigated the effect on GDGT yields of changes in the corona current, the temperatures involved in the vaporization of the sample (vaporizer temperature), and the ion transfer to the vacuum region in the detector (capillary temperature). While the tested corona intensities (3−15 μA) did not significantly change the relative GDGT yields, a larger

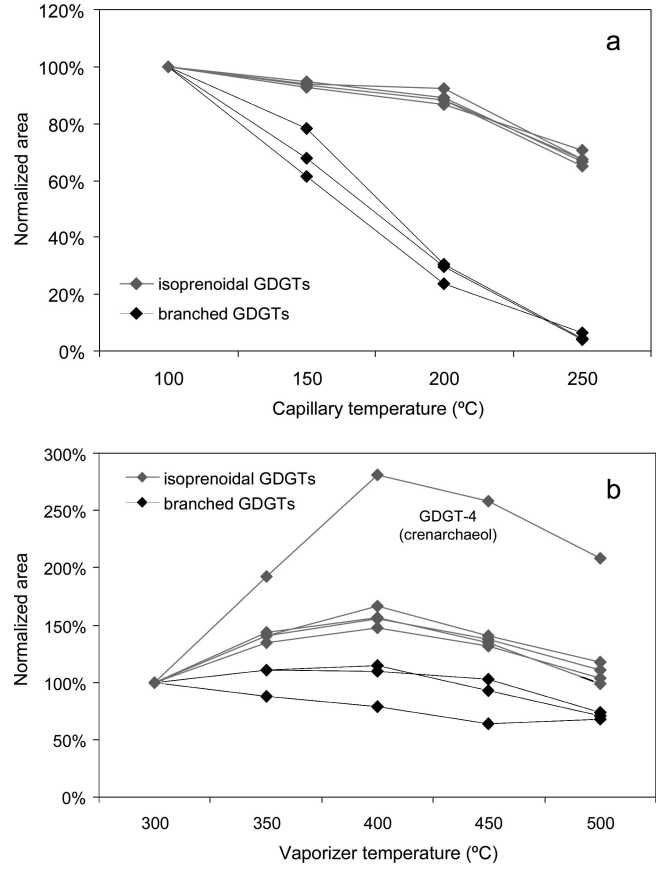

Figure 5. Effect of vaporizer temperature and capillary temperature on the branched (GDGT-5−7) and isoprenoidal (GDGT-1−4′) GDGTs yields. Data points reflect only one injection and were obtained with a Dionex HPLC coupled to a Thermo Finnigan TSQ Quantum Discovery Max mass spectrometer via an APCI interface.

effect was observed for the temperatures (Figure 5). The ionization and transfer efficiency as derived from the peak areas differ between isoprenoidal GDGTs and branched GDGTs at different vaporizer temperatures (300−500 °C; Figure 5b), and even more at different capillary temperatures (100−250 °C; Figure 5a). This raises the question of how the indices TEX_{86} and BIT are affected by the optimization or tuning of the APCI. We

observed a maximum difference in TEX_{86} of 0.05 or ~2.5 °C (result from a single analysis). However, the BIT value of a sample rose from 0.15 to 0.45 when the capillary temperature was lowered from 200 to 100 °C. The BIT values are more sensitive to the APCI conditions than TEX_{86}, as the BIT index is based on measuring two types of GDGTs, i.e., the branched and isoprenoidal (see eq 3), while TEX_{86} is based only on the isoprenoidal ones (see eq 1). Given that the APCI conditions are usually not optimized simultaneously using both isoprenoidal and branched GDGTs, it is likely that values of BIT between various instruments are not comparable. Clearly much more investigation is needed to fully understand the ionization and transfer process of GDGTs in the APCI and the repercussions on the derived TEX_{86} and BIT indices, but we urge special caution when comparing BIT values between laboratories.

CONCLUSIONS

In this study, we show the applicability and investigate the reliability of alternatives to the common analytical protocols and equipment used to analyze archaeal and bacterial GDGTs in sediments for the measurement of the TEX_{86} and BIT indices. The cleanup experiments show that alkaline hydrolysis (saponification) is a valid alternative to the fractionation on activated alumina as long as the water extraction of the hexane fraction is avoided to minimize low recoveries of the GDGTs. Although alumina fractionation and alkaline hydrolysis are both widely used cleanup methods in paleoceanographic studies, alkaline hydrolysis might be especially useful to purify samples that are very rich in certain organic compounds. Thus, GDGT analyses can be readily performed in multiproxy biomarkers studies in samples which require saponification of the organic extracts. Regarding the low recovery of GDGT-0 when water is used to remove salts from hexane, we hypothesize that the GDGT might be preferentially solubilized by water due to the relative polarity of the compound. Silica and alumina used for column fractionation either activated or deactivated at 5% provide comparable results for TEX_{86} but not for BIT. The degree of adsorbent activation seems to bias the BIT index and hence the use of nonactivated adsorbents is preferable. A reduction of flow in the HPLC after a change of HPLC columns with the same phase but different particle size, diameter, and manufacturer did not yield statistically significant differences of TEX_{86} and BIT values. Finally, TEX_{86} and BIT measurements on an ion-trap MS are compared for the first time to measurements obtained with a quadrupole MS. The ion-trap system is shown to be as precise as the quadrupole analyzer for both indices, and they also provide comparable TEX_{86} but significantly different BIT values. It appears that the ionization and transfer efficiency between branched and isoprenoidal GDGTs is different enough so that BIT values are very sensitive to MS operational conditions. This is especially important as at present much of the calibration work and provision of reference values to interpret the GDGT indices in a paleoclimatic context is derived from a single laboratory.[7,17] Our results suggest that to use such reference values, the MS conditions should first be optimized so that the relative responses of the branched vs isoprenoidal GDGTs are comparable to the published reference values. This would be facilitated if a reference sample was available with which laboratories could tune their HPLC−MS systems to obtain comparable values among the increasing community analyzing the GDGT indices.

ACKNOWLEDGMENT

A. Eustaquio, J. M. Paulís, J. Abián, and M. Carrascal are thanked for their technical support. S. Schouten and E. Hopmans are acknowledged for constructive discussion of the results. The research was partly supported by MEC Projects CTM2006-1193 and CGL2007-61579/CLI. M.E. thanks the Generalitat de Catalunya for an F.I. studentship, and S.F. thanks the support from the Deutsche Forschungsgemeinschaft (DFG).

Received for review December 31, 2008. Accepted February 17, 2009.

AC8027678

The Meteoritical Society

Meteoritics & Planetary Science 43, Nr 11, 1777–1782 (2008)
Abstract available online at http://meteoritics.org

Archaeabacterial lipids in drill core samples from the Bosumtwi impact structure, Ghana

Marina ESCALA[1], Antoni ROSELL-MELÉ[1, 2*], Susanne FIETZ[1], and Christian KOEBERL[3]

[1]ICTA, Universitat Autònoma de Barcelona, Bellaterra 08193, Catalonia, Spain
[2]ICREA, Passeig Lluís Companys 23, Barcelona 09010, Catalonia, Spain
[3]Center for Earth Sciences, University of Vienna, Althanstrasse 14, Vienna, A-1090, Austria
*Corresponding author. E-mail: antoni rosell@uab.cat

(Received 16 January 2008; revision accepted 11 July 2008)

Abstract–Meteorite impacts are associated with locally profound effects for microorganisms living at the terrestrial surface and the subsurface of the impact zone. The Bosumtwi crater in Ghana (West Africa) is a relatively young (1.07 Myr) structure with a rim-to-rim diameter of about 10.5 km. In a preliminary study targeting the subsurface microbial life in the impact structure, seven samples of the impact breccia from the central uplift of the Bosumtwi crater were analyzed for the presence of typical archaeal membrane-lipids (GDGTs). These have been detected in four of the samples, at a maximum depth of 382 m below the lake surface, which is equivalent to 309 m below the surface sediment. The concentration of the GDGTs does not show a trend with depth, and their distribution is dominated by GDGT-0. Possible origins of these lipids could be related to the soils or rocks predating the impact event, the hydrothermal system generated after the impact, or due to more recent underground water transport.

INTRODUCTION

The Bosumtwi impact structure, in Ghana, West Africa, was the subject of the ICDP Bosumtwi Crater Drilling Project in 2004 (e.g., Koeberl et al. 2007). This relatively young crater (age of 1.07 Myr; Koeberl et al. 1997) was excavated in about 2.2 Ga metavolcanics and metasedimentary rocks and has a rim-to-rim diameter of about 10.5 km. The structure has a pronounced central uplift, presumably originating from the rebound of the target rocks (Scholz et al. 2002). It is almost completely filled with a lake that has a current maximum depth of 78 m. At present, underneath the lake there is a 150 to 310 m thick layer of post-impact lake sediments, with typical seismic velocity values of unconsolidated and water-saturated sediments (Scholz et al. 2007). The lake sediments, in turn, are underlain by about 200 m of various polymict and monomict impact breccias (see, e.g., Koeberl et al. 2007 for a summary). The velocities for the impact breccia are also relatively low, which suggests that the Bosumtwi impact structure is composed of highly fractured material (e.g., Scholz et al. 2007).

The interest in such impact events is not restricted to the geological structures originating as a consequence of the collisions, but they also have important geochemical and biological implications. For instance, moderate-sized impacts and the subsequent hydrothermal systems generated can have profound effects on the organic matter abundance and composition, via processes including maturation, melting, and irradiation (Parnell and Lindgren 2006). Moreover, asteroid and comet impacts can have a profound effect on the availability and characteristics of habitats for the microorganisms living in the terrestrial surface and subsurface. Several estimates suggest that the biomass contained in microbial communities living at the terrestrial subsurface (terrestrial deep biosphere) is very large and that the total number of prokaryotes in this environment is close to the total number of microbial cells in the entire ocean (e.g., Gold 1992; Whitman et al. 1998; Karner et al. 2001). A common process associated to meteorite impacts is bulking, which increases the porosity of the shock rock lithologies and thus the surface area where lithophytic organisms can grow (e.g., Cockell et al. 2003, 2005). Furthermore, large impacts have the potential of locally sterilizing the soil, given high shock pressures and high temperatures that can persist in the impact-generated hydrothermal systems. This issue has recently been discussed for the Chesapeake Bay impact structure at the east coast of North America (Cockell et al. 2007; Glamoclija and Schieber 2007; Voytek et al. 2007). The Bosumtwi site, as it is a well-preserved and young impact structure, is an excellent site to explore the presence and structure of subsurface microbial life.

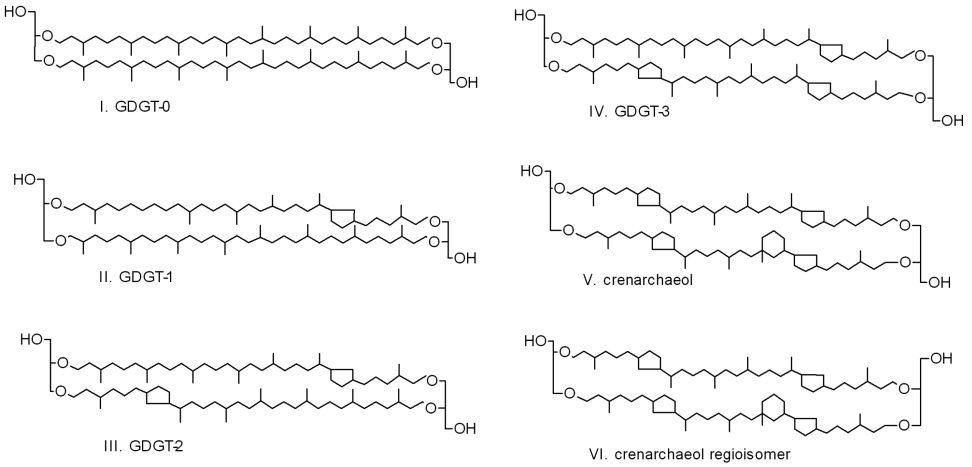

Fig. 1. Molecular structures of glycerol dialkyl glycerol tetraethers (GDGTs).

When searching for microbial life, the two prokaryotic domains of life, Archaea and Bacteria, are the usual targets of any molecular or geochemical survey. This preliminary study considers the presence of lipid biomarkers of prokaryotic life in the impact breccias. In particular, we focus on archaeal lipids, which are very refractory and thus are preserved and accumulated in sediments and soils (e.g., Schouten et al. 2000). Figure 1 shows the structures of the archaeal lipids investigated in this study, which are glycerol dialkyl glycerol tetraethers (GDGTs). The analysis of these biomarkers from Archaea in highly diverse environments, such as ocean water and surface sediments (e.g., Hoefs et al. 1997), deep-sea sediments (Fredricks and Hinrichs 2005), soils (e.g., Weijers et al. 2006), peats (e.g., Weijers et al. 2004), lakes (e.g., Powers et al. 2004), and hot springs (e.g., Pearson et al. 2004), has been used to corroborate that Archaea are ubiquitously distributed on Earth.

During the ICDP Bosumtwi Crater Drilling Project, several cores were retrieved from the geological structure. Here we report an exploratory survey of archaeabacterial biomarkers in the impactite rocks recovered from a core drilled in the Bosumtwi crater.

SAMPLES AND METHODS

Impact breccia samples were recovered from underneath the lacustrine sediments in core LB08 drilled near the central uplift of the Bosumtwi impact structure (cf. Koeberl et al. 2007), at 235.77, 240.04, 280.30, 283.50, 353.95, 382.17, and 417.60 meters below the lake surface (water column depth at this site was 73 m). The outer layer of the rock pieces was discarded in order to avoid contamination from handling. The samples were then finely ground by means of mortar and pestle, and approximately 2 g of rock powder were extracted with an organic solvent mixture of methylene chloride/methanol (3:1, v/v), using microwave assisted extraction (Kornilova and Rosell-Melé 2003). Along with the samples, a laboratory blank was run. Extracts were hydrolyzed overnight with a solution of 8% KOH in methanol, and the neutral lipid fraction was recovered with hexane by liquid extraction. The solvent was removed by vacuum rotary evaporation and the samples were redissolved in *n*-hexane/*n*-propanol (99:1, v/v), and filtered through 0.45 μm Millipore PVDF filters. All solvents used in the laboratory process were of high purity (Suprasolv® or Lichrosolv®, Merck).

The target archaeal lipids were separated by means of high performance liquid chromatography (HPLC) using an Agilent 1100 HPLC instrument. Sample extracts were eluted using a Nucleosil Cyano column (4 × 150 mm, 5 μm; Tracer) at 30.0 °C in a gradient flow using a mixture of hexane/*n*-propanol. Flow rate was 1 ml·min^{-1} and 10 μl of sample were injected. The lipids were detected and identified by mass spectrometry (MS), using a Bruker ion trap Esquire 3000 MS with an APCI (Atmospheric Pressure Chemical Ionisation) interface. For mass spectrometry, positive ion spectra were generated with the following parameters: corona voltage 5000 V, capillary voltage 4200 V, vaporizer temperature 300 °C and dry N_2 flux at 250 °C. The target GDGTs were monitored at *m/z* 1302 (I), 1300 (II), 1298 (III), 1296 (IV), 1292 (regioisomers V and VI), 1050, 1036, and 1022.

RESULTS AND DISCUSSION

Archaeal lipids were detected in four of the seven impactite rock samples analyzed (i.e., at 235.77, 240.04, 283.50, and 382.17 m) and none of the target lipids was detected in the laboratory blank. The highest concentration of GDGT lipids was found at 382.17 m depth. By comparison with external standards, we can estimate that the concentration of GDGTs in some samples is at most a few ng/g. However, given the reproducibility of the mass spectrometric method to quantify GDGTs (approximately 10% relative precision) and that internal standards were not used for this exploratory study, normalized concentrations

are presented instead of absolute concentrations. Figure 2 shows the depth profile of total archaeal lipids (GDGTs) and specifically GDGT-0 concentrations, both normalized to the maximum concentration of total GDGTs. Archaeal lipid concentrations were dominated by GDGT-0 in the four samples where GDGTs were detected. In two of these samples (240.04 and 382.17 m), GDGT-0 was the only archaeal lipid detected, whereas for the other two samples (235.77 and 283.50 m depth), GDGT-0 concentration was 81% and 38% of total GDGT concentration, respectively. The other GDGTs identified were GDGT-1, GDGT-2, GDGT-3 and crenarchaeol, which, in contrast to GDGT-0, show some degree of cyclization (see Fig. 1). These results show no trend of archaeal lipid concentration versus depth.

The rock samples analyzed in the laboratory come from the inner part of the cores and we can also rule out laboratory contamination. Thus, we infer that archaeal presence in the Bosumtwi crater is revealed by the occurrence of typical biomarker lipids, GDGTs, in the impactite rocks of this geological structure. The origin of the archaeal community is however difficult to evaluate at this time given the available data. Little information can be derived from the distribution of the detected GDGTs: GDGTs 0–3 (see Fig. 1) have been described in environmental samples including soils and lakes and ascribed to mesophilic Archaea (e.g., Powers et al. 2004; Weijers et al. 2004), but the same structures have been also observed in membranes from thermoacidophilic species (e.g., Shimada et al. 2002). Conversely, crenarchaeol is considered a marker for mesophilic Archaea, especially abundant in aquatic environments although it has also been observed, in less abundance, in soil samples (e.g., Weijers et al. 2004). However, those bacterial GDGTs that are ubiquitous in soils (Weijers et al. 2006) were not detected. The relatively high abundance of GDGT-0 in the studied Bosumtwi samples is more unusual and can provide more insights on the origin of the lipids, as discussed below.

We have considered three main pathways for the GDGTs to reach the breccia samples, which are not mutually exclusive and are discussed below: i) from soils and rocks pre-dating the impact event, ii) generation during the post-impact hydrothermal system, and iii) from hydrogeological activity.

First, it can be considered that lipids found in the rocks are from pre-impact archaeal lipids, accumulated in surface soils older than 1.07 Myr that have survived the impact event originating the Bosumtwi crater. Archaeal lipids have been found in sedimentary rocks as old as 112 Myr (Kuypers et al. 2001) and therefore, it is plausible that the lipids detected are fossil remnants of the archaeal cells that dwelled in former soils. Signatures of fossil biological activity have been found in other impact craters. For instance, in the Haughton impact structure (Nunavut, Canada) several biomarkers were identified in the melt breccias and are considered to have survived the impact event and the ensuing relatively high

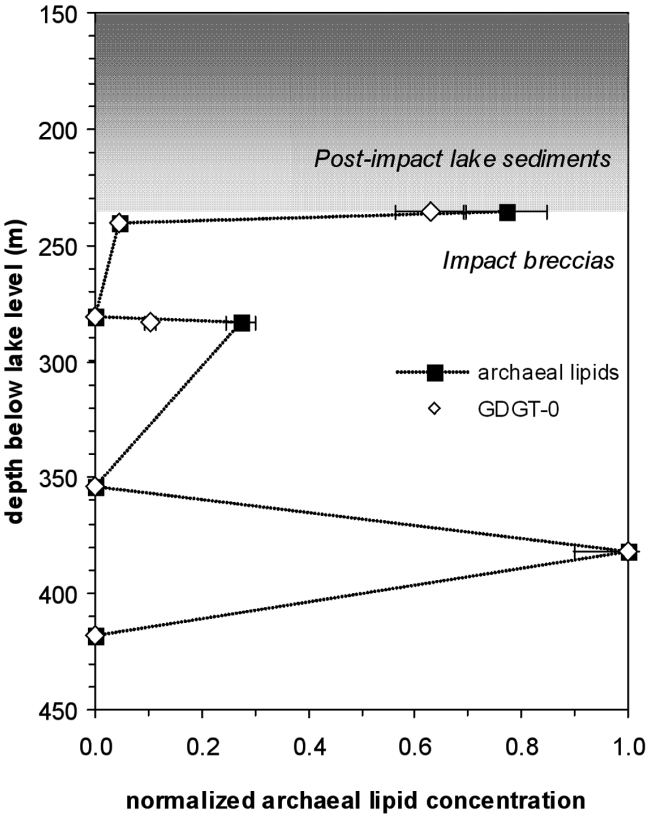

Fig. 2. Depth profile of normalized total archaeal lipid and GDGT-0 concentrations in impactites from drill core LB08 from the Bosumtwi impact structure. The archaeal lipids studied were only detected in four of the seven samples analyzed and in two of those samples only one archaeal lipid, GDGT-0, was found. Lake depth at this site is 73 m.

temperatures (around 210 °C) that lasted for ~5 kyr (Parnell et al. 2005; Lindgren et al. 2006). However, temperature effects on GDGT stability should also be taken into account. There is evidence from pyrrhotite deformation in the impact rocks of Bosumtwi suggesting peak shock temperatures at the drilling site around 250 °C (Kontny et al. 2007). There is also evidence of a moderately high-temperature post-impact hydrothermal alteration event near the central uplift, with calculated temperatures not higher than 300–350 °C (Petersen et al. 2007), although geochemical analysis suggests that this did not produce a particularly severe alteration or involved a limited volume of fluid percolating through the impacted breccias (Ferrière et al. 2007). Thus we might consider the possibility that Archaea were present in the impact target soils and they were in contact with high-temperature fluids during a relatively long time, of a few thousand years. Schouten et al. (2004) investigated the thermal maturation of GDGTs using hydrous pyrolysis and found that GDGTs exposed to temperatures above 240 °C for 72 h decreased rapidly and they were virtually completely degraded at 300 °C. Given that these values seem to be the peak temperatures reached during the impact event and post-impact hydrothermal processes, it is difficult to ascertain whether GDGTs were able

to survive the thermal conditions in the recent Bosumtwi impact structure. However, it is interesting to note that Schouten et al. (2004) also found that GDGT-0 seemed more thermally stable than the other GDGTs investigated, which is consistent with our results, where lipid distribution in rock samples is dominated by GDGT-0. The distribution of GDGTs in the sample from 283.50 m could just reflect the lipid distribution in pre-impact soils, in accordance with soil samples investigated so far (e.g., Weijers et al. 2006). But the clear dominance of GDGT-0 in the other samples, including the one at 235.77 m where little amounts of other lipids were detected, suggests an additional source for this lipid. Thus, a third explanation for the dominance of GDGT-0 within the set of investigated archaeal lipids is a large contribution of methanogenic Archaea, which are known to contain high amounts of GDGT-0 in their membranes (Koga et al. 1993).

Alternatively, the GDGTs could be of post-impact origin. Although the process of biological recovery after an impact is unique for each event and site, Cockell and Lee (2002) proposed a generalized sequence of post-impact succession. The three stages the authors distinguish after an impact event, which can include partial sterilization of the area, are (i) phase of thermal biology, characterized by thermal activity and associated microbial ecology, (ii) phase of impact succession and climax, when greater colonization of the impact crater takes place, and (iii) phase of ecological assimilation, which culminates with the erosion or burial of the impact structure. Based on studies of Haughton impact crater (about 24 km wide), the duration of the phase of thermal biology would be of the order of several thousands of years, although this will scale with the dimension of the event (Cockell and Lee 2002). Although there is a lack of global data on biological signatures which can be unequivocally associated with this phase of development of any impact crater, it can be reasonably argued that at this stage at Bosumtwi crater, the transient hydrothermal system generated provided an ideal habitat for thermophilic Archaea. Thus, the GDGTs could be remnants of this relatively recent hydrothermal system.

Otherwise, the GDGTs could be of even more recent origin. During the second phase of succession and climax proposed by Cockell and Lee (2002), crater lakes typically develop in the impact craters. In this scenario, recolonization of crater surface rocks and crater lakes can take place very rapidly, in some cases within a few months (see Cockell and Lee (2002), and references therein), with organisms that can be wind-borne, for instance. Since the meteorite impact took place (1.07 Ma), arguably enough time has passed by for prokaryotic communities (Bacteria and Archaea) to have developed in the surface of former air-exposed breccias and the lake filling the crater. The GDGTs present in the deep rocks of the Bosumtwi structure could have been carried by the water percolating from the sediments and of the lake above. In fact, mesophilic Archaea occur ubiquitously in the water column and sediments of lakes (e.g., Powers et al. 2005; Escala et al. 2007), and seismic reflection data from Bosumtwi structure suggest highly fractured impact material and water-saturated lake sediments (Scholz et al. 2007). In the same context, post-impact soils from the crater rim could be a likely source for the archaeal lipids, given that there is hydrological contact between the brecciated crater-rim rocks and the sub-lake breccias. However, the surface of the crater rim is very small compared to the size of the lake and thus the contribution of these soils in comparison to the production of GDGTs in the lake is probably not very significant. Furthermore, those GDGTs typically present in soils (Weijers et al. 2006) were not detected in the samples. If the lake waters are indeed the source of the archaeal lipids in the breccias, the high relative abundance of GDGT-0 could be explained by the presence of archaeal methanogens in sediments, which could produce the CH_4 observed in surface sediments and deep water in the Bosumtwi lake (Koeberl et al. 2007).

The lack of correlation of GDGTs concentration with depth could be explained in this case by the vertical heterogeneity in lithology and grain size that has been reported for this core (Ferrière et al. 2007). For instance, high concentrations of GDGTs in the shallowest sample (235.77 m) just below the lake sediment can be connected to the presence of carbon-rich shale clasts in the upper meters of the impactite rocks. The depth-independent concentration of archaeal lipids is also consistent with the reported vertical structure in microbial distribution in the Chesapeake Bay impact structure, which is attributed to processes of sterilization and microbial recolonization linked to the impact cratering (Cockell et al. 2007).

SUMMARY AND CONCLUSIONS

Seven samples of impact breccia from the central uplift of the Bosumtwi crater were analyzed for the presence of typical archaeal membrane-lipids (GDGTs). These have been detected in four of the samples, at a maximum depth of 382 m below lake level, and the distribution of the analyzed GDGTs is dominated by GDGT-0. The origin of these lipids is discussed and three hypotheses are considered as possible explanations: (i) pre-impact lipids in soil that survived the impact event, (ii) lipids synthesized by hyperthermophilic Archaea in the post-impact hydrothermal system, and (iii) lipids synthesized by Archaea thriving in the lake and/or crater-rim rocks that have percolated into the impactites. Additional data are needed to discriminate between these possible modes of origin for these lipids, but our preliminary results suggest that studies on the microbial community in the deep interior of the Bosumtwi structure would be rewarding.

Acknowledgments—Drilling operations at Bosumtwi were supported by the International Continental Drilling Program (ICDP), the U.S. NSF-Earth System History Program under

grant no. ATM-0402010, the Austrian FWF (project P17194-N10), the Canadian NSERC, and the Austrian Academy of Sciences. Drilling operations were performed by DOSECC, Inc. The analytical services of the UAB (A. Eustaquio and J. M. Paulís) are thanked for their technical support. M. E. thanks the Generalitat de Catalunya for an F. I. studentship. C. K. was supported by the Austrian Science Foundation (projects P17194-N10 and P18862-N10). S. F. was supported by the German Research Foundation (DFG FI 1466/1-1). M. R. Talbot and an anonymous reviewer are thanked for their insightful comments.

Editorial Handling—Dr. Uwe Reimold

REFERENCES

Cockell C. S. and Lee P. 2002. The biology of impact craters—A review. *Biological Reviews* 77:279–310.

Cockell C. S., Lee P., Broady P., Lim D. S. S., Osinski G. R., Parnell J., Koeberl C., Pesonen L., and Salminen J. 2005. Effects of asteroid and comet impacts on habitats for lithophytic organisms —A synthesis. *Meteoritics & Planetary Science* 40: 1901–1914.

Cockell C. S., Osinski G. R., and Lee P. 2003. The impact crater as a habitat: Effects of impact processing of target materials. *Astrobiology* 3:181–191.

Cockell C. S., Voytek M. A., Gronstal A. L., Kirshtein J., Finster K., Schippers A., Reysenback A., Gohn G., Sanford W. E., and Horton J. W. 2007. Influence of impacts on the deep subsurface biosphere—Preliminary results from the ICDP-USGS Chesapeake Bay Impact Structure Drilling Project. *Geological Society of America Abstracts with Programs* 39:534.

Escala M., Rosell-Melé A., and Masqué P. 2007. Rapid screening of glycerol dialkyl glycerol tetraethers in continental Eurasia samples using HPLC/APCI-ion trap mass spectrometry. *Organic Geochemistry* 38:161–164.

Ferrière L., Koeberl C., Reimold W. U., and Mader D. 2007. Drill core LB-08A, Bosumtwi impact structure, Ghana: Geochemistry of fallback breccia and basement samples from the central uplift. *Meteoritics & Planetary Science* 42:689–708.

Fredricks H. F. and Hinrichs K. 2005. Probing subsurface life with intact membrane lipids. *Astrobiology* 5:284.

Glamoclija M. and Schieber J. 2007. Fossil microbial signatures from impact induced hydrothermal settings; preliminary SEM results from the ICDP-USGS Chesapeake Bay Impact Structure Drilling Project. *Geological Society of America Abstracts with Programs* 39:316.

Gold T. 1992. The deep, hot biosphere. *Proceedings of the National Academy of Sciences* 89:6045–6049.

Hoefs M. J. L., Schouten S., de Leeuw J. W., King L. L., Wakeham S. G., and Sinninghe Damsté J. S. 1997. Ether lipids of planktonic archaea in the marine water column. *Applied and Environmental Microbiology* 63:3090–3095.

Karner M. B., DeLong E. F., and Karl D. M. 2001. Archaeal dominance in the mesopelagic zone of the Pacific Ocean. *Nature* 409:507–510.

Koeberl C., Bottomley R., Glass B. P., and Storzer D. 1997. Geochemistry and age of Ivory Coast tektites and microtektites. *Geochimica et Cosmochimica Acta* 61:1745–1772.

Koeberl C., Milkereit B., Overpeck J. T., Scholz C. A., Amoako P. Y. O., Boamah D., Danuor S., Karp T., Kueck J., Hecky R. E., King J. W., and Peck J. A. 2007. An international and multidisciplinary drilling project into a young complex impact structure: The 2004 ICDP Bosumtwi Crater Drilling Project—An overview. *Meteoritics & Planetary Science* 42:483–511.

Koga Y., Nishihara M., Morii H., and Akagawamatsushita M. 1993. Ether polar lipids of methanogenic bacteria—Structures, comparative aspects, and biosyntheses. *Microbiological Reviews* 57:164–182.

Kontny A., Elbra T., Just J., Pesonen L. J., Schleicher A. M., and Zolk J. 2007. Petrography and shock-related remagnetization of pyrrhotite in drill cores from the Bosumtwi Impact Crater Drilling Project, Ghana. *Meteoritics & Planetary Science* 42: 811–827.

Kornilova O. and Rosell-Melé A. 2003. Application of microwave-assisted extraction to the analysis of biomarker climate proxies in marine sediments. *Organic Geochemistry* 34:1517–1523.

Kuypers M. M. M., Blokker P., Erbacher J., Kinkel H., Pancost R. D., Schouten S., and Sinninghe Damsté J. S. 2001. Massive expansion of marine archaea during a mid-Cretaceous oceanic anoxic event. *Science* 293:92–94.

Lindgren P., Parnell J., Bowden S. A., Taylor C., Osinski G. R., and Lee P. 2006. Preservation of biological signature within impact melt breccias, Haughton impact structure (abstract #1028). 37th Lunar and Planetary Science Conference. CD-ROM.

Parnell J. and Lindgren P. 2006. The processing of organic matter in impact craters (abstract #288838). First International Conference on Impact Cratering in the Solar System. European Space Agency.

Parnell J., Osinski G. R., Lee P., Green P. F., and Baron M. J. 2005. Thermal alteration of organic matter in an impact crater and the duration of post impact heating. *Geology* 33:373–376.

Pearson A., Huang Z., Ingalls A. E., Romanek C. S., Wiegel J., Freeman K. H., Smittenberg R. H., and Zhang C. L. 2004. Non-marine crenarchaeol in Nevada hot springs. *Applied and Environmental Microbiology* 70:5229–5237.

Petersen M. T., Newsom H. E., Nelson M. J., and Moore D. M. 2007. Hydrothermal alteration in the Bosumtwi impact structure: Evidence from $2M_1$-muscovite, alteration veins, and fracture fillings. *Meteoritics & Planetary Science* 42:655–666.

Powers L. A., Johnson T. C., Werne J. P., Castaneda I. S., Hopmans E. C., Sinninghe Damsté J. S., and Schouten S. 2005. Large temperature variability in the southern African tropics since the last glacial maximum. *Geophysical Research Letters* 32, doi: 10.1029/2004GL022014.

Powers L. A., Werne J. P., Johnson T. C., Hopmans E. C., Sinninghe Damsté J. S., and Schouten S. 2004. Crenarchaeotal membrane lipids in lake sediments: A new paleotemperature proxy for continental paleoclimate reconstruction? *Geology* 32:613–616.

Scholz C. A., Karp T., Brooks K. M., Milkereit B., Amoako P. Y. O., and Arko J. A. 2002. Pronounced central uplift identified in the Bosumtwi impact structure, Ghana, using multichannel seismic reflection data. *Geology* 30:939–942.

Scholz C. A., Karp T., and Lyons R. P. 2007. Structure and morphology of the Bosumtwi impact structure from seismic reflection data. *Meteoritics & Planetary Science* 42:549–560.

Schouten S., Hopmans E. C., Pancost R. D., and Sinninghe Damsté J. S. 2000. Widespread occurrence of structurally diverse tetraether membrane lipids: Evidence for the ubiquitous presence of low-temperature relatives of hyperthermophiles. *Proceedings of the National Academy of Sciences* 97:14421–14426.

Schouten S., Hopmans E. C., and Sinninghe Damsté J. S. 2004. The effect of maturity and depositional redox conditions on archaeal tetraether lipid palaeothermometry. *Organic Geochemistry* 35: 567–571.

Shimada H., Nemoto N., Shida Y., Oshima T., and Yamagishi A. 2002. Complete polar lipid composition of *Thermoplasma*

acidophilum HO-62 determined by high-performance liquid chromatography with evaporative light-scattering detection. *Journal of Bacteriology* 184:556–563.

Voytek M. A., Amirbahman A., Cockell C. S., Jones E. J. P., Kirshtein J. D., Ohno T., and Sanford W. E. 2007. Biogeochemical evidence for in situ microbial metabolism in the Chesapeake Bay impact structure. *Geological Society of America Abstracts with Programs* 39:535.

Weijers J. W. H., Schouten S., Spaargaren O. C., and Sinninghe Damsté J. S. 2006. Occurrence and distribution of tetraether membrane lipids in soils: Implications for the use of the TEX86 proxy and the BIT index. *Organic Geochemistry* 37: 1680–1693.

Weijers J. W. H., Schouten S., Van Der Linden M., van Geel B., and Sinninghe Damsté J. S. 2004. Water table related variations in the abundance of intact archaeal membrane lipids in a Swedish peat bog. *FEMS Microbiology Letters* 239:51–56.

Whitman W. B., Coleman D. C., and Wiebe W. J. 1998. Prokaryotes: The unseen majority. *Proceedings of the National Academy of Sciences* 95:6578–6583.